INVESTIGATION OF ANTI-PRION, NEUROPROTECTIVE AND ANTI-CHOLINESTERASE ACTIVITIES OF ACRIDINE DERIVATIVES

NGUYEN THI HANH THUY
(B. Sc. (Pharmacy) (Hons), NUS)

A THESIS SUBMITTED

FOR THE DEGREE OF DOCTOR OF PHILOSOPHY

DEPARTMENT OF PHARMACY

NATIONAL UNIVERSITY OF SINGAPORE

2010

Acknowledgements

Table of Contents

Publications and Conferences

Hanh Thuy Nguyen Thi, Chong-Yew Lee, Kenta Teruya, Wei-Yi Ong, Katsumi Doh-ura, Mei-Lin Go. Antiprion activity of functionalized 9-aminoacridines related to quinacrine. Bioorganic & Medicinal Chemistry (2008), 16(14), 6737-6746

Nguyen, T.H.T., Go. M. L. Investigation on neuroprotective potential of acridine derivatives. Poster presentation at the Medicinal Chemistry Symposium. Jan 2008. National University of Singapore.

Nguyen, T.H.T; Lee, C.Y.; Ong, W.Y.; Doh-ura, K.; Go, M.L. Investigation on antiprion activities of acridine derivatives. Poster presentation at the European school of medicinal chemistry. Symposium of medicinal chemistry in neurodegerative diseases July 2008. Urbino, Italy.

Summary

The objective of this thesis was to investigate the activity of functionalized aminoacridines in neurodegenerative conditions. To this end, a library of forty acridine derivatives and several related tetrahydroacridine and quinoline analogues were synthesized and evaluated for (i) antiprion activities against different prion strains including two mouse strains (RML and 22L) and one human strain (Fukuoka-1) (ii) neuroprotection against glutamate-induced oxytosis (iii) anti-acetylcholinesterase and anti-butyrylcholinesterase activities. The compounds were classified into seven groups based on nature of side chain and ring template.

Almost all the compounds demonstrated activity on the murine RML strain-infected neuroblastoma (ScN2a) model, with EC_{50} values ranging from 0.03 µM to 4 µM. A number of compounds were active on the 22L strain-infected cells (N167) model as well as cells overexpressing cellular prion (Ch2) model. Most importantly, some Group 2 and Group 3 compounds were more potent than quinacrine on PrP^C-overexpressed neuroblastoma cells infected with a human prion strain (F3 model) with EC_{50} values at a low micromolar range. They were also able to clear aggregates of abnormal prion proteins (PrP^{Sc}) completely at a concentration less than 3 µM. Surface plasmon resonance revealed that the compounds bind to PrP^C. The high lipophilicity of the 9-aminoacridined contributes to its potential to cross the blood brain barrier as demonstrated from the PAMPA-BBB assay. One analog which was active on all four tested prion models had a lower susceptibility to be a Pgp substrate when tested on a cell monolayer overexpressing Pgp. Thus, the 9-aminoacridine template was found to be a promising template from

which potential antiprion agents with good in vitro potencies and drug-like properties for BBB permeability may be derived.

An –NH– group flanked by a phenyl and an acridine is crucial for neuroprotection against glutamate-induced oxytosis. The compounds were able to "rescue" cells exposed to 5mM glutamate for up to 12 hours. All 9-(phenylamino)acridines were able to quench ROS level as seen from the TEAC assay. These compounds effectively reduced the mitochondrial ROS levels and the intracellular Ca^{2+} level. Both these mechanisms were late-stage events linked to glutamate-induced cell death and were proposed to contribute to the latent protective effects of the active compounds.

The optimal ring scaffold for AChE inhibition was the 6-chlorotetrahydroacridine ring which had low nanomolar IC_{50} values. The side chain determined potency and selectivity for AChE versus BChE inhibition. The 1-benzyl-4-piperidinyl side chain was associated with the most potent activity. Most of the compounds were mixed inhibitors of AChE and competitive inhibitors of BChE. Compounds with the 6-chlorotetrahydroacridine template (Group 6) and those that had 1-benzyl-4-piperidinyl side chains attached to the 6-chloro-2-methoxyacridine ring (Group 3) were more selective inhibitors of AChE compared to BChE. Docking of active compounds onto the crystal structures of AChE and BChE shed light on the binding mode of these compounds.

In conclusion, this thesis had shown that functionalized aminoacridines were attractive starting points for the design of compounds for antiprion activity, inhibition of

oxytosis and inhibition of AChE. While structural requirements for these activities were

different, they are found in compounds that bear a common template.

List of abbreviations

ABTS: 2,2'-azino-bis(3-ethylbenzthiazoline-6-sulphonic acid)

Aβ: amyloid-β peptides

AChE: acetylcholinesterase

AD: Alzheimer's disease

m-AMSA: Amsacrine

APCI: atmospheric pressure chemical ionization

BBB: blood brain barrier

BChE: butyrylcholinesterase

BCRP: breast cancer resistant protein

BINAP: 2,2'-bis(diphenyl phosphino)-1,1'-binaphthyl

BSA: bovine serum albumin

CJD: Cruetzfeldt-Jakob disease

^{13}C NMR: carbon-13 nuclear magnetic resonance

DACA: N-(2-dimethylamino)ethyl)acridine-4-carboxamide

DMEM: Dulbecco's modified Eagle's medium

DMSO: dimethyl sulfoxide

DPPD: N,N-diphenyl-p-phenylenediamine

DTNB: dinitrothiocyanobenzene

EC$_{50}$: the concentration of substance that provides 50% of the maximum activity

ER: endoplasmic reticulum

ESI: electron spray ionization

FAA: full antiprion activity

FBS: fetal bovine serum

GPI: glycosyl phosphatidylinositol

GSH: glutathione

GSS: Gerstmann-Sträussler-Scheinker syndrome

HBSS: Hank's buffered saline solution

H_2DCF: 2',7'-Dichlorofluorescein diacetate

^1H NMR: proton nuclear magnetic resonance

HPLC: high performance liquid chromatography

IC_{50}: the concentration of substance that provides 50% of the maximum inhibition

LC/MS/MS: Liquid chromatography/Mass spectrometry/Mass spectrometry

MS: mass spectra

MTT: 3-(4,5-dimethylthiazol-2-yl)-2,5-diphenyltetrazolium bromide

NAPDH: nicotinamide adenine dinucleotide phosphate

PAMPA-BBB: parallel artificial membrane permeation assay for blood brain barrier

        permeability

PAS: peripheral anionic site

PBS: phosphate buffer saline

Pgp: P-glycoprotein

PI: propidium iodide

PMSF: phenylmethanesulphonyl fluoride

PMD: protein misfolding disorder

PrP: prion protein

PrP^C: cellular prion protein

PrP^{Sc}: scrapie prion protein

RU: response unit

ROS: reactive oxygen species

SAR: Structure-activity relationship

SDS PADE: sodium dodecyl sulfate polyacrylamide gel electrophoresis

SPR: surface plasmon resonance

TC: tolerant concentration

TEAC: Trolox equivalent antioxidant capacity

TEER: transepithelial electrical resistance

TLC: thin layer chromatography

TSE: transmissible spongiform encephalopathies

Chapter 1: Introduction

Acridine is a nitrogen heteroaromatic compound that is structurally related to anthracene (Figure 1.1). In acridine, the –CH= in the central ring of anthracene is replaced by an azomethine nitrogen (-N=), the presence of which imparts basicity to the heterocycle. Acridine is a weak base with a pK_a of 5.6 that is comparable to that of pyridine.
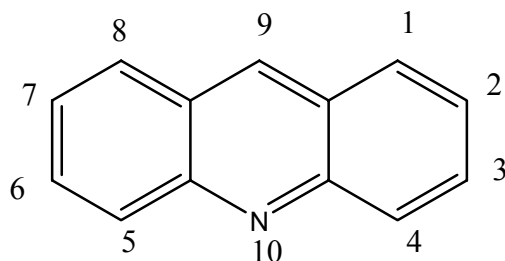
Figure 1.1: Structure and numbering of acridine (also known as dibenzo(b,e)pyridine, 2,3,5,6-dibenzopyridine, 2,3-benzoquinoline, 10-azaanthracene)

Acridine itself has no therapeutic utility but functionalized acridines like aminoacridines, and reduced acridines like tetrahydroacridines are represented in several important drugs. This has boosted the reputation of acridine as a privileged scaffold and explains the sustained interest in this template for drug design, particularly for agents targeted against microbial infection, cancer, neurodegeneration and inflammation.

1.1 Antimicrobial activity

The first antimicrobial acridines were dyestuffs, namely acriflavine which was found to possess activity against the parasitic disease trypanosomiasis by Ehrlich and Benda in 1912 and proflavine whose antibacterial activity was reported by Browning in

1913.[1] Acriflavin was subsequently found to have antibacterial activity, which led to widespread use of acriflavin and proflavin as wound antiseptics during the First World War. Interest in the antimicrobial activitiy of acridines continued unabated after the War and resulted in the development of cyanine and styryl derivatives of quaternary acridines, quinolines and phenazines,[1] as well as quinacrine which was widely employed as an antimalarial substitute for quinine during the ensuing Second World War.[2] The post-war period of the 1940s and 1950s saw a decline in research interest in the antibacterial properties of acridines due to the discovery of the highly efficacious penicillins as antibiotics in the 1950s. Nonetheless, antibacterial acridines like proflavin and acriflavin are remembered to this day for plugging the "antibacterial gap" between Ehrlich's Salvarsan and Fleming's penicillin. The research of Steck *et al.*[3] on anti-rickettsial acridines and Elslager *et al.*[4] on anti-bacterial acridine N-oxides were the last major investigations on the antimicrobial properties of acridines.[5] Ironically, it was a better understanding of the antibacterial activity of the acridines that caused the waning of interest.
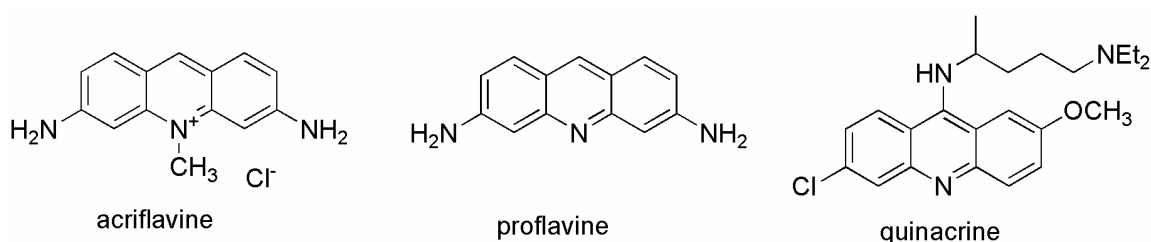
Figure 1.2: Structures of early acridine-based antimicrobials.

Nucleic acids are the established sites of action of aminoacridine derivatives in bacteria. The planar tricyclic acridine nucleus intercalates perfectly between nucleotide base pairs in the DNA helix, with the positively charged acridinium moiety directed

towards the negatively-charged phosphate groups. The principal driving forces for intercalation are stacking and charge-transfer interactions, with hydrogen bonding and electrostatic forces playing stabilization roles. Intercalation destroys the regular helical structure of DNA, causing it to unwind at the site of binding and consequently interfering with the action of the DNA-binding enzymes (DNA topoisomerases, DNA polymerases). In fact, the targeting of nucleic acids by acridines open a new front for their deployment as anticancer agents as described in Section 1.2. However, it also raised misgivings over the widespread use of acridines as main stream antibacterials for fear that its intercalating properties would result in undesirable frameshift mutagenesis in mammalian cells. These fears had since been challenged by investigations demonstrating that simple intercalators like acridines were weak clastogens and not associated with widespread mutagenic properties.[6,7]

The intercalating propensity of the acridine template is influenced by the type of substituents on the ring. Introducing bulky substituents such as propyl and tertiary butyl groups resulted in analogues that were significantly weak intercalators.[8] The presence of a methyl group at C2 of 9-aminoacridine was also reported to diminish both DNA intercalative ability and mutagenicity.[9]

The past decade had seen a modest resurgence in the research on antimicrobial acridines, prompted in part by the growing resistance to available drugs. Denny and co-workers described structure-activity relationships for the antileishmanial and antitrypanosomal activities of 1'-substituted-9-anilinoacridines.[10] Guetzoyan *et al.* reported new 9-substituted acridyl derivatives that were active against chloroquine-resistant strains of *Plasmodium falciparum.*[11] Biagini and co-workers designed

dihydroacridinediones as potent antimalarials with nanomolar IC_{50} values and greater selectivity for the parasite (and not host) mitochondrial bc1 complex.[12] More recently, hybrid molecules designed from 4-aminoquinoline and clotrimazole resulted in potent and selective antimalarials with promising pharmacokinetic profiles.[13]

1.2 Anticancer activity

The ability of the acridine ring to intercalate within the double-stranded DNA structure forms the basis of its anticancer activity. For most of these acridines, their cytotoxicity is determined not only by its affinity for DNA but the ability to form a relatively stable complex with DNA that can inhibit the topoisomerase enzymes. Briefly, topoisomerases play a crucial role in the control of the structural organization of DNA in cells and in the release of negative and positive constraints generated by DNA replication, transcription and repair processes. To release the constraints on the global structure of DNA, topoisomerase I makes transient cleavages on one strand of the DNA double helix[14] while topoisomerase II breaks both strands of the duplex.[15,16] This leads to the formation of a covalent topoisomerase-DNA complex ("cleavable complex") which in normal cells will break down to restore a native relaxed DNA strand and the free functional enzyme. This process can be inhibited at various levels such as the DNA binding or DNA cleavage step, but the most potent inhibitory process in terms of cellular toxicity is the stabilization of the cleavable complex through inhibition of the re-ligation step. Two major families of acridines were identified to act in this manner, namely the 9-anilinoacidines represented by amsacrine (m-AMSA) and carboxamidoacridines of which DACA [N-(2-dimethylamino)ethyl)acridine-4-carboxamide] is an example (Figure 1.3).
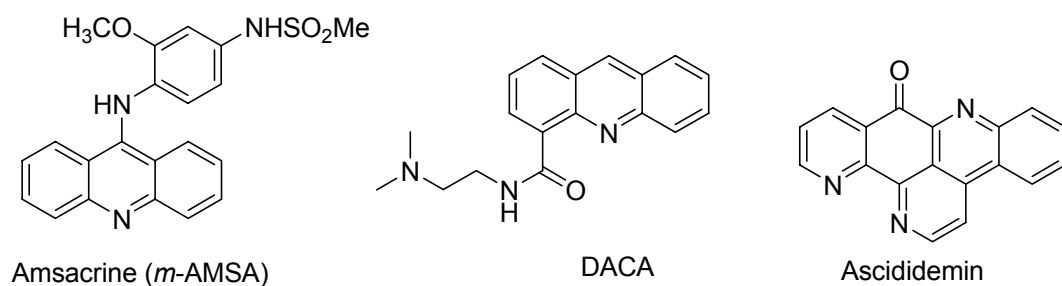
Figure 1.3: Structures of representative topoisomerase inhibitors.

Amsacrine (*m*-AMSA) has been used as an antileukaemic agent since 1976. Its mode of action involves the stabilization of the topoisomerase II - DNA complex[17] by intercalation of the acridine ring[18] and specific interactions between the substituted aniline ring and the enzyme.[19] Modification of substituents on the acridine core and 9-anilino moiety had resulted in interesting novel AMSA-like derivatives like 3-(9-acridinylamino)-5-(hydroxymethyl)anilines (AHMA),[3] 5-(9-acridinylamino) toluidines[20] and anisidines[21] which were more potent as anticancer agents and less toxic to the host.

While most topoisomerase inhibitors were selective towards either topoisomerase I or II, DACA was unusual in its ability to inhibit both enzymes. DACA was evaluated in phase II clinical trials for efficacy against non-small cell lung cancer and advanced ovarian cancer[22,23] but further trials were discontinued in the face of poor results.

Quadruplex nucleic acids are four-stranded structures comprising short tracts of guanine (G)-rich sequences that are held together by intervening sequences (loops).[24] Their occurrence has been extensively characterized at the telomeric ends of eurkaryotic chromosomes, whose DNA consists of tandem repeats of the sequence d[(TTAGGG)$_n$] and where the extreme 3' ends are single stranded.[25] These guanine-rich single strands can adopt higher–ordered and functionally useful G-quadruplexes.[26] The induction and

stabilization of telomeric G-quadruplexes by small molecules interfere with telomere function, inhibit telomerase activity and eventually alter telomere maintenance.[27-29] Telomere maintenance is necessary if cancer cells are to retain their unlimited proliferative potential,[30,31] thus the design of drugs targeting the telomeric G-quadruplex is a rational and promising approach for cancer chemotherapy.[32] Several acridines were identified as selective ligands for the telomeric G-quadruplex DNA. These were the 3,6,9 -trisubstituted analog BRACO-19,[33,34] the pentacyclic acridinium RHPS4[35-37] and aminoglycoside-quinacridine conjugates.[38] Aminoglycosides were known for their ability to recognize RNA residues and this property was exploited to good advantage in the conjugates which targeted the RNA element of telomerase.
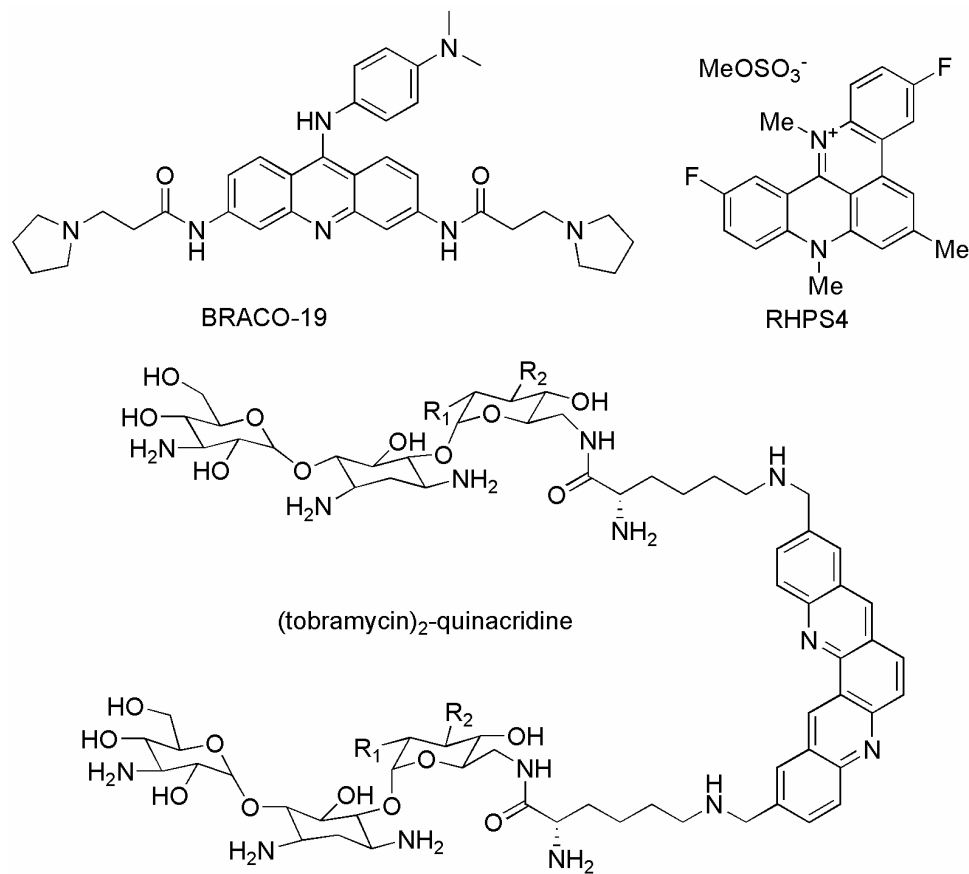
Figure 1.4: Structures of representative telomerase inhibitors.

Acridine derivatives were reported to inhibit cyclin-dependent kinases (CDK) that were frequently over-expressed in cancer cells. For example, 3-amino-9-thio(10*H*)-acridone (3-ATA) was a selective inhibitor of CDK4. 10-Benzyl-1-hydroxy-3-morpholinoacridin-9(10H)-one sensitized cancer cells and caused DNA lesions by inhibiting DNA-dependent-protein-kinase-induced phosphorylation of a p53 peptide substrate.[39]

3-ATA

10-benzyl-1-hydroxy-3-morpholinoacridin-9(10*H*)-one
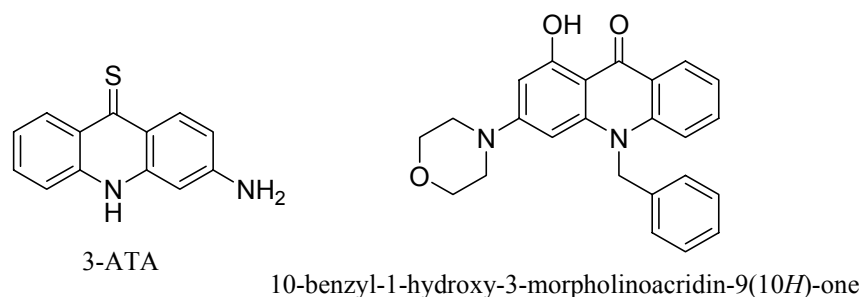
Figure 1.5: Structures of representative acridine-based kinase inhibitors.

Besides amsacrine, the only other acridine derivative in clinical use as an anticancer agent is nitracrine [1-nitro-9-(3',3'–dimethylaminopropylamino)acridine] (Figure 1.6). The reduction of the nitro group in nitracrine is one of the activation steps leading to covalent binding to DNA and other proteins.[40] This process predominated in cells with limited oxygen content which is a characteristic feature of growing tumors.
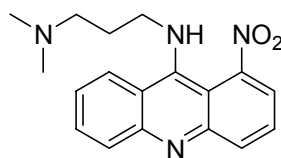
Figure 1.6: Structure of nitracrine (Ledarin ®)

1.3 Efficacy in neurodegenerative conditions

Only two acridine derivatives have been used for neurodegenerative disorders. They are quinacrine for Cruetzfeldt-Jakob disease (CJD) and tacrine for Alzheimer's disease (AD). Quinacrine was found to be effective in a cell-based model of prion infection at submicromolar EC_{50} values.[41-43] Although it failed to demonstrate activity in scrapie-infected mice,[44-46] it was used on compassionate grounds in a few patients with CJD. The decision was prompted mainly by the absence of a therapeutic agent for prion diseases as well as the relatively good safety record of quinacrine as an antimalarial agent.[47] Tacrine is an inhibitor of the acetylcholinesterase (AChE) enzyme and the first centrally acting AChE inhibitor to be approved for AD. It was used to treat the symptoms of the disease but did not offer a curative solution. Tacrine has been largely replaced by safer and more effective AChE inhibitors like rivastigmine for Alzheimer's disease[48] but it still remains an interesting template for the design of hybrid agents for cognitive disorders.[49-52]

1.3.1. Prion Diseases

Prion diseases, also termed transmissible spongiform encephalopathies (TSEs), belong to a class of neurodegenerative disorders that arise from the misprocessing and aggregation of normally benign soluble proteins. The causative agent is the prion protein originally defined by Prusiner as "a small proteinaceous infectious particle that is resistant to inactivation by most procedures that modify nucleic acid."[53] The only known component of the prion is a modified form of the cellular prion protein PrP^C, a cell surface glycoprotein[54] of unknown function that is found in all mammals examined to date. The central event in prion pathogenesis is the conformational conversion of PrP^C

into PrP^{Sc}, an insoluble and partially protease resistant isoform that propagates itself by imposing its abnormal conformation onto PrP^{C} molecules. The precise molecular mechanism of the PrP^{C} to PrP^{Sc} conversion is unknown. Two models have been proposed to explain this phenomenon.
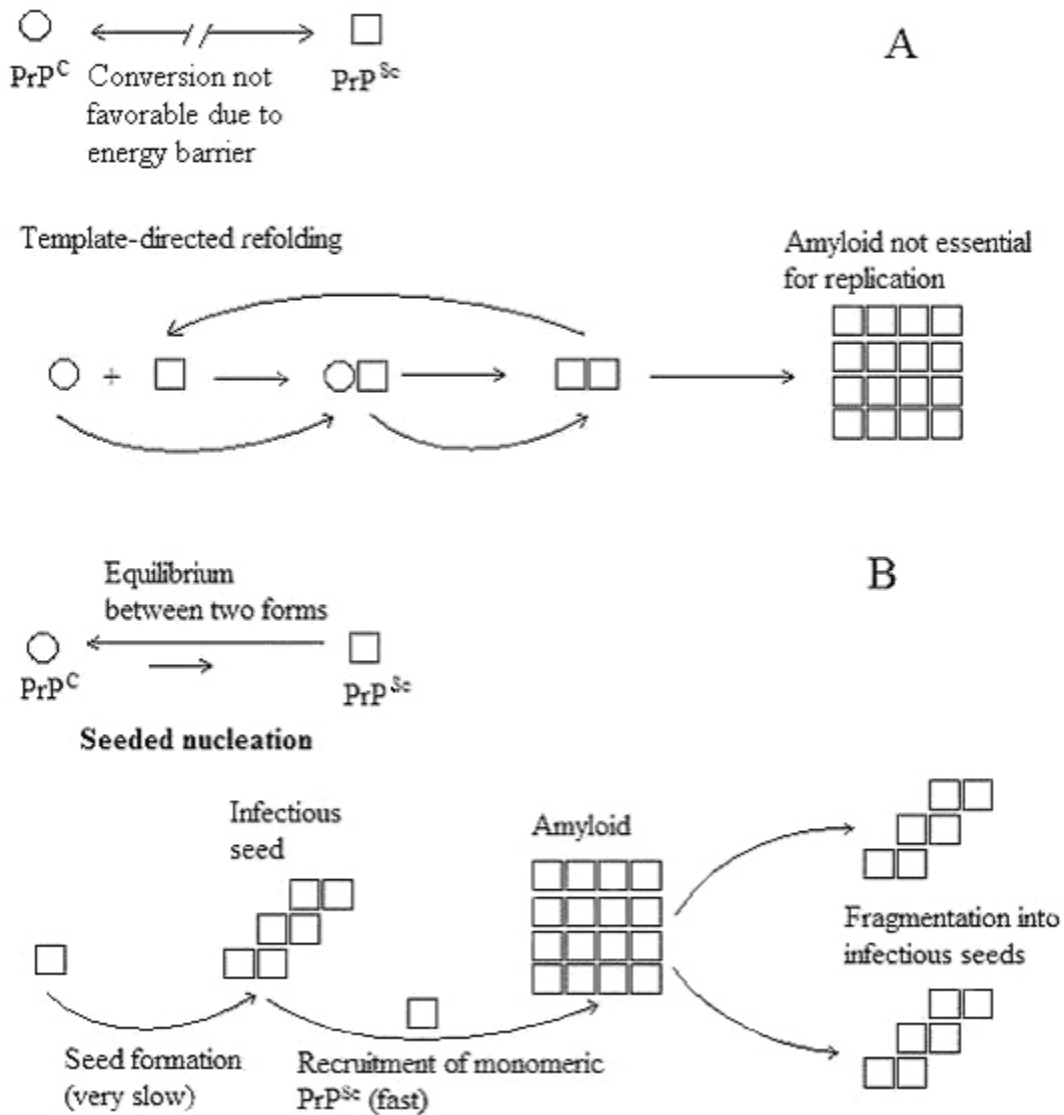
Figure 1.7: Theoretical models for the formation of PrP^{Sc} amyloid from PrP^{C}

Figure 1.7-A shows the template-assisted model which proposed an interaction between exogenously introduced PrP^{Sc} and endogenous PrP^{C}. PrP^{Sc} induced the conversion of PrP^{C} to PrP^{Sc}, which then aggregated to form the amyloid. Without a PrP^{Sc} template, spontaneous conversion from PrP^{C} to PrP^{Sc} was energetically unfavorable because of the presence of a kinetic barrier that favored the thermodynamically more stable PrP^{Sc}.[55] A role for putative heat shock protein (Protein X), presumably as a molecular chaperone that binds PrP^{C} and assists in the change of conformation has been proposed.[55]

Figure 1.7-B illustrates the "seeding" or nucleation-polymerization model which proposed that PrP^{C} and PrP^{Sc} existed in a reversible thermodynamic equilibrium.[56] In the non-disease state, the equilibrium favored PrP^{C} and only small amounts of non-infective monomeric PrP^{Sc} were present. The monomeric PrP^{Sc} slowly assembled to form a highly ordered "seed" which recruited more monomeric PrP^{Sc} to form large aggregates (amyloid). The latter fragmented into smaller infectious seeds which were able to initiate further aggregate formation. This model may also apply to amyloid formation in other protein misfolding disorders (PMDs) like Alzheimer's disease, Parkinson's disease and Huntington's disease. Protein conformational changes associated with the pathogenesis of most PMDs resulted in the formation of abnormal proteins that were rich in β-sheet structures, partially resistant to proteolysis and had a propensity to form larger-order self-propagating aggregates.

While the conversion of PrP^{C} to PrP^{Sc} is central to the pathogenesis of TSEs, the question as to whether PrP^{Sc} is directly responsible for the neurodegenerative process remains unanswered. More likely, its toxicity depends on some PrP^{C}-dependent process

that contributes to neuronal dysfunctions.[57,58] The role of PrP^C in this context has been reviewed[59] and is summarized in the following paragraphs.

(i) Alteration of PrP^C mediated signaling: It is noteworthy that depletion of PrP^C per se did not trigger scrapie pathology. However, when depleted in mice with an established prion infection, disease progression was slowed down, even in the presence of high levels of extraneuronal PrP^{Sc}. The implication was that PrP^{Sc} might not be directly responsible for neurodegeneration. Rather its toxicity was related to some PrP^C-dependent process that led to neuronal dysfunction and death. PrP^C may function as a signaling molecule with an important cytoprotective role. Its conversion to PrP^{Sc} could abrogate this function, thus inducing neurodegeneration. Alternatively, the binding of PrP^{Sc} to PrP^C may trigger a signal transduction pathway leading to neuronal damage.

(ii) PrP^C mislocalization: PrP^C is synthesized, folded and glycosylated in the endoplasmic reticulum (ER) where its glycosyl phosphatidylinositol (GPI) anchor is added, followed by further modification in the Golgi complex. PrP^C was found to assume at least two unusual transmembrane topologies in the ER: ^{Ctm}PrP and ^{Ntm}PrP which were distinguished by having either the COOH or NH$_2$ terminus in the endoplasmic reticulum lumen respectively. These misfolded and aberrantly processed PrP forms normally comprise a small proportion of cellular PrP^C but may increase in some PrP mutations. Such an increase could lead to neurotoxicity even without PrP^{Sc} formation. Under normal circumstances, misfolded (and wild type) forms of PrP^C underwent retrograde transport to the cytosol where they were ubiquitinylated and degraded by the proteasome through a process called ER-associated degradation pathway. When this pathway was overwhelmed (as would happen during proteosomal inhibition or malfunction during prion disease), the

11

excess PrP molecules were routed to the cytoplasm where they accumulated and caused neurotoxicity. Therefore aberrant PrP^C trafficking leading to mislocalization may contribute to PrP^{Sc} associated neurotoxicity.

(iii) PrP-derived oligomeric species: The currently accepted view of the causative agents of prion disease are not the highly organized amyloidal aggregates but the smaller oligomeric species of approximately 20 molecules.[60] The toxicity of small aggregates has also been proposed for Alzheimer's disease[61,62] and Parkinson's disease.[63] The disease potential of small aggregates may exceed that of large aggregates because small aggregates expose a higher proportion of residues on their surfaces. These residues may be normally buried within the core of the protein but are uncovered during the misfolding process and can participate in improper interactions with cellular components such as cell membranes, metabolites, proteins or other macromolecules that would ultimately lead to the malfunctioning of the cellular machinery.[64]

1.3.2. Oxidative stress and protein misfolding diseases

Although each protein misfolding disorder has its own molecular mechanisms and clinical symptoms, some general pathways are recognized in the different pathogenic cascades. Protein misfolding and aggregation is one common feature. Yet another is the role of oxidative stress and free radical formation as either a cause or consequence of the neurodegenerative cascade.[65] The brain is highly susceptible to oxidative stress-related degeneration for many reasons. Neural cells are rich in mitochondrial content and possess a high level of aerobic metabolism. Invariably a proportion of the consumed oxygen will end up as incompletely reduced reactive oxygen species (ROS). Brain tissue is also very

sensitive to oxidative stress due to low levels of some antioxidant enzymes, susceptibility of brain membranes to peroxidation and high content of iron.[66] There is mounting evidence that neurodegenerative disorders further increase the oxidant load and thus subject the brain to further oxidative stress. Pappolla *et al.* presented *in vitro* and *in vivo* models in support of the hypothesis that the neurotoxicity of the Aβ protein in Alzheimer's disease was mediated by free radicals.[67] Antioxidant enzymes such as catalase, superoxide dismutase, glutathione peroxidase and glutathione reductase were elevated, an indication that oxidative stress plays a significant but as yet undefined role in this disorder.[68,69] Oxidative biomarkers such as cholesterol hydroperoxide, malondialdehyde, protein adducts of 4-hydroxy-2-nonenal and 8-hydroxy-2-deoxyguanosine were detected in higher levels in Parkinson's disease.[70,71] Analysis of the dopaminergic neurons in patients with Parkinson's disease revealed a significant decline in reduced glutathione (>60%) and a moderate increase in oxidized glutathione (29%) levels.[72,73] Oxidative stress markers such as malondialdehyde and heme oxygenase-1, as well as superoxide radicals were markedly elevated in the brains of scrapie-infected mice. The mitochondrial manganese-superoxide dismutase was substantially decreased in these mice.[74] Analysis of the brains of CJD patients and scrapie-infected Syrian hamsters revealed elevated levels of products of oxidation, lipoxidation, and glycoxidation.[75] However, the administration of one or a few antioxidants to address the problem of neurodegeneration would be naïve and several clinical studies had shown limited benefits with this approach.[76] In view of the multifactorial nature of neurodegenerative diseases and the fact that cells can often exploit the redundancy of the system to compensate for a protein whose activity was moderated by a drug, Melchiorre and co-workers proposed

multi-targeting drugs against neurodegenerative disorders instead of the current practice of deploying "one-molecule, one-target"-type of therapeutics.[77]

1.3.3 Prion diseases and other protein misfolding conditions

Prion diseases share similar underlying pathogenic conditions with other neurodegenerative diseases like Alzheimer's, Huntington's, Parkinson's diseases, Lewy Body dementia. The underlying pathogenesis is the conversion of a soluble protein into an insoluble isoform, leading to an accumulation of abnormal protein mass[78]. In Huntington's disease, fragments of the Huntingtin proteins aggregate to form toxic inclusion bodies within brain cells.[79] The hallmark in Parkinson's disease and Lewy Body dementia is an abnormal accumulation of the α-synuclein protein bound to ubiquitin forming Lewy bodies. In Alzheimer's disease, normal soluble amyloid-β peptide (sAβ) is converted to Aβ plaques, forming neuritic plaques. In prion diseases, the central event is conversion of soluble cellular prion protein (PrP^C) to insoluble scrapie prion protein (PrP^{Sc}). Both Aβ and PrP^{Sc} are rich in β-sheet content. Common early neurologic symptoms are memory loss, speech impairment, jerky movements, balance and coordination dysfunction. These diseases are all caused by formation of insoluble misfolded proteins. All of these disorders except prion diseases are not infectious.[78]

There are evidences of interconnection between AD and prion pathologies. AD and CJD share a common spatial pattern of protein deposition.[80] Recently, there are fresh findings that link PrP^C to the culprit of Alzheimer's disease, amyloid-β (Aβ) peptides. Aβ-positive senile plaques in AD brains commonly contain PrP deposit[81] while they are also identified in brains of CJD and GSS patients.[82] Lauren *et al.*[83] have found out that

PrP^C has greater affinity for Aβ oligomers than for monomeric and non-toxic Aβ. Aβ oligomers inhibit long-term potentiation, which is a measure of synaptic plasticity related to learning and memory, in hippocampal slices from normal mice, but not in slices from mice lacking PrP^C.[83] Thus PrP^C seems to be a main receptor for Aβ oligomers and mediates synaptic dysfunction. On the other hand, Pera *et al.*[84] showed that AChE, well-known for triggering amyloid plaques formation in Alzheimer's disease, also accelerated the fibrillization of amyloid plaques in brains of patients with GSS. In contrast, PrP^C was reported to promote β-amyloid plaque formation in mice.[81]

1.3.4. The antiprion activity of quinacrine and other acridine derivatives

Quinacrine is a potent antiprion compound in cell culture models of prion disease[85,86] but failed to demonstrate efficacy in infected animals[9,87,88] and human clinical trials.[89] Besides quinacrine, other acridines have been explored for antiprion activity. May and co-workers[90] found bis-acridines like compound A (Figure 1.8) to have more potent *in vitro* antiprion activity than quinacrine. Csuk *et al.* found that replacing the 2-methoxy-6-chloro substituents on the two acridine rings with 3-nitro-5-methoxy improved antiprion activity.[91] Klingenstein and co-workers[13] observed the synergistic antiprion effects of quinacrine and iminodibenzyl-derived antidepressants, and this led to the synthesis of potent hybrid molecules like quinpramine (corresponding to fused quinacrine and imipramine moieties) and compound B (EC$_{50}$ of 20 nM in cell based assay).[92] Investigations into the structure-activity relationships of quinacrine showed that antiprion activity was influenced by several structural features, namely, the length of the alkyl linker attached to the 9-amino functionality, the groups attached to the distal tertiary

amino group of the alkyl side chain and the substitution pattern on the acridine ring.[42,93] The latter feature was also identified as an important determinant of cellular cytotoxicity. For example, 3-fluoro-6-methoxy-4-methyl groups were associated with greater cytotoxicity than 2-methoxy-6-chloro groups on the acridine ring of quinacrine.[93] Cope and co-workers synthesized several substituted N-phenylacridin-9-amines and found electron withdrawing groups on the N-phenyl ring to be particularly favorable for activity. The most promising compound in their series (Compound C, Figure 1.8) had an EC$_{50}$ of 1.0-2.5 μM on the scrapie mouse brain (SMB) cell model.[94]

Compound A

Compound B

Quinpramine
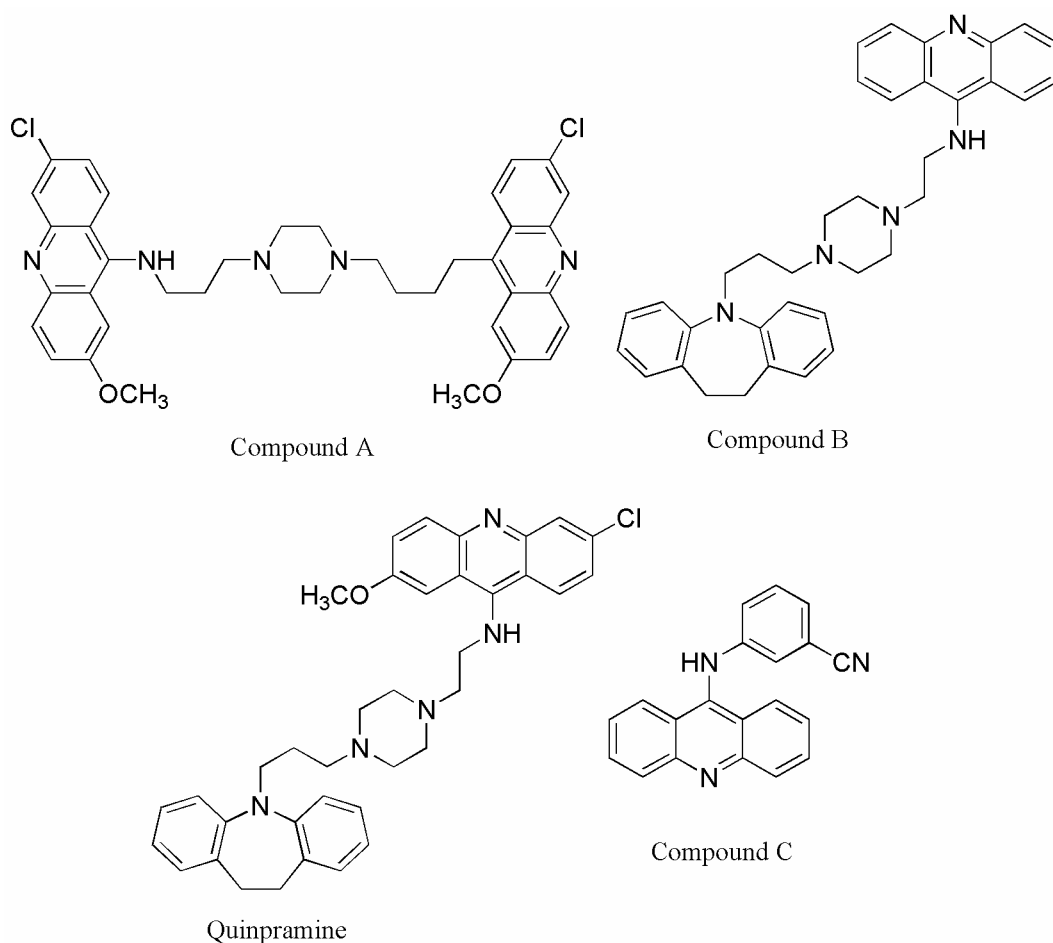
Compound C

Figure 1.8: Structures of some antiprion acridines: compound A : 6-chloro-N-(3-{4-[4-(6-chloro-2-methoxyacridin-9-yl)butyl]   piperazin-1-yl}propyl)-2-methoxyacridin-9-amine,

compound B :5-(3-{4-[2-(acridin-9-ylamino)ethyl]piperazin-1-yl}propyl)-10,11-dihydro-5H-dibenzo[b,f]azepine, compound C :3-(acridin-9-ylamino)benzonitrile, quinpramine : 5-(3-{4-[2-(6-chloro-2-methoxyacridin-9-ylamino)ethyl]   piperazin-1-yl}propyl)-10,11-dihydro-5H-dibenzo[b,f]azepine.

Pharmacokinetic factors have often been cited for the failure of quinacrine therapy in prion infected animals and human subjects.[95,96] The insufficient accumulation of quinacrine in the infected brain was attributed to its active efflux by ABCB1 (p-glycoprotein)[95] which is found in the blood brain barrier and widely linked to multidrug resistance.[97,98] Indeed, it was shown that when administered orally to mice that had *mdr* genes deleted (MDR$^{o/o}$), brain levels of quinacrine exceeded 100 μM.[99] Despite this high concentration in the brain, it still failed to extend the survival times of prion inoculated MDR$^{o/o}$ mice.[99] These results suggested that the failure of quinacrine *in vivo* was not solely due to its pharmacokinetic properties. The authors proposed that chronic quinacrine treatment eliminated a specific subset of PrP^{Sc} conformers, resulting in the survival of drug-resistant prion conformations that could not be removed by continued drug treatment.[99] Interestingly, the quinacrine-resistant conformers could not propagate in the absence of quinacrine and thus should not be considered as a stably propagating strain. The formation of quinacrine-resistant prions was evident only in cells that were not actively dividing, possibly because the probability of a partially resistant conformation surviving drug treatment would be increased in quiescent but not actively dividing cells. If this was the case, then screening for antiprion compounds in quiescent

cells rather would offer a better chance of identifying compounds that were effective *in vivo*.[99]

The suggestion that continuous quinacrine treatment is associated with the emergence of drug-resistant prions should not diminish interest in the antiprion potential of quinacrine/acridine analogs. It should be noted that drug-resistant prions emerged only on chronic dosing of quinacrine (40 mg/kg/day) for up to 60 days (given at 10-day intervals). The fact that untreated control mice could tolerate this regimen confirmed the remarkable safety profile of quinacrine, a property that may be shared by other structurally-related acridine analogs. It results in the need of compounds that combine greater antiprion potency with a better pharmacokinetic profile than quinacrine, which would make high dosing regimens unnecessary and possibly diminish the probability of resistance. In due course, the co-administration of multiple antiprion compounds may be a necessary step to keep resistance at bay.

The mechanism of action of quinacrine in prion disease remains unknown. A direct interaction with PrP^C was unlikely as demonstrated from investigations employing surface plasmon resonance[100] and NMR spectroscopy.[101] Phuan *et al.* suggested that the 9-aminoacridines like quinacrine bind to PrP^{Sc} and inhibited its replication by occluding necessary epitopes for templating PrP^C conversion or by altering the stability of PrP^{Sc} oligomers.[102] A site on PrP^C (alpha helix 2) located near the "protein X" epitope, a hypothetical factor that participates in the conformational transformation of cellular prion proteins (PrP^C) into the scrapie form was proposed based on NMR spectroscopy.[103] Turnbull *et al.*[104] proposed that quinacrine was an antioxidant and that this property was

linked to the ability of quinacrine to reduce the toxicity of the prion peptide PrP106-126 which shared several similarities to PrP^{Sc}.

1.4. Statement of purpose

The acridine template is a privileged scaffold that is associated with antimicrobial, anticancer and neuroprotective activities. The objective of this thesis was to investigate functionalized aminoacridines for their activity against prion diseases, a class of protein misfolding disorders associated with severe neurodegeneration and death. Quinacrine is the prototype aminoacridine derivative that has been widely investigated for its antiprion properties. Not withstanding its limitations as a CNS targeting agent for prion disease (Pgp substrate, moderate potency, poor *in vivo* properties, likelihood of resistance), the literature has shown that it is a fruitful lead structure which on structural modification had yielded promising analogues with improved antiprion potencies. The bis-acridine (Compound A) and the quinacrine-imipramine hybrid molecules quinpramine and compound B are examples (Figure 1.8). Despite their improved potencies, the limited follow up on the antiprion activities of these compounds in the literature did not bode well. A likely deterrent to clinical application may be the accessibility of these agents to the brain which is the site of action of antiprion agents. The above mentioned compounds had molecular weights that exceeded 500D (quinacrine 399D), lipophilicities (estimated by ClogP) that were greater than that of quinacrine and with more hydrogen (H) bond donor and acceptor atoms. These features would deter penetration across the blood brain barrier.[105] It is proposed that a more profitable approach would be to focus on smaller and less lipophilic mono-acridines and to carry out modifications that would not lead to overt

increases in size, lipophilicity and H bonding ability as these features would disqualify the resulting compound from further pharmaceutical development. To examine this proposal, modifications were made to (i) the side chain at the 9-amino position and (ii) the acridine ring, namely to replace it with the bicyclic quinoline and the partially reduced tetrahydroacridine template. The objective was to establish how these modifications affected antiprion activity and access across the blood brain barrier.

There is broad agreement in the scientific community that the multi-factorial nature of neurodegenerative disorders would benefit from a multi-target therapeutic approach and that structural scaffolds with this property would be valuable starting templates for drug design. Thus, a related aspect of this thesis was to investigate the ability of the synthesized acridine derivatives to exert neuroprotective activity. Here the ability to protect against glutamate-induced oxytosis (a process that depletes cells of glutathione, the major intracellular antioxidant) and inhibit acetylcholinesterase activity (a recognized target for cognitive and movement disorders) would be explored. The purpose was to establish the potential of the aminoacridine analogs to act on one or more targets linked to neurodegenerative conditions.

To achieve these objectives, the following work was planned:

(i)   Design and synthesize acridine analogues based on the lead compounds reported in literature, e.g. quinacrine and tacrine, with the aim to fulfill the structure-activity relationships for the three biological activities including antiprion, neuroprotective, and anticholinesterase activities (Chapter 2).

(ii)   Screen compounds for antiprion activities using several cell lines infected with different prion strains and investigate compounds' effects on expression of total

PrP^C and cell surface PrP^C levels as well as their binding affinities to PrP^C using surface plasmon resonance. The blood brain barrier permeabilities of these compounds were also investigated in a cell free system as well as a cell-based assay. (Chapter 3).

(iii)   Screen compounds for neuroprotective activity using a murine hippocampal cells challenged with a high concentration of glutamate to induce oxytosis. Mechanisms of action of these compounds investigated include ROS scavenging, inhibition of calcium influx, and effect on glutathione synthesis (Chapter 4).

(iv)   Screen compounds for acetylcholinesterase and butyrylcholinesterase inhibition and investigate binding poses of these compounds with the two above enzymes using molecular docking simulation. (Chapter 5).

Chapter 2: Design and synthesis of 9-aminoacridine analogs

2.1 Introduction

The design and synthesis of target compounds evaluated for antiprion and neuroprotective activities are described in this chapter. The compounds were structurally related to quinacrine (Figure 2.1) and were assigned to 7 groups based on their structural features. A search on the SciFinder Scholar (March 2010) showed that 29 of the 60 target compounds were novel. Some of the compounds presented in this chapter were synthesized by other members of the laboratory. Compounds **1-6**, and **9** were prepared by Dr Lee Chong Yew; compounds **8**, **10**, **11,** and **46** by Dr Liu Jianchao; compound **48** by Ms Yap Peiling.
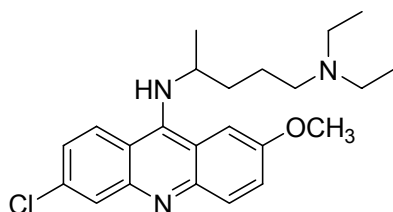
Figure 2.1. Structure of quinacrine.

Compounds were designed at two stages. The first batch included compounds **1-16**, **32**, **44**, **46-48**. Inspired by their antiprion actitivies and neuroprotective activity, the rest of the compounds were designed to further explore the potential of emerging templates.

2.2 Design Approach

In keeping with the design approach which was based on quinacrine as the lead structure, nearly ¾ of the compounds retained the 2-methoxy-6-chloro-9-aminoacridinyl

motif of quinacrine. Variations were made to the side chain attached to the 9-amino functionality.

2.2.1. Group 1

Table 2.1: Structures of compounds in Group 1
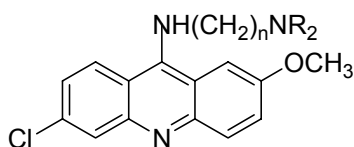
Compound	Substituent (R)
1[#]	n=2, R=C_2H_5
2[#]	n=3, R=CH_3
3[#]	n=3, R=C_2H_5
4[#]	n=4, R=C_2H_5

The compounds in Group 1 (**1-4**) retained the dialkylaminoalkyl side chain of quinacrine (Table 2.1). The alkyl chain separating the two nitrogen atoms varied from 2 to 4 carbon atoms and the substitution state of the distal tertiary nitrogen was similar to quinacrine (N,N-diethylamino), except for **3** where it was N,N-dimethylamino. A notable modification was the absence of branching in the side chain of Group 1 compounds, unlike quinacrine. Hence, the compounds were achiral in contrast to quinacrine which is chiral. It was reported that the *(S)*-quinacrine had more *in vitro* antiprion activity than *(R)*-quinacrine.[106] No stereoselectivity was reported for the antimalarial activity of quinacrine.[107] The decision to synthesize Group 1 compounds without the chiral centre was based on the following reasons: (i) to facilitate synthesis and purification; (ii) to investigate the importance of a chiral side chain for antiprion activity.

[#] Compound was synthesized by other lab members.

2.2.2. Group 2

An aliphatic side chain attached to the 9-amino group of the 9-aminoacridine template was reported to be essential for the inhibition of PrP^C to PrP^{Sc} conversion.[108] Less is known of how an aromatic or heterocyclic ring at this position would affect activity. For this reason, a series of functionalized 9-N-phenylaminoacridines (Group 2, Table 2.2) and 9-N-(4-piperidinyl)aminoacridines (Group 3, Table 2.3) were prepared. The first batch of compounds that were synthesized and evaluated was those that had basic functionalities attached to the phenyl ring (**5-16**). Only tertiary amines (dimethylamino, diethylamino, various heterocyclic amines like pyrrolidine, piperidine, morpholine, 4-methylpiperazine) attached (mostly) to the meta (3') and para (4') positions of the aromatic ring were examined, in part to mimic the distal tertiary amino function of quinacrine. The analog with the 4'-(4-methylpiperazin-1-yl) side chain (**16**) was found to possess promising *in vitro* antiprion activity and this prompted further structural variation of the 4-methylpiperazinyl moiety. These variations were (i) replacing the methyl group with its ethyl homolog (**17**) and the more hydrophilic 3-hydroxypropyl sidechain (**18**), (ii) converting the distal basic nitrogen of piperazine into a non-basic amide by attaching a methylcarbonyl (**19**), cyclohexylcarbonyl (**20**) or phenylcarbonyl (**21**) moiety, and (iii) inserting an additional methylene (**22**) or carbonyl (**20**) group between the phenyl and piperazine rings. A piperidyl analogue of **22** was also prepared (**24**). A small number of compounds (**25-31**) in Group 2 have non-basic groups (H, OCH_3, OH, F, CN) on the phenyl ring. These compounds were not evaluated for antiprion activity but were tested for neuroprotective and antioxidant properties. The substituents were selected to ensure adequate coverage of Hansch σ (electron donating /

withdrawing) and Hammett π (lipophilicity) values as guided by the Craig Plot.[109] Mono

and dihydroxy substituents (**30, 31**) are included in view of their free radical quenching

potential.
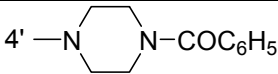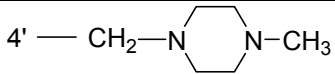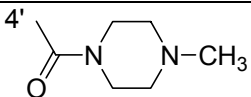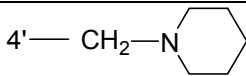
Table 2.2: Structures of compounds in Group 2

Compound	Substituent (R)	Compound	Substituent (R)
5[#]	2'-$N(CH_3)_2$	6[#]	3'-$N(CH_3)_2$
7	4'-$N(CH_3)_2$	8[#]	3'-$N(C_2H_5)_2$
9[#]	4'-$N(C_2H_5)_2$	10[#]	3' —N (pyrrolidine)
11[#]	3' —N (piperidine)	12	4' —N (piperidine)
13	3' —N O (morpholine)	14	4' —N O (morpholine)
15	3' —N N—CH_3	16	4' —N N—CH_3
17[*]	4' —N N—CH_2CH_3	18[*]	4' —N N—$CH_2CH_2CH_2OH$
19[*]	4' —N N—$COCH_3$	20[*]	4' —N N—COC_6H_{11}

[#] Compound was synthesized by other lab members.
[*] Novel compound

21[*]	4' —N⟨ ⟩N—COC₆H₅	22[*]	4' — CH₂—N⟨ ⟩N—CH₃
23[*]	4' —C(O)—N⟨ ⟩N—CH₃	24[*]	4' — CH₂—N⟨ ⟩
25	H	26	4'-CN
27[*]	4'-F	28[*]	3',4'-diF
29	4'-OCH₃	30[*]	3'-OH
31[*]	3',4'-diOH		

2.2.3. Group 3

The Group 3 compounds had an N-substituted piperidine attached to the 9-amino group. The first compound to be synthesized was **32** which had a N-(1-benzylpiperidin-4-yl) sidechain. **32** was found to have outstanding in vitro antiprion activity and this prompted further variation of the benzyl side chain to give the other compounds (**33-41**) in Group 3. The variations included: (i) preparing homologs of the benzyl ring (n=1 to n=3) and (ii) introducing representative groups with different Hansch σ and Hammett π values on the phenyl ring. Attention is drawn to compounds **24** and **32** which differed in the positioning of the phenyl and piperidine rings on the side chain.

---

[*] Novel compound

Table 2.3: Structures of compounds in Group 3
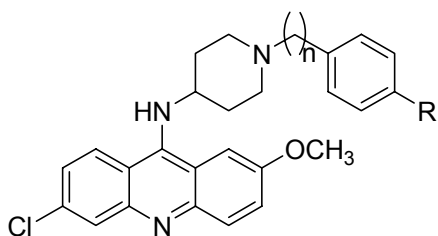
Compound	Substituent
32	n=1, R=H
33*	n=1, R=CH₃
34*	n=1, R=Cl
35*	n=1, R=OCH₃
36*	n=1, R=CN
37*	n=2, R=H
38*	n=2, R=CH₃
39*	n=2, R=Cl
40*	n=2, R=OCH₃
41*	n=3, R=H

2.2.4. Group 4

Group 4 comprise miscellaneous compounds that were synthesized to address specific structure-activity relationship (SAR) issues (Table 2.4). To determine the importance of the N-substituted secondary amino function at position 9 of the acridine ring, compounds **44-46** were proposed. **44** was a common intermediate in the synthesis of Group 1 and 2 compounds and had a phenoxy group in place of the amino functionality. To assess the importance of a secondary amino function at position 9, **46** (primary amino) and **45** (tertiary amino) were synthesized. The remaining two compounds (**42, 43**) were structurally related to **16** and **32** respectively. In **42**, the phenyl ring was replaced by butenyl-2,3, a moiety often considered as an aromatic ring equivalent because it is

electron rich, can participate in π-π stacking interactions and is structurally constrained like the aromatic ring.[110] **43** and **32** were structurally related in that the flexible piperidine ring of **32** was replaced by the conformationally more rigid 8-azabicyclo[3.2.1]oct-8-yl ring. With two additional methylene groups, **43** is also bulkier and more lipophilic than **32**.

Table 2.4: Structures of compounds in Group 4
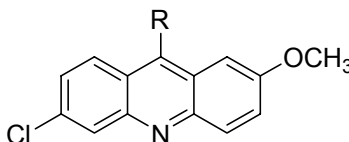
Compound	Substituent (R)	Compound	Substituent (R)
42[*]		43[*]	
44	OPh	45[*]	
46[#]	NH₂		

2.2.5. Group 5

To evaluate the importance of the 2-methoxy and 6-chloro substituents on the acridine template, compounds without these two substituents were synthesized (Table 2.5) Only two compounds (**47, 48**) were synthesized in this Group in spite of several attempts to prepare more analogs.[85] This template appears to have limited stability.[111]
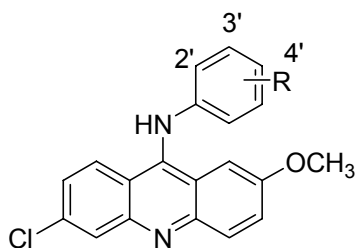
---

[*] Novel compound
[#] Compound was synthesized by other lab members.

Table 2.5: Structures of compounds in Group 5
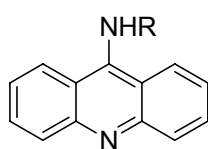
Compound	Substituent (R)
47[+]	H
48[#]	

2.2.6. Groups 6 and 7

In Groups 6 and 7, the acridine ring was replaced by 3-chloro-5,6,7,8-tetrahydroacridine and 7-chloroquinoline respectively (Tables 2.6 and 2.7). The tetrahydroacridine ring is less planar than acridine but just as lipophilic while the quinoline ring will be as planar but less bulky compared to acridine. These ring structures may have diminished DNA-intercalating properties. Like the compounds in the other groups, the 9-amino (of Group 6) and 4-amino (of Group 7) were substituted with representative aliphatic, phenyl and piperidine side chains. Notable inclusions were the N-[4'-(4-methylpiperazin-1-yl)phenyl and N- (1-benzylpiperidin-4-yl) side chains found in the promising compounds **16** and **32** respectively.

Table 2.6: Structures of compounds in group 6
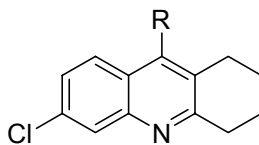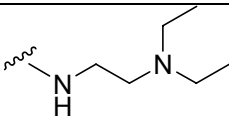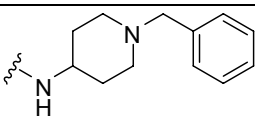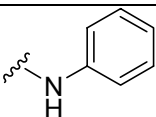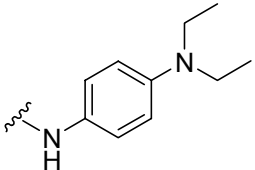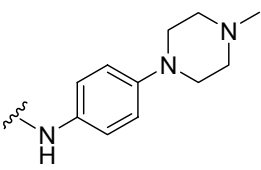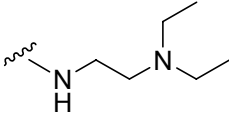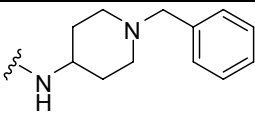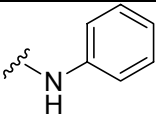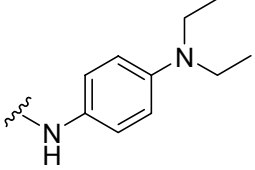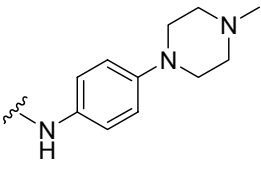
Compound	Substituent (R)	Compound	Substituent (R)
49	NH$_2$	50[*]	
51[*]		52	
53[*]		54[*]	

Table 2.7: Structures of compounds in group 7
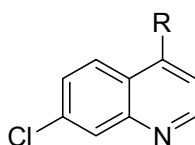
Compound	Substituent (R)	Compound	Substituent (R)
55	NH$_2$	56	
57		58	
59[*]		60	

2.3. Chemical Considerations

---

[*] Novel compound

2.3.1. N-substituted 9-aminoacridines

As most of the compounds synthesized in this thesis were 9-aminoacridines, the physicochemical properties and reactivities of this structure are briefly discussed in this section. 9-Aminoacridine is a stronger base (pK$_a$ *ca* 10) than acridine (pK$_a$ *ca* 5).[112] In the present series of compounds, the 9-aminoacridine ring was substituted with 2-methoxy (electron donating) and 6-chloro (electron withdrawing) groups. These groups were not expected to alter the basicity of the aminoacridine ring significantly.
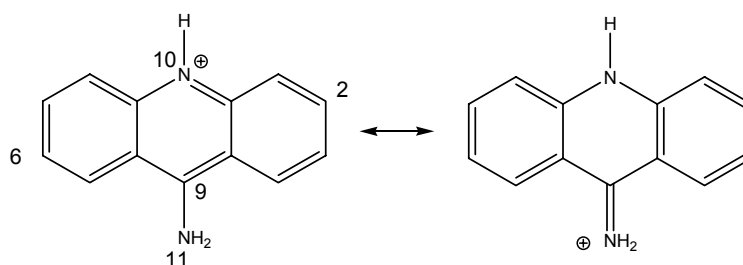
Figure 2.2: Canonical structures of 9-aminoacridine.

In the aromatic 9-aminoacridine system, the attached amino group is sp^2-hybridized, and in conjugation with the ring nitrogen (Figure 2.2). This renders the ring nitrogen basic, and protonation occurs preferentially at this site. However, when bulky groups are attached to the amine nitrogen, these force the N atom out of coplanarity, and disrupt the conjugation. When this happened, the 9-amino group would be susceptible to displacement by nucleophiles, like water (Figure 2.3).[112]
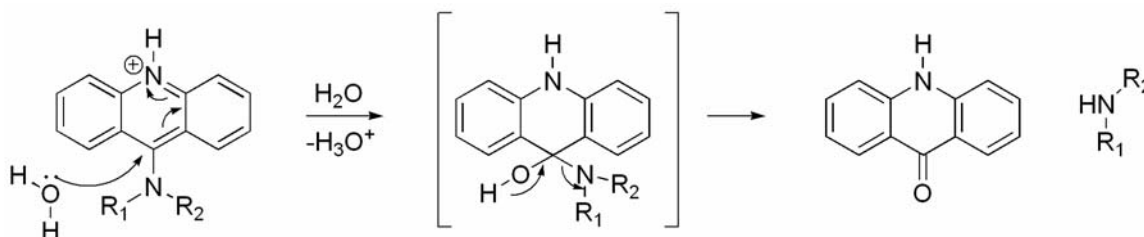
Figure 2.3: Formation of 9-acridone due to nucleophilic attack by water on the 9-substituted amino acridine (R$_1$ and R$_2$ are bulky groups).

Goodell and co-workers investigated the effect of steric bulk at the 9-substituted amino group on the rate of hydrolysis of the resulting compound.[111] Their findings are summarized as follows:

(i) 9-Aminoacridines with dimethylaminoethyl or dimethylaminopropyl side chains attached to the 9-amino group were susceptible to hydrolysis at a pH that was close to the pK_a value of the distal tertiary amino groups (*ca* 8-10) and higher. At acidic pH, the compounds were stable because the distal tertiary amino group was protonated and assumed an extended conformation to minimize charge repulsion with the positively charged 9-amino group. In contrast, at higher pH, more of the non-protonated side chain was present and intramolecular H bonding occurred (Figure 2.4). As a result, steric bulk at the vicinity of the 9-amino group was increased, co-planarity was compromised and hydrolysis was accelerated. This finding is relevant to the Group 1 compounds and serves to highlight the importance of avoiding high pH values (>7.5) when evaluating biological activity.
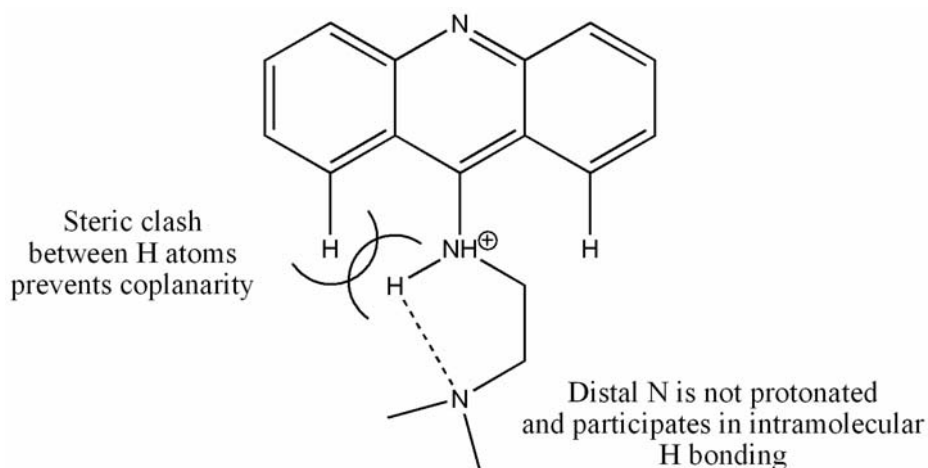
Figure 2.4: Illustration of the proposed intramolecular hydrogen bond in Group 1 compounds.

(ii) The 9-aminoacridine with a benzylpiperidinyl side chain (like **32** in Group 3) was found to be remarkably stable over pH 5-10. The inflexibility of the side chain would make intramolecular H bonding highly improbable. Thus there is minimal steric bulk at the 9-amino group and this permits electron delocalization to occur unimpeded.

(iii) The 9-aminoacridine with an N-(4-methylpiperazin-1-yl) side chain (Figure 2.5) was found to be unstable over the pH range of 5-10. The added constraint of the piperazine ring is likely to force the ring out of plane, resulting in hydrolysis at C9-N bond.
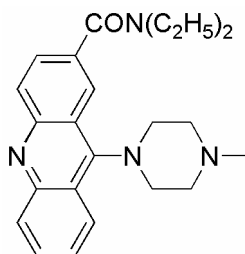
Figure 2.5 : 9-aminoacridine analog with N-(4-methylpiperazin-1-yl) side chain.[111]

9-Aminoacridines have been reported to undergo partial amine exchange reactions in organic solvents.[113] The mechanism of reaction was proposed to proceed reversibly via formation of a 9,9-diaminoacridine hemiaminal intermediate (Scheme 2.1).
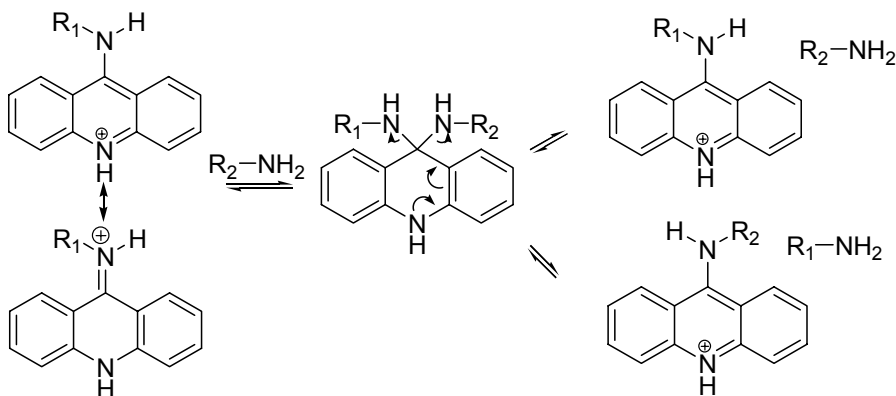
Scheme 2.1: Proposed mechanism for reversible amine exchange reaction on 9-aminoacridine.[113]

This reaction was influenced by the strength of the C9-N11 bond. Thus, as steric interactions around the C9 position increased, the C9-N11 bond was weakened making it susceptible to amine displacement. The occurrence of amine exchange was unlikely to pose as a complicating factor in the synthetic reactions explored in this report because only one amine was present at any one time in the reaction mixture. However, the likelihood of displacement of the 9-substituted amino function of the functionalized acridine under physiological conditions should not be discounted. Paul and Ladame[113] proposed that the telomerase inhibitor BRACO-19 participated in an amine exchange reaction *in vivo* and that this may have implications on its mode of action.

2.3.2. General approach to the synthesis of the 9-aminoacridines of Group 1-5.

The Group 1-5 aminoacridines were synthesized by reacting 6,9-dichloro-2-methoxyacridine or 6-chloroacridine (in the case of Group 5) with the corresponding amine in the presence of catalytic HCl in ethanol as solvent (Scheme 2.2)[43,114] or via the formation of phenoxy intermediates (Scheme 2.3).[43,92]
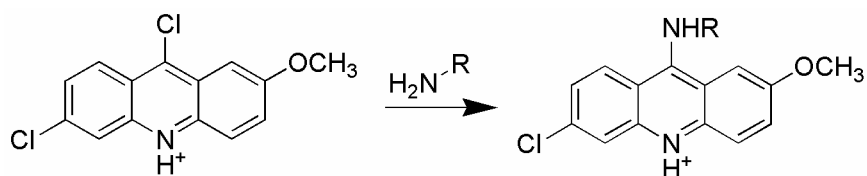
Scheme 2.2: Ethanol, cat. HCl, reflux, 24 hours.
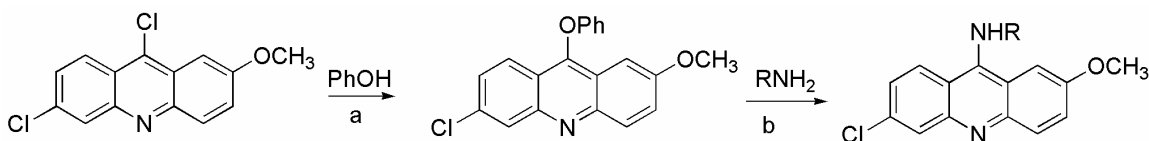
Scheme 2.3: a) 1h, 100°C b) 4-5 h, 100°C.

In both instances, the mechanism of reaction involved the displacement of the 9-chloro atom by the nucleophilic amine or phenol. The C9-Cl was selectively displaced in preference to the C6-Cl because of its proximity to the electron withdrawing N of the ring and the stability of the resulting intermediate. When the reaction was carried out in presence of HCl/ethanol, the acridine N was protonated and this served to further increase the electrophilicity of C9 (Figure 2.5). However, the attacking amine would also be protonated and hence, a weaker nucleophile.
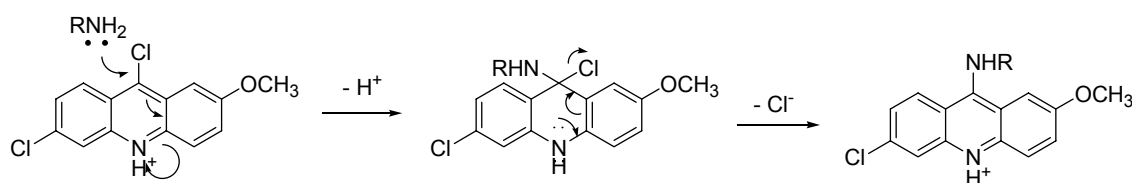
Figure 2.5: Nucleophilic substitution of 9-Cl by amine.

When the reaction was carried out in phenol as solvent, a phenoxide intermediate was formed *in situ* and subsequently displaced by the reacting amine.[111] As the reaction was not carried out under acidic conditions, C9 would be activated by the non-protonated acridine N (weaker electron withdrawing effect compared to its protonated state) but the attacking amine would be more nucleophilic because of the larger number of non-protonated species. As a leaving group, the phenol was more readily displaced than chloride (Figure 2.5) by the attacking amine. The formation of acridones as a byproduct of hydrolysis of 9-chloroacridines was also minimized.[88] The phenoxide intermediate 44 was isolated and characterized (Appendix 1).
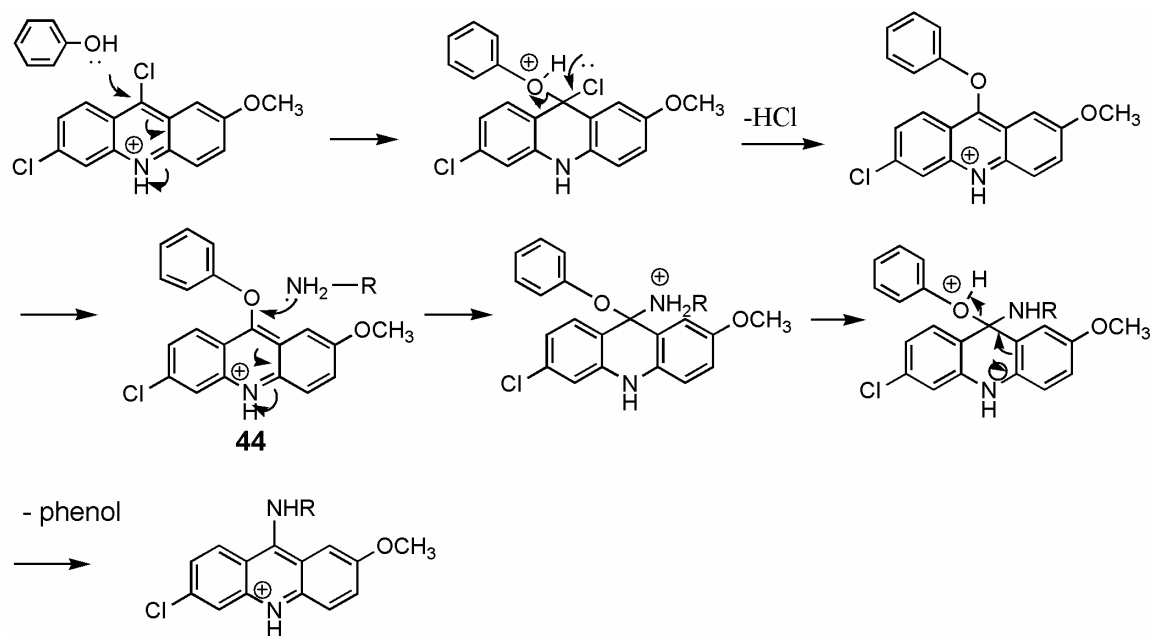
Scheme 2.4: Nucleophilic substitution of 9-Cl to give phenoxide **44**, followed by displacement of phenol by amines.

It was generally found that both approaches gave comparable yields but workup procedures were more favorable when ethanol was used as solvent. In cases where yields in ethanol were unsatisfactory, the reaction was repeated in phenol. Most of the amines involved in the condensation reactions were purchased. However there were some amines that were not commercially available and these were synthesized as described in the following sections.

2.3.3. Synthesis of substituted anilines for Groups 2, 6, and 7 by Hartwig-Buchwald amination reaction

3-Morpholinoaniline, 3-(4-methylpiperazin-1-yl)aniline, 4-(4-methylpiperazin-1-yl)aniline, 4-(4-ethylpiperazin-1-yl)aniline, 3-[4-(4-aminophenyl)piperazin-1-yl] propan-

1-ol, 1-(4-(4-aminophenyl)piperazin-1-yl)ethanone, (4-(4-aminophenyl)piperazin-1-yl)(cyclohexyl)methanone and [4-(4-aminophenyl)piperazin-1-yl]phenylmethanone were required for the synthesis of **12-21** in Group 2 and **54, 60** in Groups 6 and 7. These amines were synthesized by the Hartwig-Buchwald amination of iodobenzene by a palladium coupling reaction, followed by catalytic reduction of the aromatic nitro group to give the aniline (Scheme 2.5).
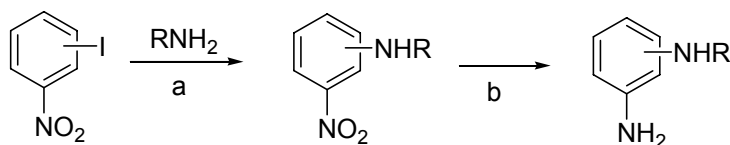
Scheme 2.5: a) Pd(OAc)$_2$, BINAP, Cs$_2$CO$_3$, anhydrous toluene, 120°C b) H$_2$, Pd/C.

The mechanism of the Buchwald-Hartwig reaction [89, 90] is illustrated in Figure 2.6. The Pd/BINAP catalyst system was used to establish the C-N bond. BINAP (*rac*-2,2'-bis(diphenylphosphino)-1,1'-binaphthyl) formed a complex with palladium diacetate Pd(II), [PdL$_2$](OAc)$_2$, which was possibly reduced by BINAP to the activated Pd(0) species PdL$_2$ which then lost one ligand to form PdL. Iodonitrobenzene (ArX) coordinated to palladium by oxidative addition to form an intermediate which was in equilibrium with its dimeric species. The iodine atom was displaced by the nitrogen atom of the attacking amine in the presence of cesium carbonate which functioned as a base to abstract a proton from the amine to form the intermediate PdL(Ar)NR$_2$. The latter underwent reductive amination to give the desired aryl amine. β-Hydride elimination could occur to give an arene and imine but this competing pathway was not found to be significant. Aryl amines were obtained with good yields (>90%). The Pd/BINAP catalyst was regenerated at the end of the cycle.
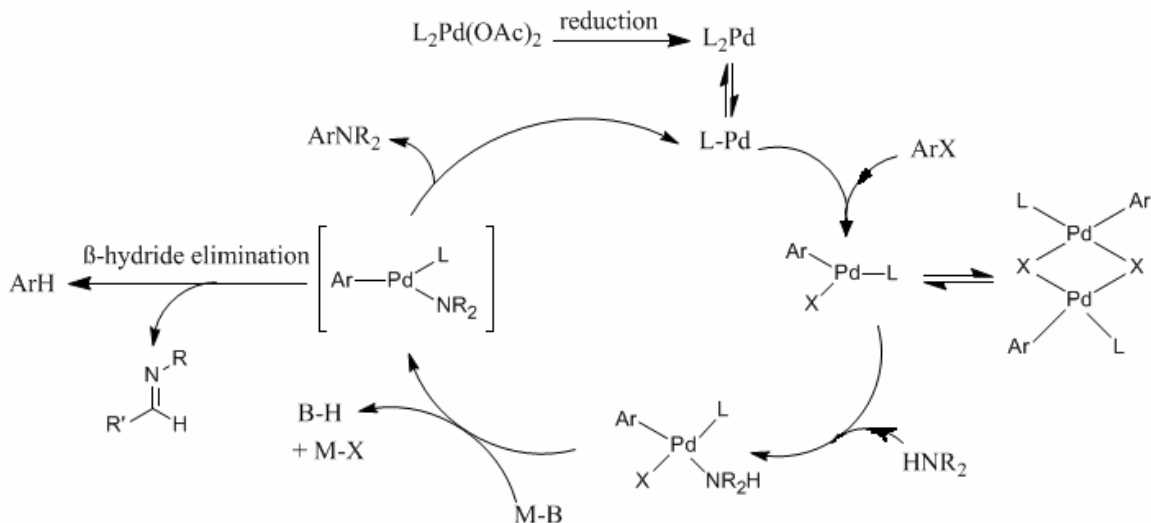
Figure 2.6: Mechanism of Buchwald-Hartwig amination[115] (X = iodine and L = BINAP).

2.3.4. Synthesis of N^1,N^1-dimethylbenzene-1,2-diamine

N^1,N^1-Dimethylbenzene-1,2-diamine was required for the synthesis of **5** in Group 2. It was synthesized by reacting 1-chloro-2-nitrobenzene with hexamethylphosphoramide (HMPA) to give the 1-dimethylamino-2-nitrobenzene. The aromatic nitro group was reduced by catalytic hydrogenation with palladium/charcoal to give the desired amine. (Scheme 2.6).
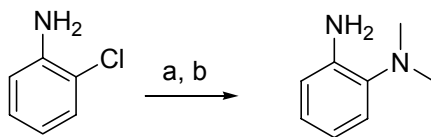
Scheme 2.6: a) HMPA 6eq, 150°C, 24h b) H_2, Pd/C, 12h

2.3.5. Synthesis of N^1,N^1-diethylbenzene-1,3-diamine

N^1,N^1-Diethylbenzene-1,3-diamine was required for **8** in Group 2. It was prepared from the acid hydrolysis of commercially available N-(3-diethylamino)phenylacetamide (Scheme 2.7).
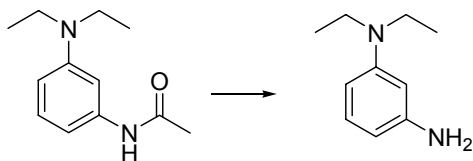
Scheme 2.7: conc. HCl, reflux 2h

2.3.6. Synthesis of 4-[(4-methylpiperazin-1-yl)methyl] aniline, 4-(piperidin-1-ylmethyl)aniline and (4-aminophenyl)(4-methylpiperazin-1-yl)methanone]

These amines were required for the synthesis of **22-24** (Group 2). The synthesis of 4-[(4-methylpiperazin-1-yl)methyl] aniline and 4-(piperidin-1-ylmethyl)aniline is shown in Scheme 2.8.

X= NCH$_3$ in **22**
= CH$_2$ in **24**
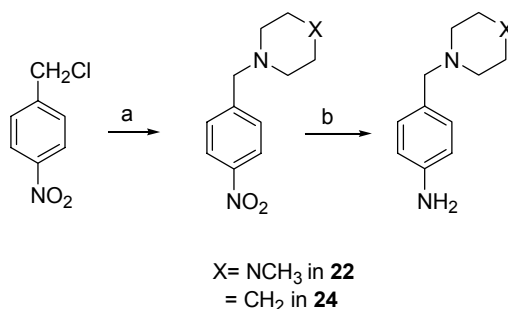
Scheme 2.8: a) Amine, TEA, THF, 70°C, 24h b) H$_2$, PtO$_2$, 50 psi, overnight.

Commercially available 1-(chloromethyl)-4-nitrobenzene was reacted with either 1-methylpiperazine or piperidine in the presence of triethylamine in tetrahydrofuran as solvent. The chloride ion was displaced by the nucleophilic secondary amine. Triethylamine was used to remove HCl released during the course of reaction. The aromatic nitro functionality was reduced to the amino by low pressure hydrogenation with Adam's catalyst. The latter was preferred to palladium/charcoal as it did not cause hydrogenolysis of the C-N bond.

A similar method was employed for the preparation of (4-aminophenyl)(4-methylpiperazin-1-yl)methanone (Scheme 2.9). Commercially available 4-nitrobenzoyl

chloride was stirred overnight (*ca* 12 h) with 1-methylpiperazine in dichloromethane at room temperature. The milder reaction conditions employed for this reaction was due to the greater susceptibility of the acid chloride to nucleophilic attack. The nitro group was reduced in the presence of hydrogen and palladium/charcoal as catalyst.
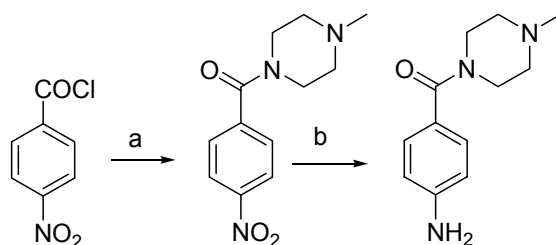
Scheme 2.9: a) 1-methylpiperazine, TEA, anhydrous DCM, rt, overnight b) H_2, Pd/C 10%, 50psi, overnight.

2.3.7 Synthesis of 1-benzyl-piperidin-4-ylamine, 1-phenethylpiperidin-4-ylamine, 1-(3-phenylpropyl)piperidin-4-ylamine and their ring substituted analogs.

n=1,2,3

R=H, CH_3, OCH_3, CN, Cl
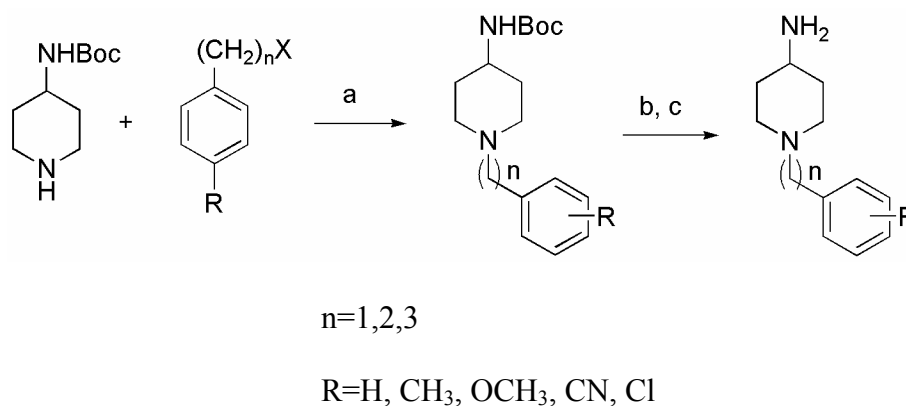
Scheme 2.10: a) TEA, THF, reflux, overnight b) TFA, DCM, rt c) aq. NaHCO_3

Scheme 2.10 outlines the reaction route for the synthesis of 1-benzyl-piperidin-4-ylamine, 1-phenethylpiperidin-4-ylamine, 1-(3-phenylpropyl)piperidin-4-ylamine and their ring substituted analogs. These amines were required for the synthesis of **33-41** (Group 3). *tert*-Butyl piperidin-4-ylcarbamate reacted with the phenylalkyl halide with

release of the hydrogen halide (HCl or HBr) which was removed by triethylamine. The protective *tert*-butoxycarbonyl (Boc) moiety was subsequently removed in the presence of trifluoroacetic acid to give the desired primary amine.

2.3.8. Synthesis of 4-chlorobenzylchloride

n=1 (for **34**) and 2 (for **39**)
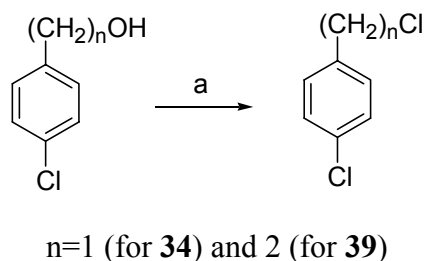
Scheme 2.11: a) SOCl$_2$, anhydrous DCM, rt, 1h.

4-Chlorobenzylchloride and 1-chloro-4-(2-chloroethyl)benzene were required for the synthesis of **34** and **39** respectively. They were prepared from the reaction of (4-chlorophenyl)methanol and 2-(4-chlorophenyl)ethanol with thionyl chloride (Scheme 2.11). Mechanistically, this was an S$_N$2 substitution reaction with thionyl chloride as the source of the nucleophilic chloride.

2.3.9. Synthesis of 4-(4-methyl-piperaziny-1-yl)-but-2-ynylamine
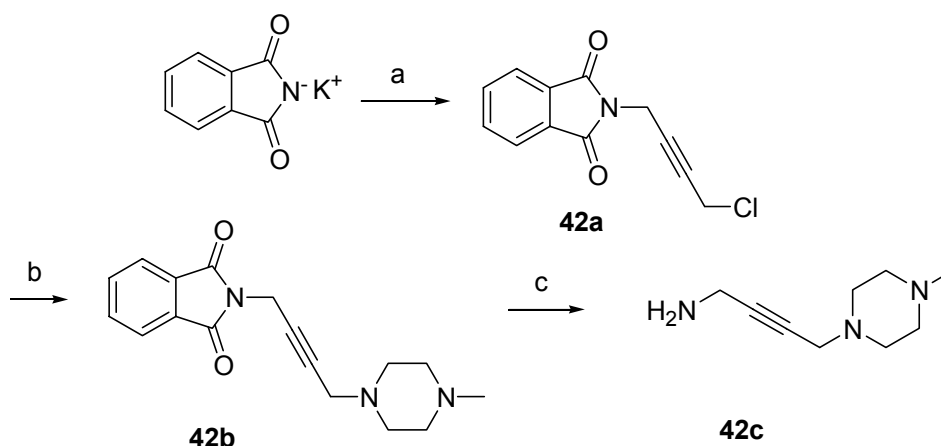
Scheme 2.12: a) 1,4-dichlorobut-2-yne, DMF, 100°C, 5h b) 1-methylpiperazine, TEA, DCM, rt, overnight c) NH$_2$NH$_2$, EtOH, reflux, 2h.

4-(4-Methyl-piperaziny-1-yl)-but-2-ynylamine was required for the synthesis of **42** (Group 4). It was prepared by the Gabriel synthesis which involved the reaction of 1,4-dichloro-2-butyne with potassium phthalimide (Scheme 2.12).[116] Excess 1,4-dichloro-2-butyne (2 equivalents) was employed to ensure that only the monosubstituted phthalimide (**42a**) was formed. The later was then reacted with 1-methylpiperazine in an S_N2 substitution reaction in which the terminal halide was displaced by the nucleophilic piperazinyl nitrogen to give **42b**. The phthalolyl group was then removed in the presence of hydrazine to give the desired amine (**42c**).

An alternative route to give **42c** was to react 1,4-dichloro-2-butyne with equivalent amounts of 1-methylpiperazine and ammonia in a stepwise manner (Scheme 2.13). However this approach gave **42c** in lower yields, mainly because both chloride atoms in 1,4-dichloro-2-butyne were displaced by 1-methylpiperazine.
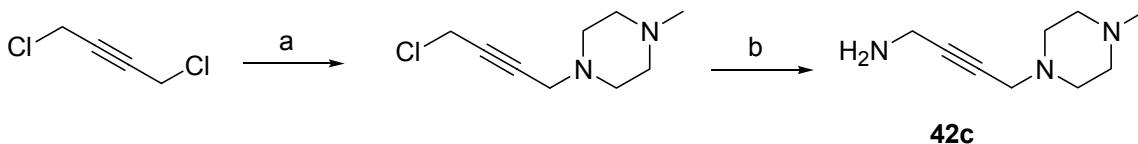
Scheme 2.13: a) 1-Methylpiperazine, TEA, DMF, heat b) NH_3, MeOH, sealed tube, heat.

2.3.10. Synthesis of 8-benzyl-8-aza-bicyclo[3.2.1]oct-3-ylamine
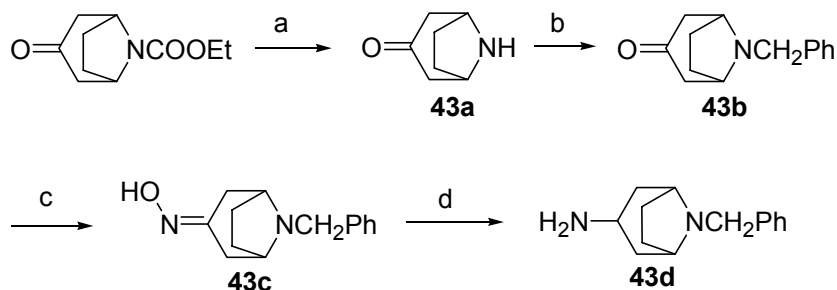
Scheme 2.14: a) KOH, water, THF, 80°C, 10h b) $PhCH_2Cl$, TEA, THF, reflux, overnight c) $NH_2OH.HCl$, MeOH, Na_2CO_3, rt, 4h d) H_2, PtO_2, 50psi, rt, overnight.

8-Benzyl-8-aza-bicyclo[3.2.1]oct-3-ylamine (**43d**) was required for the synthesis of **43** (Group 4). Its synthesis is shown in Scheme 2.14. Starting from the ethyl ester of 3-oxo-8-aza-bicyclo[3.2.1]octane-8-carboxylic acid, the ethoxycarbonyl group was removed by alkaline hydrolysis to give the secondary amine **43a**. The latter was reacted with benzyl chloride in an S_N2 type reaction to give 8-benzyl-8-aza-bicyclo[3.2.1]oct-3-one (**43b**). The ketone carbonyl was derivatized to give the oxime **43c** which was then reduced in the presence of Adam's catalyst (PtO_2) to give the desired amine **43d.**

2.3.11. Synthesis of the 3,9-dichloro-5,6,7,8-tetrahydroacridine
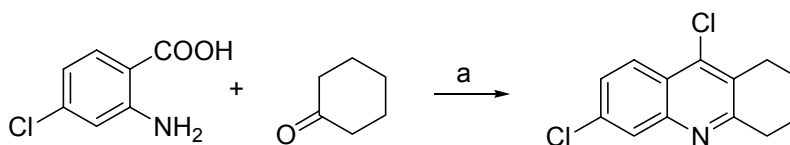
Scheme 2.15: a) $POCl_3$, reflux, 2h.

While the starting materials for the acridine (6,9-dichloro-2-methoxyacridine) and quinoline (4,7-dichloroquinoline) templates were commercially available, this was not the case for the tetrahydroacridine template. The starting material (3,9-dichloro-5,6,7,8-tetrahydroacridine) for the Group 6 compounds had to be synthesized and this was achieved by a three-step-one-pot reaction (Scheme 2.15).

2.3.12. Synthesis of 6-chloro-2-methoxyacridin-9-amine monohydrochloride (46)

Compound **46** was synthesized by reacting 6,9-dichloro-2-methoxyacridine with sodium methoxide in methanol. The 9-chloro group was displaced by methoxide to give 6-chloro-2,9-dimethoxyacridine. In the next step, 6-chloro-2,9-dimethoxyacridine was reacted with NH_4Cl to give the desired product (Scheme 2.16). However, this method did

not work for the synthesis of **49** and **55** which were prepared by displacing the chloro atoms of their respective starting materials with hydrazine, followed by reduction to give the desired amines **49** and **55** (Section 2.3.13).
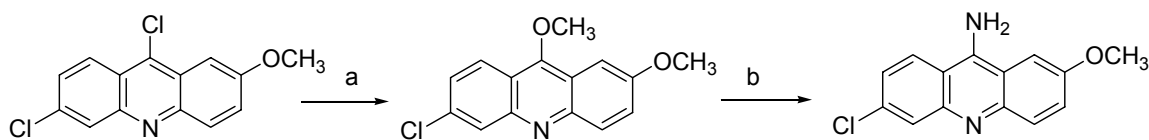
Scheme 2.16: a) CH$_3$ONa, MeOH, reflux, 2h b) NH$_4$Cl, MeOH, 70°C, 2h.

2.3.13. Synthesis of 6-chloro-1,2,3,4-tetrahydro-acridin-9-ylamine (49) and 7-chloroquinolin-4-amine (55)
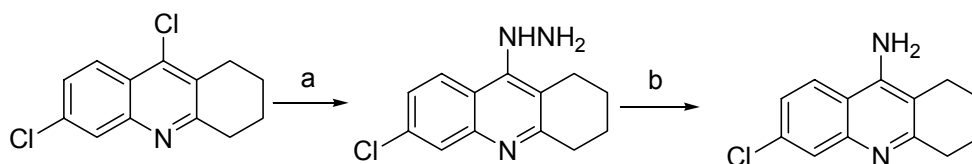
Scheme 2.17: a) NH$_2$NH$_2$.H$_2$O, mw, 150°C, 10min b) NiCl$_2$, NaBH$_4$, rt, 1h

6-chloro-1,2,3,4-tetrahydro-acridin-9-ylamine (**49**) was synthesized by reacting 6,9-dichloro-1,2,3,4-tetrahydro-acridine with hydrazine followed by reduction of the resulting hydrazide with nickel chloride and sodium borohydride to give the desired amine (Scheme 2.17).[117] The same method was used for the synthesis of **55** which was synthesized from 4,7-dichloroquinoline.

Another approach to **49** and **55** was to react 6,9-dichloro-1,2,3,4-tetrahydro-acridine or 4,7-dichloroquinoline with ammonia by heating (170°C) in a close reaction vessel at high pressure.[118] This method was not adopted because it involved the high pressure/temperature conditions.

2.4. Experimental methods

2.4.1 General experimental methods

^{1}H-NMR and ^{13}C-NMR spectra were recorded on a Bruker DPX 300MHz spectrometer and chemical shifts were reported in δ (ppm) relative to the internal standard TMS. Mass spectra (MS, nominal) were collected on a LCQ Finnigan MAT mass spectrometer. Atmospheric pressure ionization (APCI) or electron spray (ionization (ESI) were used as probes. Reactions were routinely monitored by thin layer chromatography using silica gel 60 F 254 plates from Merck, with UV light as a visualizing agent. Column chromatography was performed using silica gel G (0.04-0.063mm) from Merck. Solvents were of analytical grade or distilled from technical grade. All chemicals were purchased from Sigma Aldrich Chemical Company (MO, USA), Tokyo Chemical Industry (Tokyo, Japan), and Alfa Aesar (MA, USA). Purity analysis was verified by high pressure liquid chromatography (HPLC) or by combustion analysis. Combustion analyses (C, H) were determined by Perkin-Elmer PE 2400 CHN/CHNS elemental analyzer by the Department of Chemistry, National University of Singapore. Spectroscopic data, melting points, yields and purities of individual compounds are listed in Appendix 1.

2.4.2. General procedure for the reaction of 2-methoxy-6,9-dichloroacridine, 9-chloroacridine and 4,7-dichloroquinoline with amines in ethanol as solvent (GP1).

This method was applied to compounds **5-31**, **45**, **48**, **58-60**. The acridine or quinoline (2 mmol) and the amine (2 mmol) were dissolved in ethanol (30 to 50 ml) and 2 drops of concentrated HCl was added. The reaction mixture was refluxed until the

reaction was completed (*ca* 24h or when starting materials were not detected on TLC).

On cooling to room temperature, the workup process depended on the solubility of the

product in ethanol. For those compounds that were insoluble in ethanol, they were

precipitated from the reaction mixture by neutralizing with cold water and ammonia

solution (25%), followed by recrystallization with methanol. Compounds which were

soluble in ethanol were extracted with dichloromethane and brine after neutralization

with either ammonia solution (25%) or NaOH (1M). The crude product was subjected to

column chromatography (gradient elution from hexane: ethyl acetate (EA) 1:4 to EA

100% to EA :methanol: NH$_3$ 90:10:1) and recrystallized with methanol to afford the

desired compound.

2.4.3. General procedure for the reaction of 2-methoxy-6,9-dichloroacridine, 3,9-dichloro-5,6,7,8-tetrahydroacridine and 4,7-dichloroquinoline with amines in phenol as solvent (GP2).

This method was applied to compounds **1-4**. The acridine (1mmol) was added to

melted phenol (10mmol) and stirred for 1 hour before adding 1-benzylpiperidin-4-amine

(1.06 mmol) or related amines. The reaction was stirred at 120°C for 4 hours. On cooling

to room temperature, diethylether was added to precipitate the crude product which was

filtered and purified by column chromatography (EA :hexane 1:1, increasing to 100%

EA).

To synthesize compounds **32-43**, **50-54**, **56-57**, the acridine or quinoline (1mmol)

was added to melted phenol (10mmol) and stirred for 1 hour before adding 1-

benzylpiperidin-4-amine (1.06 mmol) or related amines. The reaction was stirred at

120°C for 4 hours. On cooling to room temperature, the mixture was neutralized with 5M NaOH, extracted with dichloromethane (20ml x 3). The organic fractions were pooled, concentrated *in vacuo* and purified by column chromatography (EA :hexane 1:1, increasing to 100% EA).

2.4.4. Synthesis of the 3,9-dichloro-5,6,7,8-tetrahydroacridine[119]

To a mixture of 2-amino-4-chlorobenzoic acid (5mmol, 0.858g) and cyclohexanone (5mmol, 0.52ml) was carefully added 5 ml of $POCl_3$ at 0°C. The mixture was heated under reflux for 2 h, then cooled to room temperature, and concentrated to give a slurry. The residue was diluted with dichloromethane, neutralized with aqueous K_2CO_3, and washed with brine. The organic layer was dried over anhydrous Na_2SO_4 and concentrated *in vacuo* to furnish 1.118g of the desired compound as a reddish brown solid (Yield 88%). ^{1}H NMR (300MHz, $CDCl_3$) δ 1.89 (m, 4H), 2.88 (t, *J*=5.3, 2H), 3.06 9t, *J*=5.3, 2H), 7.34 (dd, *J1*=1.9, *J2*=8.9, 1H), 7.89 (m, 2H). ^{13}C NMR (75MHz, $CDCl_3$) δ 22.1, 22.2, 27.1, 33.4, 123.3, 124.7, 126.8, 127.1, 128.9, 135.1, 141.4, 145.9, 160.5. MS(APCI) *m/z* [M[+]] 252.7.

2.4.5. Synthesis of 6-chloro-1,2,3,4-tetrahydro-acridin-9-ylamine (49)

A solution of hydrazine monohydrate (2mmol) was added to 3,9-dichloro-5,6,7,8-tetrahydroacridine (1mmol) in ethanol (5ml). The solution was subjected to heating (150°C, 10min) on a microwave reactor (Biotage Initiator[TM], Biotage AB, Uppsala, Sweden). The hydrazine [1-(3-chloro-5,6,7,8-tetrahydroacridin-9-yl)hydrazine] was isolated by filtration as a red solid. ^{1}H NMR (300MHz, $CDCl_3$) δ 1.94 (m, 4H), 3.04 (m,

4H), 7.45 (dd, $J1$=1.9, $J2$=9.0, 1H), 7.96 (d, J=1.7, 1H), 8.06 9d, J=9.0, 1H). ^{13}C NMR (75MHz, CDCl$_3$) δ 22.2, 22.7, 23.8, 30.1, 111.2, 115.0, 120.3, 125.7, 126.9, 139.2, 140.6, 154.5, 155.9.

The hydrazine intermediate was transferred to a round bottom flask to which was added NiCl$_2$.6H$_2$O (1mmol) and NaBH$_4$ (3mmol). The mixture was stirred at room temperature for 1 hour and then filtered through a Celite pad. The filtrate was concentrated under vacuum, dissolved in ethyl acetate and extracted with brine three times. The organic layers were combined, concentrated under vacuum and purified by column chromatography (EA/hexane) to give the final pure product (**49**). Spectroscopic details of 49 are given in Appendix 1.

2.4.6. Synthesis of 4-amino-7-chloroquinoline (55)

A solution of hydrazine monohydrate (2mmol) was added to 4,7-dichloroquinoline (1mmol) in ethanol (5ml) and heated in a microwave reactor as described in Section 2.4.5. The hydrazine [1-(7-chloroquinolin-4-yl)hydrazine] was isolated and characterized: ^{1}H NMR (300MHz, DMSO-d6) δ 7.10 (d, J=6.9, 1H), 7.69 (d, J=9.0, 1H), 7.92 (9s, 1H), 8.44 (d=8.1, 2H). MS(APCI) m/z [M+H$^+$] 194.6.

The hydrazine was reduced by NiCl$_2$.6H$_2$O and NaBH$_4$ (3mmol) and purified as described in Section 2.4.5 to give the final pure product (**55**). Spectroscopic details of **55** are given in Appendix 1.

2.4.7. 6-chloro-2-methoxyacridin-9-amine monohydrochloride (46)

6,9-Dichloro-2-methoxyacridine (0.1 mol) was dissolved in 200ml of methanol and refluxed for 2 hours with a solution of sodium methoxide, prepared by dissolving sodium (0.12 mol) in 50 ml of methanol. The precipitated sodium chloride was removed by filtration and the filtrate treated with water to precipitate out the 6-chloro-2,9-dimethoxyacridine. This alkoxyacridine (0.01 mol) was dissolved in 20ml of alcohol and treated with ammonium chloride (0.012 mol) dissolved in 2ml of water. The mixture was maintained at 60-70^{0}C for 2 hours, during which the salt of the 6-chloro-9-amino-2-methoxyacridine was crystallized from the reaction mixture. The desired compound was obtained as a yellow solid. Spectroscopic details of **46** are given in Appendix 1.

2.4.8. Synthesis of substituted nitrobenzenes for Groups 2, 5, 6, and 7 by Hartwig-Buchwald amination reaction (GP3)

Cs$_2$CO$_3$ (25mmol) and BINAP (0.8 mmol) were added into a reaction flask under argon. 1-Iodo-3 (or 4) – nitrobenzene (10mmol) and amine (25mmol) were dissolved in dry toluene (30-50 ml) in another round bottom flask and purged with argon. The mixture was transferred to the reaction flask by a canula. Pd(OAc)$_2$ (0.6mmol) was added to the reaction flask quickly. The reaction mixture was heated (90°C) and the reaction mixture monitored on TLC. Heating was stopped when the iodobenzene, was not detected on TLC. On cooling to room temperature, the reaction mixture was filtered and concentrated to give the crude product which was then purified by column chromatography (50% ethyl acetate/hexane increasing to 100% ethyl acetate and then to 10% methanol in ethyl acetate + few drops of NH$_3$) to give the desired product in good yield.

1-(3-Nitrophenyl)pyrrolidine as obtained from 1-iodo-3-nitrobenzene and pyrrolidine following GP3. Yellow solid. ^{1}H-NMR (300MHz, CDCl$_3$) δ 2.06 (m, 4H), 3.34 (t, *J*=6.6, 4H), 6.80 (dd, *J1*=2.1, *J2*=8.0, 1H), 7.32 (m, 2H), 7.46 (dd, *J1*=1.7, *J2*=8.0, 1H). MS(ESI) *m/z* [M+H$^+$] 193.4.

1-(3-Nitrophenyl)piperidine was obtained from 1-iodo-3-nitrobenzene and piperidine following GP3. Yellow solid. ^{1}H-NMR (300MHz, CDCl$_3$) δ 1.63 (m, 2H), 1.72 (m, 4H), 3.26 (m, 4H), 7.18 (dd, *J1*=2.3, *J2*=8.3, 1H), 7.34 (t, *J*=8.2, 1H), 7.60 (dd, *J1*=1.6, *J2*=8.0, 1H), 7.71 (t, *J*=2.1, 1H). MS(ESI) *m/z* [M+H$^+$] 207.3.

4-(3-Nitrophenyl)morpholine was obtained from 1-iodo-3-nitrobenzene and morpholine following GP3. Yellow solid. ^{1}H-NMR (300MHz, CDCl$_3$) δ 3.251 (t, 4H, *J*=5.3) 3.886 (t, 4H, J=5.3), 7.183 (dd, *J1*=1.92, *J2*=8.40, 1H), 7.399 (t, *J*=8.08, 1H), 7.707 (m, 2H). MS(ESI) *m/z* [M+H$^+$] 209.1.

1-Methyl-4-(3-nitrophenyl)piperazine: was obtained from 1-iodo-3-nitrobenzene and 1-methylpiperazine following GP3. Yellow solid. ^{1}H-NMR (300MHz, CDCl$_3$) δ 2.304 (s, 3H) 2.584 (t, *J*=5.3, 4H) 3.303 (t, *J*=5.3, 4H) 7.367 (m, 2H) 7.660 (m, 2H). MS(ESI) *m/z* [M+H$^+$] 222.3.

1-Methyl-4-(4-nitrophenyl)piperazine: was obtained from 1-iodo-4-nitrobenzene and 1-methylpiperazine following GP3. Yellow solid. ^{1}H-NMR (300MHz, CDCl$_3$) δ 2.36 (s, 3H), 2.56 (m, 4H), 3.44 (m, 4H), 6.83 (d, *J*=9.4, 2H), 8.13 (d, *J*=9.4, 2H). MS(ESI) *m/z* [M+H$^+$] 222.3.

1-Ethyl-4-(4-nitrophenyl)piperazine was obtained from 1-iodo-4-nitrobenzene and 1-ethylpiperazine following GP3. Yellow solid. ^{1}H-NMR (300MHz, CDCl$_3$) δ 1.11

(t, *J*=7.2, 3H), 2.46 (q, *J*=7.2, 2H), 2.57 (m, 4H), 3.42 (m, 4H), 6.80 (d, *J*=9.4, 2H), 8.10 (d, *J*=9.4, 2H). MS(ESI) *m/z* [M+H$^+$] 236.2.

3-(4-(4-Nitrophenyl)piperazin-1-yl)propan-1-ol was obtained from 1-iodo-4-nitrobenzene and 3-(piperazin-1-yl)propan-1-ol. Yellow solid. ^{1}H-NMR (300MHz, CDCl$_3$) δ 1.79 (p, *J*=5.5, 2H), 2.68 (m, 6H), 3.44 (m, 4H), 3.84 (m, 2H), 6.83 (d, *J*=9.4, 2H), 8.13 (d, *J*=9.4, 2H). MS(ESI) *m/z* [M+H$^+$] 266.3.

1-(4-(4-Nitrophenyl)piperazin-1-yl)ethanone was obtained from 1-iodo-4-nitrobenzene and 1-(piperazin-1-yl)ethanone following GP3.. Red solid. Yield 92%. ^{1}H-NMR (300MHz, CDCl$_3$) δ 2.16 (s, 3H), 3.47 (m, 4H), 3.68 (m, 2H), 3.80 (m, 2H), 6.82 (d, *J*=9.4, 2H), 8.13 (d, *J*=9.3, 2H). MS(ESI) *m/z* [M$^+$] 248.9.

Cyclohexyl(4-(4-nitrophenyl)piperazin-1-yl)methanone was obtained from 1-iodo-4-nitrobenzene and cyclohexyl(piperazin-1-yl)methanone following GP3.. Yellow solid. Yield 87%. ^{1}H-NMR (300MHz, CDCl$_3$) δ 1.26 (t, *J*=8.1, 3H), 1.68-1.85 (m, 6H), 2.50 (m, 1H), 3.45 (m, 4H), 3.75 (m, 4H), 6.83 (d, *J*=9.4, 2H), 8.16 (d, *J*=9.4, 2H). (ESI) *m/z* [M+H$^+$] 318.2.

(4-(4-Nitrophenyl)piperazin-1-yl)(phenyl)methanone was obtained from 1-iodo-4nitrobenzene and phenyl(piperazin-1-yl)methanone following GP3.. Orange solid. Yield 80%. ^{1}H-NMR (300MHz, CDCl$_3$) δ 3.44 (m, 4H), 3.81 (m, 4H), 6.85 (d, *J*=9.4, 2H), 7.45 (s, 5H), 8.16 (d, *J*=9.3, 2H). (ESI) *m/z* [M+H$^+$] 312.1.

2.4.9. General procedure for catalytic reduction of substituted nitrobenzenes (GP4)

To an ethanolic solution of the nitrobenzene obtained from the Hartwig-Buchwald reaction (section 2.3.3) was added 10% Pd/C (5%w/w) in the presence of nitrogen. The

mixture was hydrogenated at 50 psi overnight on a Parr hydrogenator. The catalyst was removed by filtration, the filtrate was concentrated in vacuo and the residue containing the aniline was used immediately for the next reaction step.

2.4.10. Synthesis of N^1,N^1-dimethylbenzene-1,3-diamine

N^1,N^1-Dimethylbenzene-1,3-diamine was required for the synthesis of **6**. 0.4 g (2.5 mmol) *ortho*-nitrochlorobenzene was added into a flask which was then sealed and flushed with argon. Hexamethylphosphoramide (15 mmol, 2.5 ml) was added into the flask and the solution was heated at 150ºC, 24 hours in the presence of argon. It was then diluted with 20 ml water, extracted with ether, after which the ether fraction was extracted with 4 × 10 ml 4M HCl. The aqueous fractions were basified with 4M NaOH and extracted with 4 × 20 ml ether and dried with anhydrous Na_2SO_4. On evaporation *in vacuo*, the residue was recrystallised with absolute ethanol to yield yellow crystals. The residue was immediately reduced to an amine following GP4 to obtain the desired product. ^{1}H-NMR (300MHz, $CDCl_3$) δ 3.091 (s, 6H) 7.14 (d, *J*=1.5, 1H) 7.57 (d, *J*=1.5, 1H) 7.88 (s, 1H).

2.4.11. Synthesis of N^1,N^1-diethylbenzene-1,3-diamine

N^1,N^1-Diethylbenzene-1,3-diamine was required for the synthesis of **8**. 1.2 g (5.8 mmol) 3-(N,N-diethylamino)acetanilide and 2.5 ml concentrated HCl was refluxed for two hours. After cooling, the pH of the solution was adjusted to 4 with 2M NaOH. The solution was added directly to an ethanolic solution of 4-methoxy-6,9-dichloroacridine following the general procedure described in Section 2.4.2 (GP1).

2.4.12. Synthesis of 4-[(4-methylpiperazin-1-yl)methyl] benzenamine

4-[(4-Methylpiperazin-1-yl)methyl]benzenamine was required for the synthesis of **22**. To a solution of 4-nitrobenzylchloride (1mmol, 0.172g) in anhydrous THF (3ml) was added 1-methylpiperazine (1mmol, 0.11ml) and triethylamine (1.5mmol, 0.21ml). The solution was heated at 70°C overnight. The reaction mixture was then extracted with dichloromethane and water. The organic fractions were combined, dried over anhydrous Na$_2$SO$_4$, and concentrated under reduced pressure. The residue was purified by column chromatography (hexane/EA 1:4) to give 0.2 g of 1-(4-nitrobenzyl)-4-methylpiperazine yellow liquid (Yield 85%). ^{1}H NMR ((300MHz, CDCl$_3$) δ 2.29 (s, 3H), 2.48 (b, 8H), 3.59 (s, 2H), 7.51 (d, J=8.7, 2H), 8.17 (d, J=8.7, 2H). MS(ESI) m/z [M^{+}] 236.1. This intermediate was dissolved in 10ml ethanol, PtO$_2$ (0.010g) was added under nitrogen. Hydrogenation was carried out on a Parr hydrogenator at 50psi for 16h. The catalyst was then removed by filtration and the filtrate was concentrated in vacuo to give the amine in quantitative yield. ^{1}H NMR ((300MHz, CDCl$_3$) δ 2.21 (s, 3H), 2.39 (b, 8H), 3.33 (s, 2H), 3.55 (b, 2H), 6.56 (d, J=6.6, 2H), 7.02 (d, J=7.2, 2H). MS(ESI) m/z [M+H^{+}] 206.1.

2.4.13. Synthesis of 4-[(piperidin-1-yl)methyl]benzenamine

4-[(Piperidin-1-yl)methyl]benzenamine was required for the synthesis of **24**. 4-Nitrobenzylchloride was reacted with piperidine as described in Section 2.4.12. 1-(4-Nitrobenzyl)piperidine was obtained as a yellow oil (85%). ^{1}H NMR (300MHz, CDCl$_3$) δ 1.47 (m, 2H), 1.67 (m, 4H), 2.48 (m, 4H), 3.65 (s, 2H), 7.59 (d, J=7.7, 2H), 8.19 (d, J=8.6, 2H). It was subjected to catalytic hydrogenation as described in Section 2.4.12 to

give the desired amine in quantitative yield. ^{1}H NMR (300MHz, CDCl$_3$) δ 1.43 (m, 2H), 1.60 (m, 4H), 2.40 (t, *J*=5.3, 4H), 3.42 (s, 2H), 6.63 (d, *J*=8.6, 2H), 7.09 (d, *J*=8.4, 2H). ^{13}C NMR (75MHz, CDCl$_3$) δ 34.2, 35.4 (2C), 58.3 (2C), 65.8, 107.6 (2C), 107.9 (2C), 120.4, 132.4. MS(ESI) *m/z* [M$^+$] 219.8.

2.4.14. Synthesis of (4-aminophenyl)(4-methylpiperazin-1-yl)methanone

(4-Aminophenyl)(4-methylpiperazin-1-yl)methanone was required for the synthesis of **23**. To a solution of 4-nitrobenzoyl chloride (1 mmol, 0.186g) in anhydrous dichloromethane (5ml) was added 1-methylpiperazine (1mmol, 0.11ml) and triethylamine (1.5mmol, 0.21ml). The solution was stirred at room temperature. The reaction mixture was then extracted with DCM and saturated NaHCO$_3$. The organic fractions were combined, dried over anhydrous Na$_2$SO$_4$, and concentrated under reduced pressure. The residue was purified by column chromatography (silica gel, hexane/ EA 1:4) to give 0.249g of (4-methylpiperazin-1-yl)(4-nitrophenyl)methanone as a yellow liquid. ^{1}H NMR (300MHz, CDCl$_3$) δ 2.33 (s, 3H), 2.40 (m, 2H), 2.51 (m, 2H), 3.39 (m, 2H), 3.82 (m, 2H), 7.57 (d, *J*=8.6, 2H), 8.28 (d, *J*=8.6, 2H). MS(ESI) *m/z* [M+H$^+$] 250.1. It was then subjected to catalytic hydrogenation as described in section 2.4.12 to give the desired amine in quantitative yield. ^{1}H NMR (300MHz, CDCl$_3$) δ 2.32 (s, 3H), 2.42 (m, 4H), 3.65 (m, 4H), 3.92 (b, 2H), 6.63 (d, *J*=8.3, 2H), 7.24 (d, *J*=8.3, 2H). MS(ESI) *m/z* [M+H$^+$] 220.1.

2.4.15 Synthesis of amines for Group 3

A solution of *tert*-butyl piperidin-4-ylcarbamate (2mmol), phenylalkyl halide (2mmol), and triethylamine (6mmol) in tetrahydrofuran (THF, 5ml) was refluxed overnight. THF was evaporated under reduced pressure. Dichloromethane was added and the mixture was extracted with dilute NaHCO$_3$. The organic fractions were combined, dried over anhydrous Na$_2$SO$_4$, concentrated *in vacuo*, and the residue purified by column chromatography (EA/hexane) to give the desired Boc-protected amine. The Boc-protected amine was dissolved in dichloromethane (4ml) and tetrafluoroacetic acid (TFA, 4 ml) was added dropwise. The reaction mixture was neutralized with saturated (5M) NaOH, extracted with dichloromethane and NaHCO$_3$ solution to give the desired amine as an oil. It was reacted with 6,9-dichloro-2-methoxyacridine by the general procedure 2 (GP2) without further characterization.

tert-Butyl 1-(4-methylbenzyl)piperidin-4-ylcarbamate: Light orange solid. Yield 95%. ^{1}H NMR (300MHz, CDCl$_3$) δ 1.35 (m, 2H), 1.43 (s, 9H), 1.88 (d, *J*=11.5, 2H), 2.06 (t, *J*=11.3, 2H), 2.32 (s, 3H), 2.78 (d, *J*=11.5, 2H), 3.43 (s, 2H), 4.53 (m, 1H), 7.10 (d, *J*=7.8, 2H), 7.18 (d, *J*=7.9, 2H). ^{13}C NMR (75MHz, CDCl$_3$) δ 20.9, 28.3 (2C), 32.4, 47.7, 52.1, 62.6, 80.0, 128.7 (2C), 129.0 (2C), 135.1, 136.4, 155.1. MS(APCI) *m/z* [M$^+$] 305.2.

tert-Butyl 1-(4-chlorobenzyl)piperidin-4-ylcarbamate: White solid. Yield 84%. ^{1}H NMR (300MHz, CDCl$_3$) δ 1.44 (s, 11H), 1.90 (d, *J*=11.3, 2H), 2.08 (t, *J*=11.4, 2H), 2.77 (d, *J*=11.6, 2H), 3.44 (s, 3H), 4.51 (s, 1H), 7.24 (d, *J*=8.7, 2H), 7.27 (d, *J*=8.6, 2H). ^{13}C NMR (75MHz, CDCl$_3$) δ 28.3 (3C), 32.4, 47.6, 52.2, 62.1, 79.1, 128.3 (2C), 130.3 (2C), 132.7, 136.7, 155.1. MS(APCI) *m/z* [M$^+$] 325.2.

***tert*-Butyl 1-(4-methoxybenzyl)piperidin-4-ylcarbamate:** White solid. Yield 93%. ^{1}H NMR (300MHz, CDCl$_3$) δ 1.38 (m, 2H), 1.43 (s, 9H), 1.87 (d, *J*=11.0, 2H), 2.03 (t, *J*=10.8, 2H), 2.77 (d, *J*=11.4, 2H), 3.39 (s, 2H), 3.76 (s, 3H), 4.71 (d, *J*=6.4, 1H), 6.83 (d, *J*=8.5, 2H), 7.19 (d, *J*=8.5, 2H). ^{13}C NMR (75MHz, CDCl$_3$) δ 28.2 (3C), 32.3, 47.6, 51.9 (2C), 54.9 (2C), 62.1, 78.7, 113.3 (2C), 130.0 (2C), 130.1, 154.9, 158.4. MS(APCI) *m/z* [M$^+$] 320.0.

***tert*-Butyl 1-(4-cyanobenzyl)piperidin-4-ylcarbamate**: Orange solid 95%. ^{1}H NMR (300MHz, CDCl$_3$) δ 1.44 (s, 9H), 1.50 (m, 2H), 1.92 (d, *J*=11.3, 2H), 2.13 (t, *J*=10.6, 2H), 2.77 (d, *J*=11.6, 2H), 3.54 (s, 2H), 4.59 (d, *J*=5.2, 1H), 7.45 (d, *J*=8.1, 2H), 7.60 (d, *J*=8.1, 2H). ^{13}C NMR (75MHz, CDCl$_3$) δ 28.2 (3C), 32.3, 47.4 (2C), 52.3, 62.2 (2C), 79.1, 110.6, 118.8, 129.3 (2C), 131.9 (2C), 144.2, 155.0. MS(APCI) *m/z* [M$^+$] 315.7.

***tert*-Butyl 1-phenethylpiperidin-4-ylcarbamate**: White solid. Yield 74%. ^{1}H NMR (300MHz, CDCl$_3$) δ 1.45 (s, 9H), 1.49 (m, 2H), 1.95 (d, *J*=11.4, 2H), 2.15 (t, *J*=11.1, 2H), 2.58 (m, 2H), 2.80 (m, 2H), 2.93 (d, *J*=10.9, 2H), 3.47 (s, 1H), 4.58 (s, 1H), 7.19 (d, *J*=5.3, 2H), 7.26 (d, *J*=6.6, 2H). ^{13}C NMR (75MHz, CDCl$_3$) δ 28.3 (3C), 32.4, 33.6, 47.6, 52.2, 60.3, 79.0, 125.9, 128.2 (2C), 128.5 (2C), 140.0, 155.1. MS(APCI) *m/z* [M$^+$] 304.7.

***tert*-Butyl 1-(4-methylphenethyl)piperidin-4-ylcarbamate**: White solid. Yield 88%. ^{1}H NMR (300MHz, CDCl$_3$) δ 1.45 (s, 9H), 1.51 (m, 2H), 1.95 (d, *J*=11.6, 2H), 2.15 (t, *J*=10.9, 2H), 2.30 (s, 3H), 2.57 (dd, *J1*=5.8, *J2*=10.4, 2H), 2.76 (dd, *J1*=5.8, *J2*=10.4, 2H), 2.92 (d, *J*=11.5, 2H), 3.47 (s, 1H), 4.59 (s, 1H), 7.07 (s, 4H). ^{13}C NMR (75MHz,

CDCl$_3$) δ 20.8, 28.3 (3C), 32.3, 33.1, 47.6, 52.2, 60.4, 79.1, 128.4 (2C), 128.9 (2C), 135.3, 136.9, 155.1. MS(APCI) *m/z* [M$^+$] 318.4.

***tert*-Butyl 1-(4-chlorophenethyl)piperidin-4-ylcarbamate**: Light orange solid. Yield 82%. ^{1}H NMR (300MHz, CDCl$_3$) δ 1.45 (s, 11H), 1.94 (d, *J*=11.8, 2H), 2.12 (t, *J*=11.2, 2H), 2.53 (m, 2H), 2.74 (m, 2H), 2.89 (d, *J*=10.9, 2H), 3.46 (m, 1H), 4.61 (b, 1H), 7.10 9d, *J*=8.0, 2H), 7.22 (d, *J*=8.0, 2H). ^{13}C NMR (75MHz, CDCl$_3$) δ 28.2 (3C), 32.4, 32.9, 47.6, 52.2, 60.0, 79.0, 128.22 (2C), 129.8 (2C), 131.5, 138.6, 155.0. MS(APCI) *m/z* [M$^+$] 338.4.

***tert*-Butyl 1-(4-methoxyphenethyl)piperidin-4-ylcarbamate**: White solid. Yield 89%. ^{1}H NMR (300MHz, CDCl$_3$) δ 1.37 (s, 9H), 1.44 (m, 2H), 1.86 (d, *J*=10.9, 2H), 2.04 (t, *J*=10.7, 2H), 2.45 (dd, *J1*=5.9, *J2*=9.6, 2H), 2.64 (m, 2H), 2.82 (d, *J*=10.7, 2H), 3.39 (b, 1H), 3.66 (s, 3H), 4.71 (b, 1H), 6.73 (d, *J*=8.3, 2H), 7.01 (d, *J*=8.3, 2H). ^{13}C NMR (75MHz, CDCl$_3$) δ 28.1 (3C), 32.2, 32.5, 47.5, 52.1, 54.8, 60.4, 78.7, 113.5 (2C), 129.2 (2C), 131.9, 154.9, 157.6. MS(APCI) *m/z* [M$^+$] 334.2.

***tert*-Butyl 1-(3-phenylpropyl)piperidin-4-ylcarbamate**: White solid. Yield 75%.^{1}H NMR (300MHz, CDCl$_3$) δ 1.44 (s, 11H), 1.81 (m, 2H), 1.93 (d, *J*=12.1, 2H), 2.05 (t, *J*=10.4, 2H), 2.36 (m, 2H), 2.62 (t, *J*=7.7, 2H), 2.84 (d, *J*=9.3, 2H), 4.47 (m, 1H), 7.17 (d, *J*=7.5, 2H), 7.26 (d, *J*=7.4, 2H). ^{13}C NMR (75MHz, CDCl$_3$) δ 28.4 (3C), 28.7, 32.5, 33.7, 47.7, 52.3, 57.9, 79.2, 125.7, 128.2 (2C), 128.3 (2C), 142.0, 155.2. MS(APCI) *m/z* [M$^+$] 318.7.

2.4.16. Synthesis of 4-(4-methylpiperazin-1-yl)but-2-yn-1-amine

4-(4-Methylpiperazin-1-yl)but-2-yn-1-amine was required for the synthesis of **42.**

2-(4-Chlorobut-2-ynyl)isoindoline-1,3-dione **(42a)**: 1,4-Dichloro-2-butyne (6mmol, 0.58ml) was added to the stirred suspension of potassium phthalimide (3mmol, 0.556g) in DMF (5ml), and heated to 100°C for 5 h. After cooling, the reaction mixture was extracted with dichloromethane and water. The organic layers were pooled, dried, and concentrated in vacuo. The residue was purified by column chromatography (hexane/ethyl acetate 1:19) to furnish 0.35g of **42a** (white solid, yield 50%). ^{1}H NMR (300MHz, CDCl$_3$) 4.11 (s, 2H), 4.51 (s, 2H), 7.75 (dd, *J1*=3.1, *J2*=5.5, 2H), 7.89 (dd, *J1*=3.1, *J2*=5.4, 2H). ^{13}C NMR (75MHz, CDCl$_3$) δ 27.1, 45.7, 46.9, 51.7 (2C), 54.7 (2C), 78.1, 78.4, 123.4 (2C), 131.9 (2C), 134.0 (2C), 166.9 (2C).

2-(4-(4-Methylpiperazin-1-yl)but-2-ynyl)isoindoline-1,3-dione (42b): **42a** was reacted with 1-methylpiperazine in the presence of TEA and anhydrous THF as solvent as described in section 2.4.12. **42b** was obtained as a yellow solid in 83% yield. ^{1}H NMR (300MHz, CDCl$_3$) δ 2.28 (s, 3H), 2.45 (m, 4H), 2.58 (m, 4H), 3.26 (s, 2H), 4.47 (s, 2H), 7.73 (dd, *J1*=3.1, *J2*=5.4, 2H), 7.88 (dd, *J1*=3.1, *J2*=5.4, 2H). MS(APCI) *m/z* [M+H^{+}] 298.2.

4-(4-Methylpiperazin-1-yl)but-2-yn-1-amine **(42c)**: A solution of **42b** (0.72mmol, 0.213g) and hydrazine (0.72mmol, 0.03ml) in 1ml of ethanol was heated at reflux for 2h. After cooling the mixture to 0°C, phthalhydrazide was removed by filtration. Evaporation of the filtrate gave the **42c** (free base). ^{1}H NMR (300MHz, CDCl$_3$) δ 2.30 (s, 3H), 2.49-2.61 (m, 8H), 3.28 (t, *J*=1.8, 2H), 3.44 (t, *J*=1.8, 2H). ^{13}C NMR (75MHz, CDCl$_3$) δ 29.7, 31.6, 46.0, 47.2, 52.0 (2C), 53.0, 54.9 (2C). MS(ESI) *m/z* [M+H^{+}] 168.1.

2.4.17. Synthesis of 8-benzyl-8-aza-bicyclo[3.2.1]octan-3-amine

8-Benzyl-8-aza-bicyclo[3.2.1]octan-3-amine was required for the synthesis of **43.**

8-Aza-bicyclo[3.2.1]octan-3-one (43a): A solution of ethyl 3-oxo-8-azabicylo[3.2.1]octane-8-carboxylic acid (2.3mmol, 0.46g) in ethanol (1ml) was mixed with KOH (0.353g) in water (5ml) and heated at 100°C for 3h. After cooling down to room temperature, the solution was diluted with 20ml of dichloromethane. The organic layer was dried and concentrated *in vacuo* to give crude 43a. ^{1}H NMR (300MHz, CDCl$_3$) δ 1.69 (m, 2H), 1.90 (dd, *J1*=4.1, *J2*=8.8, 2H), 2.31 (m, 1H), 2.36 (m, 2H), 2.56 (m, 2H), 3.87 (m, 2H). ^{13}C NMR (75MHz, CDCl$_3$) δ 30.0 (2C), 50.8 (2C), 54.9 (2C), 209.7.

8-Benzyl-8-aza-bicyclo[3.2.1]octan-3-one (43b): **43a** was reacted with benzyl chloride as described for 1-(4-nitrobenzyl)-4-methylpiperazine (Section 2.4.12). ^{1}H NMR (300MHz, CDCl$_3$) δ 1.63 (m, 2H), 2.16 (m, 4H), 2.72 (m, 2H), 3.50 (m, 2H), 3.76 (m, 2H), 7.34 (m, 5H). ^{13}C NMR (75MHz, CDCl$_3$) δ 27.7 (2C), 48.1 (2C), 55.1, 58.6 (2C), 127.2, 128.4 (2C), 128.5 (2C), 138.9, 210.1. MS(APCI) *m/z* [M$^+$] 215.3.

8-Benzyl-8-aza-bicyclo[3.2.1]octan-3-one oxime (43c): Hydroxylamine hydrochloride (1.7mmol, 0.117g) was stirred in methanol (7ml) at 0°C. The slurry was treated with Na$_2$CO$_3$ (0.09g) and stirred for 5min. A solution of **43b** (1.36mmol, 0.2934g) in 1ml of methanol was added and the reaction mixture was allowed to reach room temperature. After stirring for 5h, methanol was removed in vacuo, the residue was treated with dichloromethane and brine, the organic fractions were combined, dried (anhydrous Na$_2$SO$_4$), and concentrated to give 0.2g of the desired product as a white solid (Yield 65%). ^{1}H NMR (300MHz, CDCl$_3$) δ 1.52 (t, *J*=9.6, 1H), 1.63 (t, *J*=9.6, 1H), 2.04 (m, 2H), 2.14 (d, *J*=14.7, 1H), 2.26 (dd, *J1*=2.7, *J2*=12.6), 2.62 (d, *J*=14.7, 1H), 2.99

(d, J=15.6, 1H), 3.36 (b, 2H), 3.66 (s, 2H), 7.25-7.42 (m, 5H). ^{13}C NMR (75MHz, CDCl$_3$) δ 26.6, 27.5, 31.3, 37.1, 55.5, 57.8, 58.4, 127.0, 128.2 (2C), 128.7 (2C), 138.9, 156.3. MS(ESI) m/z [M+H$^+$] 231.1.

8-Benzyl-8-aza-bicyclo[3.2.1]octan-3-amine (43d): The oxime (**43c**) was reduced with Adam's catalyst as described for 4-[(4-methylpiperazin-1-yl)methyl]benzenamine (Section 2.3.6). **43d** was obtained as a yellow oil (Yield 76%) which was used immediately for the synthesis of compound **43**. MS(ESI) m/z [M+H$^+$] 217.4.

2.4.18. Synthesis of 1-chloro-4-(chloromethyl)benzene

To a solution of 4-chlorobenzylhydroxy (5mmol, 0.713g) in anhydrous dichloromethane (5ml) was added SOCl$_2$ (15mmol, 1.1ml) dropwise at 0$^{\text{o}}$C. The reaction mixture was allowed to reach room temperature, stirred for 1h, and then cooled down to 0$^{\text{o}}$C again. It was then carefully diluted with water, and neutralized with saturated NaHCO$_3$. The reaction mixture was extracted with dichloromethane and washed with water to afford the product as a yellow oil (0.64g, 80%) ^{1}H NMR (300MHz, CDCl$_3$) δ 4.54 (s, 2H), 7.32 (s, 4H). ^{13}C NMR (75MHz, CDCl$_3$) δ 45.3, 128.9 (2C), 129.9 (2C), 134.3, 135.9.

2.4.19 Synthesis of 1-chloro-4-(2-chloroethyl)benzene

1-Chloro-4-(2-chloroethyl)ethanol was reacted with SOCl$_2$ as described in Section 2.4.18. 1-Chloro-4-(2-chloroethyl)benzene was obtained as a yellow oil in quantitative yield. ^{1}H NMR (300MHz, CDCl$_3$) δ 2.99 (t, J=7.2, 2H), 3.65 (t, J=7.2, 2H), 7.11 (d,

J=8.4, 2H), 7.25 (d, J=8.1, 2H). ^{13}C NMR (75MHz, CDCl$_3$) δ 38.2, 44.6, 128.6 (2C), 130.1 (2C), 132.6, 136.4.

2.5. Summary

The synthesis of 47 compounds was successfully achieved. All compounds were characterized by ^{1}H NMR, ^{13}C NMR and MS. The purity of compounds was determined by elemental analysis or reversed phase HPLC using two different mobile phases. The threshold requirement for purity was 95% and compounds that complied with this requirement were considered suitable for biological evaluation. Yields, NMR chemical shifts, MS data, yield and purity of synthesized compounds are given in Appendix 1.

Chapter 3: Antiprion activity of acridine analogues

3.1. Introduction

This chapter describes the screening of selected synthesized compounds from Chapter 2 for antiprion activity. Evaluation was carried out in cells that were stably infected with scrapie protein PrP^{Sc} and capable of active replication of the protein (without associated cytotoxicity to the cells) leading to the accumulation of PrP^{Sc} in readily detected amounts. In the presence of an active antiprion agent, PrP^{Sc} levels were reduced and served as a means of evaluating the potency of the test compound. The synthesized compounds were evaluated in two stages. In the first stage, 42 compounds (all Group 1 and 5 compounds, selected compounds in Groups 2, 3 and 4) were screened. From the results, two hits were identified and chemical modification of these compounds gave analogs that were evaluated in the second stage of screening.

In an effort to understand the mode of action of the present series of compounds, two aspects were investigated, namely their interactions with cellular PrP by surface plasmon resonance and effect on cellular levels of PrP^C. Surface plasmon resonance has been widely used by many investigators[100,120,121] to investigate the binding of small ligands with prion protein. It is generally thought that binding to PrP^C served to stabilize it and thus render the conformational change to PrP^{Sc} energetically less favourable. Binding may also affect the cellular localization of PrP^C or cause a change in PrP^C mediated signaling pathways that are critical to the disease progression. Hence, a correlation between binding affinities and antiprion activities is generally expected. However, there were instances where a compound with potent antiprion activity was

found to have low binding affinity for PrP^C, or inactive compounds that had exceptionally good binding affinities. These may arise from non-specific binding (false positives) or instances where binding required additional modulation factors that were not present in the binding assay (false negatives). In spite of these exceptions, a compound that binds to PrP^C is more likely to have antiprion activity than one that fails to exhibit any binding. As for the effect on cellular levels of PrP^C, the assumption made was that a compound that reduced PrP^C content would lead to a reduction in abnormal PrP formation and thus delay disease progression.

An added requirement for an agent targeted for antiprion activity is its ability to transverse the blood brain barrier to reach its site of action in the brain. The blood brain barrier comprises endothelial cells and associated astrocytes found in the inner surfaces of blood capillaries that innervate the brain tissue. It is a "barrier" in the sense that it excludes most substances from the brain except those that are actively transported or have suitable physicochemical properties that permit passive diffusion to take place. These properties include molecular weight, hydrogen bonding capabilities and lipophilicity.[105] Even if compounds comply with these properties, access to the brain may be minimal if they are substrates of the many ATP-binding cassette efflux transporters like P-glycoprotein (Pgp, ABCB2) and breast cancer resistant protein (BCRP, ABCG2) that are found in the blood brain barrier. Hence, an attempt was made to assess the potential of the active analogs identified in this chapter to transverse the blood brain barrier. Selected actives were evaluated by the PAMPA-BBB assay[122] which measures their permeability across polycarbonate filters impregnated with porcine brain lipids and

one active analog (**16**) was tested on a cell line that over-expressed Pgp to determine if it was a substrate of this efflux protein.

3.2. Experimental methods

3.2.1. Evaluation of antiprion activity

The cell models (ScN2a, N167, Ch2, F3) were provided by Dr Byron Caughey (Laboratory of Persistent Viral Diseases, Rocky Mountain Laboratories, National Institute of Allergy and Infectious diseases, National Institutes of Health, Hamilton, Montana) and the experiments were carried out in the laboratory of Dr Katsumi Doh-ura, Department of Prion Research, Tohoku University, Sendai, Japan. The assay was performed following reported methods.[123-125] The cells were grown in minimal essential medium (Opti-MEM, Invitrogen) supplemented with 10% fetal calf serum, penicillin and streptomycin (0.1g/L each).

Approximately 2×10^6 cells were seeded into each well of a six-well plate. Stock solutions of the test compounds were prepared in DMSO and aliquots were added to the wells to achieve the desired concentration. The final concentration of DMSO in each well was kept at less than 0.5% v/v. When the cells reached confluency after 3 days, they were examined microscopically (10x magnification) for signs of abnormal morphology. The medium was then removed from each well by aspiration, the cells were rinsed with cold PBS (2 ml) and treated with lysis buffer (500 µl) which comprised 0.5% Nonidet P-40 and 0.5% sodium deoxycholate in PBS. The solution was transferred to safe-lock tubes for centrifugation at 6,000x *g*, 5 min, 4°C. The supernatant was treated with 5 µl of proteinase K (1 µg/µl, Merck) for 30 min (37°C), cooled on ice (2-3 min), followed by

addition of phenylmethanesulphonyl fluoride (PMSF, 5 µl of 0.1 M solution) to stop the reaction. The protein was precipated with 20 µl of glass fog solution 1% (Qbiogene Inc). The mixture was rolled over for 5 min and then centrifuged at 13,000x g for 2 min.

After removal of supernatant, the protein precipitate was dispersed in 20 µL of sample loading buffer and denatured for 5 min at 95°C. On cooling to room temperature, the protein samples were loaded on to polyacrylamide SDS-PAGE gel for electrophoresis. The prion proteins were detected using SAF83 (1:5,000; SPI-Bio, France), a primary antibody against a human PrP fragment (amino acids 142-160) and an alkaline phosphatase-conjugated secondary antibody (anti-mouse IgG H&L, 1:20,000; Promega [®]), followed by chemiluminescence. Immunoreactive signals were visualized with CDP-Star detection reagent (Amersham®) and were analyzed by densitometry with the ImageJ program (National Institute of Health, Bethesda, USA). Three independent assays were performed for each concentration of test compound. EC_{50} values and 95% confidence intervals were obtained by non-linear regression using the sigmoidal dose-response equation from GraphPad Prism version 4.03 (GraphPad Software Inc., CA, USA).

3.2.2. Determination of total and cell surface prion proteins

The total level of normal cellular PrP was determined in non-infected N2a cells treated with test compound following the procedure described in Section 3.2.1. The difference was that samples were not treated with proteinase K and a smaller volume of supernatant (20 µl) was mixed with 5 µl of 5x concentrated sample loading buffer, boiled and then analyzed by immunoblotting as described.

For the determination of cell surface prion protein, the method of Doh-ura et al.[126] was followed. Briefly, N2a cells were seeded and exposed to test compound for 3 days as described in Section 3.2.1. After this time, the medium was removed by aspiration, cells were rinsed with 2 ml cold PBS [without $MgCl_2$ and $CaCl_2$, referred to as PBS(-)] and the cells detached by adding the same PBS solution containing 0.1% collagenase (Wako Pure Chemical Industries Inc., Osaka, Japan) for 3 min at 37^oC. 500μl of culture medium was then added to each well to inhibit the action of collagenase. The cell suspension from each well was dispensed into two tubes (approximately $0.5-2.5x10^6$ cells/tube) which were then centrifuged (500x g, 4^oC, 1 min). Cell pellets were resuspended in 500μl washing buffer which contained 0.5% inactivated fetal bovine serum in PBS (-) (FBS/PBS), centrifuged again and incubated with SAF83 (1:500) or isotype-matched control IgG1 for 20 min on ice. They were then washed with FCS/PBS and incubated with goat F(ab')2 fragment anti-mouse IgG(H+L)-PE (1:100) (Beckman Coulter Inc., CA) for 20 min on ice. After washing, fluorescent intensities were recorded using the EPICS XL-ADC flow cytometer (Beckman Coulter Inc., CA).

3.2.3. Evaluation of binding affinity by surface plasmon resonance

Recombinant human prion protein (amino acids 121-231; hPrP121-231, molecular weight 12,544.97 Da) was a gift from Dr. Katsumi Doh-ura, Department of Prion Research, Tohoku University Graduate School of Medicine, Sendai, Japan. The assay was performed on a BIAacore 3000 platform (BIAcor, Uppsala, Sweden). The sensor chip CM5 and amine coupling kit were purchased from GE Healthcare Bio-

sciences AB (Uppsala, Sweden). The running buffer was prepared by filtering and degassing a phosphate buffer 1x, pH 7.4 containing 2.5% DMSO.

The hPrP121-231 was dissolved in 10mM sodium acetate buffer, pH 4.5 (10μg/ml) and immobilized on the CM5 chip to reach a density of *ca.* 3000 response units (RU) using amine coupling. A reference surface was prepared by treating a blank flow cell in the same way as the flow cell containing the immobilized peptide. Stock solutions of test compounds (2mM) were prepared in DMSO and diluted to 50 μM with phosphate buffer 1x, pH 7.4. Each analytical cycle consisted of running buffer for 60 seconds (stabilization phase), a sample injection of 50 μM in running buffer for 120 seconds (association phase) and running buffer for 150 seconds (dissociation phase). Flow rates were kept at 30 μl/min. Surface regeneration of the chip was carried out by injecting 10 mM NaOH (30 s, flow rate of 30μl/min). After regeneration, the surface was allowed to stabilize for *ca* 60 seconds before the next injection. The binding response curve was obtained by subtracting the background signal (from the reference flow cell) from that of the sample flow cell in order to correct for non-specific binding and bulk effects due to the analyte. The binding affinity was taken as the maximum response at the end of the association phase as seen from the binding response curve. Binding was expressed as % RU_{max} which is defined as the % theoretical maximum binding resonance units (RU) and determined by the following equation assuming a 1:1 stoichiometry:

$$\% \, RU_{max} = \frac{RU \text{ of compound}}{RU \text{ of immobilized protein}} \, x \, \frac{MW \text{ of protein}}{MW \text{ of compound}} \, x100\%$$

3.2.4. Evaluation of permeability by the PAMPA-BBB assay

Porcine polar brain lipid (PBL) (catalog no. 141101) was purchased from Avanti Polar Lipids, Inc. (Alabaster, Alabama, USA). Dodecane was obtained from Sigma-Aldrich. The acceptor plate was a 96-well filter plate (MultiscreenTM-IP, catalog no. MAIPN4510, PVDF membrane, pore size is 0.45μm) from Millipore (Bredford, USA) and the donor plate was a 96-well plate (catalog no. MATRNPS50, Millipore, Billerica, MA, USA). The 96-well UV plate (catalog no. 3535) was purchased from Corning Inc. (NY, USA).

Compounds were dissolved in DMSO at 10mM, and diluted in phosphate buffer solution 1x, pH 7.4 to 50 μM or 30 μM depending on their aqueous solubilities. An aliquot (300 μl) of the diluted solution was transferred to the donor well. The filter membrane was coated with 5 μl of 20 mg/mL PBL in dodecane and the acceptor well was filled with 150 μl of the same phosphate buffer solution. The donor plate was carefully aligned to the acceptor plate such that the underside of the membrane remained in contact with buffer solution in the donor wells. The sandwich assemble was incubated in an airtight humid box at room temperature for 10 hours. The concentrations of compound in the acceptor, donor and reference wells were determined by UV absorbance at 270nm using the Tecan Infinite 200 microplate reader.

Permeability rate (P_e) and membrane retention (R) were calculated using the following equations:

$$P_e = - \frac{2.303\, V_A}{A.t} \left[\frac{1}{1+r_v} \right] \log_{10} \left\{ 1 - \left[\frac{1+r_v^{-1}}{1-R} \right] \frac{C_A(t)}{C_D(0)} \right\}$$

$$R = 1 - \frac{V_A\, C_A(t) + V_D\, C_D(t)}{V_D\, C_D(0)}$$

where A is the active surface area of membrane ($0.24cm^2$), t is the incubation time (s), V_A and V_D are the volumes (cm^3) of the acceptor and donor chambers, $r_V = V_D/V_A$, C_A and C_D are drug concentrations in the acceptor and donor chambers.

3.2.5. Cell-based bidirectional transport assay

Dulbeco's Modified Eagle's medium (DMEM) was purchased from Sigma (MO, USA). Fetal bovine serum was from Hyclone Lab Inc. (Logan, UT, USA). The MDCK-WT (wild type) and MDCK-MDR1 (overexpressing Pgp) were gifts from Dr. Piet Borst (Netherlands Cancer Institute, University of Amsterdam, Netherlands). Western blotting was performed on these two cell lines to confirm the overexpression of Pgp by another laboratory member, the results of which had been published.[127] Transwell® plates (Cat. no 3401, 12mm diameter, 0.4μm pore size) were obtained from Costar Corp. (Cambridge, MA, USA). The Millicell-ERS system was from Millipore Corp. (Bedford, MA, USA). Transport medium was Hank's balance salt solution (HBSS) from Invitrogen (CA, USA) supplemented with 10mM HEPES at pH7.4 (HBSS-HEPES).

10mM stock solutions of quinacrine and **16** were prepared in DMSO and further diluted to 10μM with the transport medium (HBSS-HEPES). The MDCK-MDR1 cell line was grown in DMEM supplemented with 10% fetal bovine serum, 100mg/L penicillin, and 100mg/L streptomycin at 37°C in an atmosphere containing 5% CO_2. For transport assay, cells with passage number 3-8 were seeded at a density of 300,000cells/well and grown for 4 days in 12-well Transwell® plates. Cell monolayers with transepithelial electrical resistance (TEER) values greater from 120-150Ωcm² were used for the experiment. On the day of assay, fresh medium was added to the cells. Two

hours later, they were washed twice and equilibrated with HBSS-HEPES medium for 30 minutes. 500µl of 10µM test compounds was added to the apical chamber and 1500µl of HBSS-HEPES was dispensed to the basolateral chamber for determining apical to basolateral (A→ B) transport. After 2h, cells were lysed with 600 µl of lysis solution (acetonitrile : water : formic acid = 70:30:0.1) for 10min and the cell debris removed by centrifugation (12,000x g, 5min, 4°C). Both chambers were thoroughly washed with 1ml of the same lysis solution and this wash solution was tested for presence of compounds adsorbing onto the plastic surface of the Transwell apparatus. Similarly, 500 µl of HBSS-HEPES was introduced to the apical chamber and 1500 µl of the test solution to the basolateral chamber to determine the basolateral to apical (B→A) transport. Aliquots (10 µl) were withdrawn from each chamber for quantification by LC/MS/MS. The experimental conditions were listed in Appendix 2.

The integrity of the monolayer was determined by TEER value and by monitoring the transport of Lucifer yellow, a fluorescent marker for paracellular transport. TEER value was calculated using the following equation:

TEER = ($R_{cell\ layer}$-R_{blank}) x A

Where $R_{cell\ layer}$ = Resistance (Ω) of the cell molayer

R_{blank} = Resistance (Ω) of the blank (insert without cells)

A = Effective surface area of the insert (1cm^2 for the 12-well insert)

Cell layers with TEER values in the range of 120-150Ωcm^2 were deemed suitable for the bidirectional assay.

Apparent permeability (P_{app}, cm/s) was calculated as: $P_{app} = \dfrac{J}{C_0} = \dfrac{V_r\ x\ C_r}{A\ x\ t\ x\ C_0}$

where J is the flux rate, C_0 is the initial concentration in the donor compartment, V_r is the volume of the receiver compartment at the end of the assay, C_r is concentration of compound in the receiver compartment at the end of the assay, A is the effective surface area of the insert, t is duration of the assay (2h).

Mass balance was determined as:

$$MB\,(\%) = \frac{C_{At}\ x\ V_A + C_{Bt}\ x\ V_B}{C_0\ x\ V_D}\,x100\%$$

where C_{At} is the concentration of compound in the apical compartment at the end of the assay, V_A is volume of the apical compartment, C_{Bt} is the concentration of compound in the basal compartment at the end of the assay, C_0 is the initial concentration in the donor compartment, V_D is the volume of the donor compartment.

3.2.6. Statistical analysis

Pearson and Spearman correlation analyses were carried out using SPSS version 13.0. (SPSS Inc., IL, USA). CLogP was determined by ChemDraw Ultra version 8.0 (CambridgeSoft Corporation, MA, USA). SlogP was determined using MOE software version 2009.10 (Chemical Computing Group, Quebec, Canada).

3.3. Results

3.3.1. Antiprion activity of compounds on cell-based models

Conventionally, prion assays detect amount of PrP[Sc] by SDS-PAGE immunoblotting by standard techniques.[92] Some groups have applied the dot-blot method to detect PrP[Sc] from cells plated in 96-well format assay to increase high throughput screening.[128,129] Blondel group has developed a cost-saving yeast-based assay to hasten the screening process.[130] However, this assay is not very popular due to skepticism regarding significant differences between yeast and mammalian cells. For the purpose of screening our compounds for antiprion activity, we applied the well-established and

widely employed Western blot method developed by Dr Doh-ura[41] eventhough it's very labour intensive. Therefore, it is easier to compare IC_{50} values of our compounds to others screened in the same assay format which have been reported in literature.

Cell lines used for screening antiprion activitites include mouse neuroblastoma N2a[41], SMB.s15 or ScGT1[129,131], mouse C1300 neuroblastoma-derived cell lines ScMNB[132]. Here we used an infected mouse neuroblastoma-derived cell-line, ScN2a (ATCC no: CCL131) was used to screen the antiprion activity of our compounds. This cell model comprises mouse neuroblastoma cells N2a that were stably infected with RML which was a mouse adapted scrapie strain.[133] Screening was also carried out on N2a cells infected with another mouse adapted scrapie strain 22L. A subclone of N2a (N2a#58) which overexpressed PrP^C by approximately 3-5 fold and stably infected with either RML or the human prion strain Fukuoka-1 was also used for screening. A compound that demonstrated activity on both cell models was deemed to be more promising than one whose activity was restricted on only one model. Table 3.1 summarizes the various cell-based models used in the investigation.

Table 3.1**:** Cultured cell models used for investigating antiprion activity of compounds

Type of cell	Prion Strain		
	RML[a]	22L[a]	Fukuoka-1[b]
Mouse neuroblastoma cells N2a	ScN2a	N167	-
Mouse neuroblastoma cells with PrP overexpression : N2a#58	Ch2	-	F3

[a]: RML[134] and 22L are mouse-adapted scrapie strains

Briefly, antiprion activity was determined by incubating the test compound with the infected cells until confluency was attained. The cells were then lysed to give lysates that were treated with proteinase K and analyzed for PrP immunoreactivity. PrP^C was readily digested by proteinase K and hence not detectable in the western blots. In contrast, PrP^{Sc} was resistant to enzymatic activity and would react sequentially with the prion antibody and secondary antibody to give a complex that was detectable by chemiluminescence. The signal levels of the immunoblots were reduced in the presence of a compound with antiprion activity and monitoring the intensities of the bands served as a means of quantifying activity. Figure 3.1 shows the results of representative immunoblots obtained at different concentrations (0-3 μM) of a representative active (compound **16**) and inactive (compound **47**) test compound.

Compound 16   Compound 47
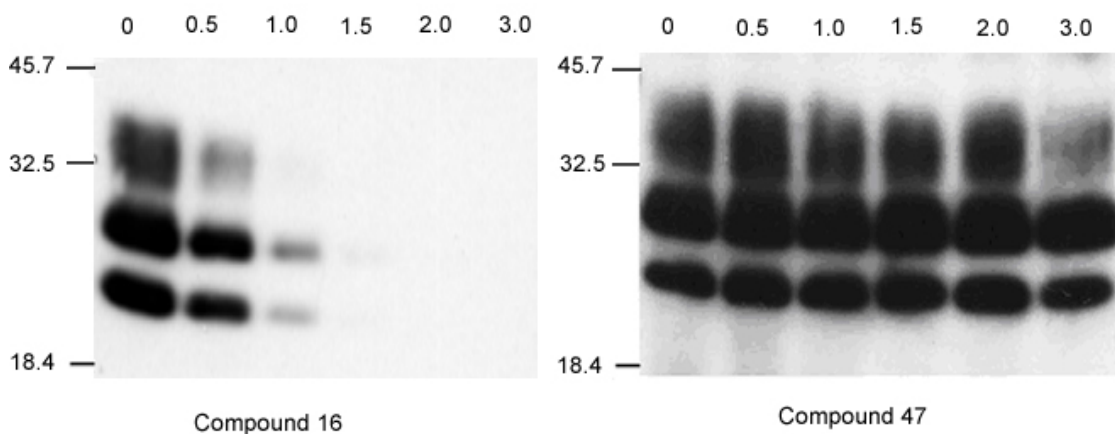
Figure 3.1: Raw immunoblots of PrP^{Sc} formation in the presence of compounds **16** and **47** in F3 cells. The top most line in each panel gives the test concentration (μM). The first column on the right ('0') represents cells that were treated with DMSO only.

Activity was quantified in terms of the EC_{50} which was the effective concentration of test compound required to reduce PrP^{Sc} content to 50% of untreated ScN2a cells. It was determined by measuring the intensities of the immunoreactive signals over a range of concentrations. The results were plotted to give a sigmoidal curve from which EC_{50} was obtained. A representative plot is given in Figure 3.2.
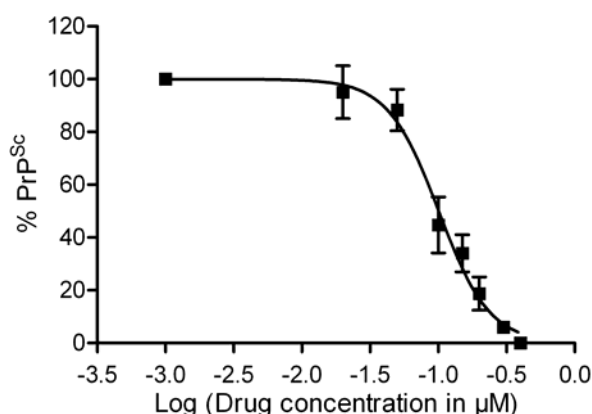
Figure 3.2: Plot of %PrP^{Sc} formation (equivalent to intensities of immunoreactive signals relative to untreated cells) in ScN2a cells treated with different concentrations of compound **16**. EC_{50} was obtained from the descending portion of the sigmoidal curve using a commercial software GraphPad Prism version 4.03 (GraphPad Software Inc., CA, USA)

Besides EC_{50}, two other parameters were concurrently determined for each test compound. These were full antiprion activity (FAA) and maximal tolerant concentration (TC). FAA was the estimated lowest concentration required to clear more than 99% of PrP^{Sc} content, while TC was the approximate highest concentration that had no effect on the viability of infected N2a cells. Ideally, an active antiprion agent should combine low EC_{50} and FAA values with a high TC. An approximate gauge of selective activity was

given by the ratio of TC to EC_{50}. In the first round of screening, 21 compounds from Groups 1-5 were evaluated on ScN2a cells.

Table 3.2: Antiprion activities of Group 1 compounds on the ScN2a cell line.
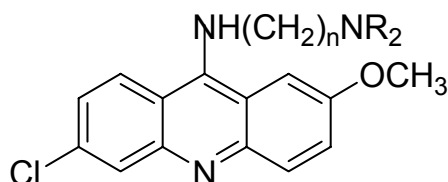
Compound	Substituent (R)	EC_{50} $(\mu M)^a$	FAA $(\mu M)^b$	TC $(\mu M)^c$	Ratio[d]
Quinacrine		0.23 (0.22, 0.25)	0.8	2.5	11
1	n=2, R=C_2H_5	0.021 (0.019, 0.023)	0.1	4.0	190
2	n=3, R=CH_3	0.11 (0.09, 0.13)	0.3	1.0	9
3	n=3, R=C_2H_5	0.14 (0.11, 0.17)	0.3	1.0	7
4	n=4, R=C_2H_5	0.15 (0.12, 0.19)	0.4	1.0	7

[a]: EC_{50} is the average of at least 3 independent determinations. 95% confidence intervals are given in the brackets.

[b]: Full antiprion activity is the estimated lowest concentration of test compound required for complete reduction of PrP^{Sc}.

[c]: Approximate maximal concentration that has no effect on the rate of cell growth to confluency.

[d]: Ratio = TC/EC_{50}.
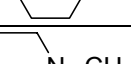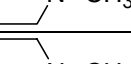
The positive control and reference compound, quinacrine was found to have an EC_{50} (0.23 μM) that was comparable to values reported by Doh-ura et al.[41] (EC_{50} 0.4 μM under similar experimental conditions) and Dollinger et al. [92] (EC_{50} 0.3 μM, incubation

period of 7 days). The Group 1 compounds were structurally similar to quinacrine which would explain why their EC_{50} values were generally comparable to quinacrine except for **1** (EC_{50} 0.021 µM) which was 10 times more potent. In **1**, the terminal N',N'-diethylamino functionality was separated from the 9-amino group on the acridine ring by two carbon atoms. Its outstanding activity may be influenced by the distance (2 carbon atoms) separating the two amino groups of the side chain since increasing the distance (as in **3** and **4**) resulted in a loss in activity. The substitution of the terminal amino function did not seem to be critical for activity as seen from the similar EC_{50} values of the N',N'-dimethylamino (**2**, EC_{50} 0.11 µM) and N', N'-diethylamino (**3**, EC_{50} 0.14 µM) analogs. The activity of **4** was noteworthy because it was structurally most alike quinacrine except for the absence of a chiral carbon in its side chain. That the EC_{50} value of **4** was very similar to quinacrine suggested that the loss of chirality did not adversely affect antiprion activity.

Table 3.3**:** Antiprion activities of Group 2 compounds on the ScN2a cell line.
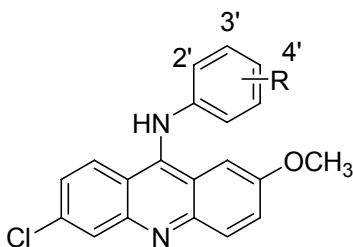
Compound	Substituent (R)	EC_{50} (µM)[a]	FAA (µM)[b]	TC (µM)[c]	Ratio[d]
5	2'-N(CH$_3$)$_2$	0.25 (0.22, 0.28)	0.8	5.0	20
6	3'-N(CH$_3$)$_2$	0.32 (0.26, 0.39)	None[e]	2.0	6
7	4'-N(CH$_3$)$_2$	0.51 (0.34, 0.77)	None[e]	2.0	4
8	3'-N(C$_2$H$_5$)$_2$	1.01 (0.85, 1.21)	2.5	3.0	3
9	4'-N(C$_2$H$_5$)$_2$	0.48	1.5	2.0	4

		(0.24, 0.93)			
10	3' —N (pyrrolidine)	1.06 (0.95, 1.18)	None^e	2.0	2
11	3' —N (piperidine)	0.18 (0.15, 0.22)	0.5	4.0	22
12	4' —N (piperidine)	4.24 (3.67, 4.90)	7.0	9.0	2
13	3' —N O (morpholine)	0.9 (0.75, 1.08)	None^e	3.0	3
14	4' —N O (morpholine)	1.28 (1.16, 1.42)	3.0	4.0	3
15	3' —N N—CH$_3$	0.29 (0.26, 0.33)	1.0	4.0	14
16	4' —N N—CH$_3$	0.10 (0.08, 0.12)	0.4	2.5	25

^{a}: EC$_{50}$ is the average of at least 3 independent determinations. 95% confidence intervals are given in the brackets.

^{b}: As defined in Table 3.1.

^{c}: As defined in Table 3.2.
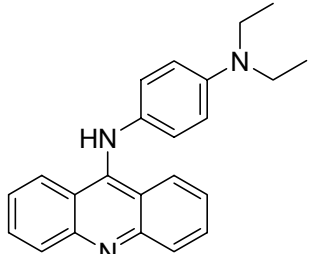
^{d}: Ratio = TC/EC$_{50}$.

^{e}: "None" denotes the compound has no effect at non-toxic concentrations.

The 12 compounds in Group 2 were characterized by the presence of a N9-(substituted phenyl) side chain with tertiary N,N-dialkylamino groups (**5-9**) or nitrogen based heterocycles (**10-16**) as substituents. The antiprion activities of this group of compounds were generally weaker than quinacrine and Group 1, with only two compounds (**11**, **16**) more potent than quinacrine and two others (**5, 15**) with comparable activity. The results showed that the following features were not critical in influencing activity, namely the type of substituent (basic heterocyclic ring or dialkylamino) attached to the ring and the position (ortho, meta, para) to which it was attached. Although the

most active compounds in Group 2 had basic heterocyclic substituents (piperidinyl in **11**, N-methylpiperazinyl in **16**), weak activities were also detected in members with similar groups (piperidinyl in **12**, morpholinyl in **14**).

Table 3.4: Antiprion activities of other compounds (Groups 3,4,5) on the ScN2a cell line.

Compound	Structure	EC_{50} $(\mu M)^a$	FAA $(\mu M)^b$	TC $(\mu M)^c$	Ratio[d]
32		0.42 (0.38, 0.46)	1.0	2.0	5
46		0.13 (0.12, 0.14)	0.4	4.0	31
47		None[e]	None[e]	2.5	
48		0.24 (0.16, 0.36)	None[e]	0.4	2

[a]: EC_{50} is average of at least 3 independent determinations. 95% confidence intervals are given in the brackets.

[b]: As defined in Table 3.1.

[c]: As defined in Table 3.2.

[d]: Ratio = TC/EC_{50}

[e]: "None" denotes the compound has no effect at non-toxic concentrations.

For the remaining compounds (Table 3.4), the most notable observation was the surprisingly good antiprion activity of **46** (EC_{50} 0.13 μM) in spite of the absence of any

substitution on its 9-amino functionality. Interestingly, removing the 6-chloro and 2-methoxy groups from the acridine ring of **46** gave **47** which was devoid of activity. While this may imply an important role for the acridine ring substituents, a comparison of the antiprion activities of the ring unsubsituted compound **48** (EC_{50} 0.24 µM) and its ring substituted analog **7** (EC_{50} 0.51 µM) showed otherwise.

Selected compounds from the first round of screening were shortlisted for evaluation on other cell models, namely N167, Ch2 and F3. They were **1, 16** and **46** which had good activities on the ScN2a cell model, and compounds that were comparable or weaker than quinacrine on ScN2a (**12, 15, 32**). The positive control quinacrine was included. The results are given in Table 3.5.

Table 3.5: Antiprion activities of quinacrine and selected compounds on different prion cell lines.

| Compound | Prion-infected cell lines | | | | | | | |
| | ScN2a | | N167 | | Ch2 | | F3 | |
	EC_{50} (µM) [a]	FAA (µM) [b]	EC_{50} (µM) [a]	FAA (µM) [b]	EC_{50} (µM) [a]	FAA (µM) [b]	EC_{50} (µM) [a]	FAA (µM) [b]
Quinacrine	0.23 (0.22, 0.25)	0.8	0.59 (0.42, 0.82)	None[c]	0.46 (0.40, 0.54)	2.0	1.88 (1.64, 2.16)	None[c]
1	0.021 (0.019, 0.023)	0.1	None[c]	None[c]	0.7 (0.41, 1.19)	3.0	None[c]	None[c]
12	4.24 (3.67, 4.90)	7.0	4.29 (3.90, 4.73)	None[c]	None[c]	ND[d]	ND[d]	ND[d]
15	0.29 (0.26, 0.33)	1.0	1.19 (0.92, 1.53)	3.0	0.38 (0.31, 0.48)	1.5	1.49 (1.34, 1.65)	3.5
16	0.10 (0.08, 0.12)	0.4	0.42 (0.41, 0.43)	1.5	0.22 (0.19, 0.27)	1.2	0.68 (0.59, 0.78)	1.5
32	0.42 (0.38, 0.46)	1.0	0.49 (0.44, 0.55)	1.5	0.41 (0.32, 0.51)	1.0	0.80 (0.64, 1.00)	None[c]

	0.13 (0.12, 0.14)	0.4	None[c]	None[c]	None[c]	None[c]	ND[d]	ND[d]
46								

[a]: Concentration (µM) required to reduce PrP^{Sc} content to 50% of untreated cells from 3 independent determinations. 95% confidence limits are given in thebracket.

[b]: As defined in Table 3.1.
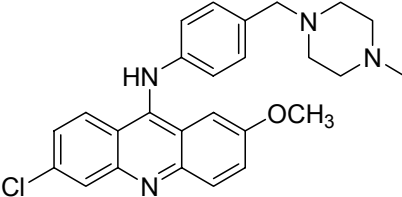
[c]: No effect at non-toxic concentrations.
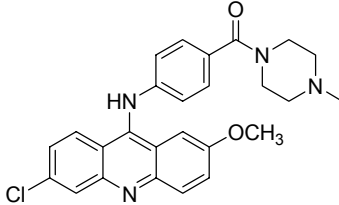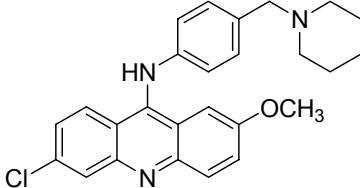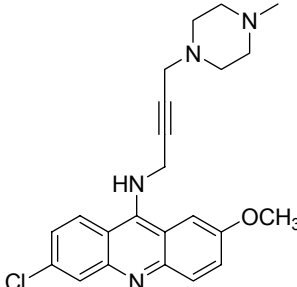
[d]: Not determined.

As mentioned earlier, a promising antiprion hit compound would be active on more than one cell model. In this regard, compounds **1, 12, 46** were not promising hits and only **15, 16** and **32** warranted further attention. Quinacrine was also active against the 4 cell models with potencies varying in the order of ScN2a (most potent) > Ch2 > N167 > F3 (least potent). No FAA value was obtained on N167 and F3 which meant that quinacrine was unable to completely eradicate PrP^{Sc} formation in these cells even when tested at the highest concentration that did not affect cell viability. Both N167 and F3 were derived from the N2a subclone that over-expressed PrP^C and this may account for their resistance to antiprion agents, as seen from the generally higher EC_{50} values on these models. Of the 3 hit compounds (**15**, **16**, **32**), **32** stood out in that it was equally active (EC_{50} 0.41-0.49 µM) on ScN2a, Ch2 and N167 cell models although it lacked an FAA value on F3. In deciding which compound to focus on for structural modification, **16** and **32** were selected because they were from different Groups and thus structurally dissimilar. **16** was preferred to **15** because it had a more desirable antiprion profile as seen from Table 3.5.

In the second phase of screening, 20 analogs related to **16** and **32** were evaluated on the ScN2a, N167 and F3 cell models. Ten analogs were prepared to interrogate the structure-activity relationship of **16**. EC_{50} and FAA values of 6 analogs are presented in Table 3.6.

Table 3.6: Antiprion activities of structurally related analogs of **16** on the ScN2a, N167, and F3 cell lines.

Cmpd	Structure	ScN2a cell line		N167 cell line		F3 cell line		TC (μM) [c]
		EC_{50} (μM) [a]	FAA (μM) [b]	EC_{50} (μM) [a]	FAA (μM) [b]	EC_{50} (μM) [a]	FAA (μM) [b]	
17		0.080, (0.063, 0.10)	1.0	0.96 (0.43, 2.11)	None[d]	None[d]	-	3
19		0.035 (0.025, 0.049)	0.1	None[d]	-	None[d]	-	5
22		0.060 (0.051, 0.069)	0.5	0.35 (0.22, 0.63)	2.0	0.86 (0.77, 0.96)	3.0	4

23		1.23 (1.09, 1.39)	5.0	4.20 (3.81, 4.63)	7.0	4.10 (3.49, 4.81)	None[d]	12
24		0.099 (0.085, 0.11)	0.5	0.51 (0.24, 1.09)	1.0	0.64 (0.52, 0.79)	3.0	5
42		0.027 (0.021, 0.036)	1.0	0.99 (0.86, 1.14)	3.0	None[d]	-	8

[a]: EC$_{50}$ values were obtained from at least 3 independent determinations. 95% confidence intervals are given in the brackets.

[b]: As defined in Table 3.2.

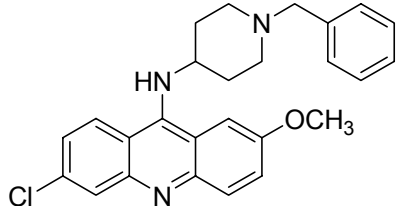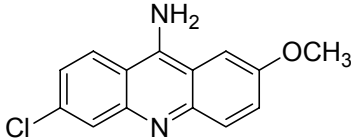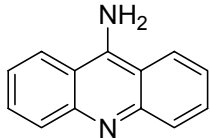[c]: Approximate maximal concentration that has no effect on the rate of ScN2a cell growth to confluency.

[d]: "None" means that the compound has no effect at non-toxic concentrations.
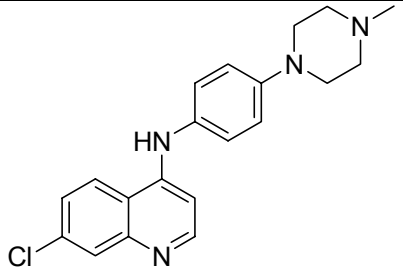
The N-methyl group of the piperazine ring in **16** was replaced by ethyl in **17** and methyl carbonyl in **19.** Both compounds were slightly more potent than **16** on ScN2a but failed to demonstrate activity on F3. It was noted that the terminal nitrogen in piperazine was now part of an amide moiety in **19** and hence not basic. But this was unlikely to have affected the activity of **19,** noting that **17** in which the terminal nitrogen of piperazine retained basic character had almost the same activity profile as **19**.

In **22**, **23** and **24**, a carbon spacer was inserted between the phenyl ring and the nitrogen heterocyle. In **22** and **24**, the carbon spacer was a methylene group and both compounds were comparable to **16** in their activities on F3. In **23**, a carbonyl group was inserted between the phenyl and 4-(1-piperazinyl) rings, thus introducing an amide bond between the 2 rings. Accordingly, the terminal basic ring (N-methylpiperazine or piperidine) of **22** and **24** would have greater conformational flexibility than the corresponding ring in **23**. It was tempting to attribute the significantly poorer activity of **23** to a loss of rotational flexibility in its side chain. However other factors (lipophilicity, H bonding) may be involved as well. While a case may be made for retaining flexibility in the linker between the two rings, the more important finding to emerge from **22**, **23** and **24** was their consistent activity against all 3 cell models. Thus separating the 2 rings by a carbon spacer generally had a more positive effect on activity while changes made to the terminal nitrogen of piperazine (**17**, **19**) were less favorable.

Compound **42** was unlike the others listed in Table 3.6 in that it had no phenyl ring. In its place was a but-2-ynyl moiety which was used here as a phenyl isostere. The effect of this replacement was not encouraging. It was inactive on F3 although it was more potent than **16** on ScN2a.

Table 3.7: Antiprion activities of compounds **25**, **45**, **54**, and **60** on the ScN2a, N167, and F3 cell lines.

Compound	Structure	ScN2a cell line		N167 cell line		F3 cell line		TC $(\mu M)^c$
		EC_{50} $(\mu M)^a$	FAA $(\mu M)^b$	EC_{50} $(\mu M)^a$	FAA $(\mu M)^b$	EC_{50} $(\mu M)^a$	FAA $(\mu M)^b$	
25		0.54 (0.36, 0.81)	None[d]	None[d]		None[d]		5
45		2.51 (2.11, 3.00)	5.0	None[d]		None[d]		8

54		0.082 (0.058, 0.11)	1.0	None[d]		None[d]		>10
60		0.14 (0.08, 0.25)	1.0	0.53 (0.41, 0.68)	2.0	2.04 (1.35, 3.07)	None[d]	10

[a]: EC$_{50}$ values were obtained from at least 3 independent determinations. 95% confidence intervals are given in the brackets.

[b]: As defined in Table 3.2.

[c]: Approximate maximal concentration that has no effect on the rate of ScN2a cell growth to confluency.

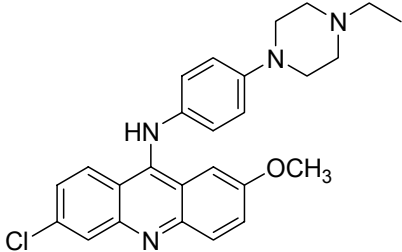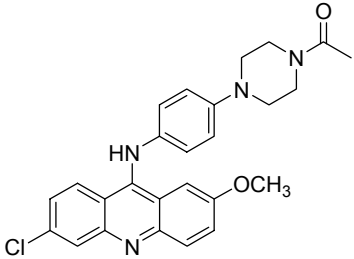[d]: "None" means that the compound has no effect at non-toxic concentrations.

Table 3.7 represents the remaining 4 compounds that were structural analogs of **16.** It was noted earlier that **46** which had only a 9-amino group demonstrated surprisingly good activity on ScN2a (EC$_{50}$ 0.13 μM). Here, it was shown that successive substitution of the 9-amino functionality with N-phenyl in **25** and N-methyl-N-phenyl in **45** resulted in a progressive loss in activity (ScN2a). The observation that no F3 activity was observed for all 3 compounds (**25**, **45**, **46**) implied that having basic substituents on the phenyl was a necessary (but still not sufficient) requirement for F3 activity. The need to keep the NH on the 9-amino functionality may also be important but required confirmation.

Compounds **54** and **60** were evaluated to provide insight on the contribution of the substituted acridine ring for antiprion activity. The 6-chloro-2-methoxyacridine ring was replaced by 6-chloro-1,2,3,4-tetrahydroacridine in **54** and 7-chloroquinoline in **60**. These replacements resulted in a significant reduction in toxicity as seen from the higher concentrations (≥ 10 μM) required to adversely affect the viability of uninfected N2a cells. Of the two compounds, the quinolinyl analog **60** gave a better antiprion profile.

Twelve analogs of **32** were evaluated to provide insight on the structure-activity relationship of **32** (Tables 3.8, 3.9, 3.10). Compounds **33-36** were modified to include a para substituent (drawn from each of the four quadrants of the Craig Plot) on the benzyl sidechain of **32**. As seen from Table 3.8, only the p-methyl analog **33** retained activity on the 3 cell models. The methyl substituent in **33** was electron donating (-σ) and lipophilic (+π) and the combination of these properties may be reason why it had a better antiprion profile than the other p-substituted analogs **34-36**.

Table 3.8: Antiprion activities of compounds **32-36** on the ScN2a, N167, and F3 cell lines.

Cmpd	R	ScN2a cell line		N167 cell line		F3 cell line		TC
		EC_{50} (μM) [a]	FAA (μM) [b]	EC_{50} (μM) [a]	FAA (μM) [b]	EC_{50} (μM) [a]	FAA (μM) [b]	(μM) [c]
32	H	0.42 (0.38, 0.46)	1.0	0.49 (0.49, 0.55)	1.5	0.80 (0.64, 1.00)	None	2
33	CH_3	0.15 (0.12, 0.19)	3.0	0.62 (0.49, 0.80)	1.0	0.63 (0.53, 0.75)	3	5
34	Cl	0.28 (0.24, 0.33)	1.0	0.34 (0.15, 0.78)	3.0	None[d]	-	12
35	OCH_3	0.082 (0.063, 0.11)	1.5	0.52 (0.47, 0.58)	2.0	None[d]	-	10
36	CN	0.55 (0.49, 0.63)	1.0	0.14 (0.081, 0.25)	1.0	None[d]	-	5

[a]: EC_{50} values were obtained from at least 3 independent determinations. 95% confidence intervals are given in the brackets.

[b]: As defined in Table 3.2.
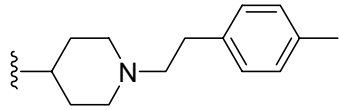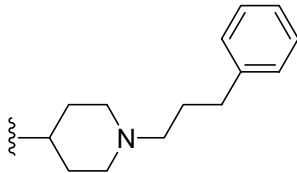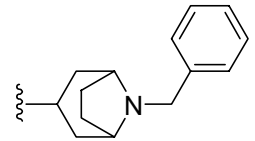
Table 3.9: Antiprion activities of compounds **32**, **37**, **38**, **41**, **43** on the ScN2a, N167 and F3 cell lines.

Cmpd	R	ScN2a cell line		N167 cell line		F3 cell line		TC (μM)[c]
		EC_{50} (μM)[a]	FAA (μM)[b]	EC_{50} (μM)[a]	FAA (μM)[b]	EC_{50} (μM)[a]	FAA (μM)[b]	
32		0.42 (0.38, 0.46)	1.0	0.49 (0.49, 0.55)	1.5	0.80 (0.64, 1.00)	None[d]	2
37		0.13 (0.10, 0.16)	0.5	0.23 (0.12, 0.42)	1.0	0.19 (0.14, 0.26)	2.0	2

89

#	Structure	EC$_{50}$		EC$_{50}$		EC$_{50}$		
38		0.076 (0.058, 0.10)	1.0	0.30 (0.14, 0.66)	1.0	0.69 (0.39, 1.19)	3.0	3
41		0.093 (0.027, 0.32)	1.0	0.32 (0.19, 0.54)	1.0	1.04 (0.77, 1.40)	3.0	4
43		0.054 (0.043, 0.067)	2.0	0.35 (0.21, 0.61)	1.0	0.54 (0.48, 0.60)	1.5	2

[a]: EC$_{50}$ values were obtained from at least 3 independent determinations. 95% confidence intervals are given in the brackets.

[b]: As defined in Table 3.2.

[c]: Approximate maximal concentration that has no effect on the rate of ScN2a cell growth to confluency
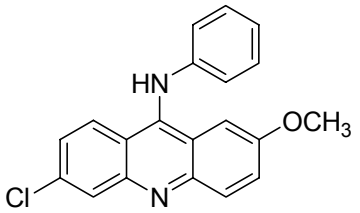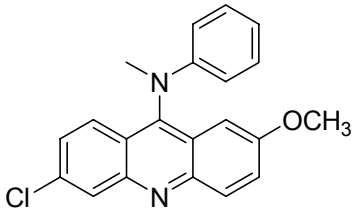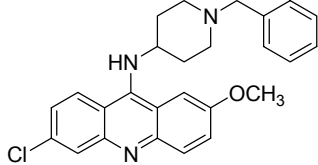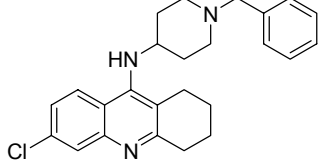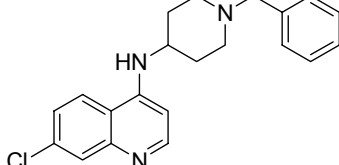
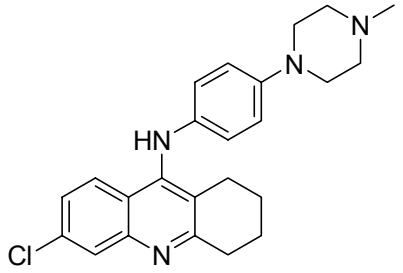[d]: "None" means that the compound did not have the effect at non-toxic concentrations.

The effect of lengthening the carbon spacer between the piperidine and phenyl rings was investigated in **37** and **41**. The results showed that both the 2-carbon (**37**) and 3-carbon (**41**) homologs retained activity on the 3 cell models but with better activity found in the 2-carbon homolog **37**. In fact, **37** was the most potent compound against F3 (EC_{50} 0.19 µM) identified in this investigation and it was able to clear PrP^{Sc} in F3 at a reasonably low concentration of 2 µM. Attaching a para-methyl group to the phenyl ring of **37** caused some loss in activity against F3. These results suggested that there was an optimal length for the carbon spacer separating the two rings possibly due to the need to maintain lipophilicity and/or flexibility of the side chain within certain desired limits.

Replacing the piperidine ring of **32** with an 8-azabicyclo[3.2.1]octane ring gave **43**. This modification restricted the conformational flexibility of the piperidine ring. Antiprion activity of **43** showed a modest improvement compared to **32** across all 3 cell models. On the other hand, **43** had the lowest FAA value (1.5 µM) among the test compounds. Thus, restricting the conformational flexibility of the piperidine ring did not adversely affect activity.

Table 3.10 gives the activities of the 6-chloro-1,2,3,4-tetrahydroacridine (**51**) and 6-chloroquinoline (**57**) analogs of **32.** The low toxicities of both compounds against non-infected N2a cells were again observed but this time, both the tetrahydroacridine and quinoline analogs had comparable antiprion profiles.

Table 3.10: Antiprion activities of compounds **32**, **51**, **57** on the ScN2a, N167, and F3 cell lines.

Cmpd	Structure	ScN2a cell line		N167 cell line		F3 cell line		TC
		EC_{50} (μM) [a]	FAA (μM) [b]	EC_{50} (μM) [a]	FAA (μM) [b]	EC_{50} (μM) [a]	FAA (μM) [b]	(μM) [c]
32		0.42 (0.38, 0.46)	1.0	0.49 (0.49, 0.55)	1.5	0.80 (0.64, 1.00)	None	2
51		0.54 (0.36, 0.80)	1.0	0.42 (0.32, 0.57)	3.0	1.19 (0.85, 1.67)	5.0	5
57		0.15 (0.13, 0.18)	1.0	0.23 (0.16, 0.33)	2.0	1.20 (0.88, 1.64)	3.0	>10

[a]: EC_{50} values were obtained from at least 3 independent determinations. 95% confidence intervals are given in the brackets.

[b]: As defined in Table 3.2.

[c]: Approximate maximal concentration that has no effect on the rate of ScN2a cell growth to confluency
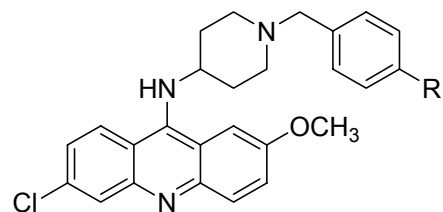
[d]: "None" means that the compound did not have the effect at non-toxic concentration.

3.3.2. Effect of lipophilicity on antiprion activity

There are two basic functionalities in quinacrine, namely the acridine N (pK$_a$ 8.2) and the side chain diethylamino group (pK$_a$ 10.2).[136] At physiological pH, it would exist predominantly in the di-protonated state (*ca* 86%) and with lesser amounts of the mono-protonated species. The ClogP of quinacrine (6.72) provides an estimate of the lipophilicity of the non-protonated (free base) species while SlogP (3.97) gives the lipophilicity of the fully protonated quinacrine.[137]

Most of the Group 1, 3 and 4 compounds have pK$_a$ values that fall within the range of quinacrine. The Group 2 compounds have a different pK$_a$ profile because the side chain basic group was directly attached to the 9-(N-phenyl) ring and would thus be a weaker base. Like aromatic amines, the pK$_a$ of this nitrogen may be in the range of 5-6. Thus, assuming a pK$_a$ of 6 for the side chain amino function, di-protonated, mono-protonated and free base species will be present at physiological pH, with the di-protonated species likely to be present in smaller amounts than the other two species. Unlike di-protonated quinacrine, the mono-protonated species of Group 2 would be protonated at the ring nitrogen and not at the less basic side chain aniline-like nitrogen.

Clog P and SlogP values have been estimated for the test compounds and are listed in Appendix 3. Neither parameter correctly reflected the lipophilicity of the compound at pH 7 but they provided a back-of-the-envelop means of ranking compounds in terms of their lipophilic character. Thus, for the same side chain present in **1** (N,N-diethylaminoethyl), the tetrahydroacridinyl analog (**50**, Group 6) was less lipophilic, and the 7-chloroquinolyl analog (**56**, Group 7) even less so. This was observed for other side chains as well (ClogP, SlogP of **32** > **51** > **57**; SlogP of **16** > **54** > **60**).

An attempt was made to correlate EC_{50} values from ScN2a and F3 models with the lipophilicity of the compounds. A significant correlation was observed only with lipophilicity (expressed as either ClogP or SlogP) and EC_{50} of F3. The Spearman coefficients were - 0.660 ($p < 0.05$, 2-tailed, n =15) for Clog P and -0.704 ($p < 0.05$, 2-tailed, n = 15) for SlogP. No correlation with lipophilicity could be established for EC_{50} from ScN2a. The relationship between EC_{50} (F3) and ClogP (or SlogP) was inverse, implying that more potent compounds were more lipophilic. The interpretation of this relationship was difficult because the predominant state (ionized or non-ionized) of the compound was not represented by either ClogP (free base) or SlogP (fully protonated species). If the putative target was intracellular, only the non-protonated form (free base) was the one to transverse the membrane barrier to reach the site of action. Lipophilicity would then be better represented by ClogP and the correlation with EC_{50} reflected the accessibility of the compound to the target site. It must then be assumed that in spite of the small amounts of non-protonated species present, the equilibrium between the species was adjusted to give more of the non-protonated from as it was transferred across the barrier. The correlation with SlogP was harder to explain and may have arisen because ClogP and SlogP were significantly correlated to each other when evaluated by either Pearson (coefficient : 0.708, $p < 0.05$, 2 tailed, n= 60) or Spearman (coefficient: 0.711, $p < 0.05$, n=60) bivariate correlation analysis.

3.3.3. Evaluation of binding affinities of test compounds to human PrP121-231 by surface plasmon resonance

Surface plasmon resonance (SPR) was used to evaluate the direct binding affinity of the compounds for PrP^C and to assess the correlation between antiprion activities and binding affinities. A truncated human prion protein comprising the carboxy-terminal polypeptide (residues 121-231) (hPrP121-231) was used for SPR measurements. It was preferred to the full length protein because of its greater solubility and stability under the experimental conditions. The protein was immobilized on a CM5 sensor chip (carboxymethylated dextran) to give a density of approximately 3000 response units (RU). Sensorgrams were obtained for the test compounds which were evaluated at a fixed concentration of 50 μM. The sensorgrams provided information on the rates at which the compound associated and dissociated from the immobilized peptide. Binding capacity was reflected by the maximum response unit (RU) obtained at the end of the association phase and quantified in terms of %RU$_{max}$, This value represented the percentage of the theoretical maximum response assuming a 1:1 stoichiometry for the interaction and was normalized to the molecular weights of both the peptide and test compound. Representative sensorgrams are given in Figure 3.3.
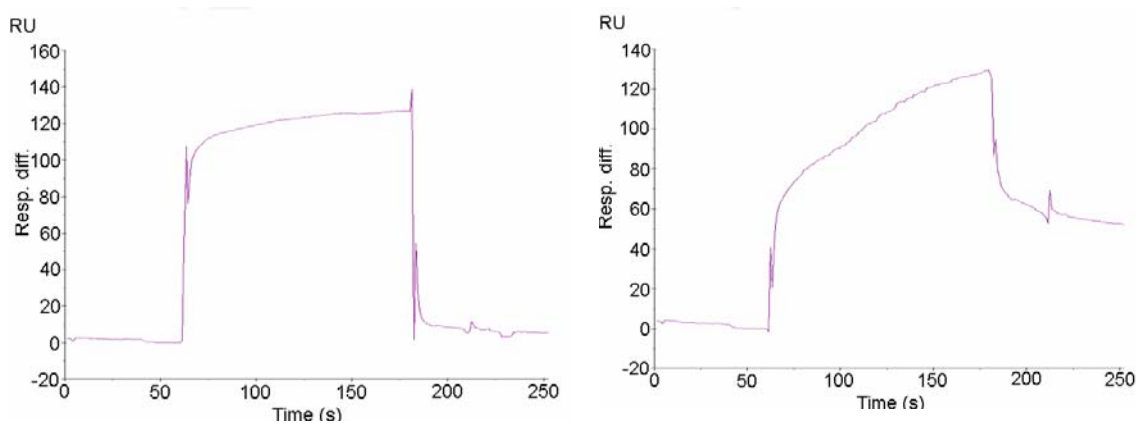
Figure 3.3: Interactions of compounds with hPrP121-231 (A) Typical sensorgram of fast on/fast off compounds (B) Typical sensorgram of slow on/slow off compounds. Spikes

seen at the start and end of injections were due to a slight time delay in the reference cell

and appeared when reference subtraction was carried out.

The left panel (A) in the figure shows a sensorgram of a typical compound that

associates rapidly with the immobilized peptide and dissociates equally fast on washing.

The maximum RU attained for this compound (quinacrine) was 101 units, equivalent to

$\%RU_{max}$ of 87. The right panel B shows the sensogram of a compound that binds slowly

and does not dissociate completely from the peptide as seen from the failure of the

descending portion of the curve to reach the base line. The $\%RU_{max}$ of this compound

(**54**) was found to be 127. Of the 38 (including quinacrine) evaluated, the majority (n =

34) had profiles that were similar to A. A few compounds (n = 2) showed an intermediate

profile in which the association and dissociation patterns were slower than A but faster

than B (for example, **34, 42)**.

Table 3.11: Binding response of test compounds (n =38) to hPrP121-231 using Surface

Plasmon Resonance and EC_{50} for ScN2a and F3 cell lines.

Cmpd	Binding response (RU)[a]	$\%RU_{max}$	EC_{50} on ScN2a cell line (µM)	EC_{50} on F3 cell line (µM)
23	248.06±21.69	231.6	1.23	4.10
19	224.94±1.82	210.0	0.04	None[b]
22	215.02±9.72	207.1	0.06	0.86
17	184.44±24.10	194.2	0.08	None[b]
4	174.15±7.28	177.6	0.15	ND[c]
37	169.48±4.04	173.9	0.13	0.19

60	125.71±10.25	165.4	0.14	2.04
2	132.16±3.75	163.6	0.11	ND[c]
47	72.09±11.09	162.2	None[b]	ND[c]
3	140.18±1.73	162.1	0.14	None[b]
35	91.8±18.78	159.8	0.08	None[b]
42	165.21±13.24	158.7	0.03	None[b]
1	115.54±18.11	153.4	0.02	ND[c]
38	169.58±1.43	147.5	0.08	0.69
24	162.7±7.12	144.4	0.10	0.64
46	83.05±17.25	139.0	0.13	ND[c]
51	92.1±7.18	138.2	0.54	1.19
9	139.08±29.38	129.4	0.48	ND[c]
54	113.75±14.38	127.2	0.08	None[b]
15	145.25±22.05	122.4	0.29	1.49
16	130.18±15.06	120.3	0.10	0.68
41	109.6±1.64	114.8	0.09	1.04
57	93.85±19.64	113.7	0.15	1.20
36	129.97±7.89	109.2	0.55	None[b]
6	94.13±11.20	107.2	0.32	ND[c]
48	100.89±1.99	102.6	0.24	ND[c]
7	99.77±4.10	100.6	0.51	None[b]
13	68.08±1.08	99.2	0.90	ND[c]

34	94.54±0.33	98.3	0.28	None[b]
8	97.69±11.88	97.7	4.24	ND[c]
Quinacrine	101.48±14.31	87.3	0.23	1.88
56	64.01±2.98	85.5	1.56	None[b]
50	75.81±10.88	82.2	0.51	None[b]
14	63.78±9.07	72.5	1.28	ND[c]
33	85.19±6.63	69.8	0.15	0.63
25	56.38±7.53	67.3	0.54	None[b]
32	67.54±10.30	65.4	0.42	0.80
45	35.00±9.48	43.2	2.51	None[b]

[a]: Binding response was obtained from the maximum response at the end of the association phase from at least 3 experiments on two different chips.

[b]: Inhibition of PrP^{Sc} formation was not observed up to the maximal tolerant concentration.

[c]: Compound was not tested on the F3 cell line.

Table 3.11 lists the binding response (RU), $\%RU_{max}$ and cell-based (ScN2a, F3) antiprion EC_{50} values of the test compounds. The $\%RU_{max}$ values are listed in order of decreasing magnitude. A few compounds (**5, 10, 11, 12, 25, 43**) were not evaluated because of inadequate solubility at the test concentration (50 μM). As seen from the Table 3.11, RU values ranged from 35 to 248. Nearly ¾ of the test compounds had $\%RU_{max}$ values that were greater than 100. Different threshold RU values had been cited to indicate binding to the immobilized protein. Heal *et al.*[138] considered compounds to

bind to PrP^C if they gave RU values of 3.5 and above while Hosokawa-Muto et al.[120] considered an RU value greater than 30 units to be indicative of strong binding. Both studies used the same Biacore CM5 sensor chip and either the full length protein (Heal et al.)[138] or the truncated mouse PrP^C (mPrP^C 121-231) (Hosokawa et al.).[120]

In this investigation, the %RU$_{max}$ of quinacrine was 87. A lower value (37) was reported by Touil et al.[121] for quinacrine, possibly because of differences in the nature of the protein (truncated human PrP^C fragment of unknown length but likely to be a C-terminal fragment) and other experimental conditions. Quinacrine was classified as a weak to moderate binder by Touil et al. [114] According to their criterion, compounds with very high %RU$_{max}$ values ($\geq$ 130) were multiple site binders while strong binders were compounds with values ranging from 50-129. Weak to moderate binders had values that were lower than 50.[121] A 1:1 stoichiometry was assumed for compounds that were not multiple site binders.

Based on these criterion set by Touil et al.[114] and using the values of quinacrine for comparison (87 in the present study versus 37 in the reported study, approximate 2-fold difference), the following %RU$_{max}$ values were proposed for multiple site, strong and weak to moderate binders: Multiple site binders : %RU$_{max}$ > 260; Strong binders : %RU$_{max}$ between 100 – 259; Weak to moderate binders %RU$_{max}$ < 100. The distribution of compounds based on their binding affinities is given in Table 3.12.

As seen from Table 3.12, none of the test compounds were identified as multiple site binders. The majority (n = 30) were strong binders. It was notable that all the Group 1 compounds (dialkylaminoalkyl side chain attached to 9-amino function) were strong binders in contrast to quinacrine (weak to moderate binder), in spite of their close

structural similarities. The Group 7 compounds (4-amino-7-chloroquinolines) were also strongly represented among strong binders. Among the moderate to weak binders (n=7), four of them had the same benzylpiperidinyl side chain (**32, 33, 51, 57**), including **32** which was a potent hit compound. The other hit compound **16** (Group 2) had stronger binding affinities. These observations were in line with those reported by others regarding the effect of relatively minor changes in structure on SPR responses.[100]

Table 3.12: Breakdown of test compounds based on Groups and %RUmax values

Group Number	Number of Strong binders (%RU$_{max}$ between 100 - 259)[a]	Number of Weak to Moderate binders (%RU$_{max}$ < 100) [a]
1	4 out of 4	0 out of 4
2	10 out of 14	4 out of 14
3	5 out of 8	3 out of 8
4	2 out of 3	1 out of 3
5	2 out of 2	0 out of 2
6	2 out of 3	1 out of 3
7	2 out of 3	1 out of 3

[a]: Based on values given in Table 3.12.

A cursory examination of compound potencies (EC$_{50}$ values on ScN2a cells) and binding affinities expressed in terms of %RU$_{max}$ suggested that more potent compounds were associated with greater binding affinities. For example, there were 9 compounds listed in Table 3.11 with EC$_{50}$ values (ScN2a) less than 0.1 µM and all had %RU$_{max}$ that

exceeded 100. To determine if this correlation is statistically significant, a bivariate Spearman correlation analysis was carried out on $\%RU_{max}$ values and EC_{50} values from ScN2a. Indeed, a significant correlation was observed (Spearman rho = -0.635, p <0.0001 (2-tailed), n=37) and the same was observed when analysis was carried out with EC_{50} (ScN2a) values and RU (Spearman rho = -0.573, p <0.0001, n=37). However, no correlation was noted for EC_{50} from F3 and RU or $\%RU_{max}$, possibly because of the small number of compounds (n=15) involved. RU and $\%RU_{max}$ values were not correlated to ClogP values of test compounds.

3.3.4. Evaluation of selected compounds for effects on the expression of total and cell-surface PrP^C by uninfected mouse neuroblastoma cells (N2a)

Having shown that almost all the compounds were strong binders of PrP^C, investigations were carried out to determine if these compounds interfered with the production of PrP^C. Interference with the synthesis of PrP^C is one way by which antiprion activity may occur. Thus, selected compounds were investigated for their effects on the expression of total PrP^C and cell-surface PrP^C.

Quinacrine and **16** were investigated for their effects on the expression of total PrP^C by non-infected N2a. Briefly, N2a cells were incubated with different concentrations of test compound for 72 hours, after which the cells were lyzed and the supernatant was analyzed for the presence of PrP^C by immunoblotting. The results are shown in Figure 3.4. It can be seen that both quinacrine and **16** did not reduce the intensity of bands that were characteristic of PrP^C even at concentrations exceeding their

EC$_{50}$ values. The effect of quinacrine was anticipated as it is known not to interfere with the synthesis of PrP^C.

Compound **16** (μM)   Quinacrine (μM)
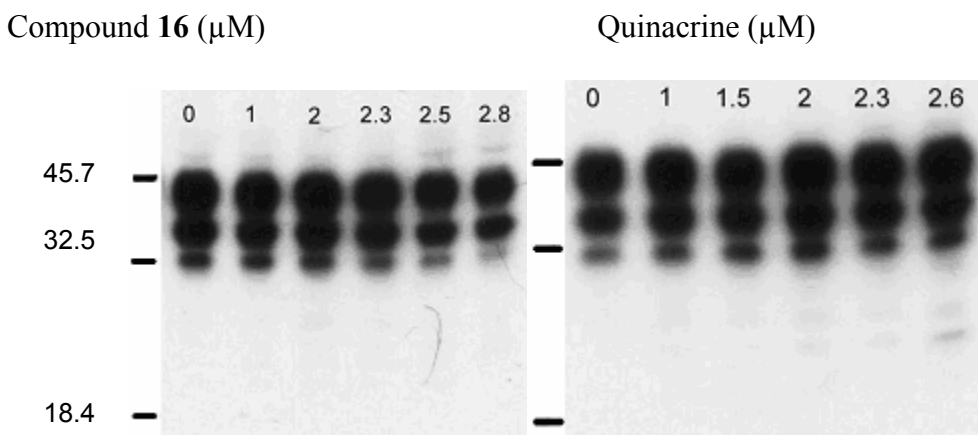
Figure 3.4: Effects of **16** and quinacrine on the total prion protein PrP^C expression. Bars on the left indicate molecular sizes of 45.7kDa, 32.5kDa, and 18kDa. The values at the top indicate the concentrations (μM) of test compounds.

PrP^C is a glycoslyated protein which is held on the cell surface by a glycophosphatidyl inositol anchor.[139] Its presence is detected by reaction with fluorescent antibodies and quantifying the intensity of fluorescence by flow cytometry.[140] This was investigated for N2a cells that were exposed to test compound as well as control cells that were left untreated. The distribution of treated and untreated (control) cells would show a close overlap if the test compound did not interfere with PrP^C expression. If the compound reduced PrP^C expression, less fluorescent antibodies would be attached to the cell surface resulting in lower fluorescence and a left shift (indicating lower fluorescence intensity) in the distribution of treated cells. As seen in Figure 3.5, overlapping curves were observed for treated and non-treated cells tagged with the fluorescent antibodies (curves 3 and 4 for each panel). Thus, quinacrine, **16** and **32** did not affect the expression

of cell surface PrP^C by normal N2a cells. It was noted that curves 1 and 2 which represented treated and non-treated cells tagged with isotype matched immunoglobulins (non-fluorescent) respectively did not show a strong overlap. This was attributed to the intrinsic fluorescence of the test compounds. They may be adsorbed on to PrP^C or the membrane surface and were not washed out during the sample preparation process. The greater displacement of curve 2 for **32** was probably due to the stronger intrinsic fluorescent property of **32**.

(a) Quinacrine at 0.4µM   (b) Compound **16** at 2µM   (c) Compound **32** at 2µM

Fluorescence intensity in log scale
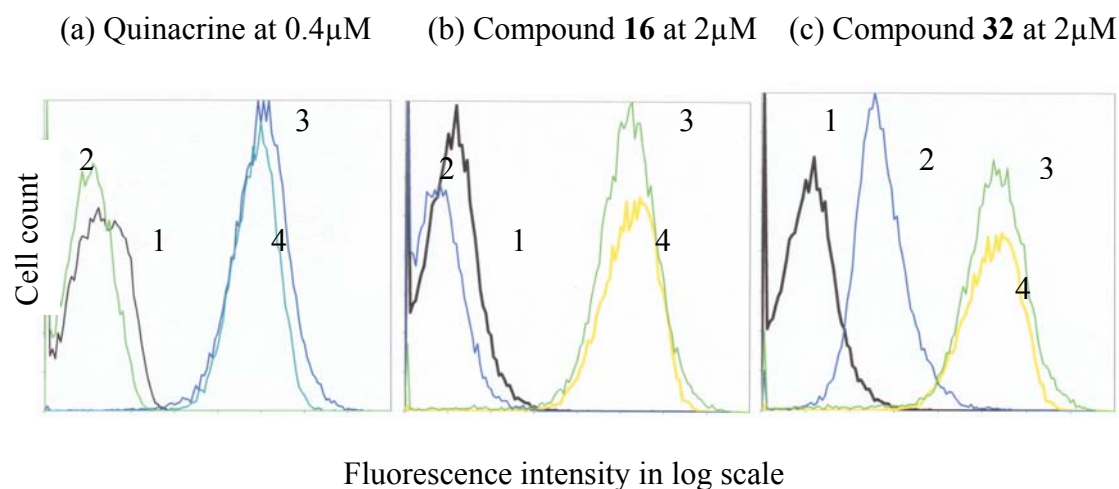
Figure 3.5: Retention of mAb-PrP^C complexes on the cell surface of N2a cells in the presence of (A) quinacrine (0.4 µM) and (B) compound **16** (2 µM) (C) compound **32** (2µM). Line 1 : N2a cells not exposed to test compound, immunostained with isotype-matched control immunoglobulin instead of anti-PrP antibody. Line 2: N2a cells exposed to test compound, immunostained with isotype-matched control immunoglobulin instead of anti-PrP antibody. Line 3: N2a cells not exposed to test compound, immunostained with anti-PrP antibody. Line 4: N2a cells exposed to test compound, immunostained with anti-PrP antibody.

3.3.5. Evaluation of the potential of test compounds to transverse the blood brain barrier

The parallel artificial membrane permeation assay (PAMPA) was introduced by Kansy[141] to predict the oral absorption of early discovery drug candidates and has since been developed into a high throughput technique by the pharmaceutical industry. An equivalent assay (PAMPA-BBB) has been developed to evaluate blood brain barrier permeabilities of target compounds.[122] Both assays operate on the same principle except that in the PAMPA-BBB assay, the barrier is made up of porcine brain lipids in dodecane instead of phospholipids for the PAMPA assay. Briefly the method involved measuring the rate at which the test compound diffused across the lipid layer separating the donor compartment (comprising of test compound at 30 or 50 μM in phosphate buffer, pH 7.4) from the acceptor compartment filled with the same buffer solution. After 10 hours, the amount of test compound in the two compartments were determined by ultra-violet spectroscopy and calculated to give the effective permeability (P_e). Validation of the method was made by determining P_e values of reference compounds (quinidine, caffeine, verapramil) and confirming that they fell within the reported values.[122] It should be noted that the assay does not provide any mechanistic insight as to how the compound moves across the barrier. It was assumed that compounds transversed the membrane by passive diffusion. Table 3.13 provides the P_e values of selected antiprion compounds. Also included are the P_e values of other compounds (**18**, **20**, **21**, **39**, **40**) that were synthesized but not evaluated for antiprion activity.

Table 3.13: Permeability values and LogP values

Compound	P_e^a (x10^{-6} cm/s)	R (membrane retention)[a]	LogP[b]
Quinidine	11.48±1.19	0.06±0.03	2.48
Caffeine	2.46±0.33[c]	0.01±0.01	-0.80
Verapamil	18.45±2.26[c]	0.26±0.10	5.69
Quinacrine	19.30±2.52	0.24±0.06	5.02
1	20.98±1.01	0.45±0.01	4.14
2	13.34±2.20	0.12±0.06	3.57
3	21.98±4.56	0.30±0.11	4.25
4	16.37±2.89	0.23±0.03	4.70
5	10.27±5.11	0.41±0.16	5.72
6	2.51±0.09	0.48±0.09	5.72
7	1.68±0.81	0.77±0.08	5.72
8	5.60±1.83	0.41±0.04	6.40
9	4.26±0.49	0.55±0.07	6.40
10	3.98±1.54	0.40±0.05	6.04
15	4.56±0.35	0.67±0.05	5.48
16	8.13±2.75	0.54±0.09	5.48
17	6.13±2.03	0.49±0.21	5.81
18	6.51±0.23	0.47±0.07	5.06
19	8.79±0.37	0.34±0.16	4.75
20	10.29±0.06	0.36±0.06	6.72

21	6.07±1.78	0.45±0.05	6.64
24	5.28±0.34	0.75±0.05	6.11
34	15.53±0.85	0.45±0.18	5.70
35	7.54±2.47	0.68±0.10	5.02
36	9.15±1.11	0.71±0.05	5.18
37	7.68±2.69	0.63±0.14	5.43
38	7.39±1.70	0.65±0.13	5.91
39	7.98±0.85	0.63±0.15	5.98
40	11.90±2.62	0.66±0.10	5.30
42	11.52±1.24	0.38±0.04	3.49
43	8.31±1.28	0.45±0.10	5.42
46	14.81±4.63	0.44±0.21	3.17
48	12.47±2.19	0.54±0.30	5.96

[a]: Values are presented as mean ± standard deviation

[b]: LogP values were determined by ChemDraw Ultra 7.0

[c]: P_e values for caffeine and verapramil were reported to be as 1.3×10^{-6} cm/s and 16×10^{-6} cm/s respectively.[122]

The P_e values of the compounds ranged from 22×10^{-6} cm/s to 1.7×10^{-6} cm/s. The average P_e values of the major groups represented in Table 3.13 were computed to give an idea of permeability changes across these groups, not withstanding the fact that not all compounds in each group were evaluated for their P_e values. It is seen that the Group 1 compounds (**1-4**) had higher mean P_e values (18.2×10^{-6} cm/s) than Group 2 (**5-**

24, 6.0 x 10^{-6} cm/s) or Group 3 (**34-40**, 9.6 x 10^{-6} cm/s) compounds. Greater permeability was thus found among functionalized acridines that had 9-dialkyaminoalkylamino side chains (Group 1) compared to those with functionalized 9-phenylamino (Group 2) or 9-(N-benzylpiperidin-4-yl)amino (Group 3) side chains.

Di *et al.*[122] proposed a means of classifying compounds as "CNS +" (high brain penetration) or "CNS –" (low brain penetration) based on PAMPA-BBB results. CNS + compounds had P_e values > 4.0 x 10^{-6} cm/s, CNS – compounds had P_e values < 2.0 x 10^{-6} cm/s while CNS+/- compounds (uncertain BBB permeation) had values between 2.0 x 10^{-6} cm/s and 4.0 x 10^{-6} cm/s. Since the present method was based on the reported protocol[122] and the P_e values of standard compounds (caffeine, verapamil) determined here corresponded closely to those indicated in the report, it was reasonable to use the reported threshold values to deduce the likely brain permeation properties of the listed compounds. Thus, except for some Group 2 compounds (**6**, **7**, **10**) which had P_e values < 4.0 x 10^{-6} cm/s, the remaining compounds had P_e values that were within the "CNS+" range.

The retention of the test compound by the barrier that separated the donor and acceptor cells was also monitored. Compounds with high permeabilities were found to have low membrane retention and vice versa. Thus, the Group 1 compounds which had the highest P_e values in Table 3.13, had low mean retention values (0.28 ± 0.14) while Group 2 and 3 compounds with lower P_e values were retained to a greater degree in the membrane. While the high level of membrane retention would hamper diffusion across the barrier, it may also function as a "depot" from which compound is released into the interior of the cell over time.

Having shown that the test compounds had permeabilities that were indicative of good penetration across the CNS, a representative compound (**16**) was evaluated to determine if it was a substrate of the efflux transporter Pgp. The Pgp transporter was involved in the efflux of quinacrine across the BBB[142] and contributed to its low levels of accumulation in the brain.[95,99] Ghaemmaghami *et al.*[99] showed that when administered to mice in which the multidrug resistant (mdr) genes responsible for expression of Pgp were removed, levels of quinacrine in the brain were nearly two orders of magnitude higher than those in normal mice. In this part of the investigation, **16** which showed promising antiprion activity in cell models, was investigated to determine if it was a Pgp substrate. As shown in Table 3.13, **16** had a P_e value of 8.13 x 10^{-6} cm/s which was indicative of good permeability into the brain. Briefly, two cell lines were used for this purpose, namely Madin-Darby Canine Kidney (MDCK) cells that were stably transfected with human MDR1 cDNA so that they had higher levels of Pgp (MDCK-MDR1) and wild-type/parental MDCK cells (MDCK-WT) that had normal levels of Pgp. Figure 3.6 shows the immunoblots from the cell lines showing the over-expression of Pgp in the same MDCK-WT and MDCK-MDR1 cells used for this bidirectional assay.

MDCKII/MDR1   MDCKII/WT

Pgp (170kDa)

β-actin

Figure 3.6: Over-expression of Pgp in MDCKII-MDR1 cells compared to its wild type MDCKII-WT. Blot was done by the labmate Sim Hong May.[127]

The cells are seeded on the insert (porous filter support) of a Transwell® cell culture chamber. When confluent, the cells covered the surface of the support to form an intact layer with minimal "gaps" in between cells that permitted the test compound to move unimpeded across the filter. To ensure the tightness of the cell layer, the transepithelial electrical resistance (TEER) of the cell layer was monitored during the period of its growth. In these experiments, the cell layer was considered suitable for experimentation when TEER values were in the range of 120-150Ωcm^2. There were two chambers in the Transwell ®, namely the apical (A) chamber which was the compartment in contact with the apical ("top") surface of the cell layer and the basolateral (B) chamber which was in contact with the basolateral ("bottom") surface of the cell layer (Figure 3.7). The test compound in buffer was placed in the A chamber and the rate at which it transversed the cell layer into the B chamber (containing only buffer) was monitored and expressed as the apparent permeability in the A to B direction ($P_{A \to B}$). The movement of the compound in the opposite direction ($P_{B \to A}$) was also monitored. If the compound was a Pgp substrate, the 2 permeability values would differ, with $P_{B \to A} > P_{A \to B}$. Compounds with $P_{B \to A}$ / $P_{A \to B}$ ("efflux ratio") that exceeded 2 were deemed to be substrates of efflux proteins.[105]
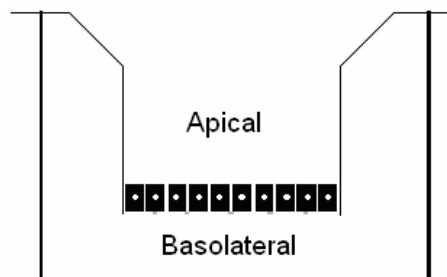
Figure 3.7: Transwell apparatus comprises of 2 compartments designated as apical and basolateral chambers separated by a layer of confluent cells.

Table 3.14 gives the $P_{B \to A}$ and $P_{A \to B}$ values of quinacrine and **16** from MDCK WT and MDCK-MDR1 cells. The efflux ratio of quinacrine in the MDCK-MDR cells was almost 4 times greater than the ratio from parental MDCK cells in keeping with the Pgp-substrate property of quinacrine. In the case of **16**, the efflux ratios in MDCK-MDR1 and MDCK-WT cells were 2.4 and 1.2 respectively. The 2 fold difference in efflux ratios of **16** suggested that it was a weaker Pgp substrate compared to quinacrine.

Mass balance measurements showed that most of quinacrine and **16** (*ca* > 50%) could be accounted in experiments involving B→A diffusion but not in the A→ B direction. The poor mass balance in the A→B direction was attributed in part to the significant amount of compounds retained by the membrane and to a lesser degree by adsorption to the walls of the cell chamber. Pgp is asymmetrically expressed in cells, with higher levels found in the apical surface than the basolaterial surface. Thus the high level of membrane retention observed in the A→B direction (60-80%, except quinacrine in MDCK-MDR1 cells) may implicate binding of the compound to Pgp or other proteins.

Table 3.14: Permeability, efflux ratio, mass balance, cell retention and % adsorption onto the Transwell apparatus of Quinacrine and

16 across MDCK-WT and MDCK-MDR1 cell monolayers.

Compound	Cell line	P_{app} (x10^{-6}cm/s)[a]		Efflux ratio P_{app}(B-A)/ P_{app}(A-B)	Mass balance (%)[a]		Cell retention (%)[a]		Adsorption on Transwell (%)[a]	
		A-B	B-A		A-B	B-A	A-B	B-A	A-B	B-A
Quinacrine	MDCK-WT	2.89±0.83	3.45±1.25	1.2	14.6±2.3	51.0±14.4	80.2±9.5	27.7±1.5	5.3±5.0	3.2±2.8
Quinacrine	MDCK-MDR1	1.32±0.05	6.70±1.14	5.1	34.8±10.3	75.8±17.8	35.5±6.2	24.5±7.3	5.5±3.6	3.9±3.1
16	MDCK-WT	0.29±0.04	0.34±0.12	1.2	11.3±1.5	75.3±7.0	66.4±29.0	27.5±12.3	11.4±8.9	3.5±2.5
16	MDCK-MDR1	0.14±0.02	0.34±0.10	2.4	12.6±10.9	73.0±13.9	67.0±14.4	44.2±12.8	6.1±3.7	3.1±2.5

[a]: Values were presented as Mean ± Standard deviation from three independent experiments.

3.4. Discussion

The ScN2a cell model is widely used for the *in vitro* screening of potential antiprion agents and many promising antiprion agents like quinoline and acridine derivatives[123] have been identified using this cell model. Here, it was noted that while many compounds demonstrated good antiprion activity on ScN2a, they were generally less active or inactive against cell models derived from other species of scrapie proteins. For example, **1** which had the lowest EC_{50} on the ScN2a model failed to demonstrate the same level of activity on Ch2, N167 and F3 models. In this investigation, promising antiprion leads were compounds that retained activity against ScN2a as well as other cell models, in particular, the F3 model. By these criteria, only 15 compounds had EC_{50} values against F3. These EC_{50} values were also higher than those obtained for other cell models infected with the mouse prion proteins. Structural requirements for activity against F3 did not always coincide with those for activity against ScN2a. Notably, lipophilicity in terms of ClogP (and SlogP) was significantly correlated to F3 EC_{50} values but not ScN2a EC_{50} values.

The first round of screening identified 2 promising hits (**16** and **32**) which had submicromolar EC_{50} values on 3 cell models (ScN2a, N167, F3). Both compounds were closely matched in terms of antiprion activity and equivalent to quinacrine in terms of EC_{50} values (< 2 μM). Structural modifications of **16** and **32** were carried out in an effort to improve antiprion activity and to provide insight into the structure-activity relationship. In this regard, modifications on **32** gave better outcomes. Two analogs of **32** (**37** and **43**) were identified which had

lower EC_{50} values on F3. Moreover, unlike **32** which had no FAA value on F3, these were available for both **37** and **43** which meant that they could eliminate PrP^{Sc} in F3 at non-toxic concentrations. In the case of **16**, modification of its structure was less promising and no analog with an improved antiprion activity was identified. Compounds **22** and **24** are possibly the most promising members to emerge but they did not offer any significant advantage in terms of antiprion profile over **16**.

An analysis of structure-activity trends showed the presence of a well defined SAR which has the following key features.

(i) Of the 7 groups, Groups 2 and 3 gave the most promising compounds, as exemplified by **16** (from Group 2) and **32** (from Group 3). Both groups were characterized by the presence of a substituted phenyl or piperidinyl ring at the 9-amino functionality of the acridine ring. There was a clear preference for these motifs over that of a dialkylaminoalkyl side chain (present in Group 1 and quinacrine) at the same position.

(ii) A basic substituent on the 9-(N-phenyl) substituent was necessary if a broad spectrum of antiprion activity was desired. Thus, **25** which did not have a basic substituent attached to the phenyl ring was moderately active on ScN2a but inactive on N167 and F3. A single basic functionality was probably adequate for activity. This was deduced from **24** which had a piperidinyl side chain but was nonetheless as potent as its piperazine analog **22**. More examples were seen in the moderately good antiprion activities (ScN2a) of **10**-**14**, all of which have monobasic heterocyclic rings.

(iii) In both hit compounds (**16**, **32**), two rings (phenyl and N-containing heterocyle) were either linked directly (**16**) or via a carbon atom (**32**). There was a trend towards improved activity when an additional carbon atom was inserted between these rings so that they were joined by a longer and more flexible linker. This was seen from **22** and **24** where the two rings are separated by a methylene moiety and in **37** where the rings were linked via a 2 carbon atom linker. The improvement in antiprion activity may be due to the increase in the number of rotatable bonds leading to greater conformational flexibility. The concurrent increase in lipophilicity may have also contributed to the improved activity profile.

(iv) Lower toxicities and slightly poorer antiprion profiles were found for the tetrahydroacridine analogs in Group 6 and quinoline analogs in Group 7. The loss in antiprion activity was dependent on the substituent attached to the 9-amino/4-amino group. From the limited examples, the loss in activity (F3) was less in compounds with the 1-benzylpiperidin-4-yl side chain of **32** (**51**, **57**) than those with the (4-methylpiperazin-1-yl) phenyl side chain of **16** (**51**, **57**).

Surface Plasmon Resonance measurements showed that almost all the compounds had strong binding affinities to a truncated C-terminal human PrP^C fragment. There was also a statistically significant correlation between binding affinities to PrP^C and EC$_{50}$ values from ScN2a, but not F3 probably because of the smaller number of compounds with EC$_{50}$ values on this cell model. Many of the compounds exhibited greater binding affinities than quinacrine on this platform but may have a different mode of interaction with the prion protein. Among these

compounds were those in Groups 1 and 7. Of the 2 potent analogs **16** and **32**, only **16** was classified as a strong binder. Interestingly, **32** and other analogs with the same side chain as **32** (benzylpiperidinyl) were weak binders. The correlation between EC_{50} (ScN2a) and binding affinities was reassuring but should not discount the involvement of other targets for these compounds. Besides showing that the target compounds investigated here have good binding affinities to PrP^C, it was seen that active analogs like **16** and **32** did not alter total cellular and surface PrP^C levels .Such a reduction is desirable as it leads to lower PrP^{Sc} levels.

The PAMPA-BBB assay was used to assess the potential of the present series of compounds to transverse the blood brain barrier by passive diffusion. The magnitude and narrow 20-fold range of the apparent permeability values (P_e) point to moderate permeabilities within this series. Many of the more potent leads identified in this study (**16**, **37**, **38**) were less permeable than quinacrine in this assay but the difference was no more than 3 fold and for **16**, may be compensated by its poorer Pgp substrate properties compared to quinacrine. Based on these preliminary investigations, the present series of target compounds had good potential to transverse the BBB. The contrasting effects of lipophilicity on antiprion activity (ScN2a) and membrane permeability (P_e) point to the need to strike a balance with regards to the lipophilicity of the compound. A compound that was highly lipophilic may have good antiprion acitivity but this may be annulled by poor permeability across the blood brain barrier.

3.5. Conclusion

Forty 9-aminoacridine analogs that were structurally related to quinacrine were evaluated for antiprion activity on a battery of cell-based models for prion infection. Almost all the compounds demonstrated activity on the ScN2a model, with EC_{50} values ranging from 0.03 μM to 4 μM (150 fold variation). A smaller number of compounds (15) were active on the F3 model and their EC_{50} values (0.2 μM to 4 μM) spanned a narrower 20 fold range. The most promising compounds were found in Groups 2 (**22**, **23**) and 3 (**37**, **43**). They have submicromolar EC_{50} values on 3 cell models (ScN2a, N167, F3) and were able to completely eradicate PrP^{Sc} in the more resistant F3 model at low concentrations (FAA ≤ 3 μM). Analysis of SAR revealed well defined trends for activity which suggested a common mode of interaction. This may involve the ability of the compounds to bind to PrP^{C} as revealed by SPR measurements. The potential of the 9-aminoacridine analogs to transverse the blood brain barrier was comparable to that of quinacrine based on their apparent permeability constants (P_e) from the PAMPA-BBB assay and one active analog (**16**) showed a lower tendency to function as a Pgp substrate. In conclusion, the 9-aminoacridine template was a promising template from which potential antiprion agents with good in vitro potencies and drug-like properties for BBB permeability may be derived.

Chapter 4: Protection of mouse hippocampal HT22 cells against glutamate induced cell death

4.1. Introduction

The glutamate-induced programmed cell death of mouse hippocampal HT22 cells, also known as oxytosis, is one of the most robust models available to characterize the oxidative mechanisms involved in neuronal degeneration.[143] HT22 cells are immortalized neuronal cells with no ionotropic glutamate receptors that could mediate excitotoxicity which involves the activation of glutamate receptors, entry of calcium ions into cells and death due in part to the generation of mitochondria-derived reactive oxygen species (ROS).[144-147] In oxytosis, the death of HT22 cells in the presence of high glutamate concentrations (*ca.* 100 μM) was triggered by diminished cystine uptake into the cell via the cystine/glutamate antiporter which carries cystine into the cells at the expense of the outflow of glutamate. The decreased cystine uptake led to the depletion of intracellular glutathione (GSH), a cysteine-containing tripeptide vital for cell survival because of its ability to act as an enzyme cofactor and antioxidant. As the intracellular GSH level diminished, there was a biphasic increase in ROS levels which was initially linear and coupled to the fall in GSH levels. This was followed by an exponential rise in ROS not linked to diminishing GSH levels. It was proposed that this second phase of ROS production was related to the activation of 12-lipooxygenase which induced an exponential burst of ROS from the mitochondria by an unknown mechanism.[148] A sharp rise in intracellular

calcium levels caused by the activation of soluble guanylate cyclase then followed,[149] triggering the massive cell death that characterizes oxytosis which morphologically resembles necrosis (mitochondrial swelling, cytoplasmic vacuolation) but is more alike apoptosis in terms of biochemical changes (requirement for RNA and protein synthesis).[143] Most discussions on glutamate-induced cell death focus on the excitotoxicity pathway but oxytosis is also relevant because many neurons do not have ionotropic glutamate receptors but are still killed by excess glutatmate in trauma and ischemia.[150]

Many compounds are reported to protect cells from oxytosis by interrupting with one or more of the three distinct events involved in the cell death cascade, namely preventing the depletion of GSH, interfering with ROS production and inhibiting calcium influx.[143] Flavonoids and tyrphostins were interesting examples of such compounds in that fairly small modifications in the parent scaffold resulted in analogs that have defined effects on oxytosis. For example, a series of flavonoids were categorized as those acting like quercetin, galangin or flavonol.[151] Quercetin-related compounds upregulated the activity of the enzyme (γ-glutamylcysteine synthetase), galangin-related compounds were antioxidants and reduced accumulated intracellular ROS while flavonol-related compounds were proposed to interfere with the influx of calcium into the cell. In the same way, changes in the substitution of the phenyl ring of tyrphostins which were derivatives of benzylidene malononitrile, resulted in compounds that interrupted specific steps in the oxytosis pathway.[152] Some tyrphostins increased the basal level of GSH, others acted as antioxidants and eliminated ROS that

accumulated as a result of glutamate treatment and yet others which were not antioxidants or did not reduce GSH levels, were mitochondrial uncouplers, collapsing the mitochondrial membrane potential and thus reducing the generation of ROS from the mitochondria.

This chapter describes the ability of the synthesized compounds to protect HT22 cells from glutamate-induced cell death. The investigations were prompted by reports that melatonin[153] and N,N-diphenyl-p-phenylenediamine (DPPD)[154] protected HT22 cells from glutamate challenge. Herrera and co-workers[153] proposed that melatonin targeted mitochondria to prevent ROS while the protective effect of DPPD was attributed to the modulation of gene expression leading to the production of proteins with presumably protective properties. Structurally, melatonin and DPPD have in common an NH group with limited or no basic properties. In melatonin, the NH is part of the indole ring while in DPPD, the NH is flanked by two aromatic rings and thus, weakly basic (Figure 4.1). A structure-activity investigation showed that 4-aminodiphenylamine retained neuroprotective activity but not phenylene diamine or aniline, thus emphasizing the need to retain the NH between two aromatic rings for activity. Herrera *et al.* reported that tryptamine and 5-methoxytryptamine, like melatonin, protected HT22 cells against glutamate challenge. However, the observation that N-acetyltryptamine failed to demonstrate activity diminished somewhat the importance of the indole NH, although it was the only shared feature among the active indole analogs.

Of the synthesized compounds, those in Group 2 (and selected members of groups 5, 6 and 7) were structurally related to DPPD in having an NH linked to two aromatic rings. This motif was absent from the other groups. Hence, it was conceivable that the Group 2 compounds would protect HT22 cells from glutamate induced cell death due to the presence of the aromatic ring-NH-aromatic ring motif while compounds in other groups that lack this structural motif would have weaker activity or none at all. To test this hypothesis, selected compounds from Groups 1-7 that had structurally diverse side chains were evaluated for their ability to protect HT22 cells from 5mM glutamate challenge. In the case of compounds identified to have protective activity, further investigations were carried out to determine if protection was due to GSH depletion, preventing ROS accumulation or interfering with calcium influx.
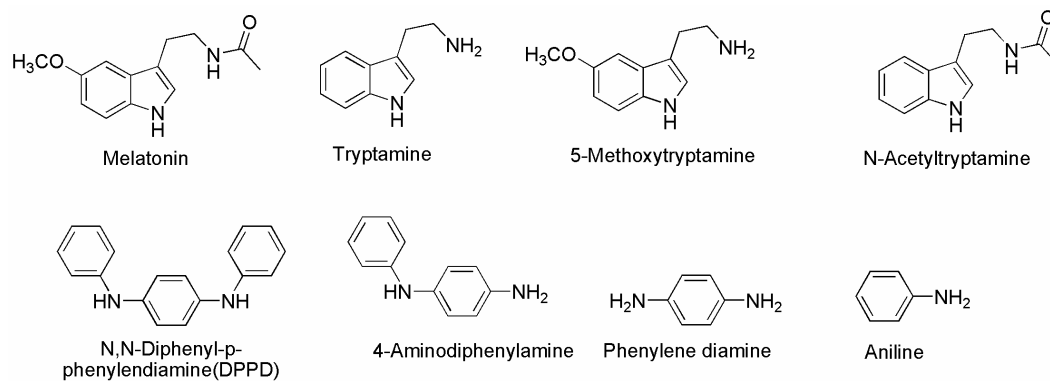
Figure 4.1: Structures of melatonin, tryptamine and its derivatives, DPPD and related compounds.

4.2. Experimental methods

4.2.1. Materials:

The following chemicals were purchased from Sigma-Aldrich Chemical Company (MO, USA): 2',7'-Dichlorofluorescein diacetate (H$_2$DCF) , propidium iodide (PI), sulfosalicyclic acid, reduced glutathione (GSH), bovine serum albumin (BSA), baker's yeast glutathione reductase (E.C. no: 1.6.4.2), potassium persulfate 99.99%, 6-hydroxy-2,5,7,8-tetramethylchroman-2-carboxylic acid 97% (trolox), 2,2'-azino-bis(3-ethylbenzthiazoline-6-sulphonic acid) (ABTS), 3-(4,5-dimethylthiazol-2-yl)-2,5-diphenyltetrazolium bromide (MTT), (2,4-dinitrophenyl) thiocyanate (DNTB), nicotinamide adenine dinucleotide phosphate (NADPH), glutamic acid, penicillin, and streptomycin. Fluo-3 AM and dihydrorhodamine 123 (D123) were obtained from Molecular Probes (Eugene, Oregon, US). Lysis buffer containing 20mM HEPES, 150mM NaCl, 1.5mM MgCl$_2$, 1mM EDTA, 1%v/v TritonX-100 and protease inhibitor, Bradford protein dye were purchased from Bio-Rad Laboratories (CA, USA). Dulbecco's Modified Eagle's medium (DMEM) was prepared by the Media Preparation Unit of National University Medical Institutes, Singapore). Fetal bovine serum (cat. no 10270-106) and trypsin 0.5% 10x with EDTA 4Na (cat. no 15400-054) were obtained from Gibco (Auckland, New Zealand). Dimethyl sulfoxide was purchased from Merck (NJ, US). Phosphate buffered saline (PBS, pH 7.4, cat. no BUF-2040-10x1L) from 1st Base (Singapore) was diluted to 1x using deionized water. PBS 1x contained 10 mM phosphate buffer, 137 mM NaCl and 2.7 mM KCl.

4.2.2. Cell Culture

HT22 cells were kindly provided by Dr David Schubert (The Salk Institute for Biological Studies, La Jolla, CA, USA). The cells (passages 3-15, taking passage number 1 for cells received from Dr Schubert) were grown on tissue culture flasks (Nunclon ™ Δ Surface, Thermo Fisher Scientific, Roskilde, Denmark) in DMEM supplemented with 10% FBS, penicillin 100mg/L, stryptomycin 100mg/L and glucose 4.5g/L. When the cells reached approximately 50% confluency, they were trypsinized and seeded into appropriate receptacles at specified cell densities and grown for 24 hours in a humidified incubator (5% CO_2, 37°C) for the various experiments. Bradford protein assay kit (cat. no #500-203) was obtained from BioRad Laboratories (CA, US).

4.2.3. Cytotoxicity Assay

HT22 cells were seeded into 96 well plates at a density of 5000 cells/well in the above mentioned DMEM (100 μl/well) and incubated for 24 h, 37°C and 5% CO_2. Stock solutions of test compounds were prepared in DMSO and serially diluted with media. A stock solution (10 mM) of glutamic acid was prepared in DMEM and diluted two fold to give a final concentration of 5 mM in each well. A control well contained only glutamate (5 mM) while test wells contained glutamate (5 mM) and test compound (at a specified concentration). For the latter, the two fold dilution of the glutamate stock solution was made with media containing test compound. Another set of wells contained only test compound at various concentrations. In all cases, the final concentration of DMSO was kept at no more than 0.1% v/v per well. After 24 h at 37°C (5% CO2), the medium in

each well was removed by decanting, PBS was carefully added to wash the cells and 100 µl of MTT solution (0.5 mg/ml prepared in PBS 1x) was added to each well for 3 h at 37^oC, 5% CO_2. Thereafter, the supernatant from each well was removed and DMSO (150µl) was added to dissolve the purple formazan crystals. The plates were incubated for an additional 30 minutes before UV absorbance readings were taken at 590 nm on a microtitre plate reader (Infinite^{TM} 200 series, Tecan Instruments Inc., NC, USA).

Cell viability at a stated concentration of test compound was expressed as follows:

% Cell viability = [A $_{Test Compound}$ - A $_{No cells}$] / [A $_{Cells Only}$ + A $_{No Cells}$] x 100

where A is the average absorbance readings of sample wells.

EC_{50} values were determined from logarithmic plots of % cell viability versus concentration using Prism GraphPad Version 4.03 (San Diego, CA, USA) with constraints set at 0-100%. At least 3-7 determinations were made for each compound at different times to give mean values. EC_{50} values were obtained for each compound in the presence of 5 mM glutamate to assess neuroprotective potential and in the absence of glutamate to determine its intrinsic cytotoxicity to HT22 cells.

4.2.4. Determination of glutathione content

5 x 10^5 HT22 cells were seeded in 100mm culture dishes and incubated for 12 h (37^oC, 5% CO_2). They were then treated with 5mM glutamate with/without

test compound (final concentration of 1 μM) or were left treated (control) for another 12h. Each treatment arm was tested in duplicate on separate plates, with one plate used for GSH determination and another for protein determination so that total GSH levels could be normalized for total protein content.

For GSH determination, the cells were washed twice with ice-cold PBS, trypsinized and centrifuged (2,000x g, 5 min, 4°C). The supernatant was discarded and cell pellets were lysed with 1 ml of 3%w/v sulfosalicyclic acid in PBS, vortexed and centrifuged (12,000x g, 5min, 4°C) to remove precipitated proteins. GSH content of the supernatant was determined by the method described by Tietze[155] with some modifications. The assay was carried out on a 96-well plate. In each well was added 140 μl of 0.3 M NADPH, 40μl of sample supernatant (diluted with sulfosalicyclic 3% in PBS if necessary) and 5 μl of 50units/ml glutathione reductase. The plate was warmed to 30°C and 20 μl 6 mM DNTB was added and quickly placed on the plate reader (Infinite™ 200 series, Tecan Instruments Inc., NC, USA) to monitor the change in UV absorbance reading at 412nm for 10 minutes at 1 minute intervals. In this assay, GSH oxidized DTNB to give the yellow colored 5-mercapto-2-nitrobenzoate anion. The oxidized GSSG (originally present in sample as well as derived from GSH oxidation) was reduced by glutathione reductase to give GSH which reacted with DTNB. The recycling process greatly improves assay sensitivity and the GSH content was proportionate to the rate at which the yellow benzoate anion was generated. For samples with low GSH content, the rate of anion formation was slow and monitored over 10 min while in cases where GSH content was high, the sample was diluted to obtain

absorbance readings within the linear range. To determine the GSH content, a standard curve (rate of anion formation versus concentration) was constructed using known amounts of GSH (1-100 µg/ml) under similar assay conditions. Each test compound was evaluated in 3 separate determinations.

For protein determination, the cells were washed twice with ice-cold PBS, trypsinized and centrifuged (2000x g, 5 min, 4°C). The supernatant was removed and cell pellet was treated with 400 µl lysis buffer, mixed and incubated at 4°C for 30min. The tubes were centrifuged at 12,000x g for 5 min to remove insoluble proteins and debris. Protein content of the supernatant was determined with the BioRad Bradford protein kit.[156] Briefly, 160 µl of the supernatant was thoroughly mixed with 40µl Bradford dye for at least 5min but not more than 30 min. Absorbance readings were taken at 595 nm. The protein content was determined from the standard curve prepared with bovine serum albumin. The total glutathione content in each sample was expressed as concentration of glutathione in nmoles per mg protein.

4.2.5. Determination of Trolox Equivalent Antioxidant Capacity (TEAC) values

TEAC measures the ability of a compound to quench free radicals (antioxidant capacity) compared to that of a standard antioxidant, trolox which is a water soluble vitamin E analog. TEAC values were measured using the ABTS decolorisation assay as described by Re *et al.*[157] The method was modified to accommodate the use of 96 well plates rather than cuvettes. Briefly, the

quenching of the stable radical cation of ABTS (ABTS$^{\bullet+}$) was accompanied by the loss of its deep purple colour (monitored at 734 nm) over time. The rate at which this loss occurred was compared to that observed under similar conditions with trolox and given as a ratio (TEAC). A stock solution of ABTS radical cation (ABTS$^{\bullet+}$) was obtained by reacting 7mM ABTS and 2.45mM potassium persulfate in PBS and allowed to stand in the dark at room temperature for 12-16 hours. This solution was diluted with PBS before each experiment to give an absorbance of 0.700±0.020 at 734nm. Test compounds were prepared in stock solutions of 2mM in DMSO. Aliquots of test compound stock solution (diluted with PBS where necessary) were dispensed into the 96-well plates and topped up with the diluted ABTS solution to 200 μl to give the desired concentration of test compound. For example, a concentration of 10 μM was obtained by adding 1 μl of test compound stock solution (2 mM) and 199 μl of the diluted ABTS solution. Absorbance was measured on a plate reader (Benchmark Plus, BioRad, PA, US) at 734 nm over 10 minutes at 1 minute interval at 30°C. The plate was shaken vigorously (but carefully) before each reading. The assay was performed in the dark or dim light. Sample containers were wrapped in aluminum foil to protect from light.

The degree of quenching was determined from the equation:

$$\text{Degree of quenching} = 1 - \frac{\text{Absorbance of ABTS}^{+} \text{ in the presence of test compound}}{\text{Absorbance of ABTS}^{+} \text{ in the absence of test compound}}$$

The degree of quenching was plotted against different concentrations (at least 5 concentrations, ranging from 1µM to 20 µM) of a test compound and the gradient of the straight line was determined. At least 3 independent determinations were made for each compound. The experiment was repeated with trolox. The ratio of the gradients of the test compound and trolox gives the TEAC. A compound with a TEAC value of 2 has twice the radical quenching ability of trolox under similar experimental conditions.

$$\text{TEAC} = \frac{\text{Gradient of the plot of test compound}}{\text{Gradient of the plot of Trolox}}$$

4.2.6. Determination of intracellular ROS levels

Intracellular accumulation of ROS was determined with H_2DCF[158] which is a cell permeant, non-fluorescent compound that accumulates in cells upon deacetylation by membrane-bound esterases. In the presence of ROS, H_2DCF is oxidized to give fluorescent 2', 7'-dichlorofluorescein (DCF).[159] HT22 cells were seeded at a density of 2×10^5 cells in a 60-mm tissue culture dish (Corning, NY, US). After incubating for 12h at 37^oC in 5% CO_2 atmosphere, the cells were either treated with 5 mM glutamic acid only or 5 mM glutamic acid in the presence of test compound and further incubated for another 12h. H_2DCF at a final concentration of 5 µM was added during the last 30 min of the incubation period.[160] Medium containing detached cells was collected and the attached cells were trypsinized. Floating and detached cells were pooled together and centrifuged at 2,000x g for 5 min at 4^oC. The pellets were washed once with ice cold phenol red-free DMEM containing 2% FBS and resuspended again in 1 ml

of the same medium containing propidium iodide (PI, 1 µg/ml). Fluorescence intensities were collected on 10,000 cells using Dako Cytomation Cyan LX (CA, US) with excitation wavelength of 488 nm and emission wavelength of 520 nm for DCF, and excitation wavelength of 488 nm and emission wavelength of 610 nm for PI. Data was analysed with the Summit software version 4.3 (Dako, Glostrup, Denmark). At least 3 independent determinations were made for each test compound. The ROS produced in the presence of test compound was expressed as a percentage of the total ROS generated in the presence of 5 mM glutamate.

4.2.7 Determination of mitochondrial ROS levels

Mitochondrial ROS production was investigated using dihydrorhodamine 123 (D123), an uncharged, non-fluorescent agent that was converted by oxidation to the fluorescent dye rhodamine 123 (R123). D123 is commonly used either as a marker of mitochondrial function or as a specific indicator of mitochondrial ROS production.[161] Cells with viable mitochondria or with high levels of mitochondrial ROS convert D123 to R123 at a faster rate than cells with dysfunctional mitochondria or with low levels of ROS. D123 (5 µM) in DMEM was loaded into HT22 cells following the protocol described in Section 4.2.6. Fluorescence intensity was collected on 10,000 cells using Dako Cytomation Cyan LX (CA, US) with excitation wavelength of 488 nm and emission wavelength of 520 nm. Data was analyzed with the Summit software version 4.3 (Dako, Glostrup, Denmark). At least 3 independent determinations were made for each test

compound. The ROS levels measured in the presence of test compound was expressed as a percentage of the ROS levels measured in cells treated with 5 mM glutamate.

4.2.8 Determination of cytosolic calcium levels

The intracellular level of calcium was determined using Fluo-3 acetyoxymethylester (AM) as described elsewhere.[162] The membrane permeable Fluo-3 AM is converted to Fluo-3 on hydrolysis by esterases in cells and Fluo-3 increases its green fluorescence when it binds to calcium ions. HT22 cells were grown and exposed to glutamate or glutamate and test compound as described in Section 4.2.6. Cells were then loaded with Fluo-3 AM (1 μg/ml) in the final 30 minutes of incubation. Cells were gently trypsinised, centrifuged (2,000x g, 5 min, 4°C), washed once with ice-cold PBS (1x, pH 7.4) and re-suspended in 1ml of phenol red-free DMEM. Fluorescence intensity was collected on 10,000 cells using Dako Cytomation Cyan LX (CA, US) with excitation wavelength of 488 nm and emission wavelength of 520 nm. Data was analysed with the Summit software version 4.3 (Dako, Glostrup, Denmark). At least 3 independent determinations were made for each test compound. The intracellular calcium levels measured in the presence of test compound was expressed as a percentage of the total calcium measured in cells treated with 5 mM glutamate.

4.2.9. Statistical Analysis

Data was analyzed for statistical significance using the nonparametric Wilcoxon signed rank test (SPSS version 13.0, IL, USA)

4.3. Results

4.3.1. Effects of test compounds on glutamate induced cell death of HT22 cells

To determine if the synthesized compounds were effective against glutamate-induced toxicity, HT22 cells were exposed to glutamate (5 mM) and test compound (at various concentrations) for 24 hours and cell viability was determined by the MTT assay. Most cells exposed to 5 mM glutamate alone were non-viable (*ca* 0-10 % viability) after 24 hours. If a compound protected against glutamate induced cell death, this profile will be reversed and greater levels of cell viability would be evident even in the presence of glutamate. Protective ability of the compound was quantified in terms of its half maximal effective concentration (EC_{50}) which was the concentration at which 50% of cells remained viable in the presence of 5 mM glutamate. EC_{50} value was determined from dose response curves, as shown in Figure 4.2 for **16**. Figure 4.2 also shows the dose response curves of **16** exposed to HT22 cells in the absence of glutamate. These determinations served to evaluate the cytotoxicity of the compound. Ideally, a compound should protect against glutamate toxicity at low EC_{50} while having no intrinsic toxicity on the HT22 cells (high EC_{50}).
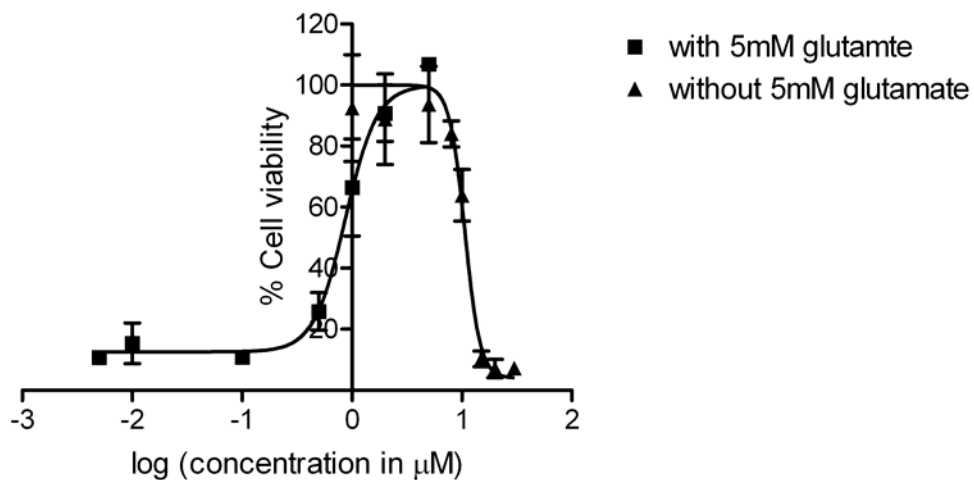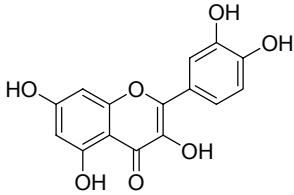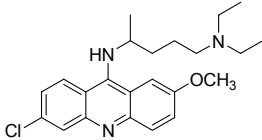
Figure 4.2: % Cell viability of HT22 cells exposed to various concentrations of compound **16** in the presence and absence of 5mM glutamate.

Table 4.1 gives the EC_{50} values of compounds in Groups 1-7 for protection from glutamate induced cell death and intrinsic cytotoxicities on HT22 cells. Quercetin was included as a positive control as its protective effects had been reported.[151] Determinations were also made for quinacrine which is the lead compound for the current series.

Table 4.1: Protective and cytotoxic ½ maximal effective concentrations (EC_{50}) values of compounds in Groups 1-7.

Compound	Structure	Protective EC_{50} $(\mu M)^a$	Cytotoxicity EC_{50} $(\mu M)^a$	Ratio of $EC_{50\mathrm{cytotoxicity}}$ and $EC_{50\mathrm{neuroprotection}}{}^b$

Quercetin	OH OH HO O OH OH O	3.13 (1.85, 4.36)	11.52 (9.04, 14.69)	3.7
Quinacrine	HN OCH$_3$ Cl N	Nil [c]	9.09 (5.48, 15.08)	N/A
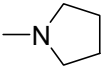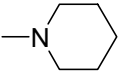
Group 1
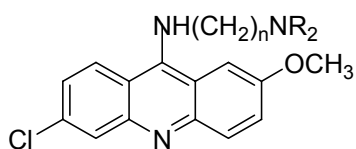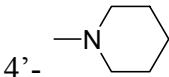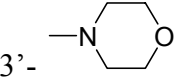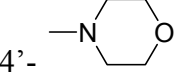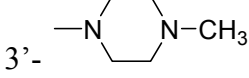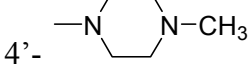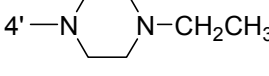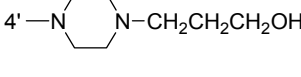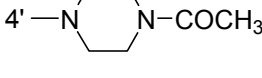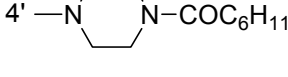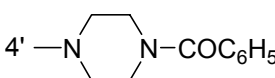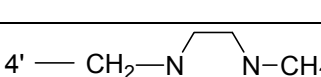
NH(CH$_2$)$_n$NR$_2$
OCH$_3$
Cl N

Compound	Side chain (R)	Protective EC$_{50}$ (μM)[a]	Cytotoxicity EC$_{50}$ (μM)[a]	Ratio of EC$_{50\text{cytotoxicity}}$ and EC$_{50\text{neuroprotection}}$[b]
1	n=2, R=C$_2$H$_5$	Nil	6.72 (4.01, 11.26)	N/A
2	n=3, R=CH$_3$	Nil	3.76 (2.20, 6.42)	N/A
3	n=3, R=C$_2$H$_5$	Nil	7.47 (4.61, 12.08)	N/A
4	n=4, R=C$_2$H$_5$	Nil	3.42 (1.76, 6.60)	N/A

Group 2
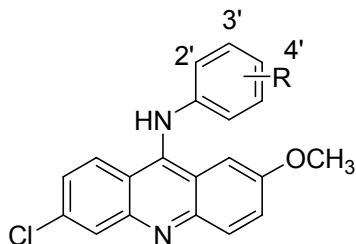
Compound	Side chain (R)	Protective EC_{50} (μM)[a]	Cytotoxicity EC_{50} (μM)[a]	Ratio of $EC_{50cytotoxicity}$ and $EC_{50neuroprotection}$[b]
5	2'-N(CH$_3$)$_2$	0.43 (0.19, 0.93)	10.37 (6.02, 17.86)	24.1
6	3'-N(CH$_3$)$_2$	0.41 (0.19, 0.85)	19.00 (14.04, 25.72)	46.3
7	4'-N(CH$_3$)$_2$	0.45 (0.23, 0.87)	9.36 (5.50, 15.92)	20.8
8	3'-N(C$_2$H$_5$)$_2$	0.44 (0.21, 0.92)	6.89 (5.53, 8.56)	15.6
9	4'-N(C$_2$H$_5$)$_2$	0.35 (0.12, 1.02)	6.83 (5.10, 9.12)	19.5
10	3'- —N⟨pyrrolidine⟩	0.27 (0.16, 0.44)	7.69 (4.89, 12.08)	28.5
11	3'- —N⟨piperidine⟩	0.30 (0.14, 0.59)	21.70 (13.58, 34.67)	72.3

#	Structure			
12	4'- —N (piperidine)	0.31 (0.11, 0.82)	14.21 (10.94, 18.46)	45.8
13	3'- —N O (morpholine)	0.5 (0.2, 1.20)	7.91 (5.84, 10.71)	15.8
14	4'- —N O (morpholine)	0.63 (0.34, 1.14)	18.17 (14.31, 23.07)	28.8
15	3'- —N N—CH$_3$	0.33 (0.18, 0.59)	5.00 (3.23, 7.73)	15.2
16	4'- —N N—CH$_3$	0.62 (0.38, 0.98)	8.94 (7.77, 10.29)	14.4
17	4'—N N—CH$_2$CH$_3$	0.64 (0.49, 0.84)	12.99 (10.23, 16.50)	20.3
18	4'—N N—CH$_2$CH$_2$CH$_2$OH	0.77 (0.64, 0.93)	16.16 (13.39, 19.51)	21.0
19	4'—N N—COCH$_3$	0.50 (0.23, 1.11)	13.65 (9.38, 16.88)	27.3
20	4'—N N—COC$_6$H$_{11}$	1.34 (0.41, 1.32)	15.12 (10.42, 18.11)	11.3
21	4'—N N—COC$_6$H$_5$	0.18 (0.046, 0.68)	19.89 (13.79, 20.70)	110.5
22	4'— CH$_2$—N N—CH$_3$	0.39	7.52	19.3

		(0.19, 0.79)	(5.74, 9.84)	
23		1.14 (0.77, 1.66)	10.88 (8.86, 13.37)	9.5
24	4'—CH₂—N (piperidine)	0.39 (0.19, 0.83)	10.67 (8.47, 13.45)	27.3
25	H	0.54 (0.44, 0.65)	14.64 (12.13, 17.67)	27.1
26	4'-CN	2.98 (2.46, 3.60)	21.15 (19.08, 23.45)	7.1
27	4'-F	0.85 (0.67, 1.08)	17.02 (14.67, 19.73)	20.0
28	3',4'-diF	0.90 (0.72, 1.13)	15.50 (12.95, 18.56)	17.2
29	4'-OCH₃	0.63 (0.47, 0.83)	7.62 (6.59, 8.82)	12.1
30	3'-OH	2.13 (1.58, 2.87)	9.75 (7.81, 12.18)	4.6
31	3',4'-diOH	2.75 (2.06, 3.36)	9.60 (8.08, 11.41)	3.5

Group 3
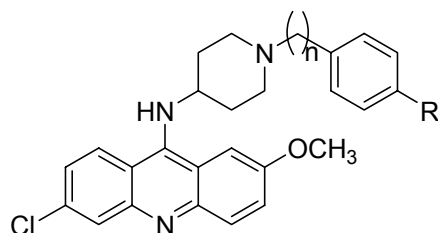
Compound	Side chain (R)	Protective EC_{50} $(\mu M)^a$	Cytotoxicity EC_{50} $(\mu M)^a$	Ratio of $EC_{50cytotoxicity}$ and $EC_{50neuroprotection}{}^b$
32	n=1, R=H	Nil	9.03 (6.65, 12.26)	N/A
33	n=1, R=CH$_3$	Nil	12.63 (9.71, 16.42)	N/A
34	n=1, R=Cl	Nil	7.69 (6.06, 9.75)	N/A
35	n=1, R=OCH$_3$	Nil	8.67 (6.29, 11.95)	N/A
36	n=1, R=CN	Nil	6.84 (4.47, 10.49)	N/A
37	n=2, R=H	Nil	2.86 (1.68, 4.87)	N/A
38	n=2, R=CH$_3$	Nil	2.37 (1.93, 2.92)	N/A

39	n=2, R=Cl	Nil	4.52 (3.07, 6.65)	N/A
40	n=2, R=OCH$_3$	Nil	4.36 (3.02, 6.30)	N/A
41	n=3, R=H	Nil	3.46 (2.10, 5.70)	N/A

Group 4

R
OCH$_3$
Cl
N

Compound	Side chain (R)	Protective EC$_{50}$ (μM)[a]	Cytotoxicity EC$_{50}$ (μM)[a]	Ratio of EC$_{50cytotoxicity}$ and EC$_{50neuroprotection}$[b]
42	(4-methylpiperazinyl butynyl amine side chain)	Nil	12.20 (9.95, 14.95)	N/A
43	(N-benzyl azabicyclo amine side chain)	Nil	3.33 (2.23, 4.98)	N/A
44	-OPh	Nil	31.36 (25.98, 34.76)	N/A
45	H$_3$C–N–phenyl	Nil	10.81 (9.27, 12.62)	N/A

137

46	-NH$_2$	Nil	7.41 (5.73, 9.57)	N/A

Group 5
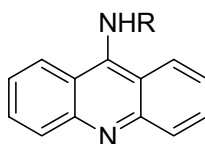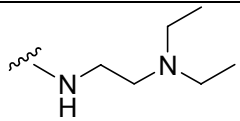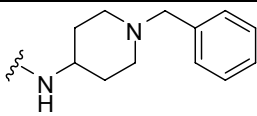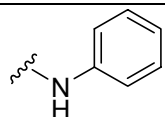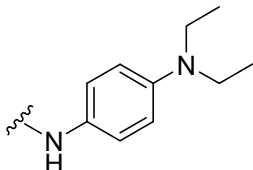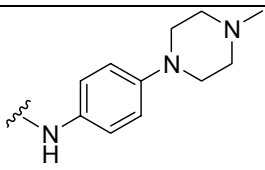
Compound	Side chain (R)	Protective EC$_{50}$ (μM)[a]	Cytotoxicity EC$_{50}$ (μM)[a]	Ratio of EC$_{50\text{cytotoxicity}}$ and EC$_{50\text{neuroprotection}}$[b]
47	-NH$_2$	Nil	9.19 (7.97, 10.60)	N/A
48		0.74 (0.50, 1.07)	6.83 (5.10, 9.13)	9.2

Group 6
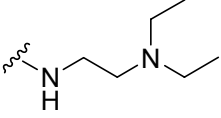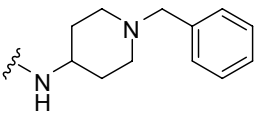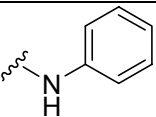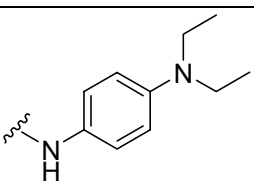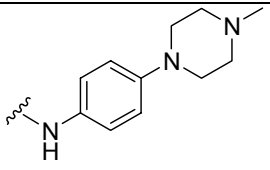
Compound	Side chain (R)	Protective EC$_{50}$ (μM)[a]	Cytotoxicity EC$_{50}$ (μM)[a]	Ratio of EC$_{50\text{cytotoxicity}}$ and

				$EC_{50neuroprotection}$[b]
49	NH_2	2.22 (1.32, 3.74)	>25	>11
50		Nil	>30	N/A
51		Nil	19.88 (16.17, 24.45)	N/A
52		Nil	>40	N/A
53		1.03 (0.85, 1.26)	>30	>29
54		3.65 (2.82, 4.17)	>40	>11

Group 7

Compound	Side chain (R)	Protective EC_{50} (µM)[a]	Cytotoxicity EC_{50} (µM)[a]	Ratio of $EC_{50cytotoxicity}$ and $EC_{50neuroprotection}$[b]

55	NH$_2$	Nil	13.28 (10.43, 16.91)	N/A
56		Nil	>25	N/A
57		Nil	16.39 (13.82, 19.45)	N/A
58		2.54 (2.07, 3.11)	> 30	>12
59		2.42 (1.46, 3.90)	12.75 (11.02, 14.76)	>5
60		2.80 (2.14, 3.67)	>25	>9

[a]: EC$_{50}$ values are the mean of 3-7 replicates. 95% confidence intervals are given in brackets..

[b]: Ratio of EC$_{50}$ values give an indication of the potential of the compound as a protective agent against glutamate induced oxytosis in HT22 cells

[c]: "Nil": Compound has no protective activity.

As seen from Table 4.1, compounds with protective activities were found in Group 2 and in lesser numbers, Groups 5, 6 and 7, with EC$_{50}$ values spanning a relatively narrow 20–fold range (0.18 μM to 3.65 μM). The positive control quercetin had an EC$_{50}$ of 3.13 μM which was comparable to its reported value (3

μM) obtained under similar conditions.[151] Quinacrine and its analogs in Group 1 were devoid of protective activity.

The following structure-activity relationships were deduced from the results.

(i) The N-phenyl ring present in the Group 2 compounds was an essential feature for activity. Removing the N-phenyl group to give the unsubstituted primary amino function (as in **46**) abolished protective activity. The N-phenyl ring was also present in the other active compounds of Groups 5, 6 and 7 and in only one instance (tetrahydroacridinyl analogs of Group 6), its omission to give the primary 9-amino function resulted in a loss of activity. The exceptional activity of **49** (EC_{50} 2.22 μM) stood in contrast to that of other compounds with the primary amino function (**46**, **47** and **55**) which were inactive. The loss of activity when the 9-(N-phenyl) substituent was replaced with 9-phenoxy (**44**) further attested to the importance of retaining this feature.

(ii) The inactivity of **45** in which the 9-NH_2 group was di-substituted with methyl and phenyl groups was a significant finding as it highlighted the importance of maintaining a secondary amino function with an intact NH group. Thus, the essential motif for activity was an aromatic ring-NH-aromatic ring feature which was present in all the active compounds (barring **49**). Replacing one of the aromatic rings with an alkyl /alkynyl side chain (as in Group 1 and **42**) or a heterocyclic ring (for example Group 3 and **43**) abolished activity altogether.

(iii) Substitution of the 9-(N-phenyl)amino moiety in Group 2 was not critical for activity but served to moderate activity, possibility by influencing the

physicochemical properties of the final compound. That substitution was not essential was seen from **25** which in spite of its un-substituted state had strong protective properties (EC_{50} 0.54 µM). The likelihood of substituents influencing activity by moderating the physicochemical profiles of the compound was suggested by the markedly weaker protective activities of compounds with hydrophilic substituents such as cyano (**26**) and hydroxyl (**30**, **31**) as compared to those with lipophilic groups like methoxy (**29**) and fluoro (**27**, **28**). Indeed, a significant and inverse relationship was noted when EC_{50} values and ClogP values of the Group 2 compounds were analyzed by Spearman bivariate correlation (Spearman rho = -0.542, n= 27, p = 0.01, 2 tailed). When extended to all compounds (n = 34, including those in Groups 5-7), the relationship was still maintained (Spearman rho = -0.594, p = 0.01 level, 2 tailed). Thus, protective activity was directly correlated to lipophilicity, which within each group was influenced by the type of substitution on the 9-amino /4-amino.

(iv) The most active compound identified from this investigation was **21** (EC_{50} 0.18 µM) which belonged to Group 2 and had a benzoylpiperazine side chain attached to the para position of the 9-(N-phenyl) ring. Replacing this side chain with structurally similar side chains like acetylpiperazine (**19**, EC_{50} 0.50 µM) and cyclohexylcarbonylpiperazine (**20**, EC_{50} 1.34 µM) reduced activity by only a narrow 7-fold margin. In fact, the variation in activity within Group 2 was limited to no more than 17 fold, an indication of the preferential status of the Group 2 motif for protective activity.

(v) Active compounds were also identified in Groups 5, 6 and 7 and the activities of these compounds showed that the acridine ring need not be substituted (Group 5), or could be replaced with other ring systems like 6-chloro-1,2,3,4-tetrahydroacridine (Group 6) and 6-chloroquinoline (Group 7). However, for the same side chain at the 9-amino (or 4-amino) functionality, the most potent compounds were those that had the 6-chloro-2-methoxyacridine ring. Compounds with the 4-diethylaminophenyl (**9**, **48**, **53**, **59**) side chain and 4-(4-methylpiperazin-1-yl) phenyl (**16**, **54**, **60**) side chain were illustrative of this point.

(vi) The cytotoxicities of the active compounds were also determined and the relative difference between cytotoxicity and protective activity for each compound was given by the ratio of the two EC_{50} values. As seen from Table 4.1, ratios ranged from 3.5 (**31**) to 110.5 (**21**), as compared to a ratio of 3.7 for quercetin. Thus, the active compounds had desirable profiles of good activities coupled with low toxicities. In terms of cytotoxicities, the Group 6 and 7 compounds had extremely low toxicities with EC_{50} values that could not be determined (> 25 µM) in many instances.

4.3.2. Effect of incubation time on protective effects against glutamate-induced cell death

In the preceding section, protective effects were evaluated by exposing HT22 cells to both test compound and glutamate, added at the same time, for 24 hours. To determine if protective effects were affected by the sequence at which test compound/glutamate was added, a time course experiment was carried out for

selected compounds (**5**, **6**, **11**, **15**, **16**, **25**) in Group 2. These compounds were chosen because they had different amino substituents (diethylamino, piperidinyl, 4-methylpiperazinyl) except for **25** which had an unsubstituted 9-(N-phenyl) ring. They also have fairly close EC_{50} values (0.30 μM to 0.62 μM). From the experiments to determine EC_{50} values, it was known that at 1 μM compound, cells were significantly rescued from the glutamate-induced cell death. At 2 μM compound, cells were completely saved from the toxic effect of 5mM glutamate. Moreover, some compounds have toxicities around 5μM. Hence, in this experiment, the compounds were investigated at only two concentrations of 1 μM and 2 μM. In view of the narrow concentration window, meaningful dose dependent effects over a broad concentration range could not be carried out. Nonetheless, the results in figure 4.3 showed that there was evidence of dose-dependent cytoprotective effects at selected incubation times as discussed in the subsequent paragraphs.

HT22 cells were incubated with glutamate for periods varying from 8 hours to 14 hours, followed by removal of the media and addition of fresh media containing test compound (at 1 μM) and glutamate (5 mM) for a period of time equivalent to 24 hours less period of exposure to glutamate. Thus, cells exposed to glutamate for 8 hours will be incubated with compound and glutamate for the remaining 16 hours while cells exposed to glutamate for 14 hours, will be incubated with compound and glutamate for only 10 hours. Cell viability was then determined after the incubation period (24 hours).

Cell viability when compound 5 was added after 5mM Glu

Cell viability (%) vs *Time of glutamate exposure (h)*

Cell viability when compound 6 was added after 5mM Glu

Cell viability (%) vs *Time of glutamate exposure (h)*

Cell viability when compound 11 was added after 5mM Glu

Cell viability when compound 15 was added after 5mM Glu

Cell viability when compound 16 was added after 5mM Glu

Cell viability when compound 25 was added after 5mM Glu

Figure 4.3: Effect of compounds added after exposure to glutamate (5 mM). Each point is a mean of 3 independent determinations. * indicates significant difference in cell viabilities when treated with 1μM and 2μM compound (p<0.05, independent T-test).

Figure 4.3 shows the effects of **5**, **6**, **11**, **15**, **16**, **25** at 1 μM and 2μM on viability of HT22 cells exposed to varying periods of glutamate. It was seen that cell viability remained at almost 100% after 8 hours glutamate exposure and was

maintained at approximately 80% viability after 12 hours glutamate exposure. With longer periods of glutamate exposure, the protective effects of these compounds were no longer evident, although at a higher concentration of 2 μM, two compounds (**6**, **16**) were able to significantly increase cell viability after 14 hours glutamate exposure as compared to 1 μM ($p<0.05$, independent T-test).

4.3.3. Effects of compounds 16, 25, 45 and 46 on glutathione levels in HT22 cells challenged with glutamate

The initiating event in oxidative glutamate toxicity is the loss of GSH from the cells which is caused by the inhibition of cystine uptake by glutamate. Cellular GSH is rapidly depleted within 8 hours of glutamate exposure.[143] The measurement of intracellular GSH is based on a cyclical process involving the oxidation of GSH by DTNB to generate the colored 5-mercapto-2-nitrobenzoate anion and oxidized GSSG. The latter is reduced back to GSH by the enzyme glutathione reductase (Figure 4.4). The recycling process greatly improves the sensitivity of the assay and GSH content is determined from the rate at which the yellow benzoate anion is generated.
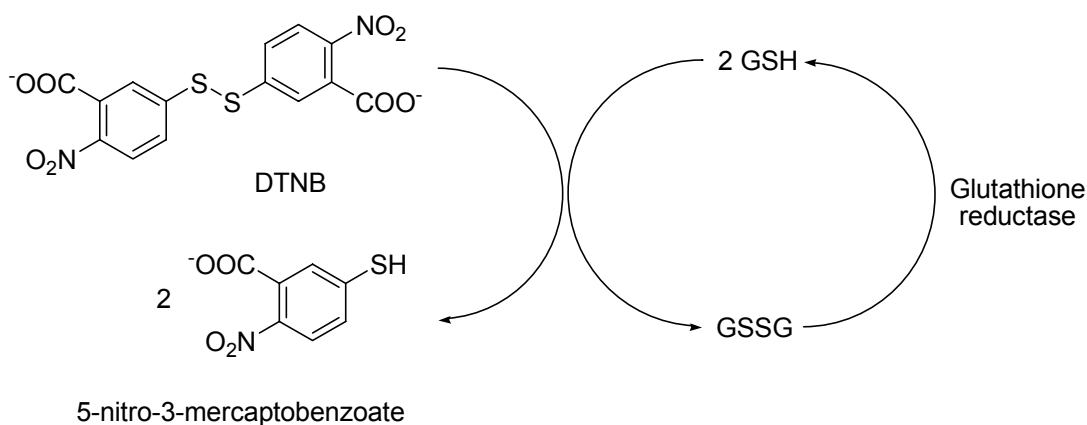
Figure 4.4: Principle of the total glutathione assay.

Compounds **16**, **25**, **45** and **46** were incubated with glutamate (5 mM) for 12 hours and GSH content was determined thereafter. The compounds were tested at 1 μM which was approximately 1.5-2 times the EC_{50} of **16** and **25**. Compounds **45** and **46** had no protective EC_{50} values (Table 4.1). As seen from Figure 4.5, none of the compounds prevented the loss of GSH caused by glutamate. Thus **16** and **25** protected HT22 cells from glutamate toxicity by a mechanism(s) that did not involve altering GSH metabolism.
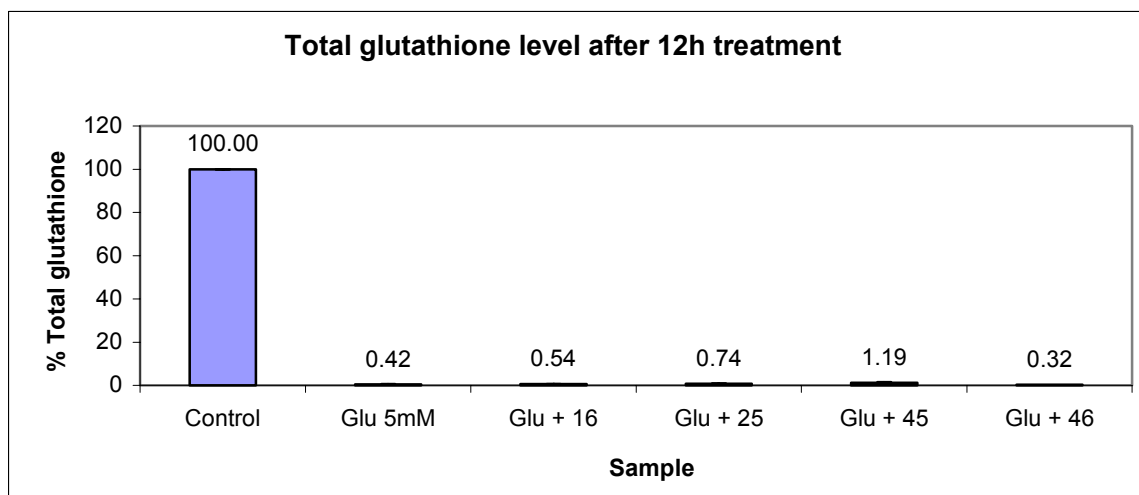
Figure 4.5: Effects of test compounds (1 μM) on the intracellular GSH levels of

149

HT22 cells exposed to glutamate (5 mM) and test compound for 12 hours. Control consists of cells treated with 0.1%v/v DMSO.

4.3.4. Quenching of the nitrogen based ABTS$^{\bullet+}$ cation radical by test compounds

The exposure of HT22 cells to glutamate leads to a biphasic increase in ROS levels. The first phase is closely linked to GSH depletion and involves a linear increase in ROS levels to about 10% of its maximum value.[143] The second phase involves an exponential rise in ROS levels to almost twice that of basal levels in untreated cells and is attributed to an increase in mitochondrial activity. The preceding section showed that selected compounds did not prevent the fall in GSH levels that accompanied exposure of HT22 cells to glutamate. As the intracellular ROS levels would be expected to increase under these conditions, it was of interest to determine if the test compounds were antioxidants with radical quenching properties. To this end, the Trolox Equivalent Antioxidant Capacity (TEAC) of selected test compounds were determined. The scavenging of the stable nitrogen radical cation (ABTS$^{\bullet+}$) which is generated from the oxidation of ABTS by potassium persulfate (Figure 4.6) is a well established procedure for obtaining TEAC values.[157] This method requires comparing the quenching ability of the test compound to that of a standard antioxidant trolox. A compound with a TEAC of 2 is said to have twice the quenching ability of trolox.
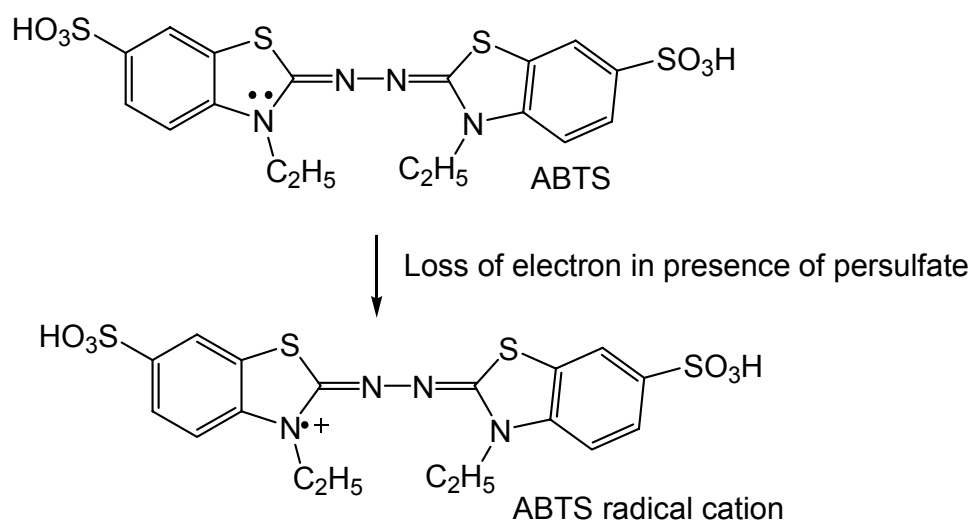
Figure 4.6: Generation of ABTS$^{\bullet+}$ from the oxidation of ABTS.

Table 4.2: TEAC and protective EC$_{50}$ values of test compounds.

Compound	Structure	TEAC values [a]	Neuroprotective EC$_{50}$ (μM) [b]
Quercetin		4.91±0.36 (Reported value 4.84[151])	3.13 (1.85, 4.36) (Reported value 3)[151]
Quinacrine		Nil[c]	Nil[c]

Group 1
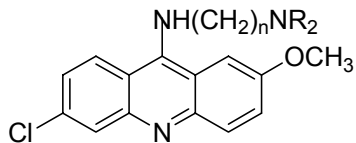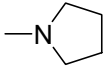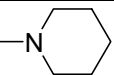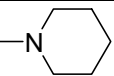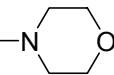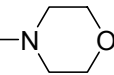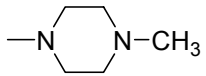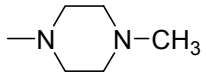
Compound	Side chain (R)	TEAC values [a]	Neuroprotective EC$_{50}$ (μM) [b]
1	n=2, R=C$_2$H$_5$	Nil[c]	Nil[c]
2	n=3, R=CH$_3$	Nil[c]	Nil[c]
3	n=3, R=C$_2$H$_5$	Nil[c]	Nil[c]
4	n=4, R=C$_2$H$_5$	Nil[c]	Nil[c]

Group 2
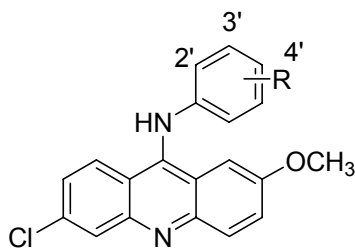
Compound	Side chain (R)	TEAC values [a]	Neuroprotective EC$_{50}$ (μM) [b]
5	2'-N(CH$_3$)$_2$	2.25±0.06	0.43 (0.19, 0.93)
6	3'-N(CH$_3$)$_2$	0.77±0.02	0.41 (0.19, 0.85)
7	4'-N(CH$_3$)$_2$	0.91±0.13	0.45 (0.23, 0.87)
8	3'-N(C$_2$H$_5$)$_2$	0.64±0.05	0.44 (0.21, 0.92)

		TEAC values[a]	Neuroprotective EC$_{50}$ (μM)[b]
9	4'-N(C$_2$H$_5$)$_2$	0.72±0.01	0.35 (0.12, 1.02)
10	3'- —N pyrrolidine	0.66±0.15	0.27 (0.16, 0.44)
11	3'- —N piperidine	0.61±0.03	0.30 (0.14, 0.59)
12	4'- —N piperidine	0.71±0.02	0.31 (0.11, 0.82)
13	3'- —N morpholine O	2.48±0.19	0.5 (0.2, 1.20)
14	4'- —N morpholine O	0.63±0.04	0.63 (0.34, 1.14)
15	3'- —N N—CH$_3$	1.03±0.25	0.33 (0.18, 0.59)
16	4'- —N N—CH$_3$	0.93±0.14	0.62 (0.38, 0.98)

Group 3
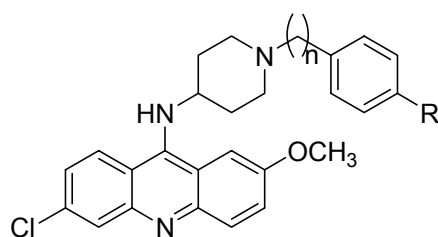
Compound	Side chain (R)	TEAC values[a]	Neuroprotective EC$_{50}$ (μM)[b]
32	n=1, R=H	Nil[c]	Nil[c]

Group 4
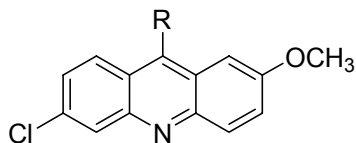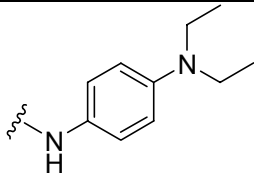
Compound	Side chain (R)	TEAC values[a]	Neuroprotective EC$_{50}$ (μM)[b]
42		Nil[c]	Nil[c]
43		Nil[c]	Nil[c]
44	-OPh	Nil[c]	Nil[c]
45		Nil[c]	Nil
46	-NH$_2$	Nil[c]	Nil[c]

Group 5

Compound	Side chain (R)	TEAC values[a]	Neuroprotective EC$_{50}$ (μM)[b]
47	-NH$_2$	Nil[c]	Nil[c]

154

48		0.90±0.01	0.74 (0.50, 1.07)

[a]: TEAC values are mean ± standard deviation for at least 3 determinations.

[b]: Values are mean of 3-7 replicates with 95% confidence intervals given in brackets.

[c]: No neuroprotective activity.

The TEAC values of selected test compounds are given in Table 4.2. The most striking observation was that compounds that were protective against glutamate-induced cytotoxicity had TEAC values while those with no protective properties, had none. There was however no significant correlation between TEAC and EC_{50} values of the active compounds, which was apparent from a casual examination of the data. For example, the isomeric 9-N-(diethylaminophenyl) analogs **5**, **6** and **7** had comparable EC_{50} values (0.41 to 0.45 μM) but **5** had a TEAC value (2.25) that was twice that of **6** and **7** (TEAC values are 0.77 and 0.91 respectively). As a whole, the TEAC values in Table 4.2 were low (< 1 in most instances).

Figure 4.7 shows a plot of % quenching (after 10 minutes of incubation with ABTS$^{\bullet+}$) versus concentration of test compound. It can be seen that for some compounds (trolox and **16**), quenching ability increased with concentration, while for others (quinacrine, quercetin, **5**), quenching tapered off after a certain concentration and did not show concentration-dependence thereafter. In the case of quinacrine, quenching of ABTS$^{\bullet+}$ reached a plateau at 5 μM and at that point,

absorbance was reduced to only 20% of the control. There was however a linear rise up to 5 μM but calculating its TEAC based on that portion of the curve actually gave quinacrine a TEAC equivalent to that of trolox. This would over-estimate its quenching properties and it was decided that no value would be assigned to quinacrine. In the case of quercetin, there was also limited concentration dependence (up to 5 μM) but the % quenching reached the maximum level before leveling off. The absence of concentration dependence for some compounds was a puzzle. One explanation may be that for these compounds, the radical species that was formed after donating a radical (likely $H^{\bullet}$) to quench $ABTS^{\bullet+}$, now in turn competed with $ABTS^{\bullet+}$ for radicals. This competition may be more significant at higher concentrations of the test compound.
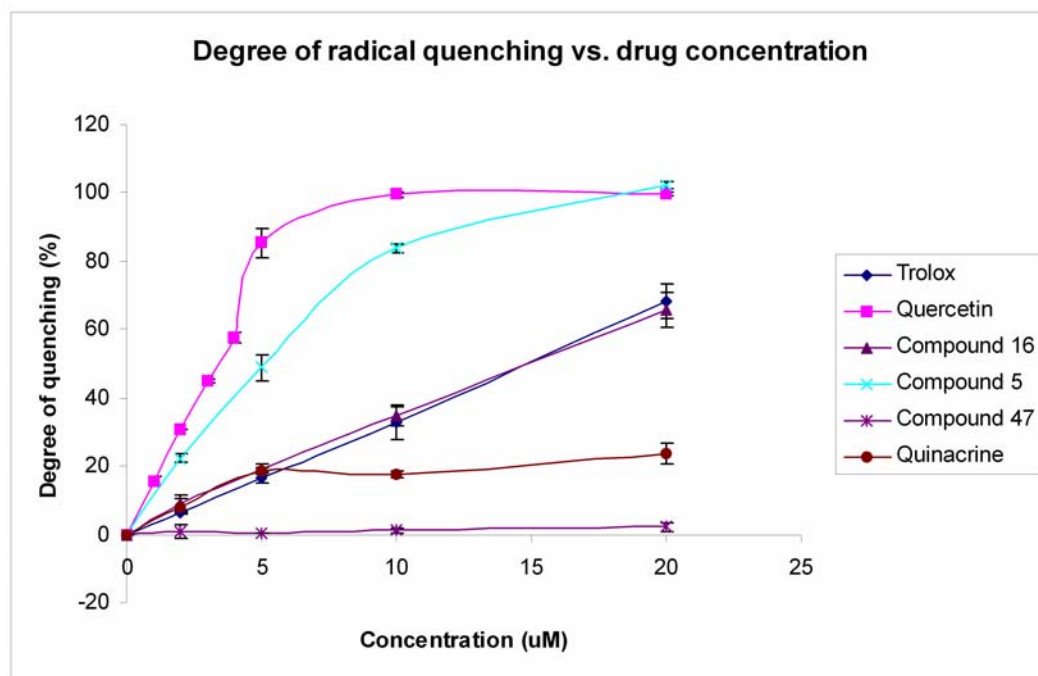
Figure 4.7: Effect of drug concentrations on the degree of scavenging $ABTS^{\cdot+}$ radicals at the 10th minute.

4.3.5. Effects of compounds 16, 25, 45 and 46 on intracellular ROS production

In the preceding section, it was found that only compounds with protective EC_{50} values against glutamate induced toxicity of HT22 cells were able to quench the ABTS radical cation. While this may imply a radical scavenging role for the test compound, the caveat is that the ABTS radical quenching assay is a non-cell based assay and free radicals (stable nitrogen based radicals) are generated in an aqueous environment. In contrast, free radical generation (predominantly ROS) in glutamate induced toxicity occurs in the cytoplasm and mitochondria. The antioxidant potential of a compound would thus depend not only on its intrinsic scavenging activity but also its ability to penetrate lipid bilayers to reach the sites of ROS generation, a property that is not adequately addressed by the quenching assay involving ABTS radical cations. Hence, in this section, the effect of selected test compounds (**16**, **25**, **45** and **46**) on intracellular accumulation of ROS was determined with H_2DCF[158] which is a cell permeant, non-fluorescent compound that accumulates in cells upon deacetylation by membrane-bound esterases.

In the presence of ROS, H_2DCF is oxidized to give fluorescent 2',7'-dichlorofluorescein (DCF).[159] The test compound (1 µM) was incubated with glutamate (5 mM) for 12 hours before the determination of ROS levels by DCF fluorescence using flow cytometry. It was found that **16** and **25** protected HT22 cells against glutamate toxicity while **45** and **46** had no protective property.

Figure 4.8 shows representative 2-dimensional data obtained from the analyses of **16** and **45** in the presence of DCF (for measurement of ROS) and propidium iodide (PI, for measurement of cell death). Panel A shows the profile of untreated HT22 cells, with most cells in the R5 section indicating live cells with basal levels of ROS. When exposed to glutamate (Panel B), more cells were found in R2 which depicted non-viable cells. Panel C shows cells challenged with glutamate in the presence of **16**. The profile differed from glutamate challenged cells (Panel B) in that there were more viable cells (R5) and fewer dead cells (R2). This was taken as an indication that **16** restored cell viability to a state resembling that of untreated cells. In contrast, **45** failed to rescue cells from glutamate challenge (Panel D) and the profile of cells treated with **45** and glutamate resembled that of cells treated with glutamate alone (Panel B).
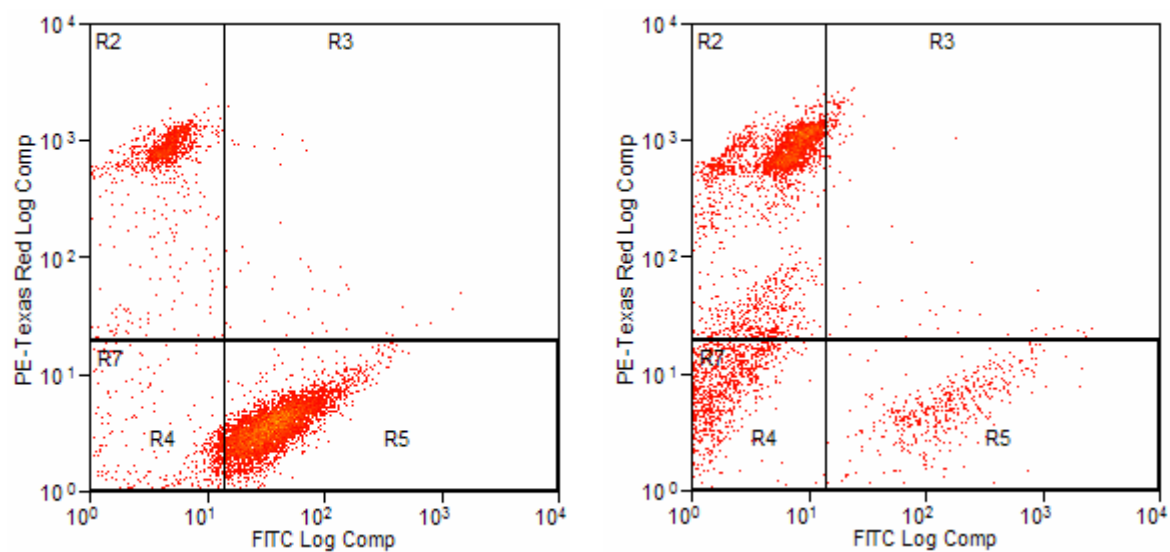
(A) DMSO   (B) Glu 5mM
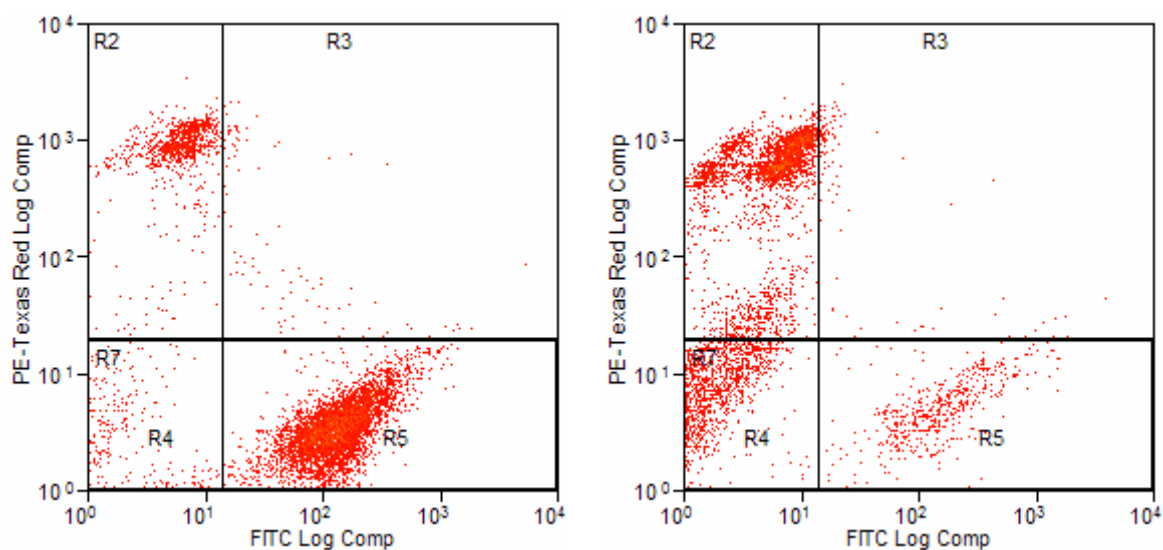
(C) Glu 5mM + compound 16 1μM   (D) Glu 5mM + compound 45 1μM

Figure 4.8: Effect of **16** and **45** on ROS levels and viability of HT22 cells treated with glutamate after 12 h of incubation. The horizontal axis displayed DCF fluorescence. The vertical axis displayed PI fluorescence. Data from 10,000 live cells were collected for each panel.

Figure 4.9 depicts the ROS levels monitored by DCF fluorescence (based on sector R5) in the presence of test compounds and glutamate. Quantification of DCF fluorescence showed that **16** and **25** significantly reduced ROS levels (p=0.08 and 0.012 respectively) compared to that observed in the presence of glutamate alone but the ROS levels were still higher than the basal levels found in untreated cells (p=0.028 and 0.018 respectively). Compounds **45** and **46** were unable to prevent the increase in ROS on glutamate exposure. The inactivity of **45** compared to the radical scavenging activity of **25** was striking and emphasized the importance of maintaining an NH moiety at position 9 of the acridine ring.
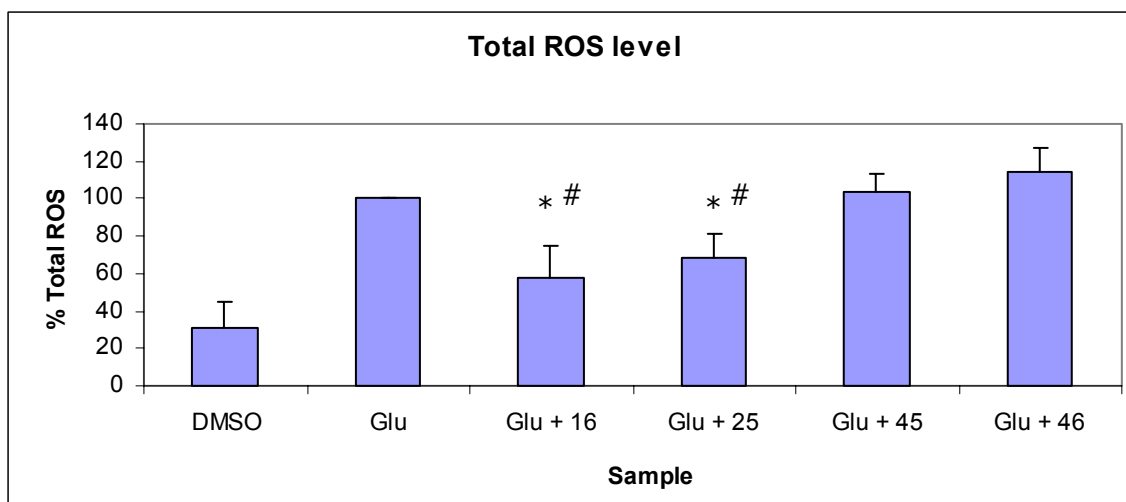
Figure 4.9: ROS levels monitored by DCF fluorescence (based on sector R5). HT22 cells were treated with glutamate acid 5mM with/without test compound at 1μM for 12h. Untreated cells exposed to media and DMSO were included as control. * indicates significant difference ($p < 0.05$) from cells treated with glutamate alone. # indicates significant difference ($p < 0.05$) from control untreated cells. Both analyses were carried out with the Wilcoxon signed rank test (SPSS v13.0).

To determine if the test compounds affected mitochondrial ROS production, cells incubated with glutamate and test compound were probed with the fluorescent ROS sensitive agent dihydrorhodamine 123 (D123) which is an uncharged, non-fluorescent agent that is converted by oxidation to the fluorescent dye rhodamine 123 (R123). D123 is commonly used either as a marker of mitochondrial function or as a specific indicator of mitochondrial ROS production.[153] Cells with viable mitochondria or with high levels of mitochondrial ROS convert D123 to R123 at a faster rate than cells with dysfunctional mitochondria or with low levels of ROS.

Figure 4.10 shows that cells treated with glutamate and **16** (or **25**) accumulated significantly lower levels of mitochondrial ROS than cells treated with glutamate alone. In fact, the ROS content of these cells were comparable to that found in untreated cells. In contrast, there was no decrease in mitochondrial ROS levels in cells co-treated with glutamate and **45** (or **46**). These results reinforced the notion that the radical quenching properties of **16** and **25** specifically targeted the mitochondria.
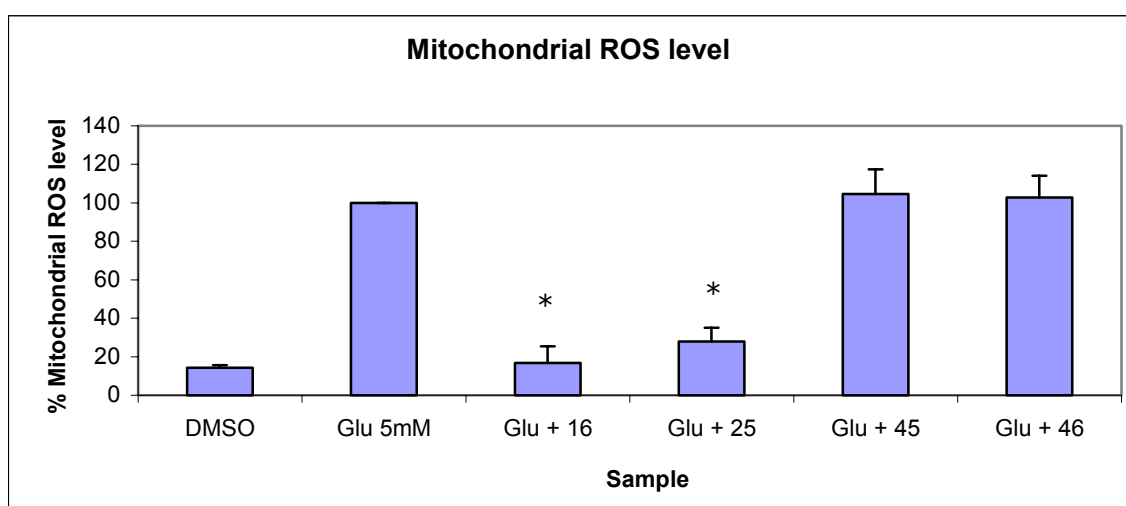
Figure 4.10: Mitochondrial ROS level monitored by D123 fluorescence. HT 22 cells were treated with glutamate 5mM with/without test compound (1µM) for 12h. Untreated cells exposed to media and DMSO was included as a control (change DMSO to control) * indicates significant difference ($p < 0.05$) from cells treated with glutamate alone. Analyses were carried out with the Wilcoxon test (SPSS v13.0).

4.3.6. Effects of compounds 16, 25, 45 and 46 on intracellular calcium levels

The increase in mitochondrial ROS levels observed in glutamate induced oxidative toxicity is closely linked to an influx of intracellular calcium which is a

necessary step that precedes cell death.[143] Thus it was of interest to determine if **16** and **25** prevented the rise in intracellular calcium levels that was linked to the demise of HT22 cells exposed to glutamate. For this purpose, calcium levels were monitored with Fluo-3 AM, a membrane permeable calcium ion specific fluorescence indicator. Fluo-3 AM is converted to Fluo-3 on hydrolysis by esterases in the cell and Fluo-3 increases its yellow-green fluorescence when it binds to calcium ions.

As shown in Figure 4.11, cells treated with glutamate showed a sharp rise in Fluo-3 fluorescence, indicating an increase in intracellular calcium levels. A sharp decline to almost basal levels was observed when cells were co-incubated with glutamate and **16** (or **25**). In the case of **45** and **46**, levels of intracellular calcium showed a rise comparable to that observed with glutamate treated cells.
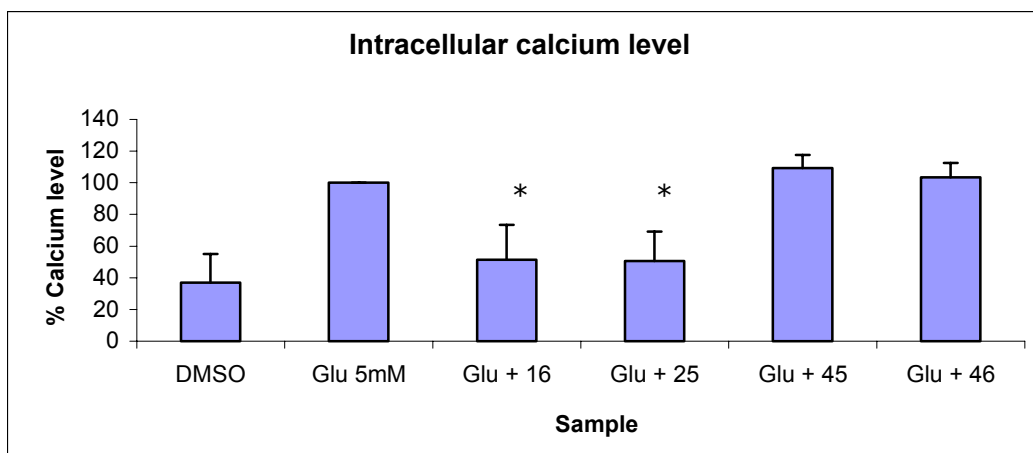
Figure 4.11: Intracellular Ca^{2+} levels monitored by Fluo-3 AM fluorescence. HT22 cells were treated with glutamic acid 5mM with/without test compound (1 µM) for 12hours. Untreated cells exposed to media and DMSO was included as a control (change DMSO to control) * indicates significant difference ($p < 0.05$)

from cells treated with glutamate alone. Analyses were carried out with the Wilcoxon test (SPSS v13.0).

4.4 Discussion

The present investigation was undertaken to provide support for the hypothesis that compounds with an aromatic ring –NH– aromatic ring motif were able to protect neuronal HT22 cells from glutamate-induced oxidative cell death. From the results obtained, it is evident that there was indeed a link between this structural feature and protective activity. Prior to this finding, only N.N-diphenyl-*p*-phenylenediamine (DPPD) and related analogs (Figure 4.1) provided evidence of this association.[154] Here it is shown that the two aromatic rings need not be phenyl but that one of them may be a N-containing heteroaromatic ring. Of the compounds that complied with this structural requirement, 80% were from Group 2 in which the heterocycle was 6-chloro-2-methoxyacridine, and the rest were from groups 5, 6 and 7 where an unsubstituted acridine, 6-chloro-tetrahydroacridine and quinoline were the heterocyclic groups.

Using the Group 2 compounds, **16** and **25**, as representative members, it was found that these compounds protected HT22 cells from glutamate challenge by influencing similar pathways. Both compounds could not prevent the fall in GSH levels that followed glutamate exposure. This may imply that there was no effect on the transcription or activity of enzymes like γ-glutamylcysteine synthetase, glutathione reductase, glutathione peroxidase involved in GSH metabolism. On the other hand, both compounds quenched and prevented the accumulation of ROS arising from glutamate exposure. Radical quenching

activity was assessed from the TEAC values and it was notable that besides **16** and **25**, only compounds with protective EC_{50} values had TEAC values, implying a radical scavenging role for the active compounds, not withstanding the limitations of the method used to generate TEAC. The monitoring of intracellular ROS levels with DCF provided more convincing evidence of the ability of **16** and **25** to cross membrane barriers and quench free radicals.

In contrast to **16** and **25**, compounds **45** and **46** which had no protective EC_{50} values did not show radical quenching properties in similar experiments. The inactivity of these compounds provided a strong case for proposing the specific involvement of the NH group when flanked by aromatic rings in the quenching of radicals. One possibility was that under certain conditions, the 9-NH lost one proton by radical abstraction by hydroxyl or similar radical to generate an amine cation radical (Figure 4.6) which would quench highly oxidizing radicals like OH•.
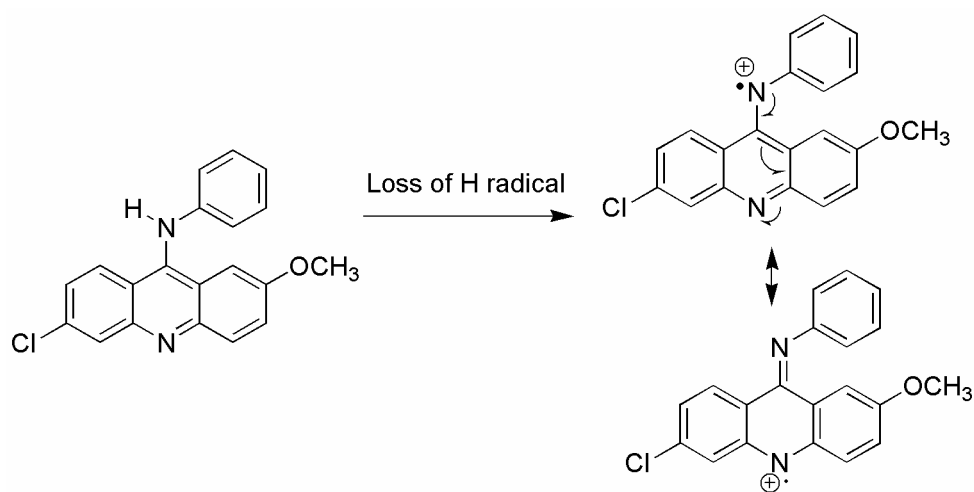
Figure 4.12: Formation of radical anion from the dissociation of the NH bond in compound **25**.

As seen in Figure 4.12 in which **25** was used as an example, electron delocalization and stabilization of the radical specie arising from the loss of H$^\bullet$ served to promote its formation and enhanced the radical quenching properties of **25**. Reference to the possible radical quenching potential of the NH bond had been alluded to in two other instances. DPPD was reported to possess antioxidant properties as it decreased intracellular ROS levels in PC12 cells.[163,164] Quinacrine was cited as an antioxidant based on electron spin resonance measurements that demonstrated its ability to scavenge hydroxyl radicals.[104] Structurally, both compounds do not have phenolic OH or tertiary CH groups that are normally linked to antioxidant activity and it was thus assumed that their radical quenching properties were due to the NH group. It was noted however that in the present investigation, quinacrine did not protect HT22 cells from glutamate toxicity and it did not have a measurable TEAC value. The discrepancy may be attributed to the non-cell based nature of the electron spin resonance experiments that were used to demonstrate the antioxidant properties of quinacrine and the high concentrations ($\geq 10~\mu$M) of quinacrine that were required for this activity. In the determination of TEAC by the ABTS$^{\bullet+}$ quenching experiments, the scavenging properties of quinacrine were observed up to 5 μM only beyond which concentration dependence was not evident.

An important feature of the protective effects of all the test compounds was their ability to rescue HT22 cells when added at the same time as glutamate. Priming of cells by initially exposing them to the test compound followed by glutamate did not appear to be necessary (although it was not investigated here).

Interestingly, this was required for DPPD and the implication was that its protective effects could involve the activation of a particular transcription pathway leading to the production of certain protective proteins. Besides rescuing HT22 cells concurrently exposed to glutamate, several Group 2 compounds (**5**, **6**, **11**, **15**, **16**, **25**) demonstrated latent protective effects in that they could rescue HT22 cells when added 10-12 hours after glutamate exposure. Latent protective effects were also reported for flavonoids and Nec-1 but at much higher concentrations of the test compound (10 µM for flavonoids, and 25 µM for Nec-1).[151,165] In comparison, the Group 2 compounds were effective at much lower concentrations (1 µM).

The latency of the protective effects of the Group 2 compounds suggested that these compounds interfered with the later stages of oxidative cell death, namely the ROS surge from the mitochondria and the influx of calcium into the cells. The finding that **16** and **25** did indeed reduce mitochondrial ROS as measured by D123, a specific indicator of mitochondrial ROS production, and also prevented the increase in intracellular calcium levels that was associated with the mitochondrial ROS surge, strongly indicated that these compounds targeted the mitochondria to bring about their protective effects. A detailed investigation as to how these two closely linked events were disrupted by **16** and **25** is beyond the scope of this thesis. Some possibilities are that the compounds function as mitochondrial uncouplers and prevent the hyperpolarization of mitochondria which results in ROS generation, or interact with channels that are responsible for calcium influx, or interfere with signaling mechanisms linking high ROS levels

and the opening of calcium channels. That **45** and **46** failed to affect either the mitochondrial ROS surge or calcium influx further emphasized the importance of the aromatic ring – NH – aromatic ring motif for activity.

4.5. Conclusion

The main findings of this chapter are summarized in the following points:

(i) Only the 9-(N-phenyl)amino-6-chloro-2-methoxyacridines of Group 2 protected HT22 cells from glutamate-induced oxidative cytotoxicity. The acridine ring may be unsubstituted or replaced with 6-chloro-1,2,3,4-tetrahydroacridine or 7-chloroquinoline with no loss of protective activity, in so far as the phenyl-NH-heterocyclic ring motif is maintained. The substituted acridine ring was associated with the most potent activity while analogs with the tetrahydroacridine and quinoline rings were less cytotoxic. For many compounds, the difference in protective and cytotoxic EC_{50} values was more than 10 folds which made them attractive lead candidates for future investigation.

(ii) A variety of substituents may be introduced at the 9-(N-phenyl) ring with relatively small variations (no more than 17 fold) in protective activity. The lipophilicity of the compound which was influenced mainly by the type of group present on the 9-(N-phenyl) ring played a significant role, with greater protective activity observed with more lipophilic compounds.

(iii) Time-related experiments showed that Group 2 compounds protected against glutamate induced cell death when present at the same time as glutamate, as well as when introduced after the addition of glutamate. Representative Group

2 compounds (**5**, **6**, **11**, **15**, **16**, **25**) were able to "rescue" cells exposed to glutamate for as long as 8-10 hours.

(iv) The protective effects of the Group 2 compounds were not related to their effects on GSH levels which remain greatly diminished in cells exposed to both test compound and glutamate. Thus, up-regulation of rate limiting enzymes involved in GSH biosynthesis may be discounted as a mode of action of these compounds.

(v) The ability to quench free radicals and/or prevent their accumulation was strongly associated with the ability of the compounds to protect cells against glutamate induced cell death. This was seen from their TEAC values which indicated antioxidant activity in a cell-free system as well as their ability to prevent the increase in intracellular ROS levels induced by glutamate. The presence of an intact NH group at the 9-position of the acridine was an important requirement for activity, suggesting that this group is linked to the antioxidant potential of the compounds.

(vi) The latent protective effects of the active compounds were attributed to their effects on mitochondrial ROS levels and influx of calcium, both of which were late-stage events linked to glutamate-induced cell death. As in (v), an intact NH at the 9 position of the acridine ring was an important requirement for activity.

Chapter 5: Anti-cholinesterase activity of synthesized compounds

5.1 Introduction

One of the objectives of this thesis was to investigate the multi-targeting potential of the acridine scaffold in neurodegenerative disorders. Thus far, the functionalized acridines synthesized in this report had demonstrated in vitro antiprion activity and were able to protect mouse hippocampal cells from glutamate induced oxytosis. In this chapter, the anti-cholinesterase activities of the synthesized compounds were explored, prompted in part by the structural resemblance of several synthesized compounds, particularly those in Group 6, to the prominent anti-cholinesterase agent tacrine.

Tacrine (9-amino-1,2,3,4-tetrahydroacridine, Figure 5.1), a reversible inhibitor of acetylcholinesterase (AChE) and butyrylcholinesterase (BChE), was the first drug to be approved by the United States Food and Drug Administration for palliative treatment of mild and moderate Alzheimer's disease (AD).[166] However, it was subsequently withdrawn because of its association to hepatotoxicity, slow pharmacokinetics and high incidence of side effects.[167] Nonetheless, interest in the tetrahydroacridine scaffold was not dampened and several derivatives were synthesized and evaluated for AChE inhibitory activity[168-170] with the aim of obtaining safer and more potent analogs for AD.

Tacrine   Donepezil
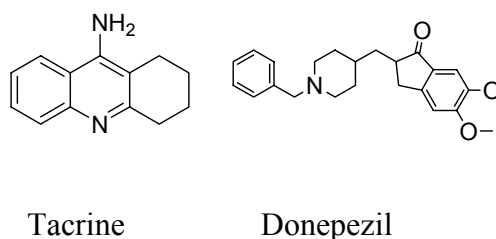
Figure 5.1: AChE inhibitors approved for the treatment of Alzheimer's Disease.

The binding interaction of tacrine with AChE had been investigated in detail. A crystalline complex of tacrine with Torpedo AChE showed that the tetrahydroacridine ring of tacrine was stacked against the indole ring of a tryptophan residue (Trp 84) which was a key component of the anionic site of AChE.[171] The ring nitrogen (protonated) of tacrine formed a hydrogen (H) bond to the main-chain carbonyl oxygen of His 440, one of the 3 amino acids of the catalytic triad (the others are Ser 200 and Glu 327) responsible for the hydrolysis of the substrate acetylcholine by a charge relay mechanism. H bonding between the 9-amino group of tacrine and water molecules were also observed.

An alternative binding mode was proposed by Pang and Kozikowski[172] based on computer aided docking. They showed that tacrine had two binding loci on the Torpedo AChE, one at the anionic site (π-π interactions with Trp 84 as described in the preceding paragraph) and another at the peripheral anionic site (PAS) which was located at the opening of the enzymatic binding pocket ("gorge") of AChE. The PAS which was rich in aromatic residues (such as Trp 279, Tyr 70, Phe 290) was proposed to be a "low affinity" binding site for tacrine, which would explain the inability of crystallography to reveal the binding of tacrine to this peripheral site. The apparent role of the PAS was to increase the

170

concentration of acetylcholine at the opening of the active site pocket, ensuring that sufficient amounts were made available to the catalytic site which lies at the base of the narrow binding pocket.[173] Thus, low affinity binding rather than tight binding of the substrate to this site was more appropriate. In the case of BChE, the sister enzyme of AChE, the number of aromatic residues at the PAS was greatly diminished because the active site of this enzyme was wide enough to permit diffusion of the putative substrate (the endogenous substrate of BChE has yet to be identified) or ligand to the catalytic site of the enzyme.[174]

Other functionalized acridines have also been reported to inhibit AChE. 9-Aminoacridine was as potent as tacrine as an inhibitor of AChE inhibitor[175] but unlike tacrine, it was proposed to bind to the aromatic residues of the PAS.[176] Alkylene-linked tacrine dimers in which the tetrahydroacridine rings were separated by 5-7 carbon atoms were exceptionally strong inhibitors of AChE.[169,170] They were proposed to bind to both the PAS and the anionic site. In view of the absence of PAS in BChE, the bis-tacrines inhibited AChE to a significantly greater extent than BChE.[169] An interesting observation was that the bis-tacrine analog in which the two rings were separated by five carbon atoms, disrupted the catalytic triad of AChE and induced unique reorientations at the active-site gorge.[170] In spite of these drastic rearrangements caused by the binding, the inhibitor was still more potent than tacrine in inhibiting AChE, suggesting that the energetics of the π-π stacking interactions could overcome the energy barrier involved in the re-orientation process.

In view of the available literature on the AChE inhibitory properties of functionalized acridines and tetrahydroacridines, it was of interest to determine if the N-substituted 9-aminoacridines (Groups 1-5), 9-amino-1,2,3,4-tetrahydroacridines (Group 6) and 9-aminoquinolines (Groups 7) synthesized here would inhibit AChE. Thus, a key objective of this chapter was to evaluate their AChE inhibitory activities and establish relevant structure-activity relationships. The inhibitory potencies of compounds **32, 51** and **57** (Figure 5.2) were of particular interest because they bear a N-benzyl-4-piperidinyl side chain which was present in donepezil, a long acting anti-AChE agent that is used clinically for the symptomatic treatment of AD (Figure 5.1). Compound **51** may be considered as a hybrid molecule incorporating the tetrahydroacridine ring of tacrine (but with an additional 6-chloro atom) and the side chain of donepezil while **32** and **57** were variants of **51**, with acridine and quinoline rings in place of tetrahydroacridine. Tacrine-donepezil hybrids had been synthesized and reported as AChE inhibitors (Figure 5.2)[177] and it would be of interest to determine how the hybrid molecules in this chapter compare in terms of AChE inhibitory activity.
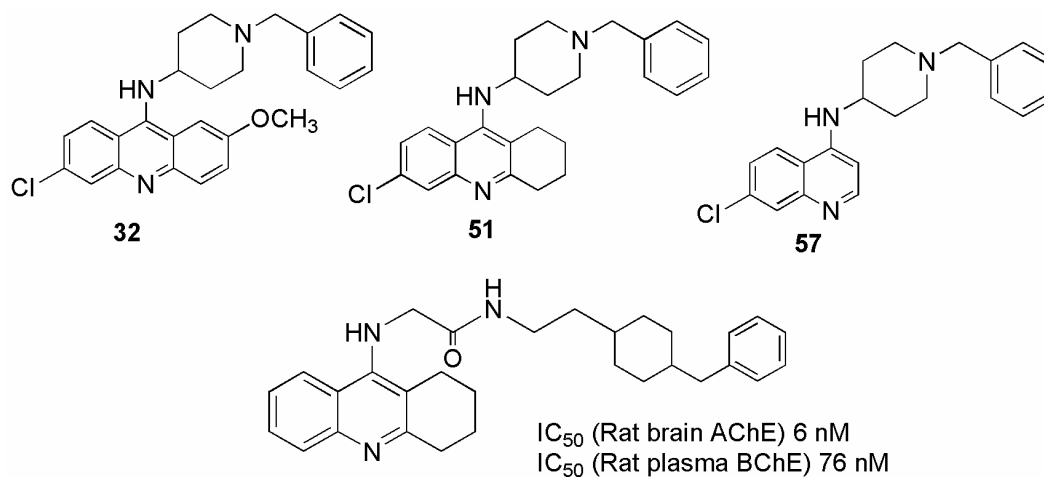
Figure 5.2: Tacrine-donepezil hybrid molecules reported by Shao *et al.*[177]

In view of the structural differences between the active sites of AChE and BChE, most inhibitors selectively inhibit one enzyme over the other. Tacrine itself was a stronger inhibitor of BChE (IC$_{50}$ 92 nM) than AChE (IC$_{50}$ 223 nM).[169] Selective inhibition of BChE had been proposed as a desirable feature for anti-AD drugs because BChE activity was found to be significantly increased in the human AD brain while AChE activity was decreased.[178,179] If so, BChE activity would then contribute significantly to the hydrolysis of acetylcholine[180] and would be a promising target for AD. Thus it was of interest to determine the AChE / BChE selectivity profiles of the synthesized compounds.

5.2. Experimental methods

5.2.1. Determination of inhibitory effects on AChE and BChE

Human acetycholinesterase (EC3.1.1.7, AChE), equine butyrylcholinesterase (EC3.1.1.8, BChE), dithiobisnitrobenzoic acid (DTNB), and substrates acetylthiocholine iodide and butyrylthiocholine iodide were purchased from Sigma Aldrich Chemical Co, Singapore. Test compounds were screened for their anti-cholinesterase activities at a final concentration of 3μM following the Ellman method.[181] The assay was carried out on a 96-well plate, with each well containing 300 μl of 0.1 M phosphate buffer (pH 8.0), 10 μl of 0.01 M DTNB, 1 μl of 2 units/ml of AChE or BChE solution, 10 μl of stock solution of test compound (prepared in DMSO) and 2 μl of 0.075 M substrate. The substrate was added last to start the reaction. Control wells containing the same composition but without test compound (10 μl DMSO) were included to give the basal

(uninhibited) AChE or BChE activity. Absorbance at 412 nm was recorded every minute for 10 minutes at 37°C on a Bio-Rad Benchmark Plus microplate reader. The rate of reaction was taken as the slope of the absorbance curve over time. To account for non-enzymatic hydrolysis of the substrate, wells containing the same composition as the above but without enzyme were concurrently monitored. Non-enzymatic hydrolysis was however not observed. The percent inhibition was calculated as the percentage of the reaction rate of test compound over that of vehicle control. Compounds with percent inhibition greater than 75% were further tested at 5 concentrations to determine IC$_{50}$ values using GraphPad Prism v4.03 (GraphPad Software Inc., CA, US).

For the determination of enzyme kinetics of selected potent compounds, a fixed amount of the enzyme (1 µl of 2 units/ml of AChE or BChE solution) was used for these determinations with substrate concentrations ranging from 0 to 450 mM for both AChE and BChE assays. Determinations were made in the absence and presence of test compound. At least 3 different concentrations of test compound were used in each instance and the experiment was repeated on 3 different occasions. Inhibition types and inhibition constants (K$_i$) were determined by SigmaPlot v11.0 and Enzyme Kinetic v1.3 add-on (Systat Software, Inc, CA, US).

The dependence of reaction rate on substrate concentration was assumed to follow the Michaelis-Menten kinetics as given in Equation (1) where v = rate of hydrolysis, [S] = substrate concentration, K$_m$ = dissociation constant for the ES complex, equivalent to the concentration of substrate required to produce a rate of

V_{max} /2 and V_{max} = maximal rate of reaction which is attained at infinite substrate concentration.

$$v = V_{max} [S] \ / \ K_m + [S] \qquad (1)$$

Taking the reciprocal of Equation 1 gives Equation 2:

$$1/v = 1/ V_{max} + K_m / V_{max} [S] \quad (2)$$

A plot of 1/v versus 1/S gives a straight line which is the Lineweaver-Burk plot. The interception of the x-axis is $-1/K_m$ and the interception of the y-axis is $1/V_{max}$. K_i is the intersection point in the Dixon plot (plot of 1/v vs. [I]).[182]

5.2.2. Molecular modeling

The x-ray crystallographic complexes of *Torpedo californica* AChE and tacrine (PDB code 1ACJ) and donepezil (PDB code 1EVE) were used for docking. The tested compounds were built and minimized by the forcefield MMFF94x in Molecular Operating Environment (MOE) 2008.10 (Chemical Computing Group, Montreal, Canada). Tacrine was removed and the protein was protonated in GOLD software (The Cambridge Crystallographic Data Center, Cambridge, UK). The binding site was defined as 15Å from the oxygen of Tyr 124 side chain as this atom was at the center of the active site.[183] 100 runs were performed for each compound using automatic genetic algorithm parameters. The default values of these parameters were: population size: 100, selection pressure: 1.1, number of operations: 105, number of islands: 5, niche size: 2, migrate: 10, mutate: 95, and crossover: 95. Finally, docked poses were visualized and examined on MOE.

Similarly, the x-ray crystallographic structure of human BChE (PDB code 1P0M) was used for docking. Since Tyr 124 was not found in the BChE binding site, the latter was defined by the following amino acid residues: Trp 82, Glu 197, Ser 198, Glu 325, His 438, Asp 70, Asn 68, Gln 119, Ala 277 which make up the anionic catalytic site, catalytic triad and peripheral anionic site.[184] Docking parameters were similar to those used for the docking onto TcAChE.

5.3. Results

5.3.1. AChE and BChE inhibitory activities

AChE and BChE activities were determined by the Ellman's method[181] which was adapted to a 96-well plate format in this study. Briefly, the assay was based on the release of thiocholine when the substrate acetylthiocholine or butyrylcholine was hydrolyzed by their respective enzymes (Figure 5.3). Thiocholine reacted with 5,5'-dithiobis-2-nitrobenzoic acid (DTNB) by a redox reaction to give colored 5-mercapto-2-nitrobenzoate anion which was detected spectrophotometrically. When the enzyme was inhibited, less of the yellow colored anion would be generated and this was used as a means of assessing the degree of inhibition.
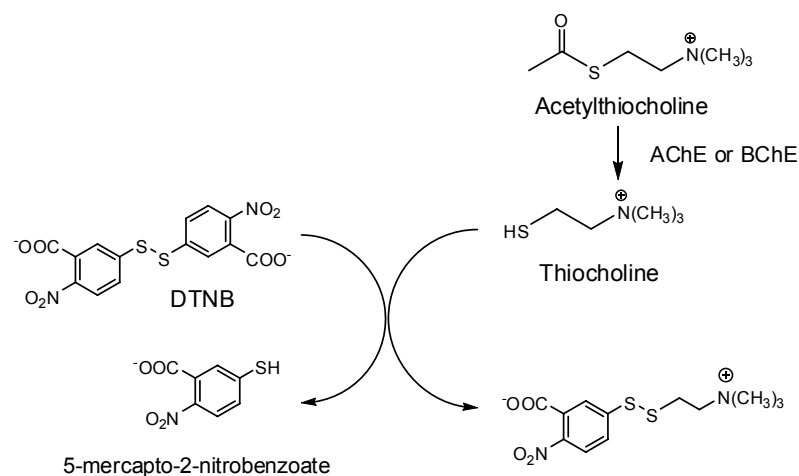
Figure 5.3: Reactions involved in the determination of AChE activity by the Ellman's method.

5.3.1.1. Inhibition of AChE and BChE at a fixed concentration (3 µM) of test compound

Table 5.1 gives the % inhibition of AChE and BChE by Group 1-7 compounds tested at a fixed concentration of 3 µM. From the results, the more potent compounds were short-listed for the determination of IC_{50} values. Noting that tacrine at 3 µM inhibited AChE and BChE by 91% and 98% respectively, a threshold value of 75% inhibition was set for identifying compounds that might be of comparable or greater potency than tacrine.

Table 5.1: Percent inhibition of AChE and BChE by compounds in Groups 1-7 tested at a fixed concentration of 3 µM.

Group 1

$NH(CH_2)_nNR_2$
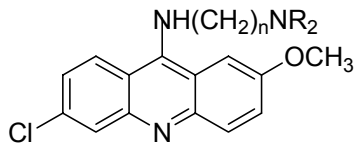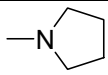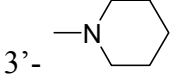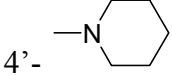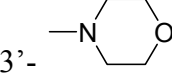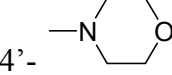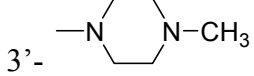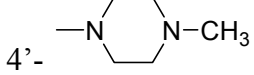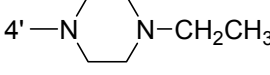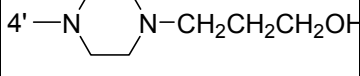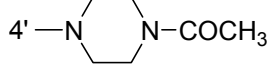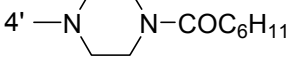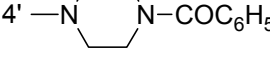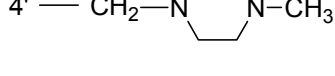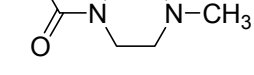
Compound	Side chain (R)	% Inhibition AChE[a]	% Inhibition BChE[a]
1	n=2, R=C_2H_5	30.4±6.0	83.9±1.5
2	n=3, R=CH_3	32.6±3.4	63.5±4.6
3	n=3, R=C_2H_5	47.4±3.9	66.3±0.4
4	n=4, R=C_2H_5	65.5±1.0	79.5±1.0

Group 2
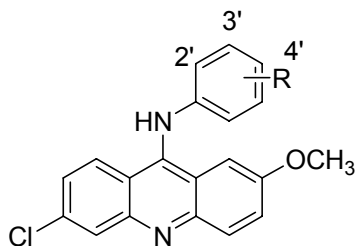
Compound	Side chain (R)	% Inhibition AChE [a]	% Inhibition BChE [a]
5	2'-$N(CH_3)_2$	34.9±1.4	48.0±9.9
6	3'-$N(CH_3)_2$	18.4±7.6	86.3±1.2
7	4'-$N(CH_3)_2$	50.6±2.8	57.1±4.6
8	3'-$N(C_2H_5)_2$	31.7±1.8	51.6±5.4
9	4'-$N(C_2H_5)_2$	64.1±0.9	55.9±2.7
10	3'- (pyrrolidine)	23.3±2.6	80.5±1.6

11	3'- —N(piperidine)	63.8±2.8	65.6±7.7
12	4'- —N(piperidine)	52.3±2.8	38.6±0.9
13	3'- —N(morpholine)O	28.3±8.5	68.3±2.7
14	4'- —N(morpholine)O	8.4±5.2	19.6±4.9
15	3'- —N(piperazine)N—CH$_3$	25.1±1.0	50.7±2.4
16	4'- —N(piperazine)N—CH$_3$	54.4±0.4	51.3±1.7
17	4'—N(piperazine)N—CH$_2$CH$_3$	52.0±4.9	68.3±2.7
18	4'—N(piperazine)N—CH$_2$CH$_2$CH$_2$OH	ND[b]	ND[b]
19	4'—N(piperazine)N—COCH$_3$	43.7±2.7	10.2±7.9
20	4'—N(piperazine)N—COC$_6$H$_{11}$	23.7±5.7	14.7±0.7
21	4'—N(piperazine)N—COC$_6$H$_5$	30.4±3.9	6.5±4.9
22	4'—CH$_2$—N(piperazine)N—CH$_3$	49.6±1.9	25.1±5.6
23	4'—CO—N(piperazine)N—CH$_3$	28.5±4.3	35.3±0.2

24	4'— CH$_2$—N⟨piperidine⟩	62.1±0.3	79.6±0.8
25	H	40.9±5.0	30.5±4.5
26	4'-CN	19.2±2.2	-1.7±3.4
27	4'-F	45.8±6.4	0.7±0.9
28	3',4'-diF	47.2±7.6	-4.6±5.6
29	4'-OCH$_3$	46.4±9.8	31.3±4.4
30	3'-OH	5.3±4.7	-3.6±1.6
31	3',4'-diOH	47.4±4.0	-1.7±3.8

Group 3
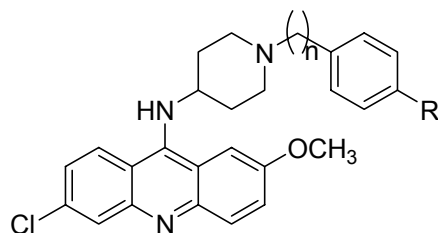
Compound	Side chain (R)	% Inhibition AChE [a]	% Inhibition BChE [a]
32	n=1, R=H	69.1±3.1	41.9±3.3
33	n=1, R=CH$_3$	38.3±1.9	12.8±3.8
34	n=1, R=Cl	64.9±4.9	32.8±3.1
35	n=1, R=OCH$_3$	34.3±2.1	8.6±5.0
36	n=1, R=CN	34.0±3.8	35.5±0.9
37	n=2, R=H	67.8±1.0	38.7±0.6
38	n=2, R=CH$_3$	71.1±5.3	36.7±2.5

180

39	n=2, R=Cl	78.5±0.2	30.5±5.1
40	n=2, R=OCH$_3$	82.0±1.6	20.9±1.5
41	n=3, R=H	95.6±0.7	37.1±5.8

Group 4
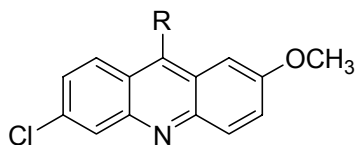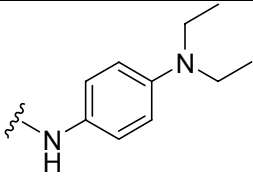
Compound	Side chain (R)	% Inhibition AChE [a]	% Inhibition BChE [a]
42		59.2±4.9	20.6±4.0
43		52.5±2.0	59.5±1.0
44	-OPh	ND[b]	ND[b]
45		46.0±6.7	1.4±0.4
46	-NH$_2$	ND[b]	ND[b]

Group 5
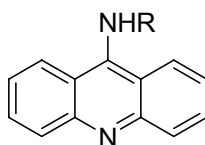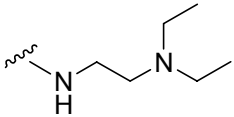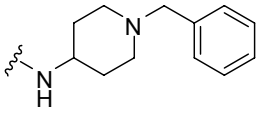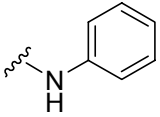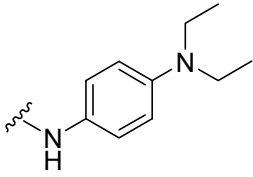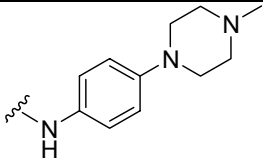
Compound	Side chain (R)	% Inhibition AChE [a]	% Inhibition BChE [a]
47	-NH$_2$	92.5±0.4	99.7±0.4

181

| 48 | | 47.6±7.1 | 86.5±1.9 |

Group 6
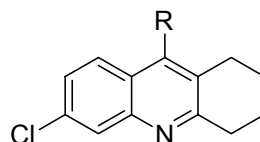
Compound	Side chain (R)	% Inhibition AChE [a]	% Inhibition BChE [a]
49	NH$_2$	97.9±0.3	98.0±0.3
50		97.0±0.1	95.3±0.4
51		97.8±0.1	88.4±0.8
52		82.1±1.3	34.6±5.3
53		81.6±3.0	50.7±5.7
54		77.7±1.0	42.9±2.9
Tacrine		91.3.± 0.5	98.3 ± 2.1

Group 7
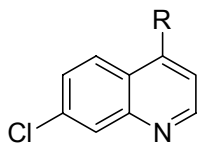
Compound	Side chain (R)	% Inhibition AChE [a]	% Inhibition BChE [a]
55	NH_2	0.4±5.4	2.0±0.5
56		6.6±1.4	4.4±1.3
57		54.0±4.3	7.6±2.6
58		15.4±4.8	7.0±0.6
59		6.2±5.8	4.1±1.7
60		31.9±2.2	6.4±1.7

[a] : % Inhibition is presented as mean ± SEM from 3 independent determinations.

[b]: Not determined

Notwithstanding the limitations of deducing structure activity relationships based on % inhibition, some important observations could be made at this stage of the investigation.

(i) Outstanding anti-AChE activity was observed in Group 6, with all 6 compounds inhibiting AChE by more than 75%. The ring scaffold in Group 6 (6-chloro-1,2,3,4-tetrahydroacridine) was structurally related to that of tacrine except for the presence of an addition 6-chloro atom on the ring. It was apparent that the 6-chloro atom did not adversely affect anti-AChE activity as seen from the comparable activities of tacrine and **49**. On the other hand, inhibitory activity was affected by the type of substitution on the 9-amino functionality. In this regard, a phenyl or substituted phenyl ring at the 9-amino group (as in **52**, **53**, **54**) was less favored as compared to a diethylaminoethyl (**50**) or 1-benzyl-piperidin-4-yl (**51**) side chain.

(ii) Three compounds in Group 3 inhibited AChE by more than 75%. The ring scaffold in this Group was 2-methoxy-6-chloroacridine, which was also present in Groups 1, 2 and 4 . But no active compounds were observed in these groups. Thus, it was clear that the anti-AChE activity of Group 3 compounds was due more to the side chain attached to the 9-amino functionality of the ring than to the ring itself. In Group 3, the side chain was 1-benzyl-4-piperidinyl (**32**) or its structural variants. Interestingly, the 1-benzyl-4-piperidinyl side chain was present in the clinically used anti-AD drug, donepezil. However, the compound in Group 3 with this side chain (**32**) was not an exceptional inhibitor of AChE (69%), suggesting that the change in scaffold (tetrahydroacridine to acridine) contributed to the diminished activity. However, this was compensated to an extent by lengthening the alkyl chain separating the terminal phenyl from the piperidine ring of the side chain to two carbon atoms (in which case substitution of the

phenyl ring was required, as seen in **39** and **40**) and three carbon atoms (as seen in **41**). The 3-carbon homolog **41** (96% inhibition) was as potent as tacrine (91% inhibition) in inhibiting AChE. On the other hand, the 2-carbon homolog **37** was a weak inhibitor (67%, and comparable to **32**) and required substitution on the phenyl ring to bring about greater inhibition.

(iii) Groups 1, 2, 4 and 7 did not yield compounds that inhibited AChE by more than 75%. Their poor activities reflected interplay of the ring scaffold and the substituent attached to the 9-amino functionality in influencing inhibitory activity. The 6-chloro-2-methoxy acridine ring was not a favored ring scaffold and when coupled with a phenyl/substituted phenyl at the 9-amino group, resulted in poor anti-AChE activity. Thus none of the 26 compounds in Group 2 inhibited AChE by more than 75%. An alkyl or alkynyl side chain attached to the same ring scaffold was also detrimental as seen from the poor activities of Group 1 and **43** of Group 4. 7-Quinoline was even less favored as a ring scaffold as seen from the exceptionally poor activities of the Group 7 compounds. In fact, for the same side chain at the 9-amino/4-amino function, compounds with the quinoline ring had the lowest anti-AChE activity.

(iv) 9-Aminoacridine (**47**) of Group 4 was a potent AChE inhibitor which was in keeping with literature reports.[175] The sharp decline in activity when a substituted phenyl was attached to the 9-amino functionality (as in **48**) provided further confirmation of the detrimental effect of this structural modification.
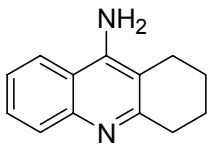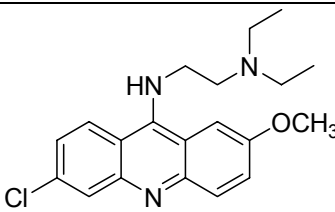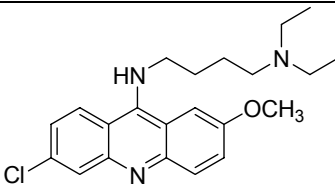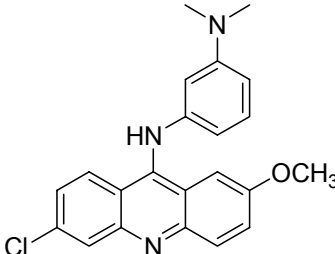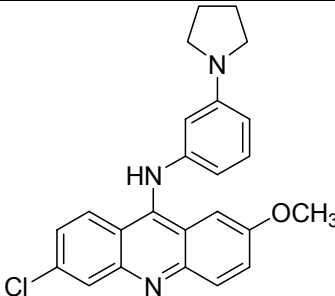
(v) Turning to anti-BChE activities of Groups 1-7, it was noted that Groups 3 and 6 which yielded the most active anti-AChE compounds were not
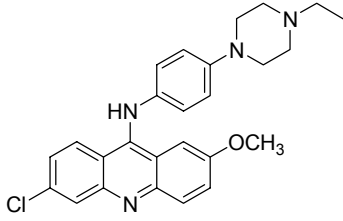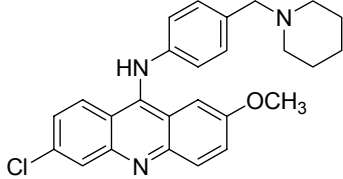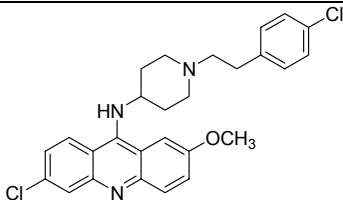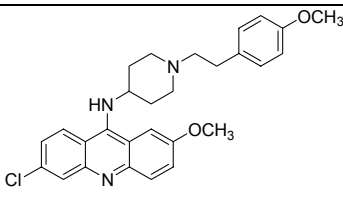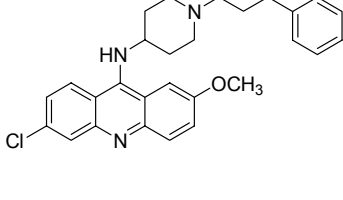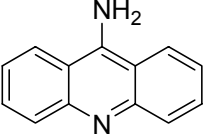
particularly outstanding as anti-BChE agents. This was most apparent in Group 3 and to lesser degree in Group 7 where 3 compounds (**49**, **50**, **51**) were still able to inhibit BChE by more than 75%. Interestingly, good BChE inhibitory activity was observed among many compounds in Groups 1 and 2 which had poor anti-AChE activities. Clearly, the dialkylaminoalkyl and substituted phenyl substitutents on the 9-amino functionality did not adversely affect BChE activity. There was an indication that an unsubstituted acridine ring may be a desirable scaffold for BChE activity but this is based on only one compound (**48**) which inhibited BChE by 86% as compared to 56% for its Group 2 analog (**9**). The N-substituted 4-amino-7-chloroquinolines of Group 7 were found to be extremely weak inhibitors of BChE.
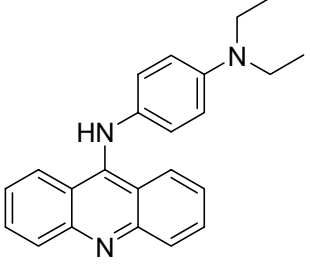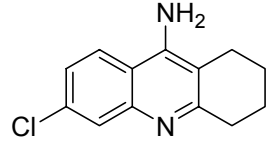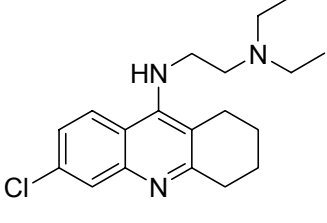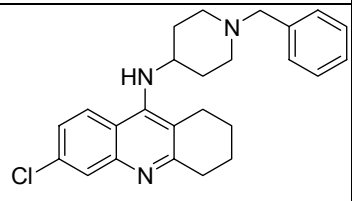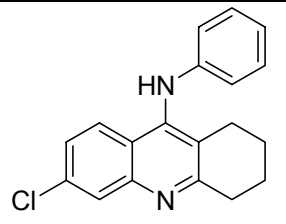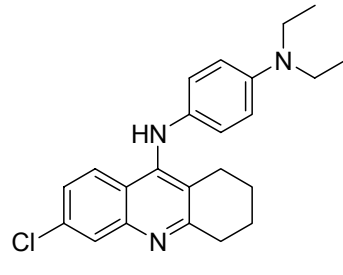
5.3.1.2. AChE and BChE inhibitory activities of selected compounds based on IC_{50} determination
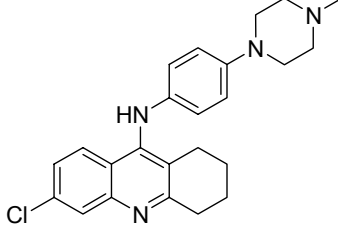
In the next stage of the investigation, IC_{50} values for AChE and BChE inhibition were determined for compounds that inhibited either enzyme by more than 75%. These were **39-41** (Group 3), **47** (Group 5), **49-54** (Group 7) which inhibited AChE by more than 75%, and **1**, **4** (Group 1), **6**, **10**, **24** (Group 2), **47**, **48** (Group 5), **49 -51** (Group 7) which inhibited BChE by more than 75%. The results are given in Table 5.2. Representative plots of % inhibition versus concentration are given in Figure 5.3.

186

Table 5.2: AChE and BChE inhibitory IC_{50} values of tacrine and selected compounds

Compound	Structures	AChE IC_{50} $(nM)^a$	BChE IC_{50} $(nM)^a$	IC_{50} AChE / IC_{50} $BChE^b$
Tacrine		182.2 (158.1, 210.0) [c]	6.6 (5.7, 7.6) [d]	27.6
1		> 3000	1149 (977.6, 1349)	2.6
4		ND	947 (735.8, 1219)	-
6		> 3000	936.0 (824.2, 1063)	3.2
10		> 3000	660.7 (495.5, 881.0)	4.5

17	7-Cl, 2-OCH₃ acridine with HN–phenyl–(4-ethylpiperazine)	≈ 3000	1336 (1203, 1483)	2.2
24	7-Cl, 2-OCH₃ acridine with HN–phenyl–CH₂–piperidine	ND^e	1634 (1483, 1801)	-
39	7-Cl, 2-OCH₃ acridine with HN–piperidine–CH₂CH₂–(4-Cl-phenyl)	597.5 (469.7, 760.1)	> 3000	0.20
40	7-Cl, 2-OCH₃ acridine with HN–piperidine–CH₂CH₂–(4-OCH₃-phenyl)	1077 (911.3, 1272)	> 3000	0.36
41	7-Cl, 2-OCH₃ acridine with HN–piperidine–CH₂CH₂CH₂–phenyl	292.2 (253.3, 337.1)	> 3000	0.10
47	9-aminoacridine (NH₂)	224.1 (191.0, 263.0)	8.6 (6.6, 11.1)	26

48		≈ 3000	1298 (1153, 1462)	2.3
49		8.8 (6.5, 11.8)	15.2 (13.4, 17.2)	0.58
50		40.8 (31.7, 52.6)	81.5 (62.6, 106.2)	0.50
51		5.7 (4.8, 6.7)	284.6 (238.4, 339.9)	0.02
52		1175 (911.9, 1515)	>3000	0.39
53		869.4 (701.8, 1077)	≈ 3000	0.29

54		1384 (1138, 1682)	> 3000	0.46

[a] IC_{50} was determined by GraphPad Prism v4.03 from at least three independent experiments. 95% Confidence intervals are given in brackets.

[b] Ratios > 1 indicate selective inhibition of BChE. Ratios < 1 indicate selective inhibition of AChE. In cases where $IC_{50} \geq 3000$ nM, a value of 3000 was taken to compute the ratio.

[c] Reported IC_{50} for human AChE : 147 nM ±11 [50], 424 nM ±21 [185]

[d] Reported IC_{50} for human BChE : 36 nM ± 4 [50]; 45.8 nM ± 3.0 [185]

[e]: Not determined.
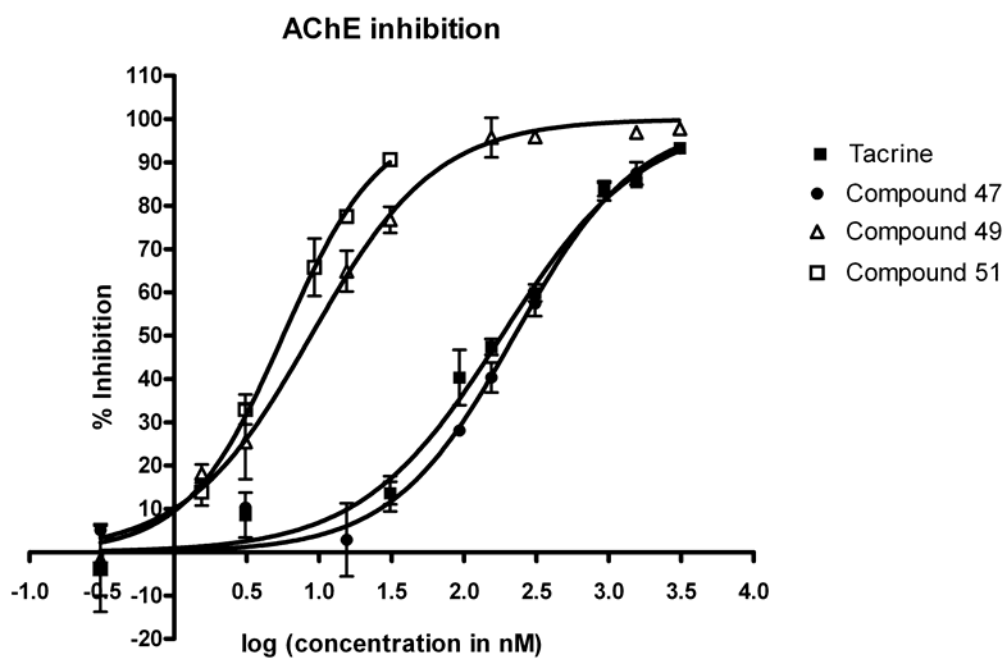
Figure 5.4: Anti-AChE activities vs. concentrations of tacrine, compounds **47**, **49**, and **51**.

   With IC_{50} values, a more definitive structure-activity relationship could be obtained, the main points of which are highlighted in the following paragraphs.

   Introducing a 6-chloro atom on to tacrine gave **49**, which was a stronger (20 folds) and more selective inhibitor of AChE. Its selectivity ratio (IC_{50AChE}/IC_{50BChE}) was 0.58 implying selective inhibition of AChE, as compared to 28 for tacrine which indicated selective inhibition of BChE. The preference for selective inhibition of AChE was observed for all the compounds in Group 6 which share the same ring structure as **49**, implying an important role for the 6-chloro atom in changing the inhibitory preference.

   When the tetrahydroacridine ring of tacrine was replaced by acridine, the resulting compound **47** (9-aminoacridine) maintained the same inhibitory profile as tacrine, both in terms of IC_{50} values and preferred inhibition of BChE. Interestingly, substitution of the 9-amino of **47** with a 4-(diethylaminophenyl) group (**48**) sharply decreased both AChE and BChE inhibitory activities, besides reducing the preference for BChE inhibition. The Group 2 compounds (**6**, **10**, **17**, **24**) were very similar to **48** in this regard: they were also poor AChE inhibitors ($IC_{50} > 3000$ nM) and had the same selectivity ratios as **48** (2.3 compared to 2.2-4.5). Thus, the poor AChE inhibitory activities of the Group 2 compounds owed more to the presence of the 9-(N-substituted phenyl)amino side chain (comparing **47** and **48**) and less to the inclusion of chloro and methoxy groups to the acridine ring. Indeed, when the substituted phenyl ring was removed and replaced by the

donepezil-like side chains of Group 3, there was a marked improvement of AChE inhibitory activity as well as a return to selective inhibition of AChE, comparable to that observed with the tetrahydroacridine analogs of Group 6. In contrast, replacing the substituted phenyl ring of Group 2 with a diethylaminoalkyl side chain (**1**, **4** in Group 1) retained the same inhibitory profile. Both Group 1 and 2 compounds were weak AChE inhibitors, with an apparent selectivity for BChE inhibition.

The most potent AChE inhibitor identified in this investigation was the compound **51** from group 6 (IC_{50} 5.7 nM). It was more potent than tacrine and also highly selective for AChE inhibition (selectivity ratio of 0.02). No compound was identified to be a more potent BChE inhibitor than tacrine although **47** (9-aminoacridine) and **49** (9-amino-6-chloro-1,2,3,4-tetrahydroacridine) had almost comparable $IC_{50\ BChE}$ values as tacrine. They were however less interesting compounds because of their under-functionalized structures. The Group 6 compound **50** was the next most potent BChE inhibitor identified here. It was also a stronger AChE inhibitor than tacrine and had a selectivity ratio of 0.5, indicating preferred inhibition of AChE.

5.3.1.3. Kinetics of the inhibition of AChE/BChE by tacrine and compounds 47, 49-51

Next, the modes of inhibition of tacrine and selected AChE and BChE inhibitors (**47**, **49**, **50**, **51**) identified in this study were investigated. The rates of AChE or BChE-catalyzed substrate hydrolysis were determined over a range of

substrate concentrations and transformed to the reciprocal Lineweaver-Burk plot for more accurate determination of K_m and V_{max} of the enzyme. When repeated in the presence of different concentrations of inhibitor, K_i of the inhibitor (dissociation constant of the enzyme-inhibitor or EI complex) was obtained and the type of inhibition (competitive, non-competitive, uncompetitive, mixed inhibition) deduced from the Lineweaver-Burk plot. Non-competitive and uncompetitive-type inhibitions are uncommon for single substrate reactions, thus the types of inhibition observed here were likely to be of the competitive or mixed inhibition types. The K_m of AChE was estimated to be 0.15 mM which was comparable to a reported value (0.17 mM) in the literature using the same method and enzyme source.[183] The K_m of BChE was found to be 0.54 mM but no value from the literature could be found for comparison. Representative Michaelis-Menten and Lineweaver Burk plots for the steady state hydrolysis of substrate by AChE and BChE, and in the presence of inhibitors tacrine, **49** and **51** are presented in Figures 5.5 and 5.6.
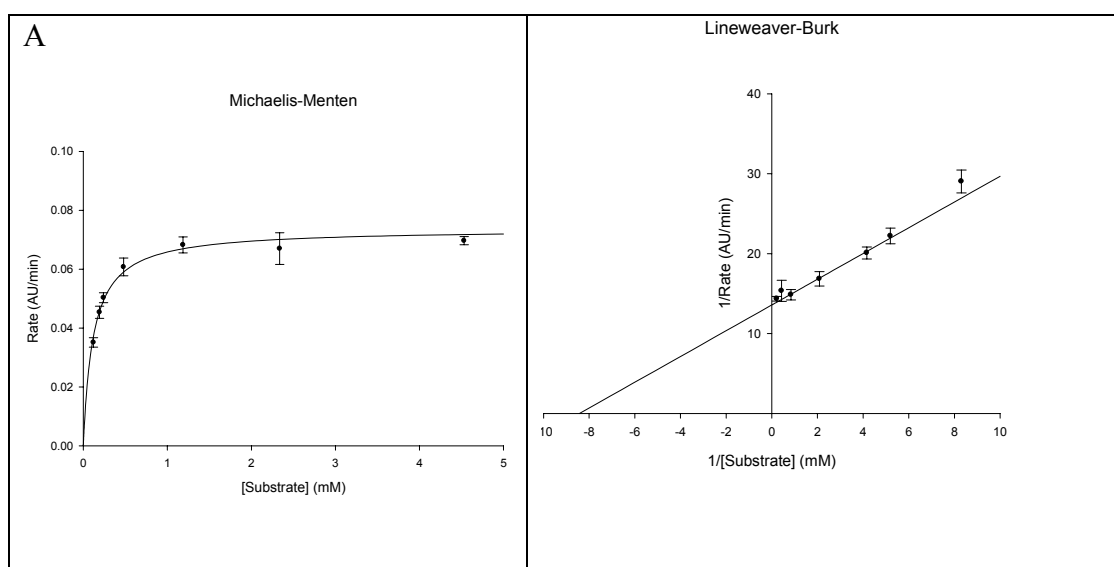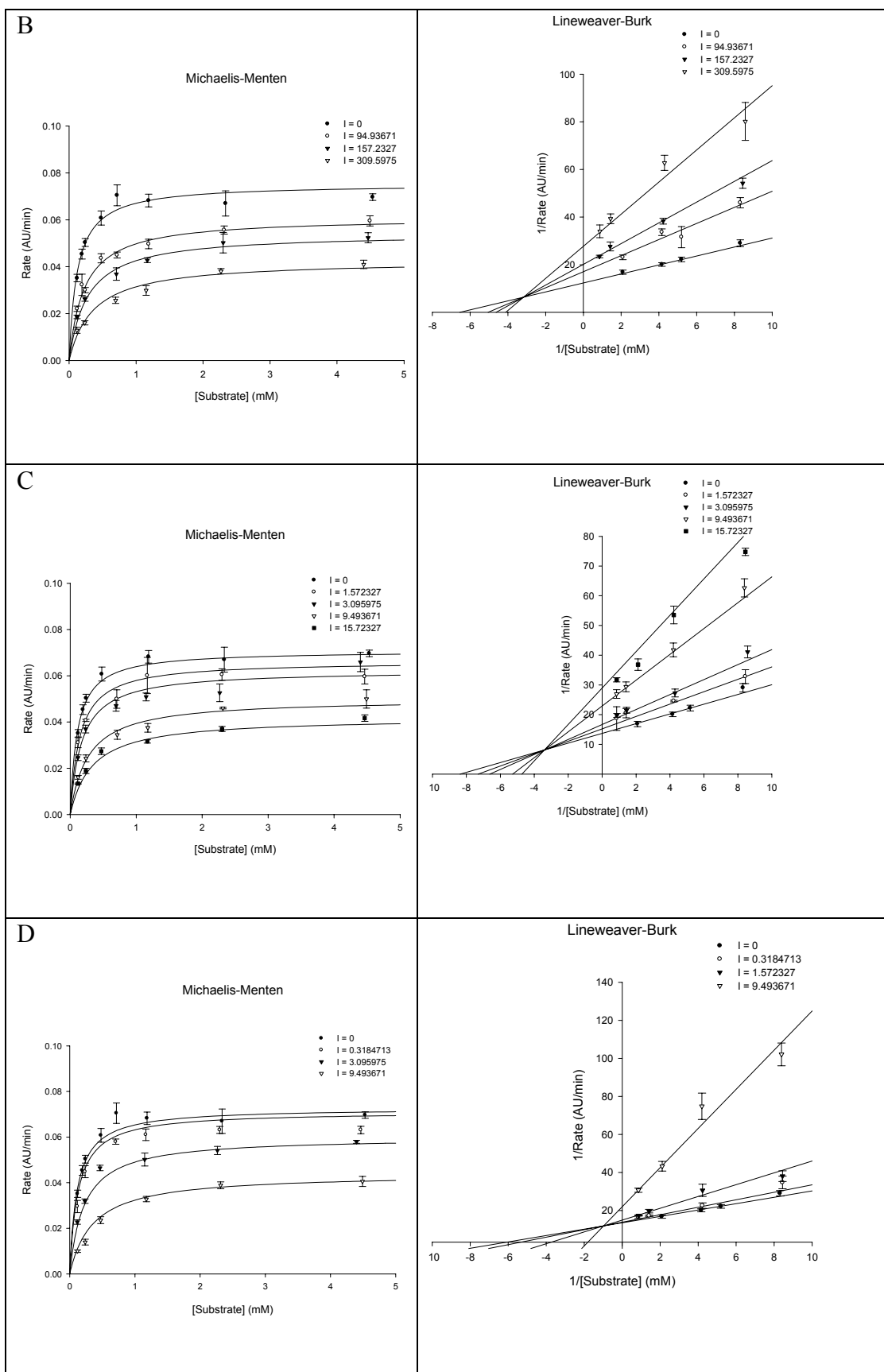
Figure 5.5: Steady-state inhibition of AChE hydrolysis acetylthicholine and Lineweaver-Burk plots of initial velocity versus substrate concentrations in (A) absence of an inhibitor, presence of inhibitors (B) tacrine, (C) **49** and (D) **51** are presented. Lines were derived from a weighted least-squares analysis of the data points.
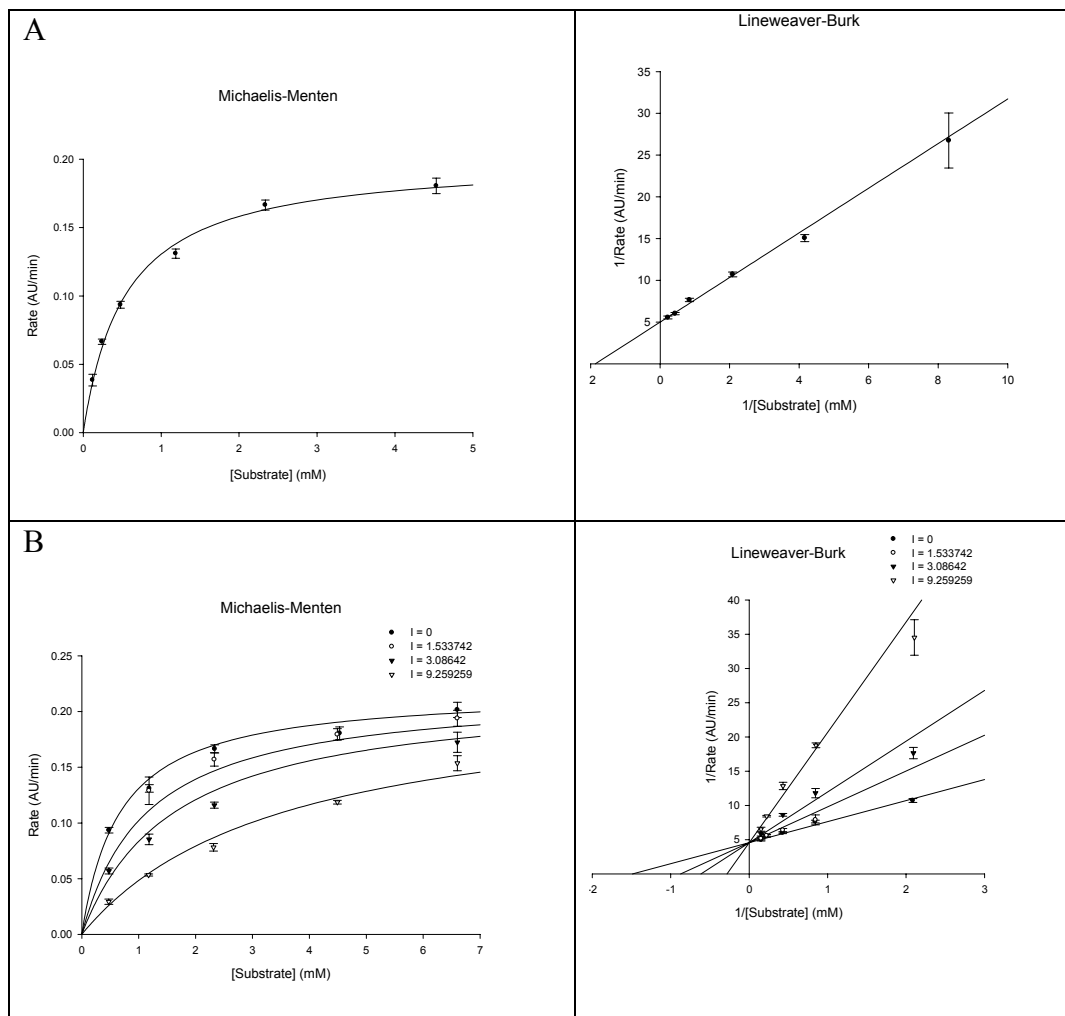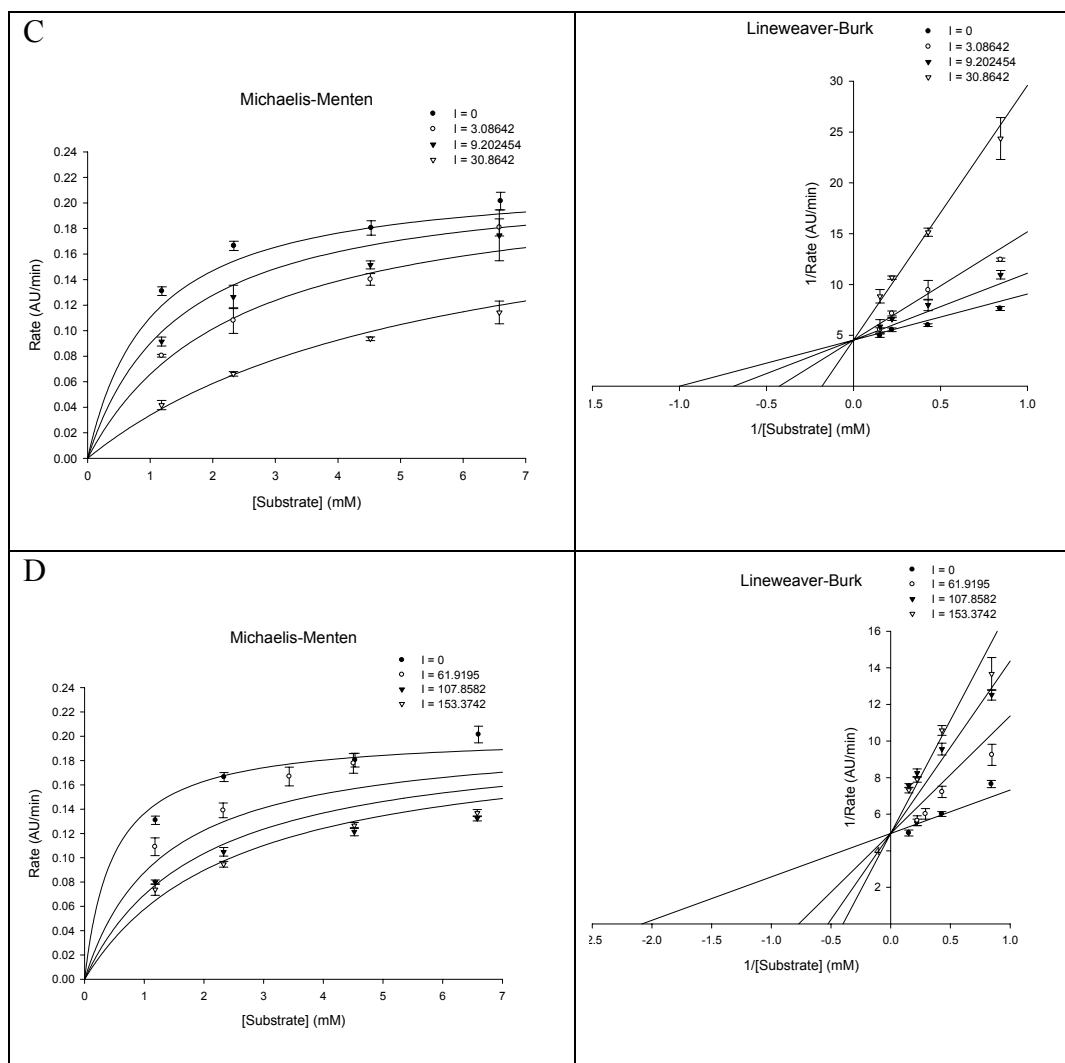
Figure 5.6: Steady-state inhibition of BChE hydrolysis acetylthicholine and Lineweaver-Burk plots of initial velocity vs. substrate concentrations in (A) absence of an inhibitor, presence of inhibitors (B) tacrine, (C) **49** and (D) **51** are presented. Lines were derived from a weighted least-squares analysis of the data points.

Inspection of the Lineweaver-Burk plots obtained for the hydrolysis of acetylthiocholine by AChE in the presence of inhibitors tacrine, **47**, **49-51** showed increasing slopes (lower V_{max}) and smaller x-intercepts (higher K_M) with increasing concentration of inhibitor. This profile was typical of mixed inhibition.

196

In mixed inhibition, the inhibitor (I) binds to both the ES (enzyme substrate) and ESI (enzyme-substrate-inhibitor) complexes. The substrate S dissociates from the ES complex at a faster rate from the ESI complex. Thus the ESI complex is nonproductive. As long as the inhibitor is present, some of the enzyme will always be in the non-productive ESI state, even at very high substrate concentrations. In effect, this lowers the concentration of the free enzyme. Therefore, V_{max} will be less than that of the free enzyme (steeper gradients in the presence of inhibitor). Moreover, a portion of the enzyme available for substrate binding will be in the low affinity EI form. Thus, the K_m will be greater than that for the free enzyme.

On the other hand, the Lineweaver-Burk plots obtained for the hydrolysis of substrate by BChE in the presence of inhibitors, tacrine, **47, 49-51** is typical of competitive inhibition. In competitive inhibition, the inhibitor competes with the substrate for binding at the active site. The affinity of the substrate for the enzyme is thus reduced (larger K_m) but at sufficiently high substrate concentrations, the inhibitor is displaced by the substrate, thus maintaining the same V_{max}. In the Lineweaver Burk plot, the substrate-only response is displaced in the presence of inhibitor to yield steeper responses that intersect at the same point on the y-axis but not at the x axis.

Table 5.3 summarizes the inhibition type, Ki and selectivity ratios of tacrine, **47** and **49-51** for the inhibition of AChE and BChE. With one exception (AChE inhibition by **47**), the sequence of inhibitory potencies expressed in terms of K_i closely parallel their IC_{50} values for both enzymes. In the case of **47**, its IC_{50}

value for AChE inhibition (224 nM) was comparable to that of tacrine (182 nM) but in terms of K_i, **47** was a stronger inhibitor than tacrine, The selectivity ratios obtained using K_i or IC_{50} values showed similar trends.

Table 5.3: Inhibition type, K_i and selectivity ratios of Tacrine, **47** and **49-51** for the inhibition of AChE and BChE.

Cmpd	AChE		BChE		Selectivity ratio $(K_{i \, AChE} / K_{i \, BChE})$
	Inhibition type	K_i (nM)	Inhibition type	K_i (nM)	
Tacrine	Mixed	120.2	Competitive	2.2	54.6
47	Mixed	87.6	Competitive	2.8	31.3
49	Mixed	5.7	Competitive	6.8	0.83
50	Mixed	7.4	Competitive	18.3	0.40
51	Mixed	1.8	Competitive	36.3	0.05

5.3.2. Docking of tacrine, compounds 49 and 51 onto the AChE and BChE binding pockets

In this section, the binding modes of tacrine and two potent inhibitors **49** and **51** at the AChE and BChE binding pockets were investigated by docking simulations using available crystallographic structures of the two enzymes. For AChE, two co-crystallized structures of ligands and Torpedo AChE (TcAChE) were explored as docking templates. They were PDB 1ACJ where the ligand is tacrine, and 1EVE where the ligand is donepezil.

The primary amino acid sequences of Torpedo AChE and human AChE (hAChE) had a relatively low similarity score of 53 but the sequences of their active sites were highly conserved.[186] This was also demonstrated by aligning the active sites of TcAChE (1ACJ) and hAChE (1B41) using the ClustalW2 program (Appendix 4) and viewing the superimposed active sites of the two enzymes by MOE (Appendix 5). The strong overlap of their active sites supported the use of TcAChE as a docking platform for this investigation.

5.3.2.1. Docking of tacrine, 49 and 51 to Torpedo AChE (1ACJ)

Before **49** and **51** were docked in the binding pocket of TcAChE derived from 1ACJ, cognate docking of tacrine was carried out. Tacrine was removed from its co-crystallized complex with the enzyme and subsequently re-docked. The pose of the re-docked tacrine was found to be similar to the original pose of tacrine in 1ACJ, thus confirming the validity of the docking protocol. The re-docked tacrine was orientated with its tricyclic ring sandwiched between the indole ring of Trp 84 and the phenyl ring of Phe 330, both of which were important residues of the catalytic anionic site. Stabilization was provided by π-π stacking of the aromatic rings. Another interaction was H bonding of the 9-amino function with two water molecules. The original pose of tacrine in 1ACJ showed H bonding between the ring N and the carbonyl oxygen of the His 440 backbone but this was not observed in the re-docked pose. The original pose of tacrine in 1ACJ and its re-docked pose in the same enzyme are shown in Figures 5.7 and 5.8.
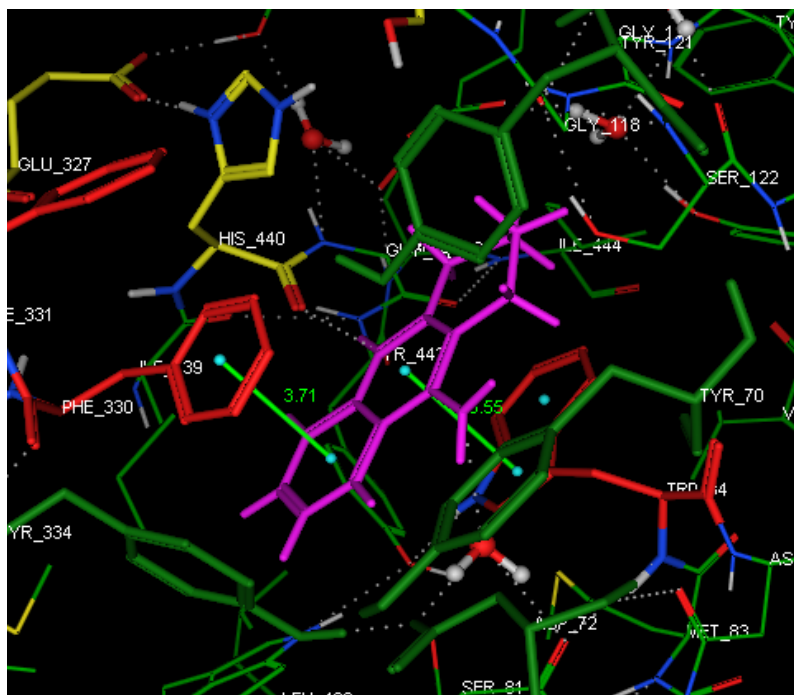
Figure 5.7: Tacrine (in pink) in the binding pocket of TcAChE (PDB code 1ACJ).
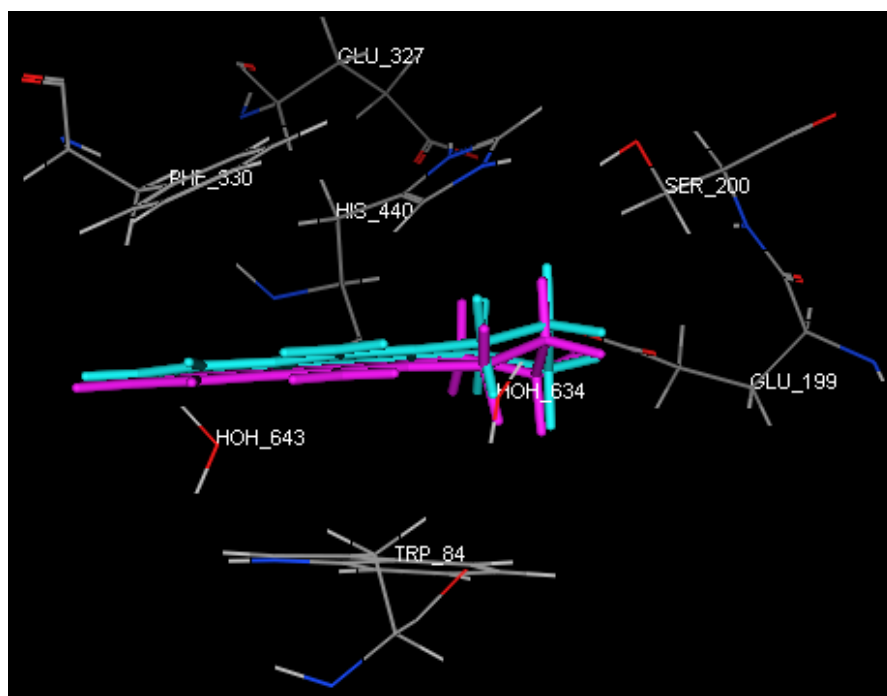
Figure 5.8: Original (pink) and re-docked (cyan) poses of tacrine in the binding pocket of TcAChE (PDB code 1ACJ).

Compound **49** (6-chlorotacrine) was a stronger AChE inhibitor than tacrine (K_i of 5.7 nM compared to 120.2 nM for tacrine, Table 5.3). Its pose in the binding pocket of the enzyme showed that like tacrine, its tetrahydroacridine ring was sandwiched between Trp 84 and Phe 330 (Figure 5.9). The ring was also aligned in such a way that there was more space at its aromatic end than the non-aromatic end. This permitted the 6-chloro atom to project into a hydrophobic pocket lined by the side chains of Trp 432 and lle 439. The extra van der Waals/hydrophobic interactions afforded by this alignment stabilized **49** in the binding pocket and would likely contribute to its greater affinity/ inhibition of AChE.
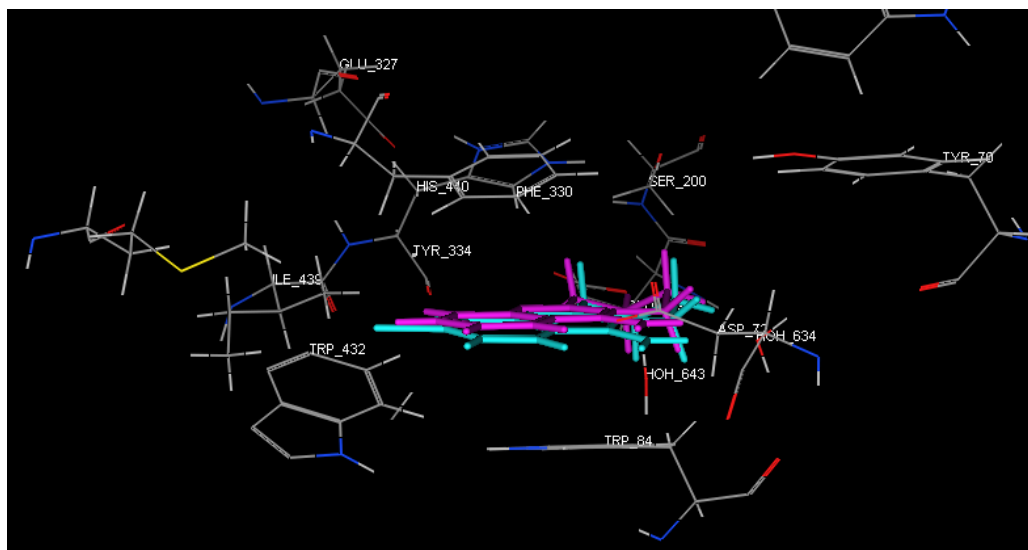
Figure 5.9: Poses of **49** (cyan) and tacrine (pink) at the AChE binding pocket (1ACJ). Goldscores of **49** and tacrine are 51.74 and 47.72 respectively.
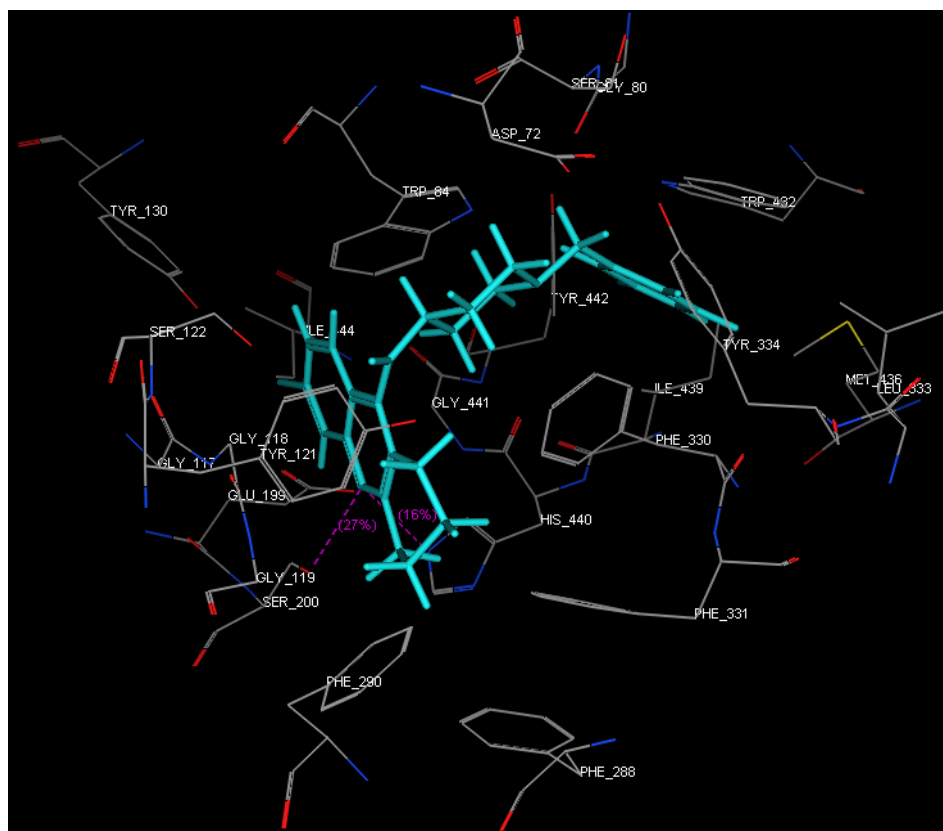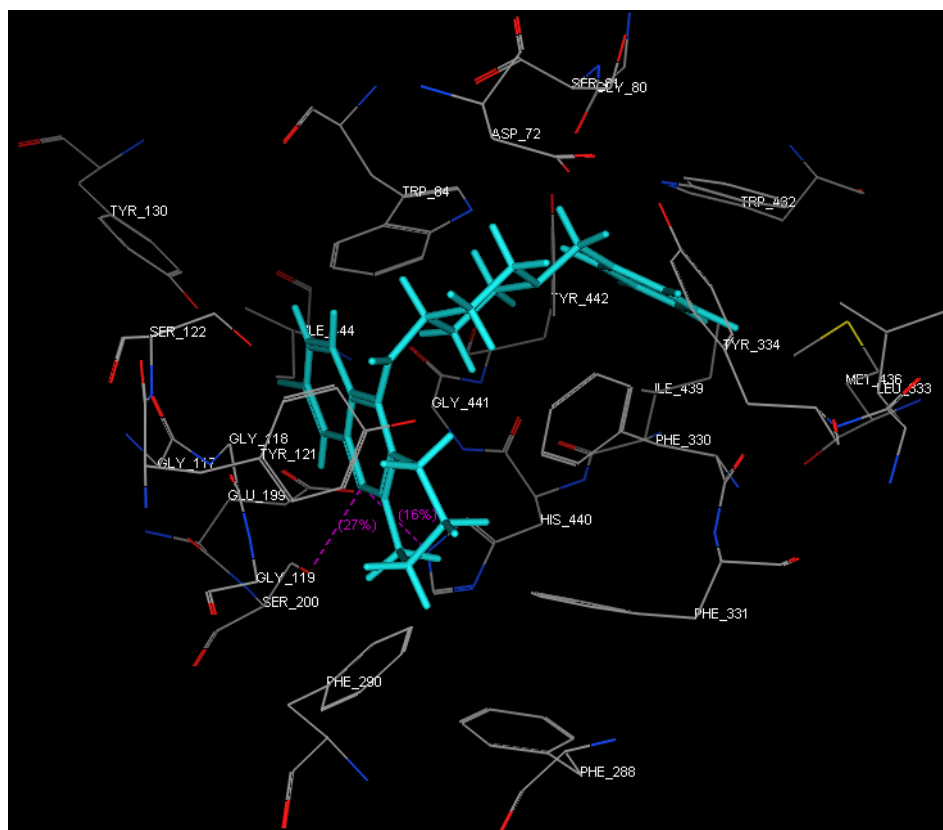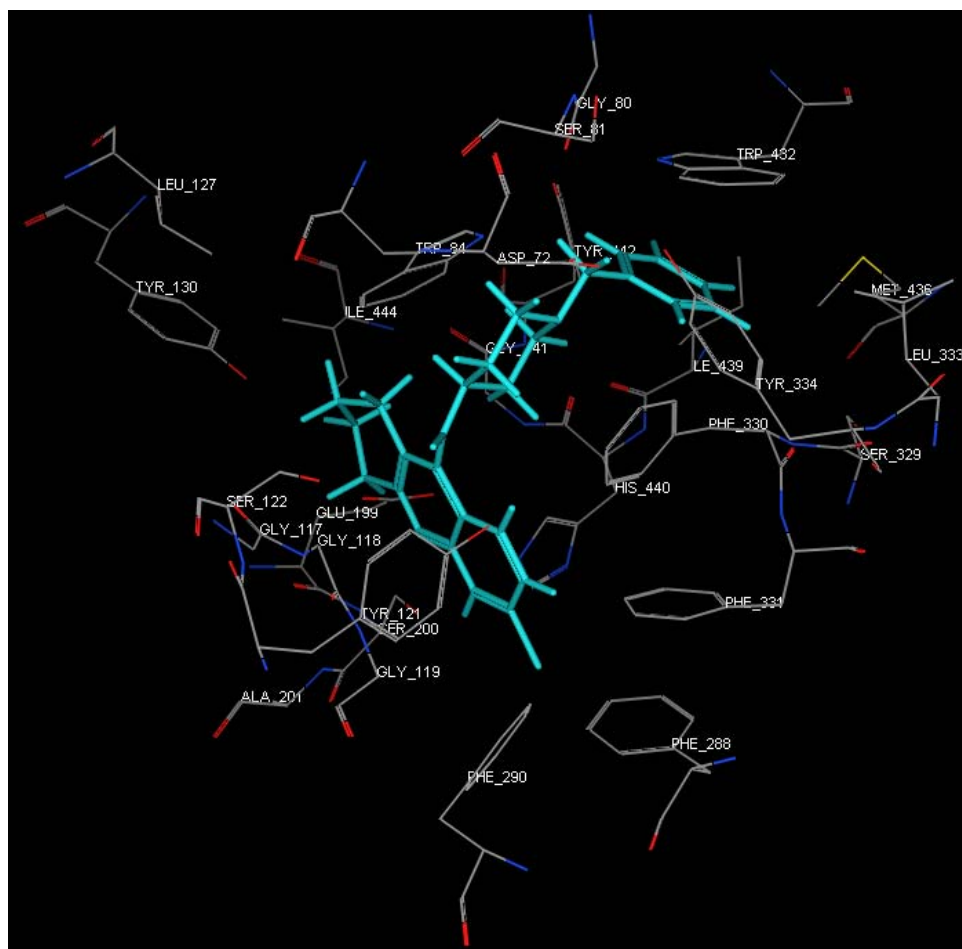
Figure 5.10: The 3D structures of three proposed docked pose of **51** in cyan.

The docking of **51** to the AChE binding pocket yielded three poses with equivalent GOLD scores (pose 1: -11.88, pose 2: -12.73, pose 3: -14.09). The magnitude of these scores did not denote strong binding affinity to the binding pocket, possibly because the pocket was "moulded" to accommodate tacrine and the cross-docking with **51** involved a structurally larger and different molecule.

The three poses shared many common binding features. First, the tetrahydroacridine ring of **51** was aligned in the vicinity of Gly 119, Gly 118, Ser 122 which were key residues of the oxyanion hole. The oxyanion hole stabilizes

the transient tetrahydral enzyme substrate complex by accommodating the negatively charged carbonyl oxygen through H bonding with the backbone NH residues of these amino acids. They are found midway down the gorge and close to the catalytic triad residues. The tetrahydroacridine ring was held in this position by H bonding between the protonated N of the tetrahydroacridine ring and the catalytic triad residue Ser 200 and van der Waals/hydrophobic interaction between the saturated ring of the tetrahydroacridine and Phe 290, Phe 288, Phe 331 which are residues found near the opening of the gorge (Trp 279 which is a PAS residue is nearby). Interestingly, in the third pose, the tetrahydroacridine ring was "flipped" so that its 6-chloro atom projected into this hydrophobic pocket.

The second common feature observed among the 3 poses was the alignment of the terminal benzyl ring at the bottom of the gorge, with one face of the ring stacked against the indole ring of Trp 432. Trp 432 and lle 429 were mentioned earlier as the amino acids that form the hydrophobic pocket into which the 6-chloro atom of 49 was inserted (Figure 5.10). Trp 432 and Trp 84 are also adjacent to each other and Trp 84 was earlier identified as one of the aromatic residues (the other is Phe 330) that formed π-π interactions with the tetrahydroacridine ring of tacrine and **49**.

Lastly, all three poses showed the protonated piperidine ring of the side chain inserted between Trp 84 and Phe 330. The distances between the rings were measured and found to exceed the optimal distance required for π-π stacking interactions. Thus, van der Waals or hydrophobic forces may be involved in interactions between the rings.

5.3.2.2. Docking of donepezil, tacrine, 49 and 51 to Torpedo AChE (1EVE)

The docking pose of donepezil in the binding pocket of TcAChE (PDB 1EVE) had the following features (Figure 5.11): (i) The aromatic ring (indanone) was aligned at the mouth of the active site gorge and formed π-π stacking interactions with the indole ring of Trp 279 which was situated at the peripheral anionic site at the mouth of the gorge; (ii) The protonated piperidine ring established cation-π interactions with Phe 330 in the middle of the gorge; (iii) The benzyl ring displayed classical parallel π-π stacking with Trp 84 at the base of the gorge.
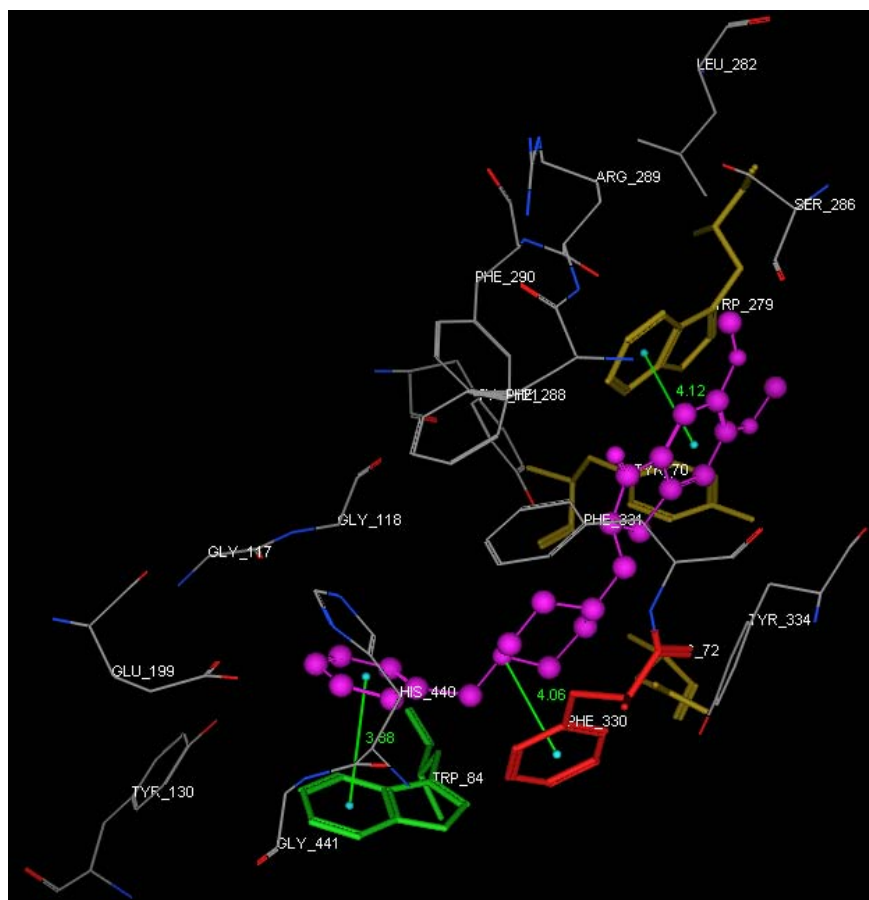
Figure 5.11: Donepezil (pink) in the binding pocket of AChE (PDB 1EVE).

Cognate docking of donepezil into the same binding pocket was successful and there was a good overlap between the poses of the original and re-docked donepezil molecules in the binding pocket (provide figure). The re-docked donepezil showed the same interactions (i) - (iii) as those observed in the original crystal structure.
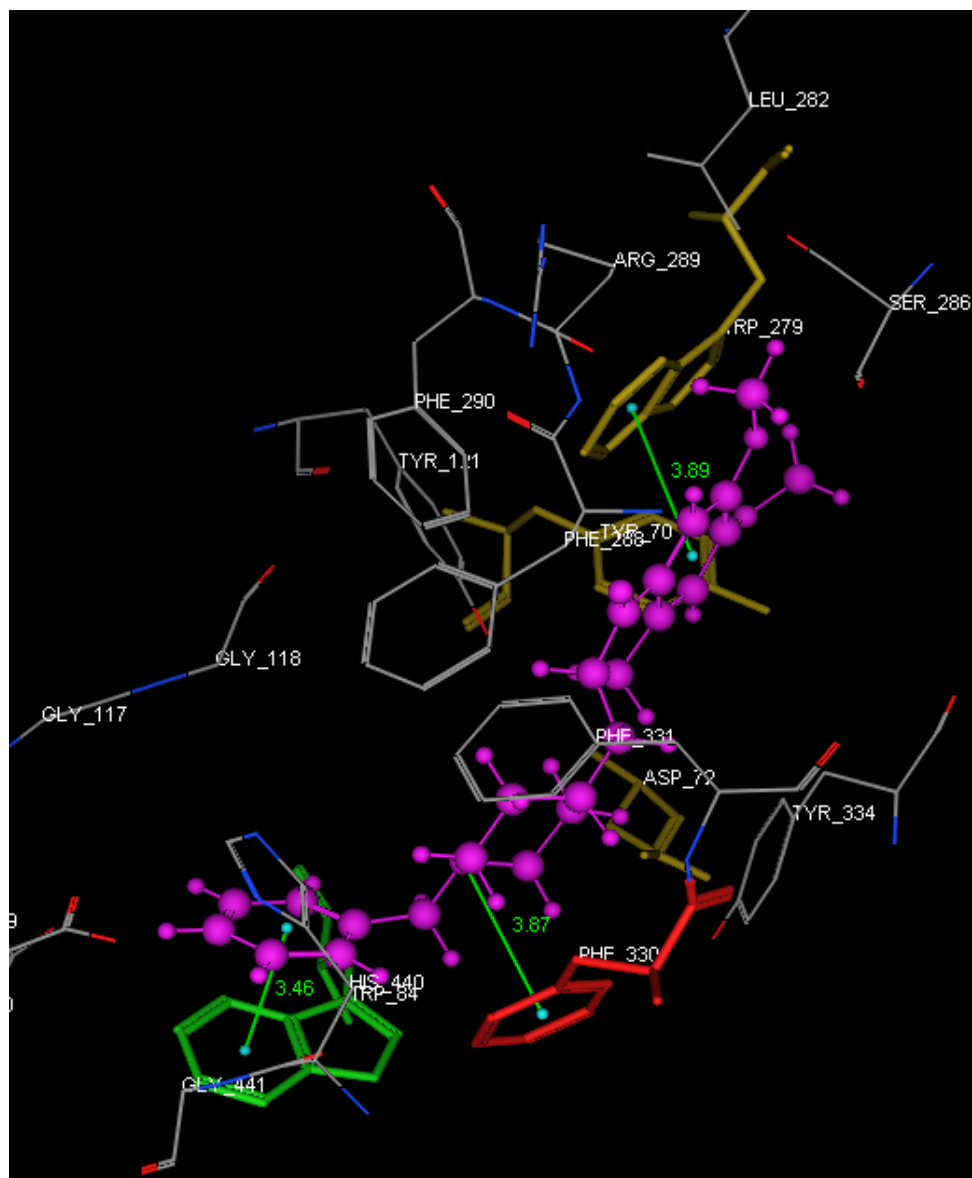
Figure 5.12: Donepezil (pink) was redocked in the binding pocket of AChE and showed the same interactions as observed in the crystal structure.

Next, tacrine was docked into the AChE binding pocket. The pose showed that the tacrine was inserted into the gorge, with π-π stacking between its middle ring and Phe 330 (distance of 3.63 Å between the mid-points of the two rings) as well as its end-aromatic ring and Tyr 334 (distance of 4.06 Å) (Figure 5.13). No H bonding was observed. The side of the tetrahydroacridine ring not facing Phe 330 and Tyr 334 was oriented towards Gly 118 and Gly 117 which are residues in the oxyanion hole.
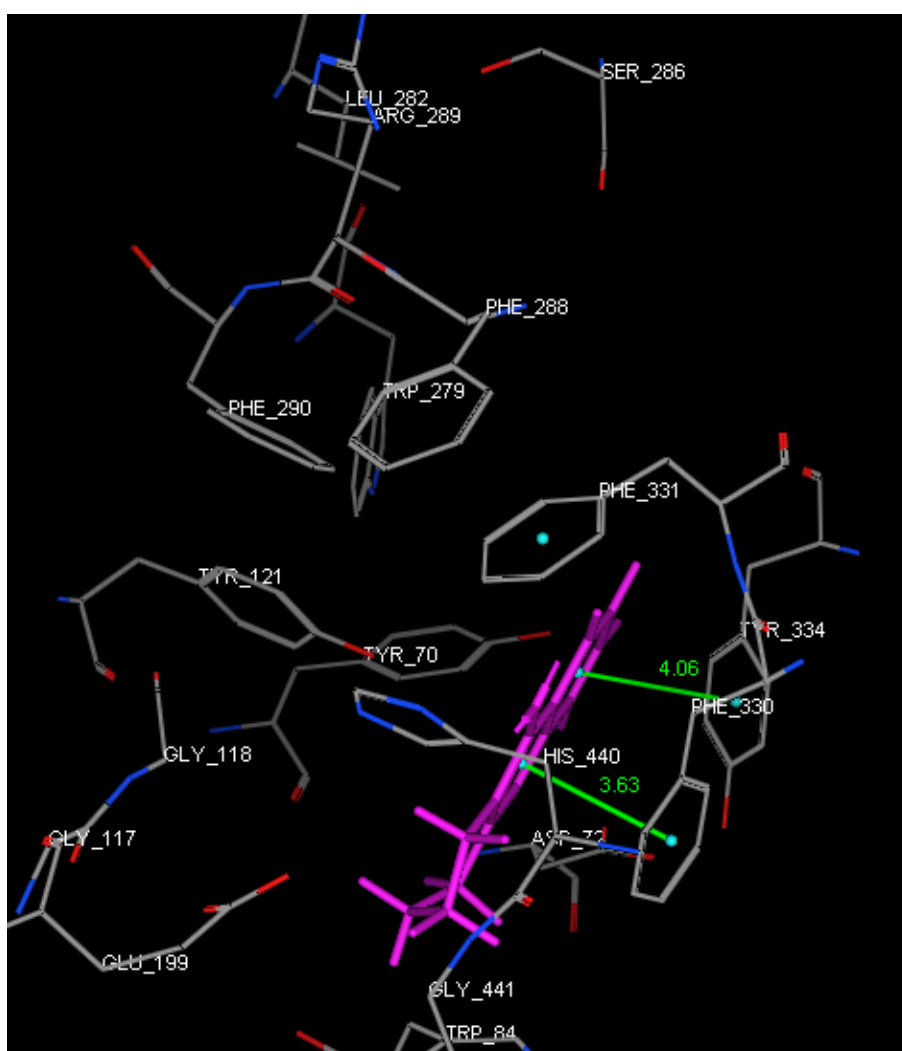
Figure 5.13: Pose of tacrine in the Torpedo AChE binding pocket (1EVE). Gold score of this pose was 45.97.

207

Compared to the pose of tacrine in the binding pocket derived from 1ACJ, obvious differences were evident. In that pose, tacrine was sandwiched between Phe 330 and Trp 84 and the ring was inserted deeper into the gorge. This was not observed in the pose derived from the binding pocket from 1EVE (Figure 5.14). Notably, the two poses were orthogonal to each other. Another observation was the change in the position of Phe 330 in the two crystal structures, which illustrated the propensity of Phe 330 to behave as a "swinging gate" that was capable of a range of conformations.[187]
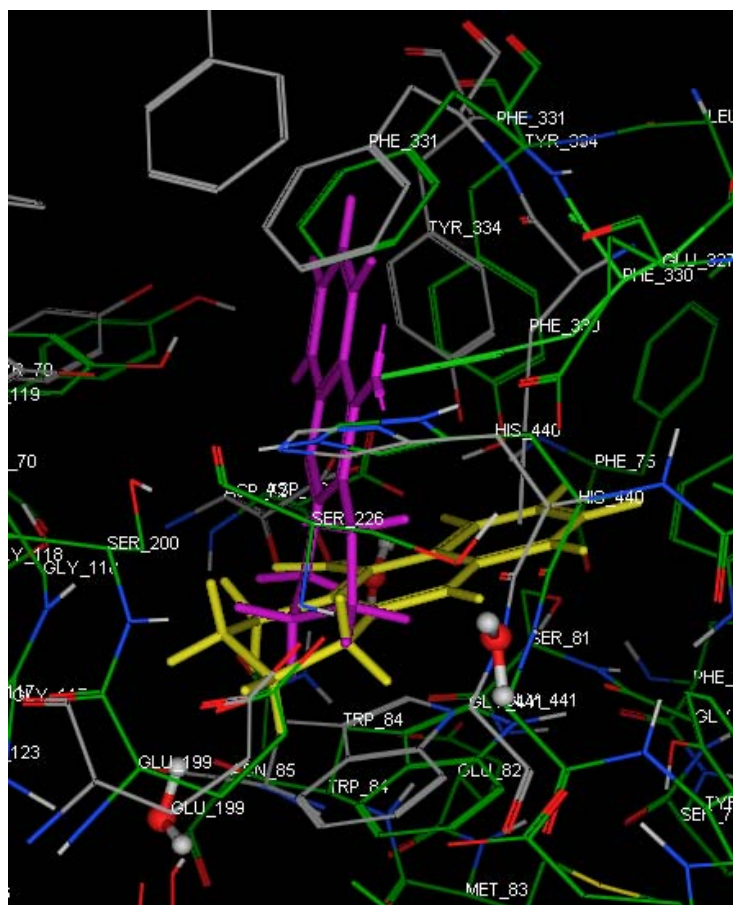
Figure 5.14: Comparison of docking poses of tacrine in binding pocket derived from 1ACJ (Yellow tacrine, amino acid residues in green) and 1EVE (pink tacrine, amino acid residues in grey).

Moving on to **49**, the docking pose of this molecule closely resembled that of tacrine in terms of the type of interactions involved (π-π stacking) and location (mid-way along the gorge). The difference however was that in **49**, the interactions now involved the middle ring of the tricyclic ring and Tyr 334 (distance of 4.53 Å) which meant that the molecule was now located near the upper reaches of the gorge. Moreover, the 6-chloro atom of **49** protruded into a hydrophobic pocket lined by Phe 330 and Trp 84 (distances 4.00 Å and 3.67 Å respectively) and there was H bonding between the ring N and Tyr 121 (2.33 Å). Hence, the position of **49** along the mid-gorge region was displaced towards the mouth of the gorge as seen in Figures 5.15b.
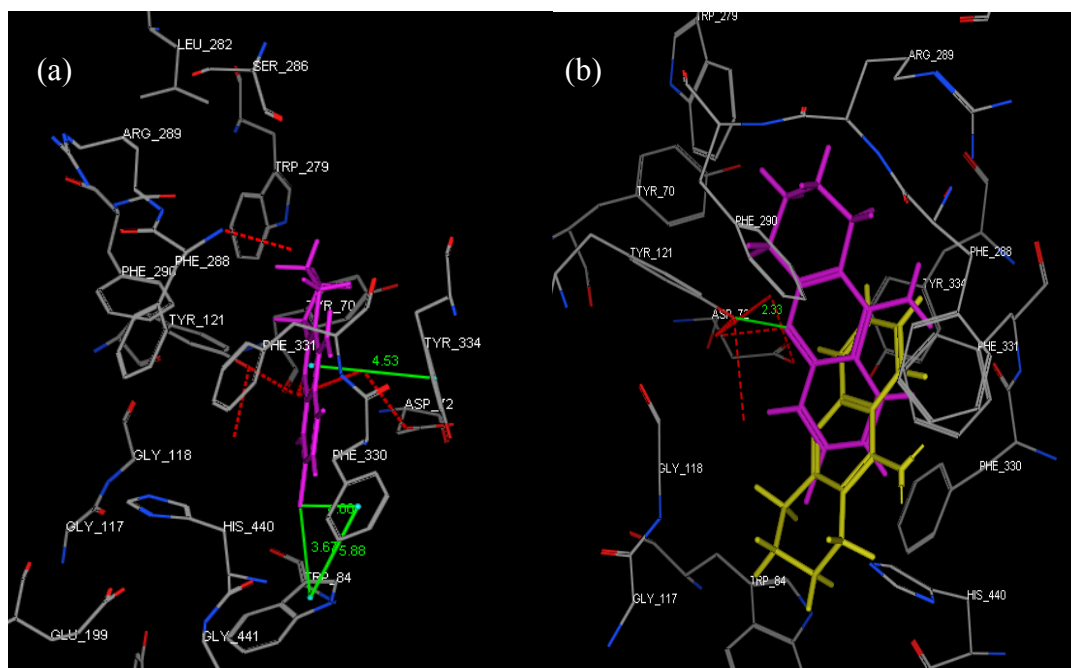
Figure 5.15: (a) Pose of compound **49** in Torpedo AChE (1EVE). (b) Pose of compound **49** (pink) and tacrine (yellow) in the Torpedo AChE binding pocket (1EVE).

Next, the docking pose of **51** in the AChE binding pocket of 1EVE was examined (Figure 5.16).
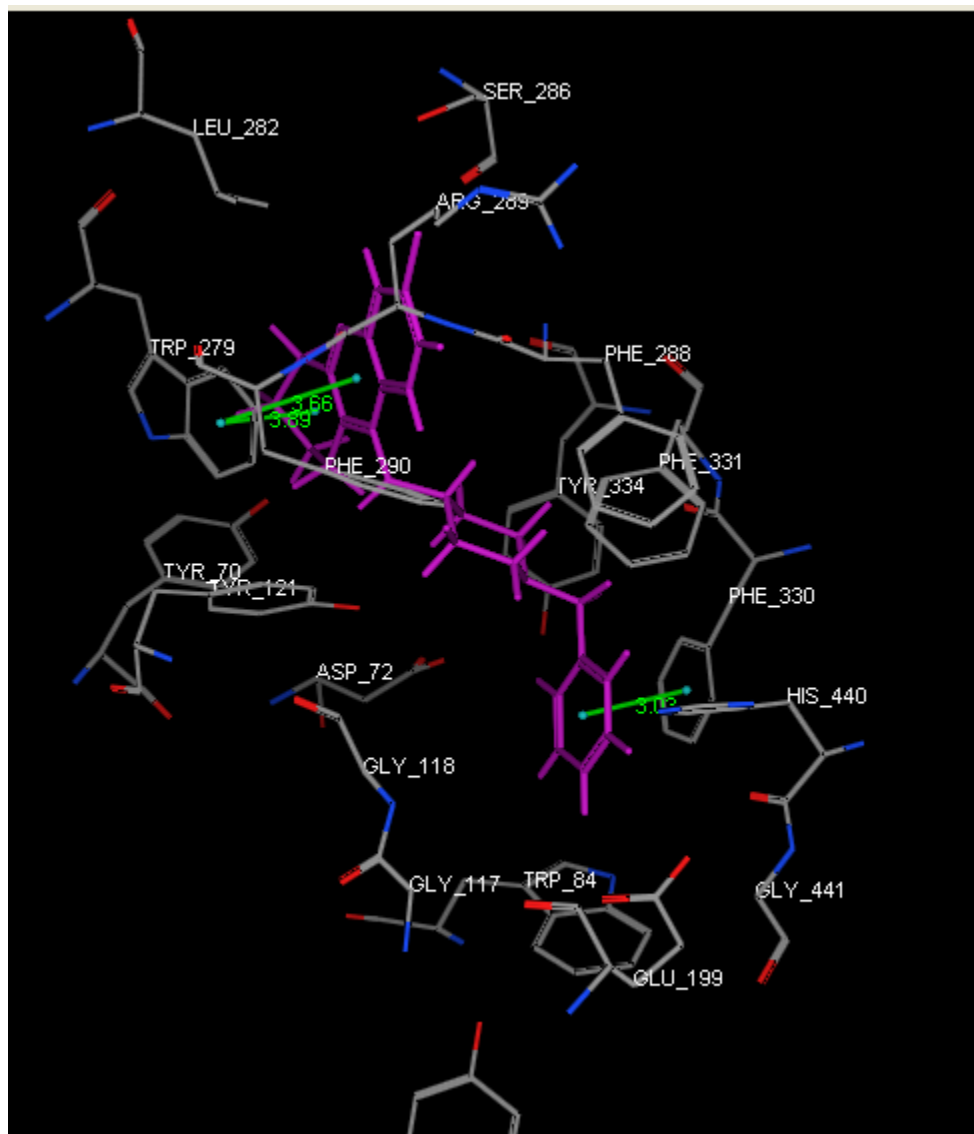
Figure 5.16: Pose of compound **51** in the AChE binding pocket (1EVE). Gold score was 54.93.

The following features were observed:

(i) The tetrahydroacridine ring of **51** was aligned near the mouth of the binding pocket, in the vicinity of Trp 279 (distance of 3.66 Å or 3.89 Å from

middle or end non-aromatic ring). In donepezil, Trp 279 formed π-π stacking interactions with the indanone ring.

(ii) The 6-chloro atom of the tetrahydroacridine ring projected into a pocket lined by some hydrophobic residues like Leu 282, Leu 287 and polar residues like Ser 286 and Arg 289.

A close-up of these interactions is shown in Figure 5.17.
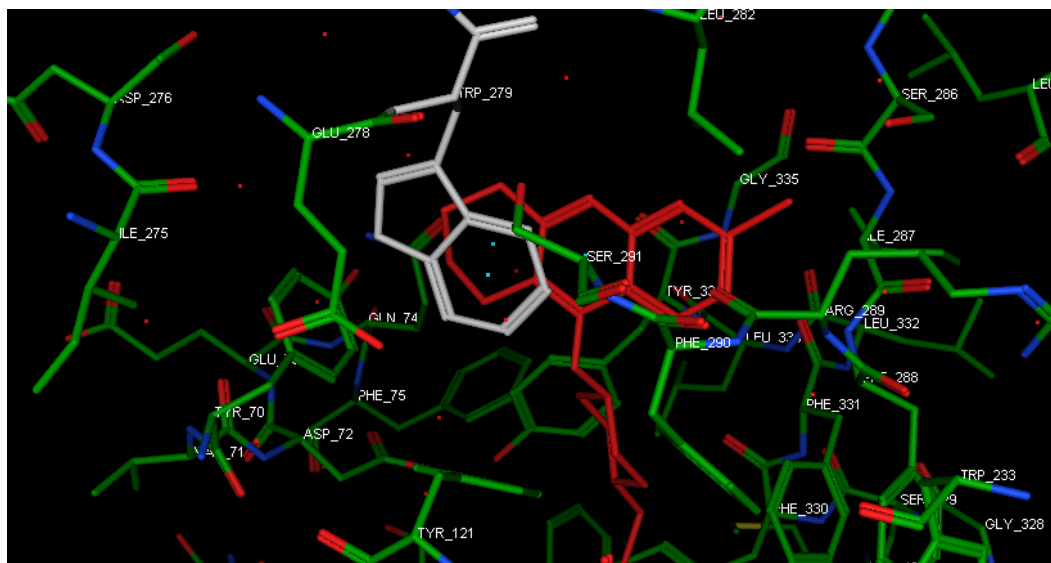
Figure 5.17: Pose of compound **51** (red) in the AChE pocket (1EVE) showing interactions involving the tetrahydroacridine ring. Trp 279 is highlighted in white.

(iii) The protonated piperidinyl ring occupied a large pocket lined by aromatic residues Tyr 121, Phe 331, Leu 333 and Tyr 334. These residues are found in the vicinity of the anionic catalytic site. However, the distances between the piperidine ring and these aromatic residues fell within the range of 4-5 Å and were unlikely to contribute towards cation – π interactions.
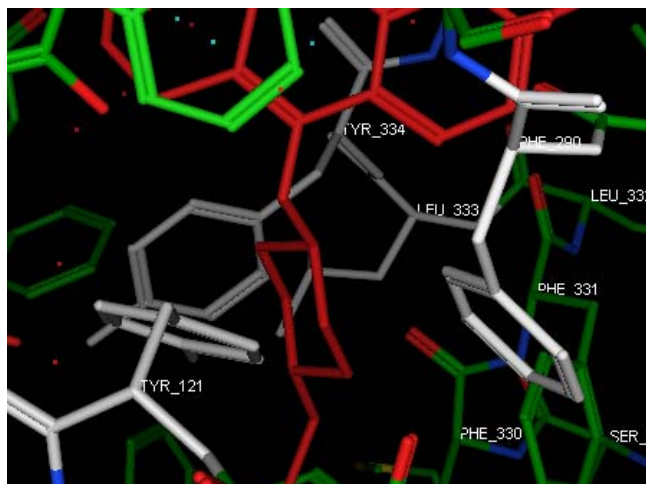
Figure 5.18: Pose of compound **51** (red) in the AChE pocket (1EVE) showing interactions involving the protonated piperidine ring. Tyr 121, Phe 331, Phe 290, Tyr 334 are highlighted in white.

(iv) The terminal benzyl ring formed π-π stacking interactions with Phe 330 (distance of 3.03 Å).
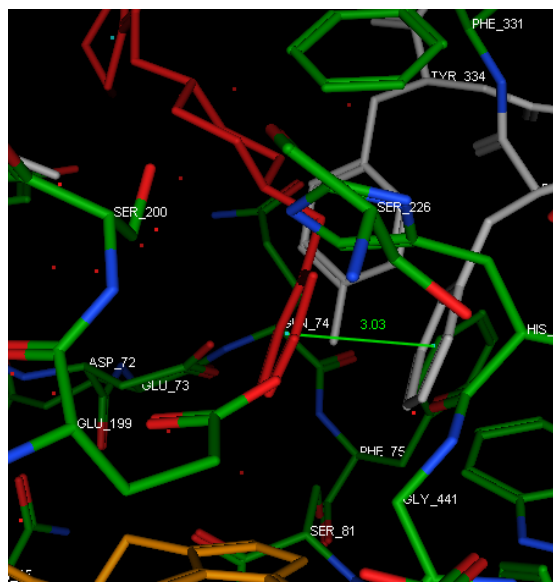
Figure 5.19: Pose of compound **51** (red) in the AChE pocket (1EVE) showing interactions involving the terminal benzyl ring and Phe 330 (white). Trp 84 which is at the bottom of the gorge is shown in gold.

When the poses of donepezil and **51** were superimposed (Figure 5.20), it was observed that both molecules made broadly similar interactions with the active site, except that different amino acid residues were involved as **51** was aligned somewhat higher up the binding pocket than donepezil. Thus, the aromatic rings of both molecules established π-π stacking interactions with Trp 279. Stacking interactions (π-π) with aromatic residues (Trp 84 for donepezil, Phe 330 for **51**) were also involved in holding down the terminal benzyl ring. The middle piperidine ring of donepezil was involved with cation π interactions with Phe 330 but these were not observed for **51**, which might explain the lower docking score assigned to **51** (54.93) compared to donepezil (63.53).
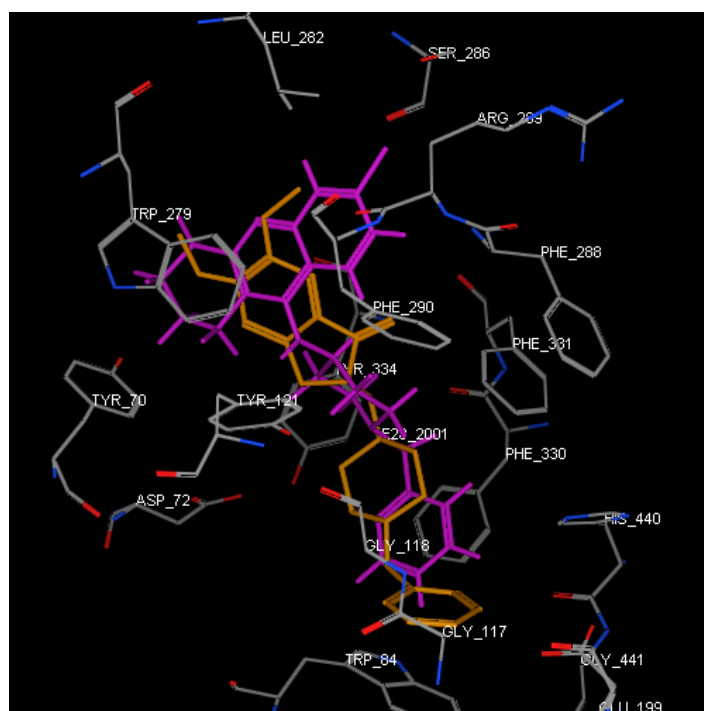
Figure 5.20: Pose of compound **51** (pink) and donepezil (orange) in the AChE pocket (1EVE).

When the poses of **51** in the two binding pockets (1EVE, 1ACJ) were compared, significant differences in orientation were observed (Figure 5.21). In 1ACJ, **51** was oriented "across" the binding pocket and the tricyclic ring was aligned at the oxyanion hold by H bonding to Ser 200 and hydrophobic interactions involving the 6- chloro atom. The middle piperidine ring was located between Phe 330 and Trp 84 and the terminal benzyl ring formed π-π stacking interactions with Trp 432 at the catalytic anionic site. In 1EVE, **51** was oriented "lengthwise" with the aromatic ring at the PAS and the benzyl ring at the catalytic anionic site (Phe 330). The piperidine ring was found in a hydrophobic pocket lined by aromatic residues found midway along the gorge.

Figure 5.21: (a) Poses of compound **51** in Torpedo AChE derived from 1EVE (pink) and 1ACJ (yellow). Gold score of the pose in 1EVE is greater than that in 1ACJ (b) As in (a) but without amino acid residues at the binding pocket.

5.3.2.3. Docking of tacrine, 49 and 51 to BChE

The BChE inhibitory properties of tacrine, **49** and **51** were investigated on equine BChE. Unfortunately, the crystal structure of equine BChE is not available for docking simulations. However, the primary sequences of equine and human BChE were known to share a high degree of similarity (89%).[188] Hence, human BChE extracted from a co-crystallized complex of human BChE in complex with a choline molecule (PDB code 1P0M) was used for the docking experiments.

There were several differences between the binding pockets of AChE and BChE. The active site of BChE is much larger (500 Å^3) than its AChE counterpart (300 Å^3). Of the 14 aromatic residues that line the active site gorge of AChE and determine its narrow aspect, six are substituted in BChE with smaller aliphatic and even polar residues. For instance, Phe 330 which is an important aromatic residue of the catalytic anionic site of AChE is replaced by Ala 528 in BChE. The absence of Phe results in diminished cation-π interactions between charged ligands and the BChE anionic site. However, the other catalytic anionic site residue Trp 82 (Trp 84 in AChE) is present in BChE.

The highest scored pose of tacrine in BChE showed the tetrahydroacridine ring stacked onto the Trp 82 residue by π-π interactions. The 9-amino function of tacrine established two H bonds with a histidine residue His 438 (one of 3 residues of the catalytic triad) and glutamic acid residue (Glu 197) (Figure 5.22). Compound **49** showed a similar binding pose as tacrine at the BChE binding pocket (Figure 5.23). The limited contribution of the 6-chloro atom of **49** to the

binding interaction was notable and could have accounted for the similar inhibitory activities of tacrine and **49** at BChE.
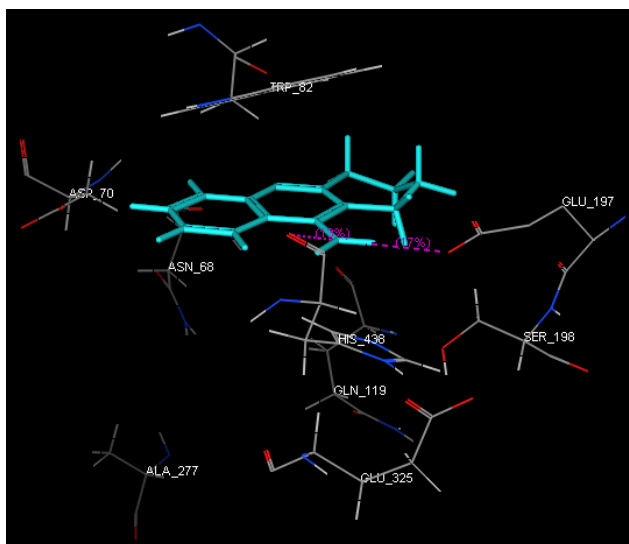
Figure 5.22: Representation of the binding mode of tacrine (shown in cyan stick) in the CAS of BChE.
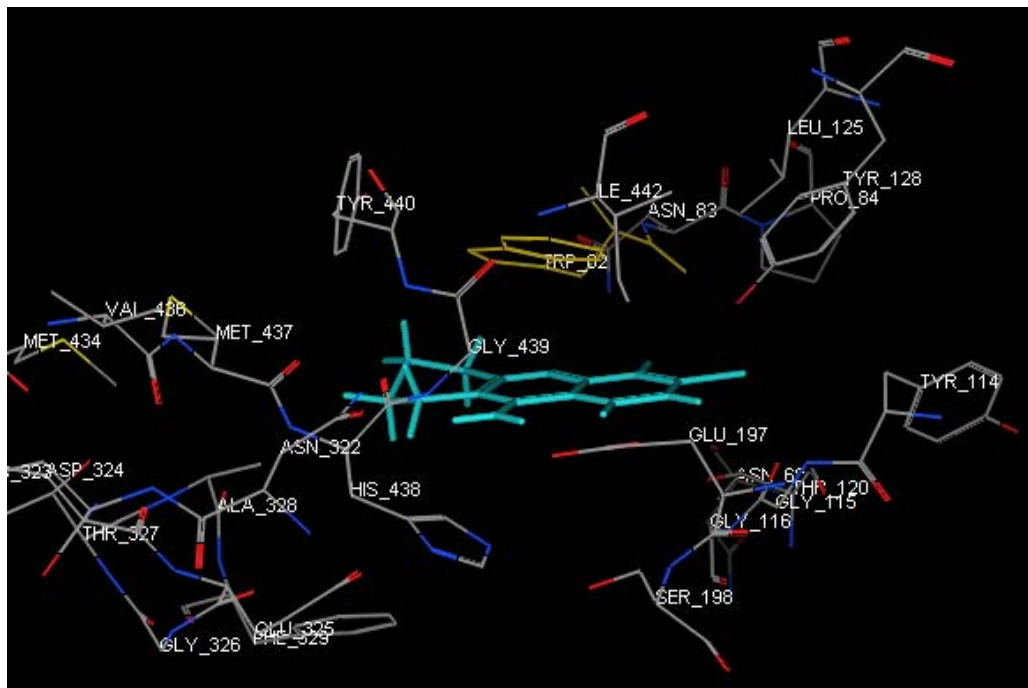
Figure 5.23: Representation of the binding mode of **49** (shown in cyan stick) in the CAS of BChE.

The highest scored binding pose of **51** at the BChE binding pocket is shown in Figure 5.24. It was observed that the tetrahydroacridine ring remained stacked onto the Trp 82 residue by π-π interactions. In addition, the protonated N of the ring formed cation-π interactions with the imidazole ring of His 438. Notably, the 4-benzylpiperidine side chain did not establish productive interactions with the binding pocket of BChE which would account for the significantly reduced BChE inhibitory activity of **51**.
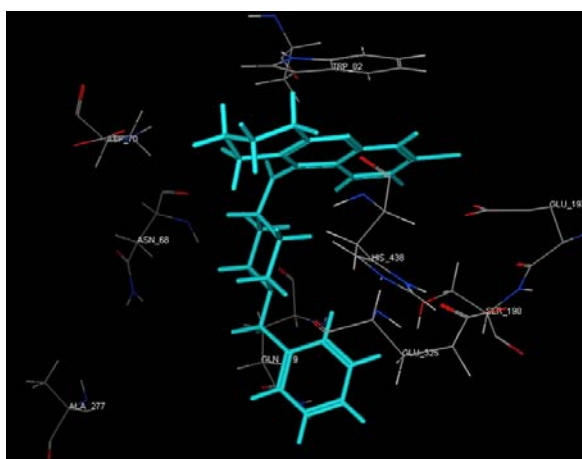
Figure 5.24: Representation of the binding mode of **51** (shown in cyan stick) in the CAS of BChE.

5.4. Discussion

The most potent AChE inhibitor identified in this investigation is **51** from Group 6. This compound was described as a tacrine-donepezil hybrid molecule in the introduction to this chapter and it was anticipated to be a potent AChE inhibitor in keeping with previously reported tacrine-donepezil hybrids.[177] Compound **51** was indeed a more potent AChE inhibitor than tacrine and of comparable activity to the other hybrid molecules reported by Shao *et al.*[177]

An analysis of the structure-activity trends showed that the 6-chloro atom on the tetrahydroacridine ring of **51** played a key role in bringing about selective affinity for AChE. Because of its lipophilic nature, the 6-chloro atom was able to establish van der Waals /hydrophobic interactions with the numerous aromatic (and non-polar) residues found in the AChE binding site. The docked poses of **49** and **51** showed that even when the tetrahydroacridine ring was oriented at different sites of the AChE binding pocket, the 6-chloro atom fitted into hydrophobic pockets that enhanced the affinity of the ring to the binding site. Thus, cross docking of **49** in 1ACJ showed the 6-chloro slotted into a hydrophobic pocket formed by Trp 432 and lle 439 at the vicinity of the catalytic anionic site near the base of the active site gorge whereas in 1EVE, the 6-chloro projected into the hydrophobic pocket formed by Phe 330 and Trp 84. In the case of **51** which showed significantly different poses when cross docked with 1ACJ and 1EVE, the 6-chloro atom still contributed to binding interactions. In 1ACJ, it fitted into a hydrophobic pocket formed by Phe 290 and Phe 288 at the peripheral anionic site while in 1EVE, it was found in a pocket was lined by hydrophobic and polar residues. Not surprisingly, the presence of the 6-chloro atom did not confer any advantage to the binding of **51** to BChE which lacked hydrophobic aromatic residues. The most highly scored pose of **51** at the BChE binding site did not show binding interactions involving the 6-chloro atom.

From the SAR, it was deduced that while compounds with the 6-chloro atom were selective inhibitors of AChE, inhibition potency was largely determined by the substituent at the 9-amino position of the acridine

/tetrahydroacridine ring. Of the various substituents investigated, the 1-benzyl- 4-piperidinyl side chain present in **51**, emerged as the most favored. An examination of the binding poses of **51** consistently showed the stacking of benzyl ring against aromatic residues like the indole ring of Trp 432 (in 1ACJ) or Phe 330 (in 1EVE). Compound **51** had two distinct docking poses depending on whether it was cross docked on 1ACJ or 1EVE. The differences between the two poses were enumerated in Section 5.3.2.2. In terms of scoring, the pose derived from 1EVE was significantly higher and thus considered more reliable, in the absence of evidence from more rigorous methods like molecular dynamics simulation. Not unexpectedly, this pose had several similarities to that observed for donepezil, namely the orientation of **51** along the length of the binding gorge, with the tricyclic ring at the PAS and the terminal benzyl ring sited within the catalytic anionic site.

It is of interest to note that the most potent tacrine-donepezil hybrid reported by Shao *et al.* (Figure 5.1) had an IC$_{50}$ of 6 nM for the inhibition of rat brain AChE. This value was comparable to that of **51** in spite of the different sources of AChE. The binding mode of the tacrine-donepezil hybrid is depicted in Figure 5.25. The orientation of this molecule in the Torpedo AChE binding pocket was very similar to that of donepezil, except for an additional H bond between the amide NH of the molecule and OH of Tyr 121. Very likely the extended nature of this molecule allowed it to span the entire length of the binding pocket and occupy both the peripheral and catalytic anionic sites. Compound **51** was not as long as this compound and its terminal benzyl ring interacted with Phe

330 found midway along the gorge, and not Trp 84 found at the base of the gorge. Nonetheless, in spite of its shorter length, **51** was as potent as the tacrine-donepezil hybrid.
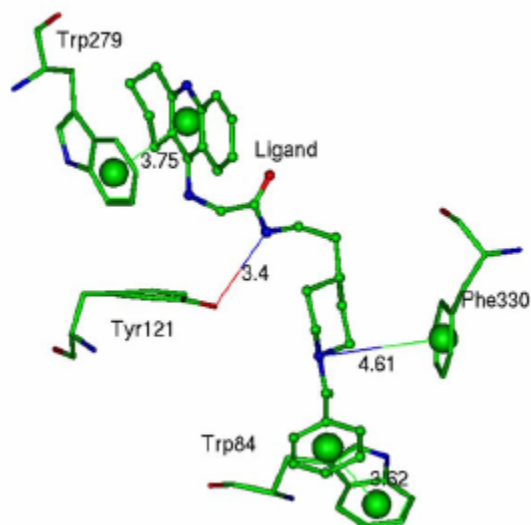
Figure 5.25: Interaction of a tacrine-donepezil hybrid molecule (IC$_{50}$ AChE from rat cortex homogenate 6 nM) reported by Shao *et al*.[177] with the Torpedo AChE binding pocket (PDB 1EVE).

When the benzylpiperidine ring was attached to other scaffolds like the 6-chloro-2-methoxyacridine ring (Group 3) and the 7-chloroquinoline ring (Group 7), AChE inhibitory activity was diminished and the selectivity for this enzyme was lost. Even then, among the different side chains attached to the 7-chloroquinoline ring, the compound with the benzylpiperidine ring remained as the most potent AChE inhibitor. Group 3 yielded 3 compounds that were potent AChE inhibitors (more than 75% inhibition at 3 μM) but the analog with the benzylpiperidinyl side chain (**32**) was not included among these potent inhibitors.

Rather, for this ring scaffold, the 2-carbon and 3-carbon homologs of (**39-41**) were identified as potent inhibitors. Docking of representative Group 3 and Group 7 compounds onto the AChE/BChE binding pockets were not done but would have provided useful insight as to how the ring scaffold and side chain of these compounds influenced affinity to the respective proteins.

5.5. Conclusion

This chapter has provided a better understanding of the structural requirements for AChE and BChE inhibitory activities of the Group 1-7 compounds. In summary, the optimal ring scaffold for AChE inhibition was the 6-chlorotetrahydroacridine ring. Attaching different side chains to the 9-amino group of this scaffold did not cause a significant loss in AChE activity as compared to the same modifications on the 6-chloro-2-methoxyacridine and 7-chloroquinoline scaffolds. Among the different side chains attached to the 9-amino /4-amino functionality, the most favoured was the 1-benzyl-4-piperidinyl side chain or its variants as seen in the Group 3 analogs. The most detrimental groups were phenyl or substituted phenyl side chains, in particularly when attached to the 6-chloro-2-methoxyacridine scaffold. In the case of BChE inhibitory activity, the most potent inhibitors were still those with a 6-chlorotetrahydroacridine ring but there was a greater tolerance for the 6-chloro-2-methoxyacridine scaffold and the 9-N-substituted phenyl side chain. Thus many Group 2 compounds were submicromolar inhibitors of BChE. In terms of selectivity for either enzyme, compounds with the 6-chlorotetrahydroacridine

template (Group 6) and those that had donepezil-like side chains attached to the 6-chloro-2-methoxyacridine ring (Group 3) were selective inhibitors of AChE. On the other hand, compounds from the other groups showed a marginal preference for BChE inhibition.

Chapter 6: Conclusions and future work

In this thesis, we tested the hypothesis that acridine is a fruitful template in neurodegenerative diseases. Sixty compounds were designed, synthesized, and tested for three biological activities: antiprion, neuroprotective, and anticholinesterase activities. Acridine analogues have different structure-activity relationships for each biological activity.

Forty seven compounds organized across seven groups were synthesized and evaluated on in vitro cell models of scrapie infected murine neuroblastoma cells. The investigation identified compounds from Groups 2 and 3 that were more potent than quinacrine against F3 cells which comprised murine neuroblastoma cells stably transfected with a human scrapie strain Fukuoka-3. The most promising compounds were **16** and **32** which were subsequently modified to give analogs with improved (in the case of **32**) or comparable (in the case of **16**) activities. Well defined structure-activity relationships were observed and key points are summarized in Figures 6.1 and 6.2. Thus, analogs of quinacrine with improved (submicromolar) potencies against cell based prion infections were successfully obtained by applying established lead optimization strategies.
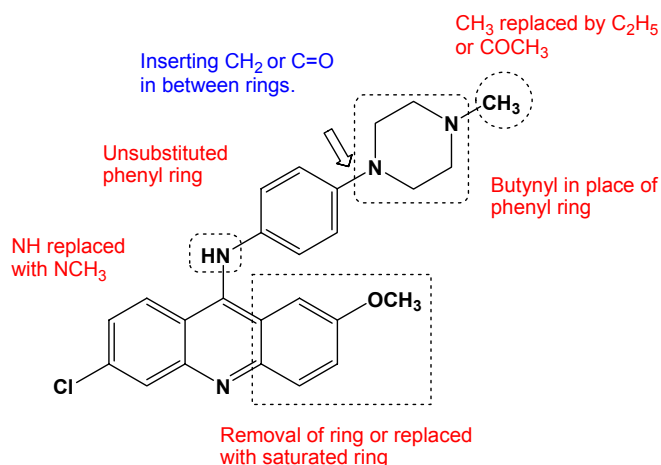
Figure 6.1: Structural modification of compound **16** and effects on antiprion activity determined on F3 cell model. Red fonts indicate changes that reduce activity while blue fonts indicate changes that enhance activity.
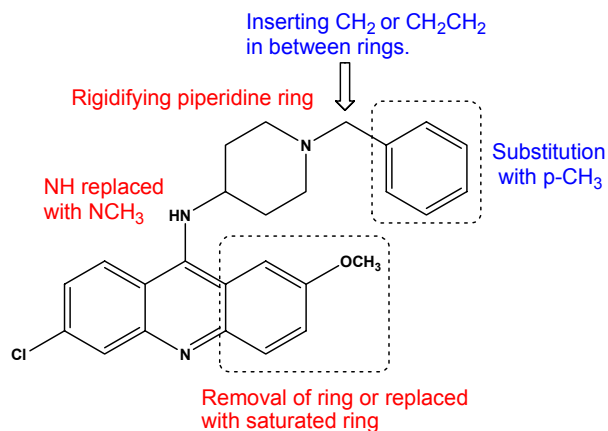
Figure 6.2: Structural modification of compound **32** and effects on antiprion activity determined on F3 cell model. Red fonts indicate changes that reduce activity while blue fonts indicate changes that enhance activity.

To determine if these compounds retained sufficient drug-like features that would permit passage across the blood brain barrier, permeability across porcine brain lipids were determined on the in vitro PAMPA BBB assay. Except for a

small number of compounds from Group 2, the other compounds tested had permeability values (P_e) that exceeded the threshold limit (4.0 x10^{-6} cm/s) proposed by Di *et al.*[122] for blood brain barrier permeability. Thus, there was a strong likelihood that these compounds including those with promising antiprion activity like **16, 24** and **37** are able to cross the blood brain barrier. In the case of **16**, it was also assessed to be a poor substrate (less so than quinacrine) of the efflux protein Pgp, high levels of which are found in the cells of the blood brain barrier. Thus, although **16** had a smaller P_e value than quinacrine (8.13 x10^{-6} cm/s versus 19.30 x10^{-6} cm/s), its weaker affinity for the efflux protein was a point in its favor. Whether this would finally translate into higher levels in the brain would require confirmation in animal models. Thus, future areas of work would include the determination of (i) pharmacokinetic profiles of the more promising antiprion agents on oral or intravenous dosing to determine if sufficient levels accumulated in brain tissues; (ii) efficacies in animal models of prion infection for those compounds identified to have acceptable pharmacokinetic profiles; (iii) Pgp affinities of a larger selection of members from the various Groups to determine if the Pgp-substrate profile of **16** (from Group 2) was also observed among other members.

Another objective of this thesis was to determine if the functionalized aminoacridines of Groups 1-7 possessed neuroprotective properties in addition to their antiprion activity. If such properties are demonstrated, it would enhance the standing of the 9-aminoacridine ring as a privilege scaffold for agents designed to act on neurodegenerative disorders. Two targets associated with

neurodegeneration / neurodegenerative disorders were selected, namely glutamate-induced cell death (oxytosis) which is a novel form of programmed cell death and acetylcholinesterase, an acknowledged target for drugs acting on Alzheimer's disease (AD).

Investigations on the ability of the synthesized compounds to protect murine hippocampal HT22 cells from glutamate-induced cell death were prompted by reports that compounds with a non-basic NH group flanked by aromatic rings were protective against cell death induced by this pathway. The hypothesis was that Group 2 compounds that had this motif would have protective properties while other groups that lacked this feature would have weaker activity, if any. This was indeed found to be true. Only the Group 2 compounds demonstrated protective properties and similar to antiprion activity, a well-defined structure-activity relationship was observed. Figure 6.3 summarizes key structural modifications of **16** (a Group 2 compound) that influenced its ability to protect HT22 cells against glutamate induced cell death. Compound **16** was found to have a neuroprotective EC_{50} of 0.62 μM and a 14 fold "safety window" as assessed from the ratio of its EC_{50} for cell cytotoxicity versus EC_{50} for neuroprotection. Modification of **16** led to **21**, the most active compound identified in this study, which had an EC_{50} of 0.18 μM and an expanded safety ratio of 110.
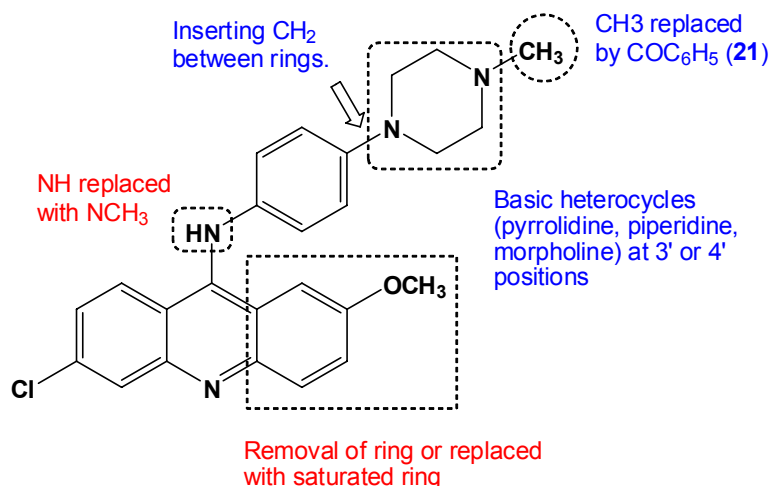
Figure 6.3: Structural modification of compound **16** and effects on EC_{50} for protection against glutamate induced toxicity of HT22 cells. Red fonts indicate changes that reduce activity while blue fonts indicate changes that enhance activity.

Mechanistically, the protective effects of **16** (and possibly other members of Group 2) were linked to its ability to quench free radicals, in particular those released by the mitochondria at the later stages of oxidative cell death. Future work in this area would be to determine how **16** and related analogs targeted the mitochondria. Some possibilities are its role as a mitochondrial uncoupler or ability to interact with channels that are responsible for calcium influx or interference with signaling mechanisms that mediate the opening of calcium channels.

Investigations of the anti-AChE activities of the Group 1-7 compounds were prompted in part by the structural resemblance of these compounds to tacrine, a known anti-AChE agent once used for the palliative treatment of Alzheimer's disease. In particular, the Group 6 compounds share the same ring

scaffold as tacrine. Furthermore, several compounds possess a side chain (4-benzyl-piperidin-4-yl) that is present in another known anti-AChE agent donepezil presently used for the symptomatic treatment of AD. Thus several members in Groups 3 and 6 were identified as "tacrine-donepezil" hybrids and they were anticipated to be more potent AChE inhibitors. This was duly observed. The Group 6 compounds yielded members with nanomolar to low submicromolar IC_{50} for AChE inhibition and the member with the donepezil like side chain (**51**) emerged as the most promising AChE inhibitor. Compound **51** was a mixed inhibitor of AChE with K_i of 1.8 nM (compared to 120.2 nM for tacrine). It was 20 times for selective for AChE inhibition compared to BChE inhibition. The structure-activity relationship for **51** is summarized in Figure 6.4.
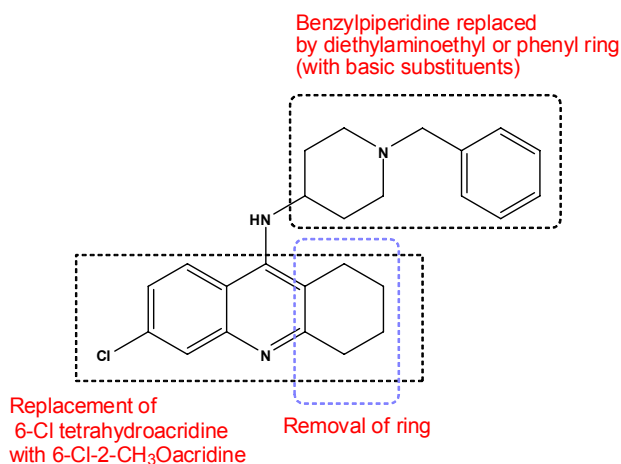
Figure 6.4: Structural modification of compound **51** and effects on IC_{50} for inihibtion of AChE. Red fonts indicate changes that reduce activity.

It is interesting to note that besides its outstanding anti-AChE profile, **51** exhibited reasonably good activity against prion infected cell lines. While it was not the most potent member, **51** had low micromolar EC_{50} values and was able to

fully clear the prion infection of all three cell lines tested. Moreover, it had limited cytotoxicity when evaluated on murine hippocampal HT22 cells (EC_{50} 20 μM) and murine neuroblastoma cells N2a (EC_{50} 5 μM). AChE was reported to play a key role in accelerating Aβ-peptide deposition and promoting of formation of Aβ-plaques in AD, and inhibition of AChE had led to the slowing down of these processes.[189,190] In view of the ability of **51** to inhibit AChE and to arrest the accumulation of scrapie prion protein (PrP^{Sc}) in cell-based assays, it would be of interest to further determine its effects on protein misfolding. **51** has submicromolar IC_{50} values in antiprion assay and low nanomolar IC_{50} value against AChE. Levels of prion proteins and AChE apparently differ from those *in vitro* assays. Therefore, it remains to be tested if combination effects of **51** is beneficial or adverse *in vivo*. Of interest would be its effects on Aβ plaque formation in the thioflavin T assay and the accumulation of protein aggregates in prion protein misfolding cyclic amplification.

In conclusion, this thesis had shown that functionalized aminoacridines were attractive starting points for the design of compounds for antiprion activity, inhibition of oxytosis and inhibition of AChE. While structural requirements for these activities were different, they were found in compounds that shared a common template. Eventhough multiple drug targets may manifest side effects, in certain cases, combined therapeutic effects may lead to fruitful clinical outcome especially in complicated diseases which involve interconnected biological conditions such as neurodegenerative disorders. Future work should focus on improving the drug-like features of promising target compounds to enhance

pharmacokinetics, of which the penetration across the blood brain barrier is foremost.

References

(1)   Greenwood, D. Conflicts of interest: the genesis of synthetic antimalarial agents in peace and war. *Journal of Antimicrobial Chemotherapy* **1995**, *36*, 857-872.

(2)   Albert, A.; Rubbo, S. D.; Goldacre, R. J.; Davey, M. E.; Stone, J. D. The influence of chemical constitution on antibacterial activity. Part II: a general survey of the acridine series. *British Journal of Experimental Pathology* **1945**, *26*, 160-192.

(3)   Demeunynck, M. Antitumor acridines. *Expert Opinion on Therapeutic Patents* **2004**, *14*, 55-70.

(4)   Adams, A. Crystal structures of acridines complexed with nucleic acids. *Medicinal Chemistry Reviews* **2004**, *1*, 405-412.

(5)   Wainwright, M. Acridine-a neglected antibacterial chromophore. *Journal of Antimicrobial Chemotherapy* **2001**, *47*, 1-13.

(6)   Wilson, W. R.; Harris, N. M.; Ferguson, L. R. Comparison of the mutagenic and clastogenic activity of Amsacrine and other DNA-intercalating drugs in cultured V79 chinese hamster cell. *Cancer Research* **1984**, *44*, 4420-4431.

(7)   Ferguson, L. R.; Denny, W. A. Genotoxicity of non-covalent interactions: DNA intercalators. *Mutation Research/Fundamental and Molecular Mechanisms of Mutagenesis* **2007**, *623*, 14-23.

(8)   Elslager, E. F.; Tendick, F. H. 9-Amino-2,3-dimethoxy-6-nitroacridine 10-oxides. *Journal of Medicinal and Pharmaceutical Chemistry* **1962**, *5*, 1149-1153.

(9)   Tomosaka, H.; Omata, S.; Hasegawa, E.; Anzai, K. The effects of substituents introduced into9-aminoacridine on frameshift mutagenicity and DNA binding affinity. *Bioscience, Biotechnology and Biochemistry.* **1997**, *61*, 1121-1125.

(10)   Gamage, S. A.; Figgitt, D. P.; Wojcik, S. J.; Ralph, R. K.; Ransijn, A. et al. Structure-Activity Relationships for the Antileishmanial and Antitrypanosomal Activities of 1'-Substituted 9-Anilinoacridines. *Journal of Medicinal Chemistry* **1997**, *40*, 2534-2642.

(11)   Guetzoyan, L.; Ramiandrasoa, F.; Dorizon, H.; Desprez, C.; Bridoux, A. et al. *In vitro* efficiency of new acridyl derivatives against *Plasmodium falciparum*. *Bioorganic & Medicinal Chemistry* **2007**, *15*, 3278-3289.

(12)   Biagini, G. A.; Fisher, N.; Berry, N.; Stocks, P. A.; Meunier, B. et al. Acridinediones: selective and potent inhibitors of the Malaria parasite mitochondrial bc1 complex. *Molecular Pharmacology* **2008**, *73*, 1347-1355.

(13)   Gemma, S.; Campiani, G.; Butini, S.; Joshi, B. P.; Kukreja, G. et al. Combining 4-aminoquinoline- and clotrimazole-based pharmacophores toward innovative and potent hybrid antimalarials. *Journal of Medicinal Chemistry* **2009**, *52*, 502-513.

(14)   Stewart, L.; Redinbo, M. R.; Qiu, X.; Hol, W. G. J.; Champoux, J. J. A model for the mechanism of human topoisomerase I. *Science* **1998**, *6*, 1534-1541.

(15)   Wang, J. C. DNA topoisomerases. *Annual Review of Biochemistry.* **1996***, 65*, 635-692.

(16)   Berger, J. M. Structure of DNA topoisomerases," in "DNA topoisomerases and topoisomerase-targeted Drugs. *Biochimica et Biophysica Acta* **1998***, 1400*, 3-18.

(17)   Denny, W. A. Chemotherapeutic effects of acridine derivatives. *Medicinal Chemistry Reviews* **2004***, 1*, 257-266.

(18)   Chourpa, I.; Manfait, M. J. Specific molecular interactions of acridine drugs in complexes with topoisomerase II and DNA. SERS and resonance Raman study ofm-AMSA in comparison witho-AMSA. *Journal of Raman Spectroscopy* **1995***, 26*, 813-819.

(19)   Chourpa, I.; Morjani, H.; Riou, J.-F.; Manfait, M. Intracellular molecular interactions of antitumor drug amsacrine (m-AMSA) as revealed by surface-enhanced Raman spectroscopy. *FEBS Letters* **1996***, 397*, 61-64.

(20)   Su, T.-L.; Chou, T.-C.; Kim, J. Y.; Huang, J.-T.; Ciszewska, G. et al. 9-Substituted acridine derivatives with long half-life and potent antitumor activity: synthesis and structure-activity relationships. *Journal of Medicinal Chemistry* **1995***, 38*, 3226-3235.

(21)   Bacherikov, V. A.; Chang, J.-Y.; Lin, Y.-W.; Chen, C.-H.; Pan, W.-Y. et al. Synthesis and antitumor activity of 5-(9-acridinylamino)anisidine derivatives. *Bioorganic and Medicinal Chemistry* **2005***, 13*, 6513-6520.

(22)   Dittrich, C.; Coudert, B.; Paz-Ares, L.; Caponigro, F.; Salzberg, M. et al. *Journal of Cancer* **2003***, 39*, 330-334.

(23)   Dittrich, C.; Dieras, V.; Kerbrat, P.; Punt, C.; Sorio, R. et al. Phase II study of XR5000 (DACA), an inhibitor of topoisomerase I and II, administered as a 120-h infusion in patients with advanced ovarian cancer. *Invest New Drugs* **2003***, 21*, 347-352.

(24)   Davis, J. T. G-Quartets 40 years later: From 5'-GMP to Molecular biology and supramolecular chemistry. *Angewandte Chemie International Edition* **2004***, 43*, 668-698.

(25)   Blackburn, E. H. Structure and function of telomeres. *Science* **1991***, 350*, 569.

(26)   Burge, S.; Parkinson, G. N.; Hazel, P.; Todd, A. K.; Neidle, S. Quadruplex DNA: sequence, topology and structure. *Nucleic Acids Research* **2006***, 34*, 5402-5415.

(27)   Gomez, D.; Paterski, R.; Lemarteleur, T.; Shin-ya, K.; Mergny, J.-L. et al. Interaction of telomestatin with the telomeric single-strand overhang. *Journal of Biological Chemsitry* **2004***, 279*, 41487-41494.

(28)   Burger, A. M.; Dai, F.; Schultes, C. M.; Reszka, A. P.; Moore, M. J. et al. The G-quadruplex-interactive molecule BRACO-19 inhibits tumor growth, consistent with telomere targeting and interference with telomerase function. *Cancer Research* **2005***, 65*, 1489-1496.

(29)   Cian, A. D.; Lacroix, L.; Douarre, C.; Temime-Smaali, N.; Trentesaux, C. et al. Targeting telomeres and telomerase. *Biochimie* **2008***, 90*, 131-155.

(30)   Bryan, T. M.; Cech, T. R. Telomerase and the maintenance of chromosome ends. *Current Opinion in Cell Biology* **1999***, 11*, 318-324.

(31)   Masutomi, K.; Yu, E. Y.; Khurts, S.; Ben-Porath, I.; Currier, J. L. et al. Telomerase maintains telomere structure in normal human cells. *Cell* **2003**, *114*, 241-253.

(32)   Neidle, S.; Parkinson, G. Telomere maintenance as a target for anticancer drug discovery. *Nature Reviews Drug Discovery* **2002**, *1*, 383-393.

(33)   Perry, P. J.; Reszka, A. P.; Wood, A. A.; Read, M. A.; Gowan, S. M. et al. Human telomerase inhibition by regioisomeric disubstituted amidoanthracene-9,10-diones. *Journal of Medicinal Chemistry* **1998**, *41*, 4873-4884.

(34)   Read, M. A.; Harrison, R. J.; Romagnoli, B.; Tanious, F. A.; Gowan, S. M. et al. Structure-based design of selective and ootent G-quadruplex-mediated telomerase inhibitors. *The Proceedings of the National Academy of Sciences U.S.A.* **2001**, *98*, 4844-4849.

(35)   Heald, R. A.; Modi, C.; Cookson, J. C.; Hutchinson, I.; Laughton, C. A. et al. Antitumor polycyclic acridines. 8.[1] Synthesis and telomerase-inhibitory activity of methylated pentacyclic acridinium salts. *Journal of Medicinal Chemistry* **2002**, *45*, 590-597.

(36)   Ellis, M. J.; Stevens, M. F. G. Antitumour polycyclic acridines. Part 13. Synthesis of 2-substituted 7H-pyrido[4,3,2-kl]acridines by thermolysis of 9-(5-alkyltriazol-1-yl)acridines. *Journal of Chemical Research* **2003**, 75-77.

(37)   Heald, R. A.; Stevens, M. F. G. Antitumour polycyclic acridines. Palladium(0) mediated syntheses of quino[4,3,2-kl]acridines bearing peripheral substituents as potential telomere maintenance inhibitors. *Organic & Biomolecular Chemistry* **2003**, *1*, 3377-3389.

(38)   Kaiser, M.; Sainlos, M.; Lehn, J.-M.; Bombard, S.; Teulade-Fichou, M.-P. Aminoglycoside-quinacridine conjugates: Towards recognition of the P6.1 element of Telomerase RNA. *ChemBioChem* **2006**, *7*, 321-329.

(39)   Halbrook, J. W.; Kesicki, E. A.; Burgress, L. E.; Schlachter, S. T.; Eary, C. T. et al.: USA, 2004; pp 149.

(40)   Gniazdowski, M.; Szmigiero, L. Nitracrine and its congeners - An overview. *General pharmacology* **1995**, *26*, 473-481.

(41)   Doh-ura, K.; Iwaki, T.; Caughey, B. Lysosomotropic agents and cysteine protease inhibitors inhibit scrapie-associated prion protein accumulation. *Journal of Virology* **2000**, *74*, 4894-4897.

(42)   Korth, C.; May, B. C. H.; Cohen, F. E.; Prusiner, S. B. Acridine and phenothiazine derivatives as pharmacotherapeutics for prion disease. *The Proceedings of the National Academy of Sciences U.S.A.* **2004**, *98*, 9836-9841.

(43)   Nguyen, T. H. T.; Lee, C. Y.; Teruya, K.; Ong, W. Y.; Doh-ura, K. et al. Antiprion activity of functionalized 9-aminoacridines related to quinacrine. *Bioorganic & Medicinal Chemistry* **2008**, *16*, 6737-6746.

(44)   Collins, S. J.; Lewis, V.; Brazier, M.; Hill, A. F.; Fletcher, A. et al. Quinacrine does not prolong survival in a murine Creutzfeldt-Jakob disease model. *Annals of Neurology*. **2002**, *52*, 503-506.

(45) Doh-ura, K.; Ishikawa, K.; Murakami-Kubo, I.; Sasaki, K.; Mohri, S. et al. Treatment of transmissible spongiform encephalopathy by intraventricular drug infusion in animal models. *Journal of Virology* **2004**, *78*.

(46) Barret, A.; Tagliavini, F.; Forloni, G.; Bate, C.; Salmona, M. et al. Evaluation of quinacrine treatment for prion diseases. *Journal of Virology* **2003**, *77*, 8462-8469.

(47) Hardman, J. G.; Limbird, L. E.; Gilman, A. G. *Goodman & Gilman's The Pharmacological Basis of Therapeutics*; McGraw-Hill Professional, 1970.

(48) Nordberg, A.; Svensson, A.-L. Cholinesterase inhibitors in the treatment of Alzheimer's disease: A comparison of tolerability and pharmacology. *Drug Safety* **1998**, *19*, 465-480.

(49) Camps, P.; Formosa, X.; Galdeano, C.; Muoz-Torrero, D.; Ramrez, L. et al. Pyrano[3,2-c]quinoline-6-chlorotacrine hybrids as a novel family of acetylcholinesterase- and beta-amyloid-directed anti-Alzheimer compounds. *Journal of Medicinal Chemistry* **2009**, *52*, 5365-5379.

(50) Marco-Contelles, J.; Leon, R.; Rios, C. d. l.; Samadi, A.; Bartolini, M. et al. Tacripyrines, the first tacrine-dihydropyridine hybrids, as multitarget-directed ligands for the treatment of Alzheimer's disease. *Journal of Medicinal Chemistry* **2009**, *52*, 2724-2732.

(51) León, R.; Ríos, C. d. l.; Marco-Contelles, J.; Huertas, O.; Barril, X. et al. New tacrine-dihydropyridine hybrids that inhibit acetylcholinesterase, calcium entry, and exhibit neuroprotection properties. *Bioorganic & Medicinal Chemistry* **2008**, *16*, 7759-7769.

(52) Fernández-Bachiller, M. I.; Pérez, C.; Campillo, N. E.; Páez, J. A.; González-Muñoz, G. C. et al. Tacrine-melatonin hybrids as multifunctional agents for Alzheimer's disease, with cholinergic, antioxidant, and neuroprotective properties. *ChemMedChem* **2009**, *4*, 828-841.

(53) Prusiner, S. B. Novel proteinacious infectious particles cause scrapie. *Science* **1982**, *216*, 136-144.

(54) Stahl, N.; Borchelt, D. R.; Hsiao, K.; Prusiner, S. B. Scrapie prion protein contains a phosphatidylinositol glycolipid. *Cell* **1987**, *51*, 229-240.

(55) Cohen, F. E.; Prusiner, S. B. Pathologic conformations of prion proteins. *Annual Review of Biochemistry.* **1998**, *67*, 793-819.

(56) Jarrett, J. T.; Lansbury, P. T. J. Seeding "one-dimensional crystallization" of amyloid: a pathogenic mechanism in Alzheimer's disease and scrapie. *Cell* **1993**, *73*, 1055-1058.

(57) Brandner, S.; Isenmann, S.; Kuhne, G.; Aguzzi, A. Identification of the end stage of scrapie using infected neural grafts. *Brain Pathology* **1998**, *8*, 19-27.

(58) Brandner, S.; Isenmann, S.; Raeber, A.; Fischer, M.; Sailer, A. et al. Normal host prion protein necessary for scrapie-induced neurotoxicity. *Nature* **1996**, *379*, 339-343.

(59) Aguzzi, A.; Calella, M. Prions: Protein aggregation and infectious diseases. *Physiology Review* **2009**, *89*, 1105-1152.

(60) Silveira, J. R.; Raymond, G. J.; Hughson, A. G.; Race, R. E.; Sim, V. L. et al. The most infectious prion protein particles. *Nature* **2005**, *437*, 257-261.

(61) Hardy, J.; Selkoe, D. J. The amyloid hypothesis of Alzheimer's disease: progress and problems on the road to therapeutics. *Science* **2002**, *297*, 353-356.

(62) Shankar, G. M.; Li, S.; Mehta, T. H.; Garcia-Munoz, A.; Shepardson, N. E. et al. Amyloid-beta protein dimers isolated directly from Alzheimer's brains impair synaptic plasticity and memory. *Nature Medicine* **2008**, *14*, 837-842.

(63) Kitada, T.; Asakawa, S.; Hattori, N.; Matsumine, H.; Yamamura, Y. et al. Mutations in the parkin gene cause autosomal recessive juvenile parkinsonism. *Nature* **1998**, *392*, 605-608.

(64) Chiti, F.; Dobson, C. M. Protein misfolding, functional amyloid, and human disease. *Annual Review of Biochemistry.* **2006**, *75*, 333-366.

(65) Andersen, J. K. Oxidative stress in neurodegeneration: cause or consequence. *Nature Medicine* **2004**, *10 (Suppl.)*, S18-25.

(66) Contestabile, A. Oxidative stress in neurodegeneration: Mechanisms and therapeutic perspectives. *Current Topics in Meidicinal Chemistry* **2001**, *1*, 553-568.

(67) Pappolla, M. A.; Chyan, Y. J.; Omar, R. A.; Hsiao, K.; Perry, G. et al. Evidence of oxidative stress and in vivo neurotoxicity of beta-amyloid in a transgenic mouse model of Alzheimer's disease - A chronic oxidative paradigm for testing antioxidant therapies *in vivo*. *American journal of pathology* **1998**, *152*, 871-877.

(68) Zemlan, F. P.; Theinhaus, O. J.; Bosmann, H. B. Superoxide dismutase activity in Alzheimer's disease: possible mechanism for paired helical formation. *Brain Research* **1989**, *476*, 160-162.

(69) Pappella, M. A.; Omar, R. A.; Kim, K. S.; Rubakis, U. K. Immunohistochemical evidence of antioxidant stress in Alzheimer's disease. *American Journal of Pathology* **1992**, *140*, 621-628.

(70) Jenner, P.; Olnaw, C. W. Oxidative stress and the pathogenesis of Parkinson's disease. *Neurology* **1996**, *47 (Suppl.)*, S161-S176.

(71) Yoitaka, A.; Hyttori, N.; Uchida, K.; Tanaka, N.; Stadtman, E. R. et al. Immunohistochemical detection of 4-hydroxynonental protein adducts in Parkinson's disease. *The Proceedings of the National Academy of Sciences U.S.A.* **1996**, *93*, 2696-2701.

(72) Damier, P.; Hirsch, E. C.; Zhang, P.; Agid, Y.; Javoy-Agid, F. Glutathione peroxidase, glial cells and Parkinson's disease. *Neuroscience* **1993**, *52*, 1-7.

(73) Sian, J.; Dexter, D. T.; Less, A. J. Alteration in glutathione levels in Parkinson's disease and other neurodegenerative disorders affective basal ganglia. *Annals of Neurology.* **1994**, *36*, 348-355.

(74) Hur, K.; Kim, J.-I.; Choi, S.-I.; Choi, E.-K.; Carp, R. I. et al. The pathogenic mechanisms of prion diseases. *Mechanisms of Ageing and Development* **2002**, *123*, 1637-1647.

(75)   Pamplona, R.; Naudí, A.; Gavín, R.; Pastrana, M. A.; Sajnani, G. et al. Increased oxidation, glycoxidation, and lipoxidation of brain proteins in prion disease. *Free Radical Biology & Medicine* **2008**, *45*, 1159-1166.

(76)   Wang, J. Y.; Wen, L. L.; Huang, Y. N.; Chen, Y. T.; Ku, M. C. Dual effects of antioxidants in neurodegeration: direct neuroprotection against oxidative stress and indirect protection via suppression of glia-mediated inflammation. *Current Pharmaceutical Design* **2006**, *12*, 3521-3533.

(77)   Cavalli, A.; Bolognesi, M. L.; Minarini, A.; Rosini, M.; Tumiatti, V. et al. Multi-target-directed ligands to combat neurodegenerative diseases. *Journal of Medicinal Chemistry* **2007**, *51*, 347-372.

(78)   Nunziante, M.; Gilch, S.; Schatzl, H. M. Prion diseases: From molecular biology to intervention strategies. *ChemBioChem* **2003**, *4*, 1268-1284.

(79)   Rubinsztein, D. C.; Carmichael, J. Huntington's disease: Molecular basis of neurodegeneration. *Expert Reviews in Molecular Medicine* **2003**, *5*, 1-21.

(80)   Armstrong, R. A.; Lantos, P. L.; Cairns, N. J. Spatial correlations between the vacuolation, prion protein deposits, and surviving neurons in the cerebral cortex in sporadic Creutzfeldt-Jakod disease. *Neuropathy* **2001**, *21*, 266-271.

(81)   Schwarze-Eicker, K.; Keyvani, K.; Gortz, N.; Westaway, D.; Sachser, N. et al. Prion protein (PrP^C) promotes beta-amyloid plaque formation. *Neurobiology of Aging.* **2005**, *26*, 1177-1182.

(82)   Miyazono, M.; Kitamono, T.; Iwaki, T.; Tateishi, J. Colocalization of prion protein and beta protein in the same amyloid plaques in patients with Gerstmann-Straussler syndrome. *Acta Neuropathologica (Berl)* **1992**, *83*, 333-339.

(83)   Laurén, J.; Gimbel, D. A.; Nygaard, H. B.; Gilbert, J. W.; Strittmatter, S. M. Cellular prion protein mediates impairment of synaptic plasticity by amyloid-b oligomers. *Nature* **2009**, *457*, 1128-1132.

(84)   Pera, M.; Martínez-Otero, A.; Colombo, L.; Salmona, M.; Ruiz-Molina, D. et al. Acetylcholinesterase as an amyloid enhancing factor in PrP82-146 aggregation process. *Molecular and Cellular Neuroscience* **2009**, *40*, 217-224.

(85)   Tabern, D. L. Antiseptic acridine compounds: US, 1953.

(86)   Tabern, D. L. Alkoxyphenylalkoxy-acridines: US, 1954.

(87)   Steck, E. A.; Buck, J. S.; Fletcher, L. T. Some 9-amino-3-nitroacridine derivatives. *Journal of the American Chemical Society.* **1957**, *79*, 4414-4417.

(88)   Piestrzeniewicz, M. K.; Wilmanska, D.; Studzian, K.; Szemraj, J.; Czyz, M. et al. Inhibition of RNA synthesis *in vitro* by acridines - relation between structure and activity. *Zeitschrift für Naturforschung. Section C. Journal of Biosciences.* **1998**, *53*, 359-368.

(89)   Hisako, F.; Mitsuo, T.; Masashi, N.; Tatsuo, Y. Prospects of the therapeutic approaches to Creutzfeldt-Jakob disease: a clinical trial of antimalarial, quinacrine. *Japanese journal of clinical medicine* **2003**, *60*, 1649.

(90)   May, B. C. H.; Fafarman, A. T.; Hong, S. B.; Rogers, M.; Deady, L. W. et al. Potent inhibition of scrapie prion replication in cultured cells by bis-acridines. *The Proceedings of the National Academy of Sciences U.S.A.* **2003**, *100*, 3416.

(91)   Csuk, R.; Barthel, A.; Raschke, C.; Kluge, R.; Ströhl, D. et al. Synthesis of monomeric and dimeric acridine compounds as potential therapeutics in Alzheimer and prion diseases. *Archiv der Pharmazie* **2009**, *342*, 699-709.

(92)   Dollinger, S.; Lober, S.; Klingenstein, R.; Korth, C.; Gmeiner, P. A chimeric ligand approach leading to potent antiprion active acridine derivatives: design, synthesis, and biological investigations. *Journal of Medicinal Chemistry* **2006**, *49*, 6591-6595.

(93)   May, B. C. H.; Witkop, J.; Sherrill, J.; Anderson, M. O.; Madrid, P. B. et al. Structure-activity relationship of 9-aminoacridine compounds in scrapie-infected neuroblastoma cells. *Bioorganic and medicinal chemistry letters* **2006**, *16*, 4913-4916.

(94)   Cope, H.; Mutter, R.; Heal, W.; Pascoe, C.; Brown, P. et al. Synthesis and SAR study of acridine, 2-methylquinoline and 2-phenylquinazoline analogues as anti-prion agents. *European journal of medicinal chemistry* **2006**, *41*, 1124-1143.

(95)   Huang, Y.; Okochi, H.; May, B. C. H.; Legname, G.; Prusiner, S. B. et al. Quinacrine is mainly metabolized to mono-desethyl quinacrine by CYP3A4/5 and its brain accumulation is limited by P-glycoprotein. *Drug Metabolism and Disposition* **2006**, *34*, 1136-1144.

(96)   Shinya, D.; Atsushi, Y.; Fuyuko, T.; Yasufumi, S.; Shun, H. et al. Uptake and efflux of quinacrine, a candidate for the treatment of prion diseases, at the blood-brain barrier. *Cellular and molecular neurobiology* **2004**, *24*, 205-217.

(97)   Silverman, J. A. Multidrug-resistance transporters. *Pharmaceutical Biotechnology* **1999**, *12*, 353-386.

(98)   Szakacs, G.; Paterson, J. K.; Ludwig, J. A.; Booth-Genthe, C.; Gottesman, M. M. Targeting multidrug resistance in cancer. *Nature Reviews: Drug Discovery* **2006**, *5*, 219-234.

(99)   Ghaemmaghami, S.; Ahn, M.; Lessard, P.; Giles, K.; Legname, G. et al. Continuous quinacrine treatment results in the formation of drug-resistant prions. *PLoS Pathogens* **2009**, *5*, 1-10.

(100) Kawatake, S.; Nishimura, Y.; Sakaguchi, S.; Iwaki, T.; Doh-ura, K. Surface plasmon resonance analysis for the screening of anti-prion compounds. *Biological & Pharmaceutical Bulletin* **2006**, *29*, 927-932.

(101) Mangels, C.; Frank, A. O.; Ziegler, J.; Klingenstein, R.; Schweimer, K. et al. Binding of TCA to the prion protein: mechanisms, implication for therapy, and application as probe for complex formation of bio-macromolecules. *Journal of Biomolecular Structure & Dynamics* **2009**, *27*, 163-170.

(102) Phuan, P.-W.; Zorn, J. A.; Safar, J.; Giles, K.; Prusiner, S. B. et al. Discriminating between cellular and misfolded prion protein by using

affinity to 9-aminoacridine compounds. *Journal of General Virology* **2007***, 88*, 1392-1401.

(103) Vogtherr, M.; Grimme, S.; Elshorst, B.; Jacobs, D. M.; Fiebig, K. et al. Antimalarial drug quinacrine binds to C-terminal helix of cellular prion protein. *Journal of Medicinal Chemistry* **2003***, 46*, 3563-3564.

(104) Turnbull, S.; Tabner, B. J.; Brown, D. R.; Allsop, D. Quinacrine acts as an antioxidant and reduces the toxicity of the prion peptide PrP106 -126. *NeuroReport* **2003***, 14*, 1743-1745.

(105) Kerns, E. H.; Di, L. Drug-like properties: concepts, structure design and methods: from ADME to toxicity optimization.; Academic Press: Amsterdam, Boston, 2008; pp Chapter 10.

(106) Ryou, C.; Legname, G.; Peretz, D.; Craig, J. C.; Baldwin, M. A. et al. Differential inhibition of prion propagation by enantiomers of quinacrine. *Laboratory Investigation* **2003***, 83*, 837-843.

(107) Webster, R. V.; Craio, J. C.; Shyamala, V.; Kirby, G. C.; Warhurst, D. C. Antimalarial activity of optical isomers of quinacrine dihydrochloride against chloroquine-sensitive and -resistant *Plasmodium falciparum in vitro*. *Biochemical Pharmacology* **1991***, 42*, S225-S227.

(108) Forloni, G.; Vari, M. R.; Colombo, L.; bugiani, O.; Tagliavini, F. et al. Prion diseases: Time for a therapy. *Current Medicinal Chemistry: Immunology, Endocrine & Metabolic Agents* **2003***, 3*, 185-197.

(109) Thomas, G. *Medicinal Chemistry: An introduction*; 2nd ed.; Wiley, 2007; pp 109.

(110) Wermuth, C. G. *The Practice of Medicinal Chemistry*; Academic Press, 2008; pp 445.

(111) Goodell, J. R.; Svensson, B.; Ferguson, D. M. Spectrophotometric determination and computational evaluation of the rates of hydrolysis of 9-amino-substituted acridines. *Journal of Chemical Information and Modeling* **2006***, 46*, 876-883.

(112) Albert, A. *The acridines: their preparation, physical, chemical, and biological properties and uses.*; 2nd ed.; Edward Arnold Ltd.: London, 1966.

(113) Paul, A.; Ladame, S. 9-Amino acridines undergo reversible amine exchange reactions in water: Implications on their mechanism of action in vivo. *Organic Letters* **2009***, 11*, 4894-4897.

(114) Aly, E. I.; Abadi, A. H. Synthesis and antitubercular activity of 6-chloro (unsubstituted)-2-methoxy-9-substituted acridine derivatives. *Archives of Pharmacal Research* **2004***, 27*, 713-719.

(115) Louie, J.; Hartwig, J. F. Palladium-catalyzed synthesis of arylamines from aryl halides. Mechanistic studies lead to coupling in the absence of tin reagents. *Tetrahedron Letters* **1995***, 36*, 3609-3612.

(116) Jeon, H.-B.; Lee, Y.; Qiao, C.; Huang, H.; Sayre, L. M. Inhibition of bovine plasma amine oxidase by 1,4-diamino-2-butenes and -2-butynes. *Bioorganic & Medicinal Chemistry* **2003***, 11*, 4631-4641.

(117) Kutschy, P.; Dzurilla, M.; Takasugi, M.; Torok, M.; Achbergerova, I. et al. New syntheses of indole phytoalexins and related compounds. *Tetrahedron* **1998**, *54*, 3549-3566.

(118) Souza, M. V. N. d.; Pais, K. C.; Kaiser, C. R.; Peralta, M. A.; Ferreira, M. d. L. et al. Synthesis and in vitro antitubercular activity of a series of quinoline derivatives. *Bioorganic & Medicinal Chemistry* **2009**, *17*, 1474-1480.

(119) Hu, M.-K.; Wu, L.-J.; Hsiao, G.; Yen, M.-H. Homodimeric tacrine congeners as acetylcholinesterase inhibitors. *Journal of Medicinal Chemistry* **2002**, *45*, 2277-2282.

(120) Hosokawa-Muto, J.; Kamatari, Y. O.; Nakamura, H. K.; Kuwata, K. Variety of antiprion compounds discovered through an *in silico* screen based on cellular-form prion protein structure: correlation between antiprion activity and binding affinity. *Antimicrobial Agents and Chemotherapy* **2009**, *53*, 765-771.

(121) Touil, F.; Pratt, S.; Mutter, R.; Chen, B. Screening a library of potential prion therapeutics against cellular prion proteins and insights into their mode of biological activities by surface plasmon resonance. *Journal of Pharmaceutical and Biomedical Analysis* **2006**, *40*, 822-832.

(122) Di, L.; Kerns, E. H.; Fan, K.; McConnell, O. J.; Carter, G. T. High throughput artificial membrane permeability assay for blood-brain barrier. *European journal of medicinal chemistry* **2003**, *38*, 223-232.

(123) Murakami-Kubo, I.; Doh-ura, K.; Ishikawa, K.; Kawatake, S.; Sasaki, K. et al. Quinoline derivatives are therapeutic candidates for transmissible spongiform encephalopathies. *Journal of Virology* **2004**, *78*, 1281-1288.

(124) Ishikawa, K.; Kudo, Y.; Nishida, N.; Suemoto, T.; Sawada, T. et al. Styrylbenzoazole derivatives for imaging of prion plaques and treatment of transmissible spongiform encephalopathies. *Journal of Neurochemistry* **2006**, *99*, 198-205.

(125) Kawasaki, Y.; Kawagoe, K.; Chen, C. J.; Teruya, K.; Sakasegawa, Y. et al. Orally administered amyloidophilic compound is effective in prolonging the incubation periods of animals cerebrally infected with prion diseases in a prion strain-dependent manner. *Journal of Virology* **2007**, *81*, 12889-12898.

(126) Doh-ura, K.; Kuge, T.; Uomoto, M.; Nishizawa, K.; Kawasaki, Y. et al. Prophylactic effect of dietary seaweed Fucoidan against enteral prion infection. *Antimicrobial Agents and Chemotherapy* **2007**, *51*, 2274-2277.

(127) Sim, H.-M.; Lee, C.-Y.; Ee, P. L. R.; Go, M.-L. Dimethoxyaurones: Potent inhibitors of ABCG2 (breast cancer resistance protein). *European journal of Pharmaceutical Sciences* **2008**, *35*, 293-306.

(128) Kocisko, D. A.; Baron, G. S.; Rubenstein, R.; Chen, J.; Kuizon, S. et al. New inhibitors of scrapie-associated prion protein formation in a library of 2,000 drugs and natural products. *Journal of Virology* **2003**, *77*, 10288-10294.

(129) Thompson, M. J.; Louth, J. C.; Greenwood, G. K.; Sorrell, F. J.; Knight, S. G. et al. Improved 2,4-diarylthiazole-based antiprion agents: switching the

sense of the amide group at C5 leads to an increase in potency. *ChemMedChem* **2010**, *5*, 1476-1488.

(130) Bach, S.; Tribouillard, D.; Talarek, N.; Desban, N.; Gug, F. et al. A yeast-based assay to isolate drugs active against mammalian prions. *Methods* **2006**, *39*, 72-77.

(131) Clarke, M. C.; Haig, D. A. Evidence for the multiplication of scrapie agent in cell culture. *Nature* **1970**, *225*, 100-101.

(132) Race, R.; Fadness, L.; Chesebro, B. Characterisation of scrapie infection in mouse neuroblastoma cells. *Journal of General Virology* **1987**, *68*, 1391-1399.

(133) Bosque, P. J.; Prusiner, S. B. Cultured cell sublines highly susceptible to prion infection. *Journal of Virology* **2000**, *74*, 4377-4386.

(134) Butler, D. A.; Scott, M. R.; Bockman, J. M.; Borchelt, D. R.; Taraboulos, A. et al. Scrapie-infected murine neuroblastoma cells produce protease-resistant prion proteins. *Journal of Virology* **1988**, *62*, 1558-1564.

(135) Milhavet, O.; McMahon, H. E. M.; Rachidi, W.; Nishida, N.; Katamine, S. et al. Prion infection impairs the cellular response to oxidative stress. *The Proceedings of the National Academy of Sciences U.S.A.* **2000**, *97*, 13937-13942.

(136) Lemke, T. L.; Williams, D. A. *Foye's Principles of Medicinal Chemistry*; 6 ed.; Lippincott Williams & Wilkins, 2002; 1377.

(137) Wildman, S. A.; Crippen, G. M. Prediction of physiochemical parameters by atomic contributions. *Journal of Chemical Information and Modeling* **1999**, *39*, 868-873.

(138) Heal, W.; Thompson, M. J.; Mutter, R.; Cope, H.; Louth, J. C. et al. Library synthesis and screening: 2,4-diphenylthiazoles and 2,4-diphenyloxazoles as potential novel prion disease therapeutics. *Journal of Medicinal Chemistry* **2007**, *50*, 1347-1353.

(139) Koster, T.; Singh, K.; Zimmermann, M.; Gruys, E. Emerging therapeutic agents for transmissible spongiform encephaopathies. *Journal of Veterinary Pharmacology and Therapeutics* **2003**, *26*, 315-326.

(140) Kim, C.-L.; Karino, A.; Ishiguro, N.; Shinagawa, M.; Sato, M. et al. Cell-surface retention of PrP^C by anti-PrP antibody prevents protease-resistant PrP formation. *Journal of General Virology* **2004**, *85*, 3473-3482.

(141) Kansy, M.; Senner, F.; Gubernator, K. Physicochemical high throughput screening: parallel artificial membrane permeability assay in the description of passive absorption processes. *Journal of Medicinal Chemistry* **1998**, *41*, 1007-1010.

(142) Dohgu, S.; Yamauchi, A.; Takata, F.; Sawada, Y.; Higuchi, S. et al. Uptake and efflux of quinacrine, a candidate for the treatment of prion diseases at the blood-brain barrier. *Cellular and molecular neurobiology* **2004**, *24*, 205-217.

(143) Tan, S.; Schubert, D.; Maher, P. Oxytosis: A novel form of programmed cell death. *Current Topics in Meidicinal Chemistry* **2001**, *1*, 497-506.

(144) Rothman, S. M. The neurotoxicity of excitatory amino acids is produced by passive chloride influx. *Journal of Neuroscience* **1985**, *5*, 1483-1489.

(145) Rothman, S. M.; Olney, J. M. Glutamate and the pathophysiology of hypoxic-ischemic brain damage. *Annals of Neurology* **1986**, *19*, 105-111.

(146) Schinder, A. F.; Olson, E. C.; Spitzer, N. C.; Montal, M. Mitochondrial dysfunction is a primary event in glutamate neurotoxicity. *Journal of Neuroscience* **1996**, *16*, 6125-6133.

(147) Castilho, R. F.; Hansson, O.; Ward, M. W.; Budd, S. L.; Nicholls, D. G. Mitochondrial control of acute glutamate excitotoxicity in cultured cerebellar granule cells. *Journal of Neuroscience* **1998**, *18*, 10277-10286.

(148) Li, Y.; Maher, P.; Schubert, D. A role for 12-lipoxygenase in nerve cell death caused by glutathione depletion. *Neuron* **1997**, *19*, 453-463.

(149) Li, Y.; Maher, P.; Schubert, D. Requirement for cGMP in nerve cell death caused by glutathione depletion. *Journal of Cell Biology* **1997**, *139*, 1317-1324.

(150) Liu, Y.; Dargusch, R.; Maher, P.; Schubert, D. A broadly neuroprotective derivative of curcumin. *Journal of Neurochemistry* **2008**, *105*, 1336-1345.

(151) Ishige, K.; Schubert, D.; Sagara, Y. Flavonoids protect neuronal cells from oxidative stress by three distinct mechanisms. *Free Radical Biology & Medicine* **2001**, *30*, 433-446.

(152) Sagara, Y.; Ishige, K.; Tsai, C.; Maher, P. Tyrphostins Protect Neuronal Cells from Oxidative Stress. *Journal of Biological Chemsitry* **2002**, *277*, 36204-36215.

(153) Herrera, F.; Martin, V.; Garcýa-Santos, G.; Rodriguez-Blanco, J.; Antolýn, I. et al. Melatonin prevents glutamate-induced oxytosis in the HT22 mouse hippocampal cell line through an antioxidant effect specially targeting mitochondria. *Journal of Neurochemistry* **2007**, *100*, 736-746.

(154) Satoh, T.; Izumi, M. Neuroprotective effects of phenylenediamine derivatives independent of an antioxidant pathway in neuronal HT22 cells. *Neuroscience letters* **2007**, *418*, 102-105.

(155) Tietze, F. Enzymic method for quantitative determination of nanogram amounts of total and oxidized glutathione. *Analytical Biochemistry* **1969**, *27*, 502-522.

(156) Bradford, M. M. A Rapid and Sensitive Method for the Quantitation of Microgram Quantities of Protein Utilizing the Principle of Protein-Dye Binding. *Analytical Biochemistry* **1976**, *72*, 248-254.

(157) Re, R.; Pellegrini, N.; Proteggente, A.; Pannala, A.; Yang, M. et al. Antioxidant activity applying an improved ABTS radical cation decolorization assay. *Free Radical Biology & Medicine* **1999**, *26*, 1231-1237.

(158) Sagara, Y. Induction of reactive oxygen species in neurons by haloperidol. *Journal of Neurochemistry* **1998**, *71*, 1002-1012.

(159) Bass, D.; Parce, J.; Dechatelet, L.; Szejda, P.; Seeds, M. et al. Flow cytometric studies of oxidative product formation by neutrophils: a graded response to membrane stimulation. *Journal of Immunology* **1983**, *130*, 1910-1917.

(160) Chew, E.-H.; Matthews, C. S.; Zhang, J.; McCarroll, A. J.; Hagen, T. et al. Antitumor quinols: Role of glutathione in modulating quinol-induced

apoptosis and identi.cation of putative cellular protein targets. *Biochemical and Biophysical Research Communications* **2006**, *346*, 242-251.

(161) Jou, M. J.; Peng, T. I.; Reiter, R. J.; Jou, S. B.; Wu, H. Y. et al. Visualization of the antioxidant effects of melatonin at the mitochondrial level during oxidative stress-induced apoptosis of rat brain astrocytes. *Journal of Pineal Research* **2004**, *37*, 55-70.

(162) Novak, E. J.; Rabinovitch, P. S. Improved sensitivity in flow cytometric intracellular ionized calcium measurement using Fluo-3/Fura Red fluorescence ratios. *Cytometry* **1994**, *17*, 135-141.

(163) Aoshima, H.; Satoh, T.; Sakai, N.; Yamada, M.; Enokido, Y. et al. Generation of free radicals during lipid hydroperoxide-triggered apoptosis in PC12 cells. *Biochimica et Biophysica Acta* **1997**, *12345*, 35-42.

(164) Satoh, T.; Sakai, N.; Enokido, Y.; Uchiyama, Y.; Hatanaka, H. Survival factor-insensitive generation of reactive oxygen species induced by serum deprivation in neuronal cells. *Brain Research* **1996**, *739*, 9-14.

(165) Xu, X.; Chua, C. C.; Kong, J.; Kostrzewa, R. M.; Kumaraguru, U. et al. Necrostatin-1 protects against glutamate-induced glutathione depletion and caspase-independent cell death in HT-22 cells. *Journal of Neurochemistry* **2003**, *103*, 2004-2014.

(166) Farlow, M.; Gracon, S. I.; Hershey, L. A.; Lewis, K. W.; Sadowsky, C. H. et al. A controlled trial of tacrine in Alzheimer's disease. The tacrine study group. *Journal of the American Medical Association.* **1992**, *268*, 2523-2529.

(167) Watkins, P. B.; Zimmerman, H. J.; Knapp, M. J.; Gracon, S. I.; Lewis, K. M. Hepatotoxic effects of tacrine administration in patients with Alzheimer's disease. *Journal of the American Medical Association.* **1994**, *271*, 992-998.

(168) Pang, Y.-P.; Quiram, P.; Jelacic, T.; Hong, F.; Brimijoin, S. Highly potent, selective, and low cost bis-tetrahydroaminacrine inhibitors of acetylcholinesterase: steps toward novel drugs for treating Alzheimer's disease. *Journal of Biological Chemsitry* **1996**, *271*, 23646-23649.

(169) Carlier, P. R.; Han, Y. F.; Chow, E. S.-H.; Li, C. P.-L.; Wang, H. et al. Evaluation of short-tether Bis-THA AChE inhibitors. A further test of the dual binding site hypothesis. *Bioorganic & Medicinal Chemistry* **1999**, *7*, 351-357.

(170) Rydberg, E. H.; Brumshtein, B.; Greenblatt, H. M.; Wong, D. M.; Shaya, D. et al. Complexes of alkylene-linked tacrine dimers with Torpedo californica acetylcholinesterase: Binding of bis(5)-tacrine produces a dramatic rearrangement in the active-site gorge. *Journal of Medicinal Chemistry* **2006**, *49*, 5491-5500.

(171) Harel, M.; Schalk, I.; Ehret-Sabatier, L.; Bouet, F.; Goeldner, M. et al. Quaternary ligand binding to aromatic residues in the active-site gorge of acetylcholinesterase. *The Proceedings of National Academy of Sciences U.S.A.* **1993**, *90*, 9031-9035.

(172) Pang, Y.-P.; Kozikowski, A. R. Prediction of the binding sites of huperzine A in acetylcholinesterase by docking studies. *Journal of Computer-Aided Molecular Design.* **1994**, *8*, 669-681.

(173) Sussman, J. L.; Harel, M.; Frolow, F.; Oefner, C.; Goldman, A. et al. Atomic structure of acetylcholinesterase from Torpedo californica:a prototypic acetylcholine-binding protein. *Science* **1991**, *253*, 872-879.

(174) Harel, M.; Sussman, J. L.; Krejci, E.; Bon, S.; Chanal, P. et al. Conversion of acetylcholinesterase to butyrylcholinesterase: modeling and mutagenesis. *The Proceedings of the National Academy of Sciences U.S.A.* **1992**, *89*, 10827-10831.

(175) Steinberg, G. M.; Mednick, M. L.; Maddox, J.; Rice, R.; Cramer, J. Hydrophobic binding site in acetylcholinesterase. *Journal of Medicinal Chemistry* **1975**, *18*, 1056-1061.

(176) Taylor, J. L.; Mayer, R. T.; Himel, C. M. Conformers of acetylcholinesterase: a mechanism of allosteric control. *Molecular Pharmacology* **1994**, *45*, 74-83.

(177) Shao, D.; Zou, C.; Luo, C.; Tang, X.; Li, Y. Synthesis and evaluation of tacrine–E2020 hybrids as acetylcholinesterase inhibitors for the treatment of Alzheimer's disease. *Bioorganic & Medicinal Chemistry Letters.* **2004**, *14*, 4639-4642.

(178) Mesulam, M.-M.; Guillozet, A.; Shaw, P.; Levey, A.; Duysen, E. G. et al. Acetylcholinesterase knockouts establish central cholinergic pathways and can use butyrylcholinesterase to hydrolyze acetylcholine. *Neuroscience* **2002**, *110*, 627-639.

(179) Li, B.; Stribley, J. A.; Ticu, A.; Xie, W.; Schopfer, L. M. et al. Abundant tissue butyrylcholinesterase and its possible function in the Acetylcholinesterase knockout mouse. *Journal of Neurochemistry* **2000**, *75*, 1320-1331.

(180) Giacobini, E. Cholinergic function and Alzheimer's disease. *International Journal of Geriatric Psychiatry* **2003**, *18*, S1-S5.

(181) Ellman, G. L.; Courtney, K. D.; Andres, V.; Featherstone, J. a. R. M. A new and rapid colorimetric determination of acetylcholinesterase activity. *Biochemical Pharmacology* **1961**, *7*.

(182) Cornish-Bowden, A. A simple graphical method for determining the inhibition constants of mixed, uncompetitive and non-competitive inhibitors. *Biochemistry Journal* **1974**, *137*, 143-144.

(183) Tumiatti, V.; Milelli, A.; Minarini, A.; Rosini, M.; Bolognesi, M. L. et al. Structure-activity relationship of acetylcholinesterase noncovalent inhibitors based on a polyamine backbone for further investigation on the inner space. *Journal of Medicinal Chemistry* **2008**, *51*, 7308-7312.

(184) Saxena, A.; Fedorko, J. M.; Vinayaka, C. R.; Medhekar, R.; Radic, Z. et al. Aromatic amino acid residues at the active and peripheral anionic sites control the binding of E2020 (Aricept) to cholinesterases. *European Journal of Biochemistry* **2003**, *270*, 4447-4458.

(185) Rosini, M.; Simoni, E.; Bartolini, M.; Cavalli, A.; Ceccarini, L. et al. Inhibition of acetylcholinesterase, ß-Amyloid aggregation, and NMDA

receptors in Alzheimer's disease: A promising direction for the multi-target-directed ligands gold rush. *Journal of Medicinal Chemistry* **2008**, *51*, 4381-4384.

(186) Kryger, G.; Sussman, J. L. 3D structure of a complex of human recombinant acetylcholinesterase with fasciculin-II at 2.7A resolution. *Structure and function of cholinesterases and related proteins.*; Plenum: NY, 1998; pp 323-326.

(187) Kryger, G.; Silman, I.; Sussman, J. L. Structure of acetylcholinesterase complexed with E2020 (Aricept®): implications for the design of new anti-Alzheimer drugs. *Structure* **1999**, *7*, 297-307.

(188) Moorad, D. R.; Luo, C.; Saxena, A.; Doctor, B. P.; Garcia, G. E. Purification and determination of the amino acid sequence of equine serum butyrylcholinesterase. *Toxicology Methods* **1999**, *9*, 219-227.

(189) Bartolini, M.; Bertucci, C.; Cavrini, V.; Andrisano, V. B-Amyloid aggregation induced by human acetylcholinesterase: inhibition studies. *Biochemical Pharmacology* **2003**, *65*, 407-416.

(190) Inestrosa, N. C.; Alvarez, A.; Perez, C. A.; Moreno, R. D.; Vicente, M. et al. Acetylcholinesterase accelerates assembly of amyloid-beta peptides into Alzheimer's fibrils: possible role of the peripheral site of the enzyme. *Neuron* **1996**, *16*, 881-891.

Appendix 1: Spectroscopic data, yield, and retention time of synthesized compounds

^{1}H-NMR and ^{13}C-NMR spectra were recorded on a Bruker DPX 300MHz spectrometer and chemical shifts were reported in δ (ppm) relative to the internal standard TMS. Mass spectra (MS, nominal) were collected on a LCQ Finnigan MAT mass spectrometer. Atmospheric pressure ionization (APCI) or electron spray (ionization (ESI) were used as probes. Reactions were routinely monitored by thin layer chromatography using silica gel 60 F 254 plates from Merck, with UV light as a visualizing agent. Column chromatography was performed using silica gel G (0.04-0.063mm) from Merck. Solvents were of analytical grade or distilled from technical grade. Purity analysis was verified by high pressure liquid chromatography (HPLC) or by combustion analysis. Combustion analyses (C, H, N) were determined by Perkin-Elmer PE 2400 CHN/CHNS elemental analyzer by the Department of Chemistry, National University of Singapore. All chemicals were purchased from Sigma Aldrich Chemical Company (MO, USA), Tokyo Chemical Industry (Tokyo, Japan), and Alfa Aesar (MA, USA).

The purity of the compounds were determined by reverse phase HPLC with two different solvent systems (methanol/water and acetonitrile/water). Compounds were considered sufficiently pure for biological evaluation if they gave a single peal on the HPLC chromatogram, with peak area not less than 95%. The test compound was dissolved in methanol and injected through a 50 µl loop at a flow rate of 1ml/min, with UV detection at 254 nm. Each compound was tested with two mobile phases: methanol-water and acetonitrile-water. Retention time (t_R in

min) and peak area of test sample (P) were recorded in each case from at least two determinations.

Mobile phases and columns used are listed in the table below

Condition	Column	Mobile phase
A1	ODS1, 4.6x250mm, 10μm, 80Å (Waters Spherisorb®)	water 10% + methanol 90% + formic acid 0.01%
A2	ODS1, 4.6x250mm, 10μm, 80Å (Waters Spherisorb®)	water 10% + acetonitrile 90% + formic acid 0.01%
B1	Zorbax Eclipse XDB-C18 (Agilent Technologies®)	water 10% + methanol 90% + formic acid 0.01%
B2	Zorbax Eclipse XDB-C18 (Agilent Technologies®)	water 30% + methanol 70% + formic acid 0.03%
B3	Zorbax Eclipse XDB-C18 (Agilent Technologies®)	water 50% + methanol 50% + formic acid 0.05%
B4	Zorbax Eclipse XDB-C18 (Agilent Technologies®)	water 10% + acetonitrile 90% + formic acid 0.01%
B5	Zorbax Eclipse XDB-C18 (Agilent Technologies®)	water 30% + acetonitrile 70% + formic acid 0.03%
B6	Zorbax Eclipse XDB-C18 (Agilent Technologies®)	water 50% + acetonitrile 50% + formic acid 0.05%

B7	Zorbax Eclipse XDB-C18 (Agilent Technologies®)	water 70% + acetonitrile 30% + formic acid 0.07%

Group 1:

6-Chloro-N-(2-(diethylamino)ethyl)-2-methoxyacridin-9-amine

dihydrochloride (1): Yellow solid. Yield 74%. ^{1}H NMR (300MHz, CDCl$_3$) δ 1.41 (t, J=7.2, 6H) 3.39 (q, J=7.2, 4H), 3.80 (t, J=6.4, 2H) 4.06 (s, 3H) 4.63 (t, J=6.4, 2H) 7.55 (dd, J1=2.7, J2=9.3, 1H) 7.67 (t, J=8.3, 1H) 7.80 (dd, J1=4.2, J2=9.2, 1H) 7.86 (d, J= 2.7, 1H) 8.01 (d, J=2.9, 1H) 8.49 (dd, J1=1.5, J2=9.4, 1H). MS (ESI) *m/z* [M$^+$] 358.1. Elemental analysis: C$_{20}$H$_{24}$N$_3$OCl.2HCl.H$_2$O found 53.33 % C (calcd 53.51%), found 6.03% H (calcd 6.24%).

6-Chloro-N-(3-(dimethylamino)propyl)-2-methoxyacridin-9-amine

dihydrochloride (2): Yellow solid. Yield 70%. ^{1}H NMR (300MHz, CD$_3$OD) δ 2.48 (q, 2H) 2.94 (s, 6H) 3.36 (t, J=7.2, 2H) 4.04 (s, 3H) 4.29 (t, J=7.2, 2H) 7.52 (dd, J1=2.1, J2=9.3, 1H) 7.64 (dd, J1=2.5, J2=9.3, 1H) 7.77 (d, J=9.3, 1H) 7.82 (d, J=2.0, 1H) 7.91 (d, J=2.3, 1H) 8.51 (d, J=9.4, 1H). MS (ESI) *m/z* [M$^+$] 344.1. Elemental analysis: C$_{19}$H$_{22}$N$_3$OCl.2HCl.2¼H$_2$O found 50.02% C (expected 49.89%), found 5.99% H (expected 6.24%).

6-Chloro-N-(3-(diethylamino)propyl)-2-methoxyacridin-9-amine

dihydrochloride (3): Yellow solid. Yield 55%. ^{1}H NMR (300MHz, CD$_3$OD) δ 1.35 (t, J=7.3, 6H) 2.48 (m, 2H) 3.45-3.30 (obs, m, 6H, in acetic acid-d) 4.04 (s,

3H) 4.30 (t, J=7.2, 2H) 7.50 (dd, $J1$=2.0, $J2$=9.3, 1H) 7.63 (dd, $J1$=2.4, $J2$=9.3, 1H) 7.76 (d, J=2.5, 1H) 7.81 (d, J=1.9, 1H) 7.92 (d, J=2.3, 1H) 8.51 (d, J=9.4, 1H). MS (ESI) m/z [M$^+$] 371.9. $C_{21}H_{26}N_3OCl.2HCl.2\frac{1}{2}H_2O$ found 51.58% C (calcd 51.48%), found 6.80% H (calcd 6.74%).

6-Chloro-N-(4-(diethylamino)butyl)-2-methoxyacridin-9-amine

dihydrochloride (4): Yellow solid. Yield 56%. ^{1}H NMR (300MHz, CDCl$_3$) δ 1.33 (t, J=7.3, 6H) 1.93 (m, 2H) 2.11 (m, 2H) 3.25 (m, 6H) 4.03 (s, 3H) 4.24 (t, J=6.8, 2H) 7.50 (d, J=8.9, 1H) 7.63 (d, J=9.0, 1H) 7.74 (d, J=9.2, 1H) 7.80 (d, J=2.2, 1H) 7.88 (d, J=2.1, 1H) 8.50 (d, J=9.3, 1H). MS (ESI) m/z [M$^+$] 386.1. Elemental analysis: $C_{22}H_{28}N_3OCl.2HCl.1\frac{3}{4}H_2O$ found 53.82% C (calcd 53.88%) found 6.71% H (calcd 6.84%).

Group 2

N^1-(6-Chloro-2-methoxyacridin-9-yl)-N^2,N^2-dimethylbenzene-1,2-diamine

hydrochloride (5): Yellow solid. Yield 70%. ^{1}H NMR (300MHz, CDCl$_3$) δ 3.31 (s, 6H) 3.77 (s, 3H), 7.45 (m, 2H) 7.53 (d, J=2.1, 1H) 7.61-7.66 (m, 2H) 7.71 (dd, $J1$=11, $J2$=2.4, 1H) 7.73.-7.88 (m, 2H) 7.98 (d, J=1.8, 1H) 8.03 (d, J=9.6, 1H). MS (ESI) m/z [M$^+$] 378.1. HPLC: condition A1 t_R=3.518min P=100%, condition A2 t_R=3.471min P=100%.

N^1-(6-Chloro-2-methoxyacridin-9-yl)-N^3,N^3-dimethylbenzene-1,3-diamine

(6): Orange solid. Yield 70%. ^{1}H NMR (300MHz, CDCl$_3$) δ 2.98 (s, 6H), 3.76 (s,

3H), 6.63 (q, *J1*=8.7, *J2*=16.0, 2H), 6.99 (m, 2H), 7.05 (dd, *J1*=2.2, *J2*=9.3, 1H), 7.20 (m, 2H) 7.30 (d, *J*=2.0, 1H), 7.84 (d, *J*=9.4, 1H), 7.98 (d, *J*=9.2, 1H), 8.13 (d, *J*=1.4, 1H), 10.81 (s, 1H). ^{13}C NMR (75MHz, CDCl$_3$) δ 40.5, 55.7, 103.0, 106.7, 110.4, 110.6, 112.8, 116.1, 118.3, 120.8, 124.8, 127.4, 128.2, 130.2, 135.1, 138.7, 140.3, 141.9, 151.5, 151.8, 155.9. MS (ESI) *m/z* [M$^+$] 378.0. HPLC: condition A1 t_R=4.313min P=100%, condition A2 t_R=3.518min P=98.5%.

N^1-(6-Chloro-2-methoxyacridin-9-yl)-N^4,N^4-dimethylbenzene-1,4-diamine (7): Purple red crystals. Yield 70%. ^{1}H NMR (300MHz, CDCl$_3$) δ 2.92 (s, 6H), 3.73 (s, 3H), 6.52 (s, 1H), 6.70 (d, *J*=8.9, 2H), 6.90 (d, *J*=8.9, 2H), 7.10 (s, 1H), 7.39 (dd, *J1*=2.0, *J2*=9.22, 1H), 7.91 (d, *J*=9.1, 1H), 8.01 (d, *J*=9.1, 1H), 8.11 (s, 1H). ^{13}C NMR (75MHz, CDCl$_3$) δ 41.1, 55.3, 99.9, 113.9, 117.3, 117.4, 119.4, 121.2, 124.7, 125.0, 127.8, 130.8, 130.9, 134.9, 144.0, 146.8, 147.2, 147.9, 156.0. MS (ESI) *m/z* [M$^+$] 377.7. HPLC: condition B2 t_R=1.516min P=99.6%, condition B5 t_R=1.504min P=99.3%.

N^1-(6-Chloro-2-methoxyacridin-9-yl)-N^3,N^3-diethylbenzene-1,3-diamine hydrochloride (8): Orange solid. Yield 41%. ^{1}H NMR (300MHz, CDCl$_3$) δ 1.10 (t, *J*= 7.0, 6H) 3.38 (q, *J*=7.0, 4H) 3.67 (s, 3H) 6.63 (d, *J*=7.7, 1H) 6.69 (t, *J*=2.0, 1H) 6.79 (dd, *J1*=2.3, *J2*=8.5, 1H) 7.33 (t, *J*=8.1, 1H) 7.41 (dd, *J1*=2.0, *J2*=9.4, 1H) 7.56 (d, *J*=2.5, 1H) 7.64 (dd, *J1*=2.6, *J2*=9.3, 1H) 7.82 (d, *J*=9.3, 1H) 7.88 (d, *J*=1.9, 1H) 8.25 (d, *J*=9.4, 1H). MS (ESI) *m/z* [M$^+$] 406.3. Elemental analysis:

$C_{24}H_{24}N_3OCl.HCl.\frac{1}{4}H_2O$ found 64.56% C (calcd 64.50%), found 5.79% H (calcd 5.64%).

N^1-(6-Chloro-2-methoxyacridin-9-yl)-N^4,N^4-diethylbenzene-1,4-diamine hydrochloride (9): Orange solid. Yield 60%. ^{1}H NMR (300MHz, CDCl$_3$) δ 1.09 (t, *J*=6, 6H) 3.25 (q, *J*=6, 4H) 6.56 (d, *J*=9, 2H) 6.84 (d, *J*=9, 2H) 7.21-7.16 (m, 2H) 7.57 (t, *J*=9, 2H) 7.94 (t, *J*=9, 4H). MS (ESI) *m/z* [M$^+$] 406.3. Elemental analysis: $C_{24}H_{24}N_3OCl.HCl$ found 65.28% C (calcd 65.15%), found 5.81% H (calcd 5.66%).

6-Chloro-2-methoxy-*N*-(3-(pyrrolidin-1-yl)phenyl)acridin-9-amine (10): Orange solid. Yield 70%. ^{1}H NMR (300MHz, CDCl$_3$) δ 1.99 (t, 4H), 3.28 (t, 4H), 3.77 (s, 3H), 6.41 (d, *J*=7.4, 1H), 6.56 (d, *J*=7.7, 1H), 6.79 (s, 1H), 6.97 (d, *J*=9.1, 1H), 7.05 (d, *J*=9.0, 1H), 7.14 (t, *J*=8.0, 1H), 7.35 (s, 1H), 7.87 (d, *J*=9.4, 1H), 7.97 (d, *J*=9.3, 1H), 8.12 (s, 1H). ^{13}C NMR (75MHz, DMSO-d6) δ 24.8, 47.2, 55.3, 102.8, 103.1, 106.6, 106.8, 115.9, 118.7, 123.1, 125.1, 127.6, 129.7 (2C), 135.3, 141.0, 144.2, 146.4, 147.2, 148.7 (2C), 155.1. MS (ESI) *m/z* [M$^+$] 404.1. HPLC: condition A1 t_R=4.275min P=100%, condition A2 t_R=3.503min P=100%.

6-Chloro-2-methoxy-*N*-(3-(piperidin-1-yl)phenyl)acridin-9-amine (11): Orange solid. Yield 70%. ^{1}H NMR (300MHz, CDCl$_3$) δ 1.59 (m, 2H) 1.68 (m, 4H), 3.19 (t, 4H), 3.76 (s, 3H), 6.79 (dd, *J1*=8.7, *J2*=11.9, 2H), 7.03 (dd, *J1*=9.2, *J2*=17.9, 2H), 7.11 (s, 1H), 7.19 (s, 1H), 7.21 (s, 1H), 7.84 (d, *J*=9.5, 1H), 7.96 (d,

J=9.1, 1H), 8.117 (s, 1H). MS (ESI) *m/z* [M$^+$] 418.1. HPLC: condition A1 t_R=3.568min P=100%, condition A2 t_R=3.628min P=100%.

6-Chloro-2-methoxy-*N*-(4-(piperidin-1-yl)phenyl)acridin-9-amine (12): Red solid. Yield 65%. ^{1}H NMR (300MHz, DMSO) δ 1.52 (b, 2H), 1.62 (b, 4H), 3.04 (b, 4H), 3.72 (s, 3H), 6.65 (s, 1H), 6.86 (b, 4H), 7.32 (d, J=8.7, 1H), 7.42 (s, 1H), 7.93 (d, J=8.8, 1H), 7.80 (s, 1H), 8.07 (d, J=8.5, 1H), 8.98 (s, 1H). ^{13}C NMR (75MHz, CDCl$_3$) δ 24.1, 25.9, 51.3, 55.3, 100.2, 117.3, 117.8, 119.4, 120.6, 124.9, 125.2, 125.4, 126.8, 129.8, 135.4, 136.7, 144.1, 145.6, 147.0, 148.4, 156.1. MS (APCI) *m/z* [M$^+$] 417.8. HPLC: condition B3 t_R=1.583min P=98.3%, condition B6 t_R=1.535min P=98.2%.

6-Chloro-2-methoxy-*N*-(3-morpholinophenyl)acridin-9-amine (13): Orange solid. Yield 83%. ^{1}H NMR (300MHz, CDCl$_3$) δ 3.04 (t, J=4.7, 4H), 3.77 – 3.79 (m, 7H), 6.32-6.41 (m, 2H), 6.52 (d, J=4.6, 1H), 7.14 (t, J=7.8, 2H), 7.31 (d, J=10.5, 1H), 7.45 (d, J=9.0, 1H), 7.98 (d, J=9.1, 1H), 8.08 (d, J=9.3, 1H), 8.18 (s, 1H). 13C NMR (75MHz, DMSO-d6) δ 49.5 (2C), 56.4, 67.1 (2C), 109.4, 109.8, 119.3, 121.7, 125.6, 126.3, 127.7, 128.6, 130.6, 132.1, 134.7, 144.3, 147.0, 147.9, 148.0, 148.8, 153.0, 153.1, 156.9. MS (ESI) *m/z* [M$^+$] 419.5. Elemental analysis: found 68.41% C (calcd 68.65%) found 5.11% H (calcd 5.28%) found 9.75% N (calcd 10.01%).

6-Chloro-2-methoxy-*N*-(4-morpholinophenyl)acridin-9-amine (14): Orange solid. Yield 69%. ^{1}H NMR (300MHz, CDCl$_3$) δ 3.10 (t, J=4.6, 4H), 3.48(s, 3H),

3.87 (t, *J*=4.5, 4H), 6.46 (s, 1H), 6.86 (b, 4H), 7.09 (s, 1H), 7.42 (d, *J*=8.0, 1H), 7.92 (d, *J*=9.3, 1H), 8.05 (d, *J*=7.8, 1H), 8.145 (s, 1H). MS (ESI) *m/z* [M$^+$] 420.1. HPLC: condition B1 t_R=1.381min P=98.9%, condition B4 t_R=1.521min P=96.5%.

6-Chloro-2-methoxy-*N*-(3-(4-methylpiperazin-1-yl)phenyl)acridin-9-amine

(15): Red solid. Yield 72%. ^{1}H NMR (300MHz, CDCl$_3$) *δ* 2.32 (s, 3H), 2.50 (t, *J*=4.4, 4H), 3.11 (t, *J*=4.5, 4H), 3.78 (s, 3H), 6.30 (d, *J*=7.6, 1H), 6.39 (s, 1H), 6.43 (s, 1H), 6.55 (d, *J*=8.3, 1H), 7.13 (d, *J*=5.8, 2H), 7.44 (d, *J*=10.3, 1H), 7.98 (d, *J*=8.9, 1H), 8.07 (d, *J*=9.0, 1H), 8.17 (s, 1H). MS (ESI) *m/z* [M$^+$] 433.4. HPLC: condition B2 t_R=1.404min P=98.2%, condition B7 t_R=1.578min P=99.1%.

6-Chloro-2-methoxy-*N*-(4-(4-methylpiperazin-1-yl)phenyl)acridin-9-amine

(16): Red solid. Yield 65%. ^{1}H NMR (300MHz, DMSO) *δ* 2.33 (s, 3H), 2.56 (t, *J*=4.8, 4H), 3.12 (t, *J*=4.6, 4H), 3.66 (s, 3H), 6.82 (b, 4H), 7.08 (s, 1H), 7.15 (d, *J*=9.1, 1H), 7.32 (d, *J*=9.4, 1H), 7.85 (d, *J*=9.2, 1H), 7.94 (d, *J*=9.0, 1H), 8.02 (s, 1H). ^{13}C NMR (75MHz, CDCl$_3$) *δ* 46.0, 49.6, 55.0, 55.4, 100.5, 116.9, 117.3, 119.2, 120.7, 125.1, 125.2, 125.6, 125.9, 126.0, 128.9, 135.8, 136.9, 144.7, 146.2, 147.4, 156.0. MS (ESI) *m/z* [M$^+$] 431.9. HPLC: condition B3 t_R=1.738min P=100%, condition B6 t_R=1.265min P=98.3%.

6-Chloro-*N*-(4-(4-ethylpiperazin-1-yl)phenyl)-2-methoxyacridin-9-amine

(17): Orange solid. Yield 68%. ^{1}H NMR (300MHz, CDCl$_3$) *δ* 1.14 (t, *J*=7.2, 3H), 2.50 (q, *J*=7.2, 2H), 2.64 (m, 4H), 3.17 (m, 4H), 3.71 (s, 3H), 6.88 (m, 4H), 7.09 (d, *J*=2.4, 1H), 7.20 (dd, *J1*=1.7, *J2*=9.2, 1H), 7.36 (dd, *J1*=2.5, *J2*=9.4, 1H), 7.89

(d, *J*=9.2, 1H), 7.98 (d, *J*=9.4, 1H), 8.07 (s, 1H). MS (ESI) *m/z* [M$^+$] 447.5. HPLC: condition A1 t_R=3.625min P=97.6%, condition A2 t_R=3.581min P=98.0%.

3-(4-(4-(6-Chloro-2-methoxyacridin-9-ylamino)phenyl)piperazin-1-yl)propan-1-ol (18): Brown solid. Yield 40%. ^{1}H NMR (300MHz, CDCl$_3$) *δ* 1.77 (m, 2H), 2.70 (m, 6H), 3.13 (m, 4H), 3.74 (s, 3H), 3.85 (t, *J*=15.9, 2H), 6.84 (m, 4H), 7.08 (d, *J*=7.7, 1H), 7.28 (s, 1H), 7.40 (dd, *J1*=7.7, *J2*=21.6, 1H), 7.90 (d, *J*=9.25, 1H), 8.00 (d, *J*=9.41, 1H), 8.10 (s, 1H). MS (ESI) *m/z* [M$^+$] 477.2. HPLC: condition A1 t_R=3.412min P=98.3%, condition A2 t_R=3.267min P=96.5%.

1-(4-(4-(6-Chloro-2-methoxyacridin-9-ylamino)phenyl)piperazin-1-yl)ethanone (19): Brown solid. Yield 83%. ^{1}H NMR (300MHz, CDCl$_3$) *δ* 2.14 (s, 3H), 3.08 (m, 4H), 3.62 (t, 2H), 3.75 (s, 3H), 3.77 (t, 2H), 6.49 (b, 1H), 6.86 (m, 4H), 7.10 (s, 1H), 7.41 (dd, *J1*=1.56, *J2*=9.15, 1H), 7.92 (d, *J*=9.37, 1H), 8.03 (m, 1H), 8.15 (s, 1H). MS (ESI) *m/z* [M$^+$] 461.2. HPLC: condition A1 t_R=3.168min P=99.7%, condition A2 t_R=3.248min P=98.7%.

(4-(4-(6-Chloro-2-methoxyacridin-9-ylamino)phenyl)piperazin-1-yl)(cyclohexyl)methanone (20): Red solid. Yield 87%. ^{1}H NMR (300MHz, CDCl$_3$) *δ* 1.28 (m, 2H), 1.54 (m, 2H), 1.72 (s, 2H), 1.80 (m, 4H), 2.49 (m, 1H) 3.08 (m, 4H), 3.66 (m, 2H), 3.73 (s, 3H), 3.76 (m, 2H), 6.87 (m, 4H), 7.10 (d, *J*=2.5, 1H), 7.22 (dd, *J1*=1.8, *J2*=9.3, 1H), 7.37 (dd, *J1*=2.6, *J2*=9.4, 1H), 7.89 (d, *J*=9.3, 1H) 8.00 (d, *J*=9.4, 1H), 8.09 (s, 1H). MS (ESI) *m/z* [M$^+$] 529.3. HPLC: condition A1 t_R=3.524min P=98.5%, condition A2 t_R=3.489min P=97.6%.

(4-(4-(6-Chloro-2-methoxyacridin-9-ylamino)phenyl)piperazin-1-yl)(phenyl)methanone (21): Red solid. Yield 80%. ^{1}H NMR (300MHz, CDCl$_3$) δ 3.12 (m, 4H), 3.62 (m, 2H), 3.74 (s, 3H), 3.92 (m, 2H), 6.88 (t, J=6.5, 4H), 7.12 (s, 1H), 7.20 (dd, $J1$=1.5, $J2$=9.3, 1H), 7.26 (s, 1H), 7.34 (dd, $J1$=2.4, $J2$=9.4, 1H), 7.43 (s, 4H), 7.88 (d, J=9.3, 1H), 7.99 (d, J=9.4, 1H), 8.09 (s, 1H). MS (ESI) m/z [M$^+$] 523.5. HPLC: condition A1 t_R=3.381min P=97.5%, condition A2 t_R=3.269min P=97.1%.

6-Chloro-2-methoxy-*N*-(4-((4-methylpiperazin-1-yl)methyl)phenyl)acridin-9-amine (22): Yellow solid. Yield 74%. ^{1}H NMR (300MHz, CDCl$_3$) δ 2.29 (s, 3H), 2.47 (b, 8H), 3.45 (s, 2H), 3.75 (s, 3H) 6.44 (s, 1H), 6.76 (d, J=8.2, 2H), 7.09 (s, 1H), 7.18 (d, J=8.4, 1H), 7.45 (dd, $J1$=2.0, $J2$=9.1, 2H), 7.97 (d, J=9.5, 1H), 8.09 (d, J=9.4, 1H), 8.19 (s, 1H). MS (ESI) m/z [M$^+$] 447.2. HPLC: condition A1 t_R=3.298min P=96.4%, condition A2 t_R=3.187min P=97.4%.

(4-(6-Chloro-2-methoxyacridin-9-ylamino)phenyl)(4-methylpiperazin-1-yl)methanone (23): Yellow solid. Yield 65%. ^{1}H NMR (300MHz, CDCl$_3$) δ 2.30 (s, 3H), 2.39 (t, 4H), 3.63 (t, 4H), 3.74 (s, 3H), 6.69 (d, J=8.3, 2H), 7.11 (d, J=1.7, 1H), 7.27 (m, 3H), 7.39 (dd, $J1$=2.0, $J2$=9.4, 1H), 7.89 (d, J=9.2, 1H), 7.99 (d, J=9.2, 1H), 8.08 (s, 1H). ^{13}C NMR (75MHz, DMSO-d6) δ 46.6, 55.6, 56.4, 101.5, 116.5, 120.4, 122.7, 126.6, 127.3, 127.8, 128.8, 129.8, 130.1, 132.4, 134.9, 142.9, 147.8, 148.2, 148.8, 157.4, 170.1. MS (ESI) m/z [M$^+$] 461.5. HPLC: condition A1 t_R=3.147min P=98.4%, condition A2 t_R=3.168min P=98.5%.

6-Chloro-2-methoxy-*N*-(4-((piperidin-1-yl)methyl)phenyl)acridin-9-amine

(24): Orange solid. Yield 90%. ^{1}H NMR (300MHz, CDCl$_3$) δ 1.41 (m, 2H), 1.57 (m, 4H), 2.36 (m, 4H), 3.41 (s, 2H), 3.68 (s, 3H), 6.74 (d, *J*=8.1, 2H), 7.05 (s, 1H), 7.17 (d, *J*=8.1, 2H), 7.24 (m, 1H), 7.36 (d, *J*=9.4, 1H), 7.90 (d, *J*=9.1, 1H), 8.08 (s, 1H). ^{13}C NMR (75MHz, CDCl$_3$) δ 24.3, 25.8, 54.3, 55.2, 63.2, 99.9, 117.0, 119.3, 121.3, 124.8, 125.4, 125.8, 130.4, 130.6, 131.1, 135.0, 142.1, 142.2, 144.0, 147.8, 156.4. MS (ESI) *m/z* [M$^+$] 432.3. HPLC: condition A1 t$_R$=3.647min P=97.2%, condition A2 t$_R$=3.589min P=97.0%.

6-Chloro-2-methoxy-N-phenylacridin-9-amine (25): Yellow solid. Yield 96%. ^{1}H NMR (300MHz, CDCl$_3$) δ 3.72 (s, 3H), 6.80 (d, *J*=7.9, 2H), 6.95 (t, *J*=7.3, 1H), 7.07 (d, *J*=1.9, 1H), 7.21 (s, 1H), 7.24 (s, 1H), 7.38 (dd, *J1*=2.3, *J2*=9.4, 1H), 7.91 (d, *J*=9.2, 1H), 8.01 (d, *J*=9.4, 1H), 8.10 (s, 1H). ^{13}C NMR (75MHz, CDCl$_3$) δ 55.4, 99.9, 117.1, 119.4, 121.4, 121.5, 124.8, 125.6, 126.0, 127.6, 129.4, 130.7, 135.2, 142.0, 145.0, 146.7, 147.6, 156.7. MS (APCI) *m/z* [M$^+$] 335.2. Elemental analysis: found 71.70% C (calcd 71.75%), found 4.34% H (calcd 4.15%), found 8.13% N, (calcd 8.37%).

4-(6-Chloro-2-methoxy-acridin-9-ylamino)-benzonitrile (26): Orange solid. Yield 96%. ^{1}H NMR (300MHz, CDCl$_3$) δ 3.81 (s, 3H), 6.75 (d, *J*=8.4, 2H), 7.07 (d, *J*=2.2, 1H), 7.38 (d, *J*=9.2, 1H), 7.45 (d, *J*=10.0, 1H), 7.50 (d, *J*=8.6, 2H), 7.91 (d, *J*=9.2, 1H), 8.06 (d, *J*=6.8, 1H), 8.17 (s, 1H). ^{13}C NMR (75MHz, dmso-d$_6$) δ 56.0, 100.4, 100.6, 115.7, 120.2, 120.7, 123.0, 126.3, 126.4, 126.9, 128.4, 131.9,

134.1, 134.5, 140.7, 147.7, 148.1, 150.2, 157.4. MS (APCI) *m/z* [M$^+$] 361.5. HPLC: condition A1 t_R=3.487min P=98.7%, condition A2 t_R=3.385min P=98.5%.

(3-Chloro-acridin-9-yl)-(4-fluoro-phenyl)-amine (27): Yellow solid. Yield 92%. ^{1}H NMR (300MHz, CDCl$_3$) δ 3.69 (s, 3H), 6.76 (dd, *J1*=4.5, *J2*=8.8, 2H), 6.93 (t, *J*=8.6, 2H), 7.01 (d, *J*=1.5, 1H), 7.21 (d, *J*=9.1, 1H), 7.34 (dd, *J1*=1.8, *J2*=9.2, 1H), 7.83 (d, *J*=9.2, 1H), 7.94 (d, *J*=9.2, 1H), 8.02 (s, 1H). ^{13}C NMR (75MHz, CDCl$_3$) δ 55.3, 100.0, 115.9, 116.2, 118.9, 121.0, 124.7, 125.4, 125.7, 127.2, 130.3, 135.2, 141.4, 142.6, 146.2, 147.3, 156.5, 159.6. MS (APCI) *m/z* [M+H$^+$] 354.4. Elemental analysis found 68.10% C (calcd 68.09%), found 3.90% H (calcd 4.00), found 7.60% N (calcd 7.94%).

6-Chloro-N-(3,4-difluorophenyl)-2-methoxyacridin-9-amine (28): Yellow solid. Yield 88%. ^{1}H NMR (300MHz, CDCl$_3$) δ 3.84 (s, 3H), 7.09 (dd, *J1*=2.8, *J2*=9.0, 2H), 7.24 (m, 4H), 7.74 (d, *J*=9.4, 1H), 7.97 (d, *J*=9.3, 1H), 8.18 (s, 1H). ^{13}C NMR (75MHz, dmso-d$_6$) δ 55.5, 103.2, 103.3, 109.6, 114.9, 115.0, 116.8, 118.0, 118.2, 123.7, 126.2, 127.6, 136.6, 142.3, 142.4, 148.0, 148.2, 151.3, 151.4, 155.5. MS (ESI) *m/z* [M$^+$] 372.2. HPLC: condition A1 t_R=3.487min P=97.4%, condition A2 t_R=3.456min P=97.8%.

(6-Chloro-2-methoxy-acridin-9-yl)-(4-methoxy-phenyl)-amine (29): Orange solid. Yield 88%. ^{1}H NMR (300MHz, CDCl$_3$) δ 3.72 (s, 3H), 3.78 (s, 3H), 6.83 (m, 4H), 7.07 (s, 1H), 7.25 (d, *J*=9.4, 1H), 7.39 (dd, *J1*=2.1, *J2*=9.4Hz, 1H), 7.89 (d, *J*=9.2, 1H), 8.00 (d, *J*=7.7, 1H), 8.10 (s, 1H). ^{13}C NMR (75MHz, CDCl$_3$) δ

55.3, 55.6, 99.6, 99.7, 114.7, 118.2, 120.0, 120.3, 124.5, 125.3, 125.5, 128.1, 131.4, 134.9, 138.1, 142.9, 148.1, 155.1, 156.3. MS (APCI) *m/z* [M$^+$] 365.7. Elemental analysis: found 69.13% C (calcd 69.14%), found 4.35% H (calcd 4.70%), found 7.35% N (calcd 7.68%).

3-(6-Chloro-2-methoxyacridin-9-ylamino)phenol (30): Yellow solid. Yield 96%. ^{1}H NMR (300MHz, CDCl$_3$) δ 3.73 (s, 3H), 6.29 (t, *J*=1.9, 1H), 6.41 (dd, *J1*=1.9, *J2*=8.1, 2H), 7.30 (d, *J*=9.3, 1H), 7.34 (d, *J*=2.3, 1H), 7.42 (dd, *J1*=2.4, *J2*=9.4, 1H), 7.89 (d, *J*=9.3, 1H), 7.95 (s, 1H), 8.11 (d, *J*=9.2, 1H). MS (ESI) *m/z* [M+H$^+$] 352.4. Elemental analysis: found 68.64% C (calcd 68.48), found 4.05% H (calcd 4.31%), found 7.67% N (calcd 7.99%).

4-(6-Chloro-2-methoxyacridin-9-ylamino)benzene-1,2-diol (31): Yellow solid. Yield 46%. ^{1}H NMR (300MHz, MeOD) δ 3.70 (s, 3H), 6.78 (dd, *J1*=2.3, *J2*=8.4, 1H), 6.87 (d, *J*=2.3, 1H), 7.48 (d, *J*=8.7, 2H), 7.58 (dd, *J1*=2.2, *J2*=9.2, 2H), 7.83 (s, 1H), 8.12 (d, *J*=9.3, 1H). ^{13}C NMR (75MHz, MeOD) δ 55.9, 103.0, 110.7, 114.4, 117.0, 119.2, 125.0, 125.1, 127.0, 127.6, 128.2, 128.3, 137.5, 138.0, 143.6, 145.2, 147.4, 157.1. MS (ESI) *m/z* [M$^+$] 368.5. HPLC: condition A1 t_R=3.248min P=96.5%, condition A2 t_R=3.149min P=96.2%.

Group 3

N-(1-Benzylpiperidin-4-yl)-6-chloro-2-methoxyacridin-9-amine (32): Yellow solid. Yield 48%. ^{1}H NMR (300MHz, CDCl$_3$) δ 1.74 (d, *J*=9.4, 2H), 2.05 (t, *J*=9.4, 4H), 2.90 (d, *J*=11.7, 2H), 3.51 (s, 2H), 3.70 (b, 1H), 3.96 (s, 3H), 4.34 (b,

1H), 7.19 (s, 1H), 7.30 (s, 4H), 7.37 (d, *J*=1.96, 1H), 7.44 (dd, *J1*=2.60, *J2*=9.41, 1H), 8.01 (t, *J*=9.47, 2H), 8.10 (d, *J*=1.83, 1H). ^{13}C NMR (75MHz, CDCl$_3$) δ 34.1, 52.4, 55.5, 57.4, 62.9, 99.2, 117.2, 119.3, 124.1, 125.1, 125.2, 127.3, 127.6, 128.3, 129.1, 130.8, 135.3, 137.8, 147.4, 149.1, 149.2, 156.4. MS (APCI) *m/z* [M$^+$] 432.4. HPLC: condition B2 t_R=1.337min P=99.4%, condition B5 t_R=1.278min P=98.2%.

N-(1-(4-Methylbenzyl)piperidin-4-yl)-6-chloro-2-methoxyacridin-9-amine dihydrochloride (33): Yellow solid. Yield 51%. ^{1}H NMR (300MHz, CDCl$_3$) δ 1.77 (d, *J*=11.20, 2H), 2.05 (t, *J*=10.6, 4H), 2.33 (s, 3H), 2.90 (d, *J*=11.2, 2H), 3.48 (s, 2H), 3.71 (b, 1H), 3.95 (s, 3H), 7.12 (d, *J*=7.9, 2H), 7.18 (m, 3H), 7.31 (dd, *J1*=1.9, *J2*=9.2, 1H), 7.39 (dd, *J1*=2.1, *J2*=9.6, 1H), 7.98 (m, 2H), 8.08 (d, *J*=1.89, 1H). ^{13}C NMR (75MHz, CDCl$_3$) δ 21.1, 34.1, 52.3, 55.5, 57.4, 62.6, 99.0, 117.3, 119.5, 123.9, 124.9, 125.2, 127.7, 128.9, 129.1, 130.9, 134.7, 135.0, 136.8, 146.2, 147.6, 148.9, 156.3. MS (ESI) *m/z* [M$^+$] 446.6. HPLC: condition A1 t_R=3.542min P=97.5%, condition A2 t_R=3.425min P=96.9%.

***N*-(1-(4-Chlorobenzyl)piperidin-4-yl)-6-chloro-2-methoxyacridin-9-amine dihydrochloride (34):** Yellow solid. Yield 56%. ^{1}H NMR (300MHz, CDCl$_3$) δ 1.80 (dd, *J1*=10.6, *J2*=21.1, 2H), 2.04 (t, *J*=10.4, 4H), 2.87 (d, *J*=11.4, 2H), 3.45 (s, 2H), 3.72 (b, 1H), 3.95 (s, 3H), 7.17-7.28 (m, 5H), 7.30 (d, *J*=1.9, 1H), 7.37 (dd, *J1*=2.4, *J2*=9.38, 1H), 7.96 (t, *J*=9.6, 2H), 8.06 (d, *J*=1.8, 1H). ^{13}C NMR (75MHz, CDCl$_3$) δ 34.1, 52.3, 55.5, 57.3, 62.0, 99.2, 116.9, 119.2, 124.0, 125.0, 125.1, 127.2, 128.3, 130.3, 130.4, 132.8, 135.3, 136.6, 145.5, 147.1, 149.2, 156.3.

MS (ESI) *m/z* [M$^+$] 465.5. HPLC: condition A1 t_R=3.426min P=97.2%, condition A2 t_R=3.412min P=96.4%.

N-(1-(4-Methoxybenzyl)piperidin-4-yl)-6-chloro-2-methoxyacridin-9-amine dihydrochloride (35): Yellow solid. Yield 57%. ^{1}H NMR (300MHz, CDCl$_3$) δ 1.75 (m, 2H), 2.04 (m, 4H), 2.88 (d, *J*=11.2, 2H), 3.45 (s, 2H), 3.71 (b, 1H), 3.80 (s, 3H), 3.96 (s, 3H), 6.85 (d, J=8.3, 2H), 7.20 (d, *J*=8.4, 2H), 7.26 (s, 1H), 7.34 (dd, *J1*=0.7, *J2*=9.2, 1H), 7.43 (dd, *J1*=1.6, *J2*=9.4, 1H), 8.00 (m, 2H), 8.09 (s, 1H). ^{13}C NMR (75MHz, CDCl$_3$) δ 34.1, 52.1, 55.1, 55.3, 57.3, 62.2, 98.8, 113.5, 117.6, 119.6, 123.8, 124.7, 125.0, 128.2, 129.9, 130.1, 131.4, 134.6, 146.7, 147.9, 148.5, 156.2, 158.6. MS (ESI) *m/z* [M$^+$] 461.8. HPLC: condition A1 t_R=3.268min P=98.6%, condition A2 t_R=3.197min P=98.2%.

4-((4-(6-Chloro-2-methoxyacridin-9-ylamino)piperidin-1-yl)methyl)benzonitrile dihydrochloride (36): Yellow solid. Yield 40%. ^{1}H NMR (300MHz, CDCl$_3$) δ 1.74 (dd, *J1*=10.5, *J2*=20.9, 2H), 2.06 (dd, *J1*=9.1, *J2*=18.2, 4H), 2.85 (d, *J*=11.6, 2H), 3.54(s, 2H), 3.70(b, 1H), 3.97 (s, 3H), 7.19 (d, *J*=2.3, 1H), 7.35 (dd, *J1*=1.7, *J2*=9.25, 1H), 7.44 (m, 3H), 7.61(d, *J*=8.1, 2H), 8.00 (m, 2H), 8.09 (d, *J*=1.6, 1H). ^{13}C NMR (75MHz, CDCl$_3$) δ 34.3, 52.6, 55.4, 57.3, 62.3, 98.9, 110.9, 117.8, 118.9, 119. 9, 123.7, 124.8, 125.4, 128.4, 129.3, 131.6, 132.1, 134.8, 144.2, 146.9, 148.1, 148.5, 156.4. MS (ESI) *m/z* [M$^+$] 457.4. HPLC: condition A1 t_R=3.184min P=95.6%, condition A2 t_R=3.082min P=95.2%.

6-Chloro-2-methoxy-*N*-(1-phenethylpiperidin-4-yl)acridin-9-amine

dihyrochloride (37): Yellow solid. Yield 57%. ^{1}H NMR (300MHz, CDCl$_3$) δ 1.79 (m, 2H), 2.09 (m, 4H), 2.61 (t, 2H), 2.81 (t, 2H), 3.02 (d, *J*=11.57, 2H), 3.73 (b, 1H), 3.97 (s, 3H), 7.20 (m, 3H), 7.27 (d, *J*=6.5, 2H), 7.35 (d, *J*=9.2, 1H), 8.01 (t, *J*=9.1, 2H), 8.10 (s, 1H). ^{13}C NMR (75MHz, CDCl$_3$) δ 33.6, 34.0, 52.4, 55.2, 57.1, 60.1, 99.68, 117.6, 119.6, 123.7, 124.6, 125.0, 125.9, 128.1, 128.2, 128.4, 131.3, 134.5, 139.9, 146.7, 147.8, 148.4, 156.1. MS (ESI) *m/z* [M^{+}] 445.2. HPLC: condition A1 t_R=3.185min P=96.8%, condition A2 t_R=3.087min P=97.0%.

6-Chloro-2-methoxy-*N*-(1-(4-methylphenethyl)piperidin-4-yl)acridin-9-amine

dihyrochloride (38): Yellow solid. Yield 67%. ^{1}H NMR (300MHz, CDCl$_3$) δ 1.80 (d, *J*=9.2, 2H), 2.03 (m, 4H), 2.30 (s, 3H), 2.57 (d, *J*=8.2, 2H), 2.73 (d, *J*=7.8, 2H), 2.98 (d, *J*=10.4, 2H), 3.66 (d, *J*=9.1, 2H), 3.93 (s, 3H), 7.07 (s, 4H), 7.16 (s, 1H), 7.30 (d, *J*=9.1, 1H), 7.40 (d, *J*=9.1, 1H), 7.97 (dd, *J1*=9.2, *J2*=16.3, 2H), 8.08 (s, 1H). ^{13}C NMR (75MHz, CDCl$_3$) δ 20.9, 33.1, 33.9, 52.5, 57.3, 60.3, 98.9, 117.6, 119.7, 123.9, 124.8, 125.1, 127.9, 128.4, 129.0, 131.2, 134.8, 135.5, 136.8, 146.6, 147.8, 148.8, 156.3. MS (ESI) *m/z* [M^{+}] 460.3. HPLC: condition A1 t_R=3.562min P=96.0%, condition A2 t_R=3.485min P=96.5%.

N-(1-(4-Chlorophenethyl)piperidin-4-yl)-6-chloro-2-methoxyacridin-9-amine

dihydrochloride (39): Yellow solid. Yield 92%. ^{1}H NMR (300MHz, CDCl$_3$) δ 1.73 (m, 2H), 2.05 (m, 4H), 2.54 (m, 2H), 2.73 (m, 2H), 2.95 (d, *J*=10.3, 2H), 3.66 (b, 1H), 3.94 (s, 3H), 7.08 (d, *J*=7.9, 2H), 7.14 (s, 1H), 7.22 (d, *J*=8.0, 2H), 7.30 (d, *J*=9.4, 1H), 7.40 (d, *J*=9.2, 1H), 7.97 (dd, *J1*=9.3, *J2*=19.1, 2H), 8.08 (s,

1H). ^{13}C NMR (75MHz, CDCl$_3$) δ 33.0, 34.1, 52.5, 55.4, 57.2, 59.9, 98.8, 117.6, 119.7, 123.8, 124.8, 125.2, 128.0, 128.4, 129.8, 131.2, 131.7, 134.7, 138.5, 146.7, 147.9, 148.6, 156.3. MS (ESI) *m/z* [M$^+$] 480.4. HPLC: condition A1 t_R=3.587min P=97.0%, condition A2 t_R=3.455min P=96.4%.

N-(1-(4-Methoxyphenethyl)piperidin-4-yl)-6-chloro-2-methoxyacridin-9-amine dihydrochloride (40): Yellow solid. Yield 90%. ^{1}H NMR (300MHz, CDCl$_3$) δ 1.66 (m, 2H), 1.99 (m, 4H), 2.48 (m, 2H), 2.64 (m, 2H), 2.88 (m, 2H), 3.79 (b, 4H), 3.87 (s, 3H), 6.75 (m, 2H), 7.02 (m, 3H), 7.22 (d, 1H), 7.34 (d, 1H) , 7.91 (m, 2H), 8.05 (s, 1H). ^{13}C NMR (75MHz, CDCl$_3$) δ 32.6, 33.9, 52.2, 54.9, 55.0, 57.0, 60.2, 98.6, 113.5, 117.4, 119.5, 123.6, 124.5, 124.8, 128.0, 129.2, 131.2, 131.8, 134.3, 146.6, 147.7, 148.2, 156.0, 157.6. MS (ESI) *m/z* [M+H$^+$] 477.8. HPLC: condition A1 t_R=3.333min P=95.7%, condition A2 t_R=3.255min P=95.0%.

6-Chloro-2-methoxy-*N*-(1-(3-phenylpropyl)piperidin-4-yl)acridin-9-amine dihyrochloride (41): Yellow solid. Yield 89%. ^{1}H NMR (300MHz, CDCl$_3$) δ 1.80 (m, 4H), 1.95 (m, 4H), 2.31 (t, 2H), 2.57 (t, *J*=7.6, 2H), 2.86 (d, *J*=11.5, 2H), 3.64 (b, 1H), 3.89 (s, 3H), 7.12 (m, 4H), 7.24 (m, 3H), 7.36 (dd, *J1*=2.1, *J2*=9.4, 1H), 7.87 (d, *J*=9.3, 1H), 7.96 (d, *J*=9.4, 1H), 8.06 (s, 1H). ^{13}C NMR (75MHz, CDCl$_3$) δ 28.5, 33.4, 33.8, 52.3, 55.1, 57.1, 57.5, 98.7, 117.3, 119.4, 123.8, 124.6, 124.8, 125.5, 127.7, 128.0, 128.1, 130.9, 134.5, 141.7, 146.4, 147.6, 148.6, 156.0. MS (ESI) *m/z* [M$^+$] 460.2. HPLC: condition A1 t_R=3.358min P=96.4%, condition A2 t_R=3.322min P=96.0%.

6-Chloro-2-methoxy-*N*-(4-(4-methylpiperazin-1-yl)but-2-ynyl)acridin-9-amine (42): Brown solid. Yield 60%. ^{1}H NMR (300MHz, CDCl$_3$) δ 2.28 (m, 4H), 2.49 (m, 7H), 3.24 (s, 2H), 3.96 (s, 3H), 4.53 (s, 2H), 7.26 (m, 2H), 7.43 (d, *J*=2.1, 1H), 7.81 (d, *J*=9.3, 1H), 7.95 (s, 1H), 8.19 (d, *J*=9.3, 1H). ^{13}C NMR (75MHz, CDCl$_3$) δ 38.8, 45.7, 47.0, 51.7, 54.6, 55.8, 80.9, 81.0, 100.6, 108.6, 114.0, 116.8,120.3, 124.6, 125.4, 125.7, 126.6, 137.0, 144.4, 151.0, 156.1. MS (APCI) *m/z* [M$^+$] 409.3. HPLC: condition A1 t_R=3.022min P=96.8%, condition A2 t_R=2.85min P=95.6%.

N-(8-Benzyl-8-aza-bicyclo[3.2.1]octan-3-yl)-6-chloro-2-methoxyacridin-9-amine (43): Yellow solid. Yield 45%. ^{1}H NMR (300MHz, CDCl$_3$) δ 1.77 (m, 2H), 1.94 (t, J=11.2, 2H), 2.31 (t, *J*=6.9, 2H), 2.57 (t, *J*=7.6, 3H), 2.86 (d, *J*=11.5, 2H), 3.64 (m, 1H), 3.89 (s, 3H), 4.44 (s, 2H), 7.11 (d, *J*=6.3, 3H), 7.23 (d, *J*=8.3, 3H), 7.36 (dd, *J1*=2.1, *J2*=9.4, 1H), 7.87 (d, *J*=9.3, 1H), 7.96 (d, *J*=9.4, 1H), 8.06 (s, 1H). ^{13}C NMR (75MHz, CDCl$_3$) δ 28.5, 33.4, 33.8, 52.3, 55.1, 57.5, 98.7, 117.3, 119.4, 123.8, 124.6, 124.8, 125.5, 127.7, 128.0, 128.1, 130.9, 134.5, 141.7, 146.4, 147.6, 148.6, 156.0. MS (APCI) *m/z* [M$^+$] 458.5. HPLC: condition A1 t_R=3.871min P=97.5%, condition A2 t_R=3.758min P=97.2%.

6-Chloro-2-methoxy-9-phenoxyacridine (44): Light yellow solid. Yield 98%. ^{1}H NMR (300MHz, CDCl$_3$) δ 3.80 (s, 3H), 6.86 (d, *J*=8.4, 2H), 7.07 (t, *J*=7.3, 1H), 7.16 (s, 1H), 7.30 (t, *J*=7.7, 2H), 7.37 (d, *J*=9.2, 1H), 7.48 (d, *J*=9.5, 1H),

7.98 (d, *J*=9.3, 1H), 8.16 (d, *J*=9.4, 1H), 8.26 (s, 1H). MS (APCI) *m/z* [M$^+$] 335.6.

HPLC: condition A1 t_R=3.455min P=96.8%, condition A2 t_R=3.42min P=95.8%.

6-Chloro-2-methoxy-N-methyl-N-phenylacridin-9-amine (45): Yellow solid.

Yield 86%. ^{1}H NMR (300MHz, CDCl$_3$) *δ* 3.52 (s, 3H), 3.77 (s, 3H), 6.56 (d,

J=7.2, 2H), 6.78 (t, *J*=7.3, 1H), 7.01 (d, *J*=2.6, 1H), 7.18 (t, *J*=7.8, 2H), 7.35 (dd,

J1=1.8, *J2*=9.2, 1H), 7.46 (dd, *J1*=2.7, *J2*=9.4, 1H), 7.80 (d, *J*=9.2, 1H), 8.14 (d,

J=9.4, 1H), 8.25 (d, *J*=1.7, 1H). ^{13}C NMR (75MHz, CDCl$_3$) *δ* 39.2, 55.5, 99.3,

112.8, 118.1, 123.3, 125.3, 125.8, 126.1, 127.6, 128.6, 129.4, 131.7, 135.0, 147.8,

148.5, 148.8, 148.9, 157.9. MS (APCI) *m/z* [M+H$^+$] 349.5. Elemental analysis:

found 72.06% C (calcd 72.31%), found 4.58% H (calcd 4.91%), found 7.65% N

(calcd 8.03%).

6-Chloro-2-methoxyacridin-9-amine (46): Yellow solid. Yield 85%. ^{1}H

NMR (300 MHz, CD$_3$OD) d 8.71–7.20 (m, 6H), 3.96 (s, 3H). MS (ESI, MeOH)

m/z [M$^+$] 258.1. HPLC: condition A1 t_R=3.572min P=100%, condition A2

t_R=3.797min P=100%.

Group 5

N^1-(Acridin-9-yl)-N^4,N^4-diethylbenzene-1,4-diamine (48): Brownish red solid.

Yield 88%. ^{1}H NMR (300MHz, CDCl$_3$) *δ* 1.09 (t, *J*=6, 6H), 3.25 (q, *J*=6, 4H),

6.56 (d, *J*=9, 2H), 6.84 (d, *J*=9, 2H), 7.21-7.16 (m, 2H), 7.57 (t, *J*=9, 2H), 7.94 (t,

J=9, 4H). MS (ESI) m/z [M$^+$] 341.2. HPLC: condition B3 t_R=1.353min P=98.9%, condition B6 t_R=1.368min P=98.9%.

Group 6

3-Chloro-5,6,7,8-tetrahydroacridin-9-amine (49): Pale yellow solid. Yield 56%. ^{1}H NMR (300MHz, CDCl$_3$) δ 1.90 (m, 4H), 2.53 (t, *J*=5.3, 2H), 2.92 (t, *J*=5.3, 2H), 7.37 (dd, *J1*=1.5, J2=9.0, 1H), 7.62 (d, *J*=1.4, 1H), 8.13 (d, *J*=9.0, 1H). ^{13}C NMR (75MHz, CD$_3$OD) δ 22.2, 22.7, 23.8, 30.1, 111.2, 115.0, 120.3, 125.7, 126.9, 139.2, 140.6, 154.5, 155.9. MS (APCI) *m/z* [M+H$^+$] 234.2. HPLC: condition A1 t_R=3.255min P=97.5%, condition A2 t_R=3.147min P=96.8%.

N'-(6-Chloro-1,2,3,4-tetrahydro-acridin-9-yl)-N,N-diethyl-ethane-1,2-diamine (50): Orange solid. Yield 60%. ^{1}H NMR (300MHz, CDCl$_3$) δ 1.05 (t, *J*=7.1, 6H), 1.88 (t, *J*=5.5, 4H), 2.58 (q, *J*=7.1, 4H), 2.67 (t, *J*=5.6, 4H), 3.01 (m, 2H), 3.55 (dd, *J1*=5.2, *J2*=10.4, 2H), 5.52 (s, 1H), 7.19 (dd, *J1*=1.9, *J2*=9.1, 1H), 7.88 (d, *J*=1.9, 1H), 7.95 (d, *J*=9.1, 1H). ^{13}C NMR (75MHz, CDCl$_3$) δ 11.6, 22.4, 22.7, 24.4, 33.4, 45.4, 45.9, 52.3, 114.6, 117.7, 123.6, 124.7, 126.6, 133.8, 147.4, 151.1, 158.6. MS (APCI) *m/z* [M+H$^+$] 333.5. HPLC: condition A1 t_R=3.213min P=96.6%, condition A2 t_R=3.248min P=96.9%.

N-(1-Benzylpiperidin-4-yl)-6-chloro-1,2,3,4-tetrahydroacridin-9-amine (51): Orange solid. Yield 56%. ^{1}H NMR (300MHz, CDCl$_3$) δ 1.68 (m, 2H), 1.88 (m, 4H), 2.00 (d, *J*=12.4, 2H), 2.12 (t, *J*=11.4, 2H), 2.67 (m, 2H), 2.89 (d, *J*=11.8, 2H), 3.07 (m, 2H), 3.54 (s, 2H), 3.64 (m, 1H), 7.28 (d, *J*=2.3, 1H), 7.31 (m, 5H),

7.83 (d, *J*=9.0, 1H), 7.97 (d, *J*=1.8, 1H). ^{13}C NMR (75MHz, CDCl$_3$) δ 22.4, 22.7, 24.7, 33.7, 34.0, 52.2, 55.6, 62.8, 117.8, 119.2, 124.1, 124.8, 127.0, 127.1, 128.1, 129.0, 134.1, 137.8, 147.3, 149.9, 159.4. MS (APCI) *m/z* [M+H$^+$] 407.6. HPLC: condition A1 t$_R$=3.358min P=96.9%, condition A2 t$_R$=3.348min P=96.5%.

(6-Chloro-1,2,3,4-tetrahydro-acridin-9-yl)-phenyl-amine (52): Orange solid. Yield 80%. ^{1}H NMR (300MHz, CDCl$_3$) δ 1.82 (d, *J*=5.5, 2H), 1.90 (d, *J*=5.9, 2H), 2.68 (t, *J*=6.0, 2H), 3.09 (t, *J*=6.3, 2H), 6.66 (d, *J*=7.8, 2H), 6.90 (t, *J*=7.3, 2H), 7.17 (m, 2H), 7.64 (d, *J*=8.9, 1H), 7.94 (d, *J*=1.3, 1H). ^{13}C NMR (75MHz, CDCl$_3$) δ 22.5, 22.6, 25.1, 33.8, 116.7, 120.9, 121.1, 123.2, 124.9, 125.6, 127.4, 129.2, 134.3, 143.4, 144.1, 147.6, 161.1. MS (APCI) *m/z* [M$^+$] 309.7. HPLC: condition A1 t$_R$=3.422min P=97.8%, condition A2 t$_R$=3.456min P=98.2%.

N^1-(3-Chloro-5,6,7,8-tetrahydroacridin-9-yl)-N^4,N^4-diethylbenzene-1,4-diamine (53): Purple solid. Yield 45%. ^{1}H NMR (300MHz, CDCl$_3$) δ 1.14 (t, *J*=7.0, 6H), 1.89 (m, 4H), 2.63 (t, *J*=3.0, 2H), 3.10 (t, *J*=3.1, 2H), 3.31 (dd, *J1*=7.0, *J2*=14.0, 4H), 6.59 (d, *J*=8.9, 2H), 6.79 (d, *J*=8.8, 2H), 7.10 (dd, *J1*=1.9, *J2*=9.1, 1H), 7.62 (d, *J*=9.1, 1H), 7.99 (s, 1H). ^{13}C NMR (75MHz, CDCl$_3$) δ 12.5, 22.3, 22.6, 24.7, 33.1, 44.6, 113.0, 117.9, 118.6, 122.2, 124.8, 125.4, 126.1, 132.3, 134.7, 144.7, 146.5, 146.7, 159.2. MS (APCI) *m/z* [M+H$^+$] 381.6. HPLC: condition A1 t$_R$=3.585min P=96.4%, condition A2 t$_R$=3.523min P=96.0%.

(6-Chloro-1,2,3,4-tetrahydro-acridin-9-yl)-[4-(4-methyl-piperazin-1-yl)-phenyl]-amine (54): Gray solid. Yield 52%. ^{1}H NMR (300MHz, CDCl$_3$) δ 1.87

(m, 2H), 2.36 (s, 3H), 2.59 (m, 4H), 2.66 (t,2H) 3.08 (m, 2H), 3.14 (m, 2H), 3.63 (b, 2H), 6.64 (d, J=8.7, 1H), 6.73 (d, J=8.8, 1H), 6.81 (dd, $J1$=4.6, $J2$=8.6, 2H), 7.14 (dd, $J1$=1.7, $J2$=9.0, 1H), 7.62 9d, J=9.0, 1H), 7.95 (d, J=1.6, 1H). ^{13}C NMR (75MHz, CDCl$_3$) δ22.5, 25.0, 33.6, 45.9, 49.6, 50.6, 55.1, 116.1, 117.2, 118.6, 119.9, 120.3, 125.1, 127.0, 134.3, 136.7, 140.1, 144.3, 146.7, 160.3. MS (ESI) m/z [M+H$^+$] 408.4. HPLC: condition A1 t$_R$=3.856min P=97.5%, condition A2 t$_R$=3.725min P=98.6%.

Group 7

7-Chloroquinolin-4-amine (55): Red solid. Yield 67%. ^{1}H NMR (300MHz, DMSO-d$_6$) 6.59 (d, J=5.1, 1H), 7.41 (d, J=8.9, 1H), 7.70 (d, J=8.9, 1H), 7.96 (d, J=0.9, 1H), 8.52 (d, J=5.0, 1H). ^{13}C NMR (75MHz, DMSO-d$_6$) δ 104.0, 105.2, 121.6, 124.7, 125.7, 128.7, 129.0, 151.7, 152.1. MS (APCI) m/z [M+H$^+$] 179.03. HPLC: condition A1 t$_R$=2.544min P=98.6%, condition A2 t$_R$=2.444min P=97.6%.

N'-(7-Chloro-quinolin-4-yl)-N,N-diethyl-ethane-1,2-diamine (56): White solid. Yield 60%. ^{1}H NMR (300MHz, CDCl$_3$) δ 1.06 (t, J=7.1, 6H), 2.59 (dd, $J1$=7.0, $J2$=14.1, 4H), 2.79 (t, J=5.4, 2H), 3.24 (t, J=5.2, 2H), 6.32 (d, J=5.3, 2H), 7.32 (d, J=7.3, 1H), 7.71 (d, J=8.9, 1H), 7.93 (s, 1H), 8.48 (d, J=5.1, 1H). ^{13}C NMR (75MHz, CDCl$_3$) δ 11.7, 39.6, 46.3, 50.4, 99.0, 117.2, 121.3, 125.0, 128.1, 134.6, 148.6, 149.9, 151.6. MS (APCI) m/z [M+H$^+$] 279.3. Elemental analysis: found 64.93% C (calcd 64.85%), found 6.76% H (calcd 7.26%), found 14.22% N (calcd 15.23%).

(1-Benzyl-piperidin-4-yl)-(7-chloro-quinolin-4-yl)-amine (57): Red solid. Yield 53%. ^{1}H NMR (300MHz, CDCl$_3$) δ 1.62 (dd, $J1$=10.3, $J2$=20.3, 2H), 2.07 (d, J=11.9, 2H), 2.16 (t, J=11.4, 2H), 2.86 (d, J=11.7, 2H), 3.45 (m, 1H), 3.51 (s, 2H), 5.24 (d, J=6.6, 1H), 6.36 (d, J=5.5, 1H), 7.24 (m, 2H), 7.30 (m, 3H), 7.66 (d, J=9.0, 1H), 7.93 (d, J=1.9, 1H), 8.46 (d, J=5.4, 1H). ^{13}C NMR (75MHz, CDCl$_3$) δ 31.5, 49.6, 51.9, 62.8, 99.1, 117.0, 121.1, 124.9, 126.9, 128.0, 128.3, 128.9, 134.6, 137.9, 148.5, 149.0, 151.6. MS (APCI) *m/z* [M+H$^+$] 353.5. HPLC: condition A1 t_R=3.278min P=96.5%, condition A2 t_R=3.335min P=97.0%.

(7-Chloro-quinolin-4-yl)-phenyl-amine (58): White solid. Yield 73%. ^{1}H NMR (300MHz, CDCl$_3$) δ 6.96 (d, J=5.3, 1H), 7.22 (t, J=7.4, 1H), 7.30 (d, J=7.5, 2H), 7.43 (d, J=8.4, 2H), 7.47 (m, 1H), 7.89 (d, J=9.0, 1H), 8.04 (d, J=2.0, 1H), 8.54 (d, J=5.3, 1H). ^{13}C NMR (75MHz, CDCl3) δ 102.4, 118.0, 121.2, 122.9, 125.1, 126.2, 128.8, 129.8, 135.4, 139.3, 147.8, 149.4, 151.7. MS (APCI) *m/z* [M$^+$] 255.6. HPLC: condition A1 t_R=3.784min P=97.0%, condition A2 t_R=3.546min P=96.5%.

N^1-(7-Chloroquinolin-4-yl)-N^4,N^4-diethylbenzene-1,4-diamine (59): Yellow solid. Yield 96%. ^{1}H NMR (300MHz, CDCl$_3$) δ 1.20 (t, J=7.0, 6H), 3.39 (q, J=7.0, 4H), 6.62 (d, J=5.5, 1H), 6.73 (d, J=8.9, 2H), 7.14 (d, J=8.8, 2H), 7.43 (dd, $J1$=2.0, $J2$=9.0, 1H), 7.85 (d, J=8.9, 1H), 8.02 (d, J=2.0, 1H), 8.42 (d, J=5.3, 1H). ^{13}C NMR (75MHz, DMSO-d$_6$) δ 12.4, 43.7, 100.3, 112.2, 117.6, 124.2, 124.4, 126.2, 127.0, 127.4, 133.6, 145.4, 149.3, 149.8, 151.7. MS (APCI) *m/z* [M+H$^+$]

326.5. HPLC: condition A1 t_R=3.325min P=95.2%, condition A2 t_R=3.358min P=95.8%.

7-Chloro-N-(4-(4-methylpiperazin-1-yl)phenyl)quinolin-4-amine (60): Green solid. Yield 94%. ^{1}H NMR (300MHz, DMSO-d$_6$) δ 2.22 (s, 3H), 2.45 (t, 4H), 3.13 (t, 4H), 6.61 (d, J=5.4, 1H), 6.99 (d, J=8.8, 2H), 7.19 (d, J=8.7, 2H), 7.52 (dd, J1=2.0, J2=9.0, 1H), 7.85 (d, J=2.0, 1H), 8.36 (d, J=5.4, 1H), 8.41 (d, J=9.1, 1H), 8.92 (s, 1H). ^{13}C NMR (75MHz, DMSO-d$_6$) δ 45.7, 48.2, 54.6, 100.5, 116.1, 117.7, 124.2, 124.5, 125.1, 127.5, 130.7, 133.7, 148.4, 149.2, 149.4, 151.8. MS (APCI) *m/z* [M+H$^+$] 353.6. Elemental analysis: found 68.34% C (calcd 68.08%), found 5.49% H (calcd 6.00%), found 15.50% N (calcd 15.88%).

Appendix 2: Liquid chromatography tandem mass spectrometry

LC/MS/MS analyses were performed using an Agilent 1100 HPLC system (Agilent Technologies, Santa Clara, CA, USA) interfaced with a hybrid triple quadrupole linear ion trap mass spectrometer (QTRAP MS) equipped with TurboIonSpray ESI source (2000 QTRAP, Applied Biosystems, Foster City, CA, USA). Chromatographic separations were performed on a Luna C_{18}(2) 3 µm 50 x 2 mm i.d. column (Phenomenex, Torrance, CA, USA). The column heater and autosampler were kept at 60°C and 4°C, respectively. The flow rate was 0.50 mL/min and the mobile phases consisted of 0.1% formic acid in 10 mM ammonium acetate (solvent A) and acetonitrile (solvent B). The optimized elution conditions for compound 16 were: 17 to 65% solvent B (0.00–3.00 min), 65 to 100% solvent B (3.00–3.01 min), isocratic at 100% solvent B (3.01–4.00 min) and isocratic at 17% solvent B (4.01–11.00 min). The optimized elution conditions for quinacrine were: 0 to 40% solvent B (0.00-2.00min), 40-100% solvent B (2.00-2.01min), isocratic at 100% solvent B (2.01-3.00min), isocratic at 0% solvent B (3.01-8.00min).

All the MS experiments were performed using electrospray positive ionization mode (ESI +ve). Multiple reaction monitoring (MRM) experiments using *m/z* 433.2 to 348.3 and 400.3 to 327.2 were performed to quantify compound **16** and quinacrine, respectively. The MS conditions for the MRM experiment are summarized in Table A2 below. All data were acquired at unit resolution and the

dwell time was set to 300 ms for both compound 16 and quinacrine. Data processing was performed using Analyst 1.4.2 software (Applied Biosystems).

Table A2. Optimized MS parameters for the detection of compound **16** and quinacrine.

Parameter	Value
Curtain gas, psi	25
IonSpray voltage, V	4500
Temperature, ^{o}C	550
Gas 1, psi	55
Gas 2, psi	55
Interface heater	ON
CAD gas	Medium
Entrance potential for compound **16**, V	10
Entrance potential for quinacrine, V	11
Declustering potential for compound **16**, V	87
Declustering potential for quinacrine, V	31
Collision energy for compound **16**, V	42
Collision energy for quinacrine, V	40
Collision cell entrance potential for compound **16**, V	22
Collision cell entrance potential for quinacrine, V	40
Collision cell exit potential for compound **16**, V	5
Collision cell exit potential for quinacrine, V	4

Figure A2. MRM chromatograms on analysis of compound **16** (A) and quinacrine (B).

B

3.54
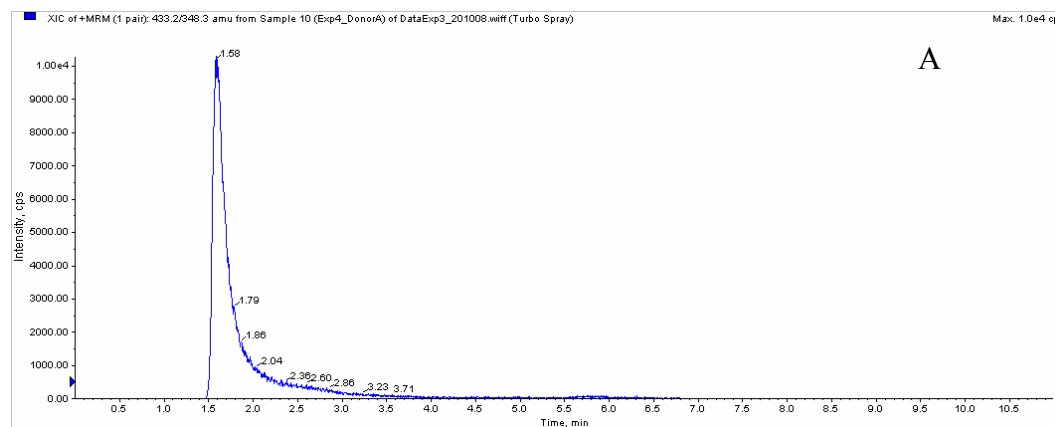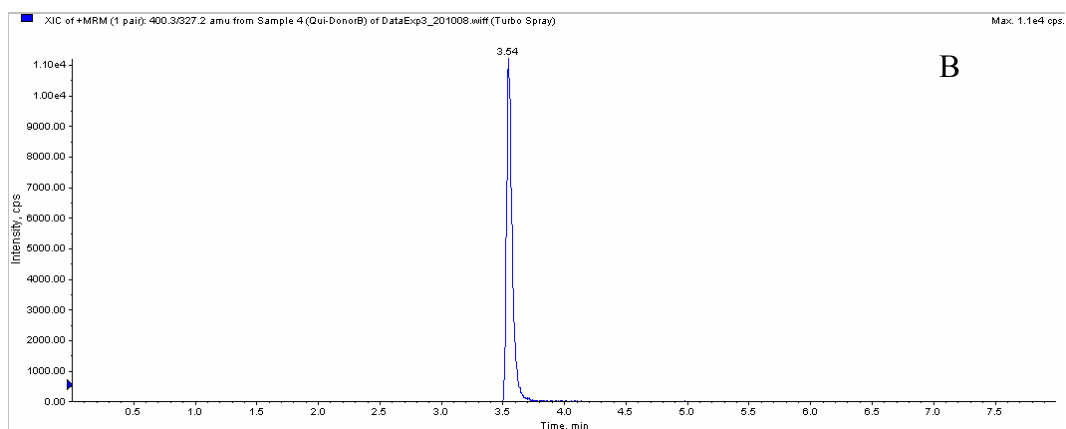
Appendix 3: ClogP and SlogP values

Compound	EC$_{50}$ in ScN2a (µM)	EC$_{50}$ in F3 (µM)	ClogP[a]	SlogP[b]
Quinacrine	0.23	1.88	6.72	3.97
1	0.021	ND[c]	6.23	2.81
2	0.11	ND[c]	5.51	2.42
3	0.14	ND[c]	6.56	3.20
4	0.15	ND[c]	6.41	3.59
5	0.25	ND[c]	7.12	5.28
6	0.32	ND[c]	7.12	5.28
7	0.51	ND[c]	7.12	5.28
8	1.01	ND[c]	8.18	6.06
9	0.48	ND[c]	8.18	6.06
10	1.06	ND[c]	7.75	5.81
11	0.18	ND[c]	8.31	6.20
12	4.24	ND[c]	8.31	6.20
13	0.9	ND[c]	6.77	5.05
14	1.28	ND[c]	6.77	5.05
15	0.29	1.49	6.17	3.55
16	0.1	0.68	6.17	3.55
17	0.08	ND[c]	6.87	3.94
19	0.035	ND[c]	4.94	4.88
22	0.06	0.86	7.14	2.39
23	1.23	4.1	6.15	3.18
24	0.099	0.64	7.98	5.05
25	0.54	ND[c]	6.95	5.21
32	0.42	0.8	6.82	4.39
33	0.15	0.63	7.32	4.70
34	0.28	ND[c]	7.53	5.05
35	0.082	ND[c]	6.74	4.40
36	0.55	ND[c]	6.25	4.27
37	0.13	0.19	6.96	4.17
38	0.076	0.69	7.46	4.48
41	0.093	1.04	7.34	4.56
42	0.027	ND[c]	5.02	0.30
43	0.054	0.54	7.13	4.93
45	2.51	ND[c]	6.94	5.24
46	0.13	ND[c]	4.17	3.05
48	0.24	ND[c]	7.09	5.40
50	0.51	ND[c]	6.15	2.52
51	0.54	1.19	6.73	4.11

54	0.082	ND^c	6.25	3.26
56	1.56	ND^c	4.58	1.64
57	0.15	1.2	5.16	3.23
60	0.14	2.04	4.68	2.39

^{a}: determined by ChemDraw version 8.0

^{b}: determined by Molecular Operating Environment version 2009.10

^{c}: not determined.

Appendix 4: ClustalW2 sequence alignment of TcAChE (PDB code 1ACJ) and hAChE (PDB code 1B41)

```
SeqA Name                        Len(aa)  SeqB Name                        Len(aa)  Score
===============================================================================================
1    1B41_A|PDBID|CHAIN|SEQUENCE  539      2     1ACJ_A|PDBID|CHAIN|SEQUENCE  537      57
===============================================================================================
```

```
1B41    --DAELLVTVRGGRLRGIRLKTPGGPVSAFLGIPFAEPPMGPRRFLPPEP 48

1ACJ    DDHSELLVNTKSGKVMGTRVPVLSSHISAFLGIPFAEPPVGNMRFRRPEP 50

          .:****..:.*:: * *: . .. :*************:*   **   ***



1B41    KQPWSGVVDATTFQSVCYQYVDTLYPGFEGTEMWNPNRELSEDCLYLNVW 98

1ACJ    KKPWSGVWNASTYPNNCQQYVDEQFPGFSGSEMWNPNREMSEDCLYLNIW 100

        *:***** :*:*: . * ****   :***.*:*******:*********:*



1B41    TPYPRPTSPTPVLVWIYGGGFYSGASSLDVYDGRFLVQAERTVLVSMNYR 148

1ACJ    VPSPRPKS-TTVMVWIYGGGFYSGSSTLDVYNGKYLAYTEEVVLVSLSYR 149

        .* ***.* *.*:***********:*:****:*::*. :*..****:.**



1B41    VGAFGFLALPGSREAPGNVGLLDQRLALQWVQENVAAFGGDPTSVTLFGE 198

1ACJ    VGAFGFLALHGSQEAPGNVGLLDQRMALQWVHDNIQFFGGDPKTVTIFGE 199

        ********* **:***********:*****::*:   *****.:**:***



1B41    SAGAASVGMHLLSPPSRGLFHRAVLQSGAPNGPWATVGMGEARRRATQLA 248

1ACJ    SAGGASVGMHILSPGSRDLFRRAILQSGSPNCPWASVSVAEGRRRAVELG 249

        ***.*******:*** **.**:**:****:** ***:*.::.*.****.:*.



1B41    HLVGCPPGGTGGNDTELVACLRTRPAQVLVNHEWHVLPQESVFRFSFVPV 298
```

```
1ACJ    RNLNCNLN----SDEELIHCLREKKPQELIDVEWNVLPFDSIFRFSFVPV 295

        : :.*   .     .* **: *** : .* *:: **:*** :*:********



1B41    VDGDFLSDTPEALINAGDFHGLQVLVGVVKDEGSYFLVYGAPGFSKDNES 348

1ACJ    IDGEFFPTSLESMLNSGNFKKTQILLGVNKDEGSFFLLYGAPGFSKDSES 345

        :**:*:. : *:::*:*:*:  *:*:** *****:**:*********.**



1B41    LISRAEFLAGVRVGVPQVSDLAAEAVVLHYTDWLHPEDPARLREALSDVV 398

1ACJ    KISREDFMSGVKLSVPHANDLGLDAVTLQYTDWMDDNNGIKNRDGLDDIV 395

         *** :*::**::.**:..**. :**.*:****:. ::   : *:.*.*:*



1B41    GDHNVVCPVAQLAGRLAAQGARVYAYVFEHRASTLSWPLWMGVPHGYEIE 448

1ACJ    GDHNVICPLMHFVNKYTKFGNGTYLYFFNHRASNLVWPEWMGVIHGYEIE 445

        *****:**: ::..: :   *   .* *.*:****.* ** **** ******



1B41    FIFGIPLDPSRNYTAEEKIFAQRLMRYWANFARTGDPNEPRDPKAPQWPP 498

1ACJ    FVFGLPLVKELNYTAEEEALSRRIMHYWATFAKTGNPNEPHSQES-KWPL 494

        *:**:**   . ******: :::*:*:***.**:**:****:. :: :**



1B41    YTAGAQQYVSLDLRPLEVRRGLRAQACAFWNRFLPKLLSAT-- 539

1ACJ    FTTKEQKFIDLNTEPMKVHQRLRVQMCVFWNQFLPKLLNATET 537

        :*:   *:::.*: .*::*:: **.* *.***:******.**
```

Note: star denotes conservation, double dot denotes exact match, single dot denotes high similarity, and blank means difference.

275

Appendix 5: Superimposing 3D structures of TcAChE and hAChE using MOE
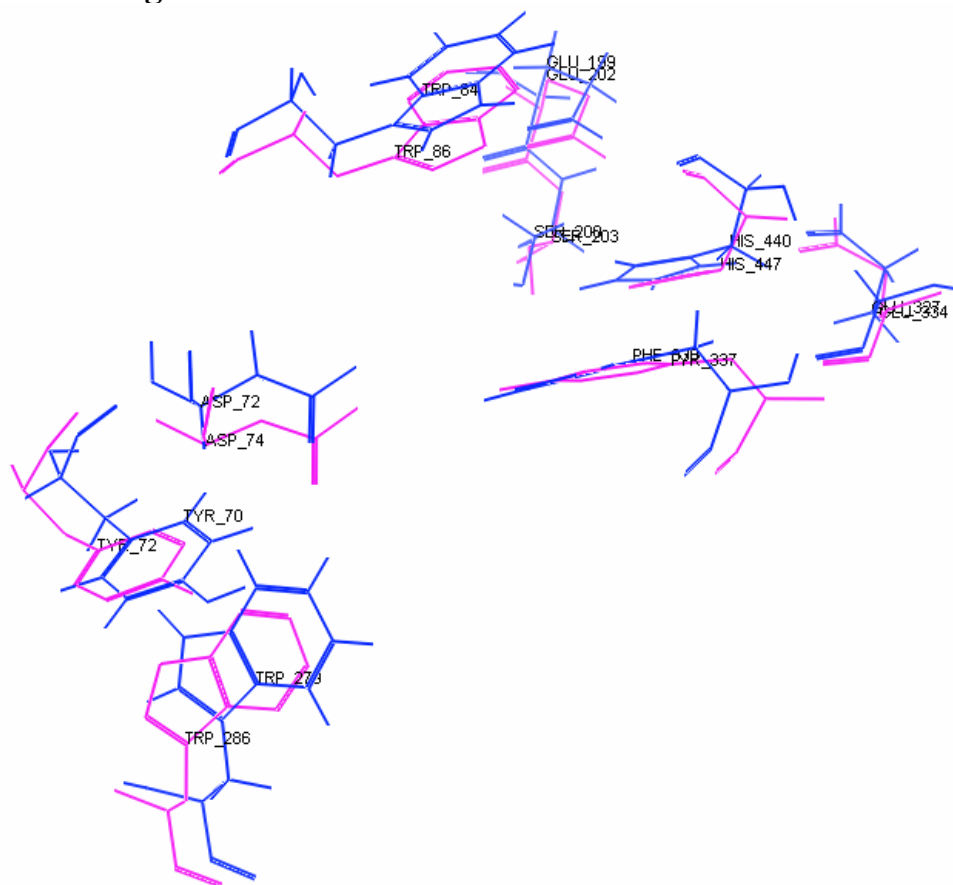
In the diagram, 1ACJ is displayed in blue and 1B41 in pink. RMSD is 4.054Å. The amino acid residues at the active site and peripheral site are well-preserved.